

**STABILITY STUDIES ON CELLULAR-WALLED
CIRCULAR CYLINDRICAL SHELLS**

by

RONG DAR ZOU

B.E., M.E.

Submitted in fulfilment of the requirements

for the degree of

DOCTOR OF PHILOSOPHY

in the

Department of Civil and Mechanical Engineering

UNIVERSITY OF TASMANIA

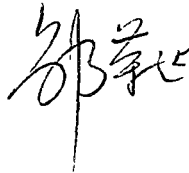
AUSTRALIA

May, 1993

DECLARATION

I hereby declare that this thesis contains no material which has been accepted for the award of any other degree or diploma in any tertiary institution and that, to the best of my knowledge and belief, this thesis contains no material previously published or written by another person, except when due reference is made in the text of the thesis.

Rong dar Zou



5. Access to, and copying of, thesis

The thesis copy lodged in the University Library shall be made available by the University for consultation but, for a period of two years after the thesis is lodged, it shall not be made available for loan or photocopying without the written consent of the author and in accordance with the laws of copyright

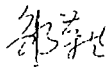
After a thesis has been examined, the following authority will apply. Please complete your request, and sign below

(i) I agree/~~do not~~ agree that the thesis may be made available for loan

(ii) I agree/~~do not~~ agree that the thesis may be made available for photocopying

(iii) I note that my consent is required only to cover the two-year period following approval of my thesis for the award of my degree. After this, access to the Library copy will be subject only to any general restrictions laid down in Library regulations

Signed



Date

24/6/93

Lodged in Morris Miller Central Library

/

/ 198

from which date the two years embargo will apply

SMED 12/86

To
My Wife and Parents

ABSTRACT

The present study deals with the stability behaviour of cellular-walled cylindrical shells subjected to simultaneous loading of axial compression and external pressure. In particular, the effect of high fluid pressure within the cells on the buckling behaviour of the shell is considered.

The form of cellular-walled shell originated from a consideration of fossil shell remains belonging to the Nautiloid Cephalopod group. These extinct animals (relatives to the modern day pearly nautilus) grew to about 300mm in length and had an exoskeleton in the form of a conical shell with a small apex angle. However, the unique feature of the shell of this fish was that it contained small closely spaced holes running longitudinally in the shell wall. Interest in these fossil shells originated from discussions with Dr. M.R. Banks¹, a paleontologist at the University of Tasmania. Dr. Banks was interested to discover why the shellfish should want to build its shell in such a particular form. Other than for the obvious conclusion that a cellular wall has better bending stiffness than a solid wall of the same mass, there appeared to be no particular reason for the specific form of this shell. From a strength point of view, there appears to be no advantage in the shell having longitudinal holes over circumferential or spiral holes, and spiral holes would be easier for the shell fish to manufacture. This study showed both theoretically and experimentally that a possible answer lies in the stability behaviour of this particular form of shell.

The cellular-walled cylindrical shell can be characterized as a pseudo-orthotropic cylindrical shell with the principal directions axially and circumferentially oriented. Different effective Young's moduli had to be used for tension and bending. A theoretical analysis, based on Flugge's linear buckling theory, resulted in simple interaction formulas for buckling under external pressure, axial compression and cell pressure.

Cellular-walled model shells have been made out of epoxy by an adaptation of the spin casting process developed by Tennyson⁶. These shells have 360 longitudinal holes each of 0.7mm diameter, shell internal diameter 153mm, wall thickness 1.2mm and length 245mm. The tests of the model shells were carried out on a rigid test machine with parallel platens. Since the shells are cast with a free surface on the inside they are internally reflective. An optical system making use of the reflective surface was used to monitor buckling and prebuckling deformations. Test data was logged into a PC. Southwell plots were then employed to predict axial buckling loads. Because of the likelihood of the shell shattering on buckling, actual collapse loads were the final values obtained. Test data confirmed the theoretical predictions.

Both theoretical and experimental results showed that shells of this type with pressurized cells exhibit significantly improved stability, hence they appear to have potential in engineering applications, particularly in marine situations.

ACKNOWLEDGEMENTS

I would like to express my sincere gratitude to my supervisor Dr. C. G. Foster and associate supervisor Dr. E. Melerski, for their constant guidance, encouragement and advice during every stage of this study.

My appreciation must be extended to many others without whose assistance this study could not have been completed. In particular I would like to thank

- : Mr. Basil Stiberc and the other staff of the engineering workshop for the manufacture of the end-rings and other apparatus used in the model shells testing.
- : All the other academic as well as non-academic staffs in the engineering faculty for their encouragement and support.
- : Dr. John Morris, of the department of computer science, for his valuable advice in writing the computing programs.
- : Mrs Gail Wilson for checking draft of the thesis.
- : Mr. Michael Koutsoukis, Reza Izadnegahdar and Ashay Prabhu, for many valuable discussions and their support.
- : Professor M. R. Davis for providing the opportunity to undertake this study in the Department of Civil and Mechanical Engineering.
- : and the University of Tasmania for providing Postgraduate Research Scholarship during Sept. 1988 to Sept. 1992.

Finally, I would like to acknowledge the forbearance and the sacrifices of my wife and child, without which this study and the preparation of the thesis would not have been possible.

TABLE OF CONTENTS

ABSTRACT	iv
ACKNOWLEDGEMENTS	vi
CHAPTER 1 INTRODUCTION	1
CHAPTER 2 BUCKLING OF ISOTROPIC CYLINDRICAL SHELLS - HISTORICAL BACKGROUND	9
2.1 Classical Linear Theory	13
2.2 Development of Large-Displacement Theory	15
2.3 Effect of Initial Imperfections	19
2.4 Effect of Prebuckling Deformation and Boundary Condition	25
2.5 Experiments on Near Perfect Shells	26
CHAPTER 3 BUCKLING OF ORTHOTROPIC AND ANISOTROPIC CYLINDRICAL SHELLS - A REVIEW OF CURRENT LITERATURE	28
3.1 Classical Buckling Theories - Perfect Cylindrical Shells	30
3.2 Limitations in the Classical Buckling Theories	34
3.3 Buckling of Geometrically Imperfect Orthotropic Cylindrical Shells	36
3.4 Experimental Data on Orthotropic Cylindrical Shells	38
CHAPTER 4 THEORETICAL BUCKLING ANALYSIS OF ORTHOTROPIC AND CELLULAR-WALLED CIRCULAR CYLINDRICAL SHELLS	41
4.1 Buckling Criterion of An Orthotropic Circular Cylindrical Shell Under Combined Loading of Axial Compression and External Pressure	43
4.1.1 Basic Equations	43
4.1.2 Buckling under Combined Loading	49
4.1.3 Buckling under External Pressure Only	54
4.1.4 Buckling under Axial Compression Only	57

4.2	Buckling Criterion of A Cellular-Walled Circular Cylindrical Shell Under Combined loading of Axial Compression and External Pressure	61
4.2.1	Buckling under Combined Loading	62
4.2.2	Buckling under External Pressure Only	63
4.2.3	Buckling under Axial Compression Only	64
	Notations	66
 CHAPTER 5 NUMERICAL ESTIMATION OF AVERAGE PROPERTIES OF CELLULAR-WALLED CIRCULAR CYLINDRICAL SHELLS		
69		
5.1	Determination of Equivalent Cell Pressure to Internal Pressure	73
5.1.1	Structure Analysis and Elements	73
5.1.2	The Empirical Relations of the Effect of Cell Pressure to That of Internal Pressure	75
5.2	Determination of Average Properties of Cellular-Walled Circular Cylindrical Shells	78
5.2.1	Determination of Average Young's Modulus E_1	78
5.2.2	Determination of Average Young's Modulus E_2	81
5.2.3	Determination of Poisson's Ratios μ_1 and μ_2	82
5.2.4	Determination of Average Young's Modulus E_{b1}	84
5.2.5	Determination of Average Young's Modulus E_{b2}	84
	Notations	89
 CHAPTER 6 THEORETICAL PERFORMANCE OF CELLULAR-WALLED CIRCULAR CYLINDRICAL SHELLS		
91		
6.1	Buckling under Combined Axial Compression and External Pressure	92
6.2	Buckling Including the Effects of Cell Pressure	106
6.3	Calculation of Buckling Loads	108
	Notations	111
 CHAPTER 7 MANUFACTURE OF MODEL SHELLS		
113		

7.1	Nylon Line Cage	114
7.2	Model Shell Casting	116
7.3	Finishing Work	121
CHAPTER 8 EXPERIMENTAL SET UP		125
8.1	Optical System	126
8.2	End Rings	133
8.3	Loading Frame	136
8.4	Data Logging	139
8.5	Southwell Plot	141
CHAPTER 9 MEASURED BEHAVIOUR OF MODEL SHELLS		145
9.1	Test Procedure	148
9.2	Buckling under Combined Loading	152
9.3	Buckling under Axial compression	168
CHAPTER 10 CONCLUSIONS AND RECOMMENDATIONS		173
10.1	Conclusions	174
10.2	Discussions and Recommendations	175
REFERENCES		177
APPENDIX A	CALCULATED DATA OF RADIAL DISPLACEMENTS w_1 AND w_2 FOR VARIOUS GEOMETRIC CONFIGURATIONS	191
APPENDIX B	PROGRAM LISTING USED IN NON-LINEAR LEAST SQUARES FITTING	218
APPENDIX C	PROGRAM LISTING USED IN DETERMINE THEORETICAL BUCKLING LOADS AND MODE	230
APPENDIX D	PROGRAM LISTING USED IN DATA LOGGING	236
APPENDIX E	CALIBRATION PLOTS.....	240
APPENDIX F	PROCEDURE LISTING USED IN PC-MATLAB	245

CHAPTER 1

INTRODUCTION

CHAPTER 1

INTRODUCTION

The present study was undertaken with the objective of investigating the buckling behaviour of a form of cellular shell suggested by fossil shell remains belonging to the Nautiloid Cephalopods group.

Nautiloid Cephalopods are a family of interesting fossil shellfish. These extinct animals, relatives of the modern day Pearly Nautilus, grew to about 300mm in length and had an exoskeleton in the form of a conical shell with a small apex angle. However, the unique feature of the shell of this fish was that it contained small, closely spaced holes running longitudinally in the shell wall. Interest in these fossil shells originated from discussions with Dr. M.R. Banks¹, a paleontologist at the University of Tasmania. The problem encountered by Dr. Banks was to discover the reason the shell is built in such a particular form. Aside from the obvious conclusion that a cellular wall has better bending stiffness than a solid wall of the same mass, there appeared to be no particular reason for the specific form of this shell. Animal structures are usually very efficient, and a cellular wall made with circumferential or spiral cells would have similar bending stiffness while providing an easier path for the manufacture of the shell.

Figure 1.1 shows an artist's impression of the living

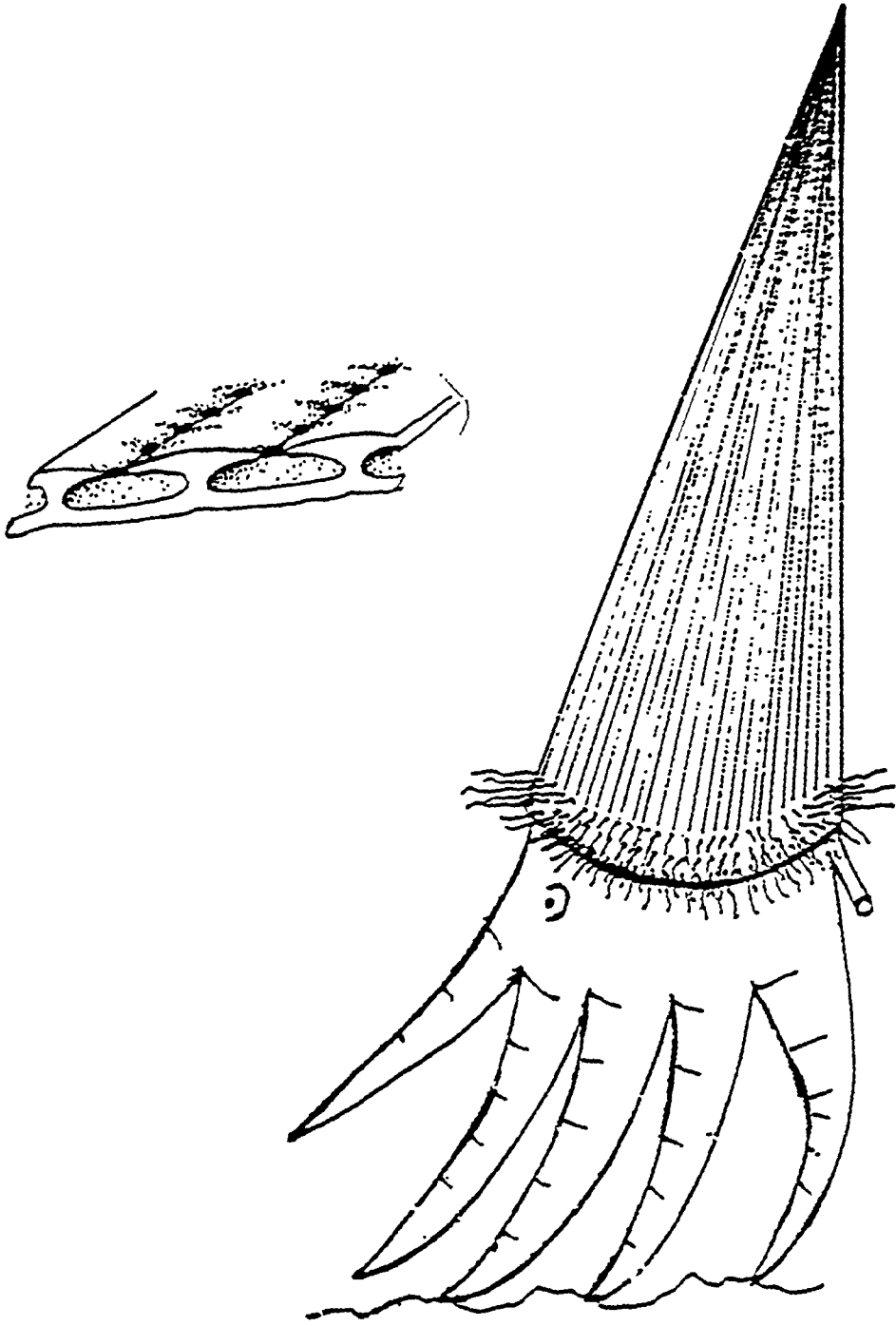


Figure 1.1
Artists impression of Nautiloid Cephalopod
and section of shell wall

shell fish together with a sketch of a section through the shell wall. This sketch is taken from actual fossil specimens. The structure is essentially a thin-walled circular shell with small, closely spaced holes running longitudinally through the wall. In addition, there are a large number of considerably smaller holes connecting these longitudinal channels with the outside of the shell. The purpose of the longitudinal holes and the smaller connecting holes is not clear. One likely explanation is that the longitudinal holes were filled with muscle while the very small connecting holes may have been for some form of nerve tissue (i.e., sensing element).

From a strength point of view, there appears to be no advantage in the shell having longitudinal holes over circumferential or spiral holes. However, if the small longitudinal holes contained muscle then it can be observed that by contracting the muscle, pressure could be applied to the inside of the holes. Large pressures could be achieved with muscle contraction, which appear to be equivalent to small pressures applied to the inside of the shell.

It is well known that by applying pressure to the inside of a thin, solid-walled cylindrical shell, its axial buckling load can be increased^{2,3,4}. One contributing factor could be that the pressure tends to make the shell more nearly circular and hence reduces the sizes of geometric defects. Internal pressure obviously must also increase the external buckling pressure. Since it was expected that high cell pressure would act in a similar fashion to

much lower internal pressure, it was thought that the purpose of the cells may have been to provide such high pressure through muscle contraction. The contraction would have been triggered by the nerve "sensing element" attached directly to the muscle and connected through the secondary holes to the outside of the shell.

If the shell did function in this manner, then it seems likely that nature had provided a solution which may have an engineering significance, hence the reason for this investigation. The equivalent structure which appeared to have possibility as a submarine containment shell was a thin-walled cylindrical shell with closely spaced longitudinal holes and with high fluid pressure applied inside the holes. Such a structure could be made somewhat lighter than a uniform shell. It could have smooth external and internal surfaces, and the inside of the shell could be maintained at relatively low pressure, e.g. suitable for human occupation.

Since the shell wall consists of a section containing a large number of circular closely spaced longitudinal holes, the line of this investigation was to consider it in a similar fashion to a longitudinal stringer-stiffened shell with the stringers closely spaced. Thus the shell wall construction was treated as homogeneous and pseudo-orthotropic, with the principal directions along the shell generators and circumference. Local variations in wall properties were ignored in determining buckling loads. Also it may be observed that axial in-plane stiffness and bending stiffness would be greater than the same properties measured in the hoop

direction. Average wall properties had to be established from a consideration of local wall geometry.

Since the shell form originated from a marine animal, and also since the most likely application of the shell form would be as a submarine structure; this investigation concentrated on the load condition of axial compression and external pressure.

The theoretical buckling analysis presented in this thesis was based on Flugge's linear elastic theory⁵. The shell was treated as homogeneous and pseudo-orthotropic. A simple form of solution for the buckling of cellular-walled cylindrical shells under simultaneous loading of axial compression and external pressure was derived, which can be simplified to the form of exact orthotropic shells, and further to the form of isotropic shells. The effect of cell pressure on the buckling load of the shell was considered.

The shell models have been made by an adaptation of the spin casting process developed by Tennyson⁶. I have been able to consistently produce shells with an internal diameter of 153mm, wall thickness 1.2mm, length 245mm. These shells had 360 holes each of 0.7mm diameter. The radius to thickness ratio for these shells is around 65. Thus they should be considered as relatively thick shells. Unfortunately, it does not appear possible to make shell models by our current technique with walls that are much thinner. Tests of the shell models on buckling load capacity have

been carried out on a rigid compression testing machine with parallel platens and incorporated with the optical examination system.

The first three chapters in the thesis, including this one, are introductory. Chapter Two gives a survey of the developments in research on the buckling behaviour of isotropic cylindrical shells loaded in axial compression, external pressure, or a combination of the two; while in Chapter Three, a review of the buckling behaviour of orthotropic cylindrical shells under various load conditions is presented. Some necessary background for the work presented in the thesis is provided in these chapters.

The next three chapters deal with theoretical investigations. In Chapter Four, theoretical buckling analysis of orthotropic and cellular-walled circular cylindrical shells are presented. Buckling solutions for both orthotropic and cellular-walled shells under simultaneous loading of axial compression and external pressure are derived. A conventional simply-supported boundary condition is used in the analysis. The difference in boundary conditions used in the buckling analysis and in the shell models test (built-in) is noted. A numerical analysis is presented in Chapter Five, which determines the effects of cell pressure. Cell pressure was considered to be the same as an internal pressure when the radial displacements of midsurface were the same in both cases. The empirical relations are established to link the effect of cell pressure to that of internal pressure. The average wall

properties of cellular-walled cylindrical shells were established using the energy method, from a consideration of local wall geometry. These properties were used in the theoretical performance of cellular-walled cylindrical shells, which is presented in Chapter Six. The buckling of shells with different geometric configurations were presented and compared. The effects of shell geometric configurations on buckling were discussed. In particular, the effects of cell pressure to the buckling of shells were demonstrated.

The experimental work of this thesis is presented in Chapters Seven, Eight and Nine. In Chapter Seven, the model shell manufacture and the main problems experienced in the processes are described. Experimental set-up, the optical examination system, end rings design, loading frame, data logging board and PCLAB program used in the test are described in Chapter Eight. The results of the tests on buckling loads are presented in Chapter Nine.

Chapter Ten provides the conclusion to the thesis.

CHAPTER 2

BUCKLING OF ISOTROPIC CYLINDRICAL SHELLS

- HISTORICAL BACKGROUND

CHAPTER 2

BUCKLING OF ISOTROPIC CYLINDRICAL SHELLS

- HISTORICAL BACKGROUND

The problem of cylindrical shell buckling has been a widespread topic of research interest over several decades, and the results have been reported in innumerable publications. Certain aspects of cylindrical shell buckling have been emphasized, namely the effect of boundary conditions and nonlinear prebuckling deformations, external loading conditions (axial compression, external pressure, torsion), postbuckling behaviour and accompanying imperfection sensitivity, and the role of material properties (isotropic, orthotropic, anisotropic).

In general, thin-walled shell structures are stiff in axial or in-plane deformations but flexible in bending. When they are subjected to axial or in-plane forces they often lose stability at very low stress levels, resulting in large bending deformations. Thus, examining the buckling problem and determining the critical load has been one of the most important investigations in the development of light-weight structures.

The type of buckling to which an axially compressed cylinder is susceptible depends on the ratio of its length to its radius, L/R , and on the ratio of its radius to its thickness, R/t .

Relatively thick-walled shells buckle into the axisymmetric "ripple" pattern illustrated in Figure 2.1. This type of buckling usually leads to yielding. Very short, thin-walled cylinders behave like flat plates that are supported along the loaded edges and are free along the unloaded edges. They buckle into a single half sine wave in the axial direction with no waves in the circumferential direction as shown in Figure 2.2a. By comparison, very long cylinders with small diameters buckle like Euler columns with minimal distortion of the circumferential cross-section (Fig. 2.2b). A third group consists of moderately long cylinders that fail by local buckling. The surface of these cylinders buckles into a series of diamond shaped dimples which are well known as Yoshimura patterns (Fig. 2.2c).

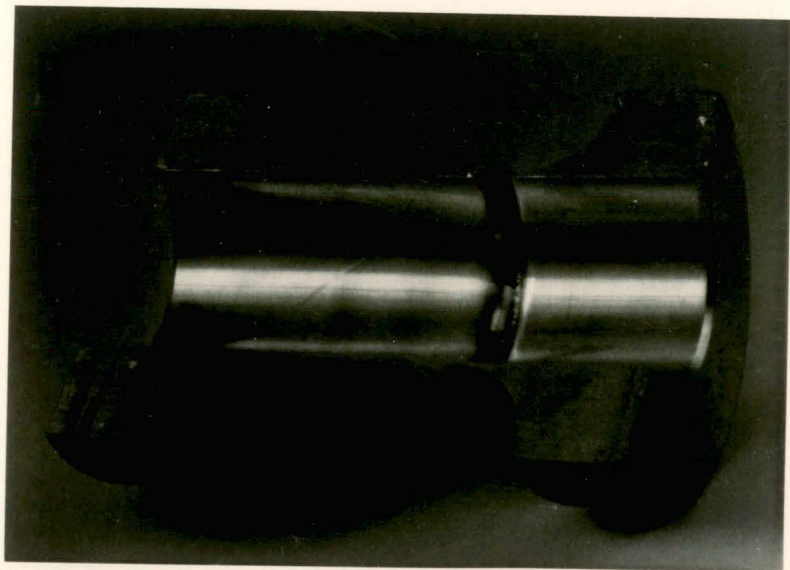
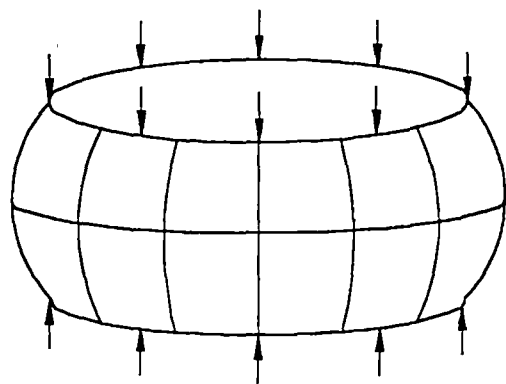
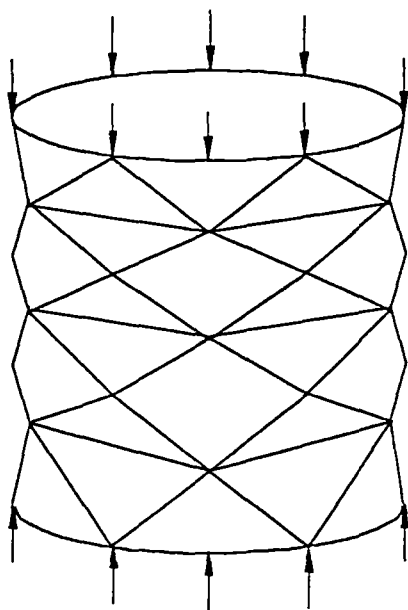


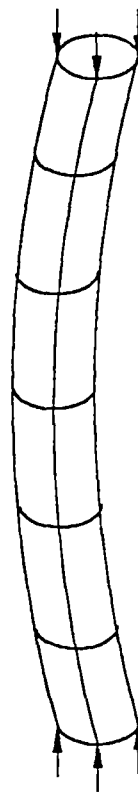
**Figure 2.1 Inelastic axial ripple buckling (Foster³⁸)
(No.2011 Aluminium cylinder $R = 12.70\text{mm}$, $t = 0.50\text{mm}$)**



(a) Very short cylinder



(c) Moderately long cylinder



(b) Long cylinder

Figure 2.2 Buckling of thin cylindrical shells

The Batdorf parameter Z is normally used to separate short cylindrical shells from moderately long cylindrical shells⁷

$$Z = (L/R)^2(R/t)\sqrt{1-\mu^2} \quad (2.1)$$

where μ is Poisson's ratio. Those cylindrical shells with $Z < 2.85$ can be characterised as very short cylindrical shells and those with $Z > 850$ as very long cylindrical shells. Cylindrical shells with Z between 2.85 and 850 can be considered as moderately long.

The single most important characteristic of moderately long cylindrical shells is that they often fail at loads well below the critical load obtained using classical linear theory. It is with this group of cylindrical shells that this thesis is mainly concerned. The major developments in both theoretical and experimental work on buckling of moderately long cylindrical shells are summarized in the following sections.

2.1 CLASSICAL LINEAR THEORY

Within the limits of elastic small-deformation linear theory, the behaviour of unstiffened isotropic cylindrical shells is usually considered to be governed by Donnell's equation^{8,9}, i.e.,

$$D\nabla^4 w + \frac{Et}{R^2} \frac{\partial^4 w}{\partial x^4} + t\nabla^4 \left(\sigma_x \frac{\partial^2 w}{\partial x^2} + 2\tau_1 \frac{\partial^2 w}{\partial x^2} + \sigma_y \frac{\partial^2 w}{\partial x^2} - \sigma_y/R \right) + \nabla^4 p = 0 \quad (2.2)$$

where $D = Et^3/[12(1-\mu^2)]$ is the flexural rigidity, E Young's modulus, t shell thickness, R shell radius, σ_x axial stress, x coordinate in axial direction, w displacement in radial direction; $\nabla^2 = \frac{\partial^2}{\partial x^2} + \frac{\partial^2}{\partial y^2}$ is biharmonic operator; ∇^4 signifies the application of ∇^2 twice and ∇^8 four times. When there is only axial stress applied on a shell, Donnell's equation (2.2) becomes:

$$D \nabla^8 w + \frac{Et}{R^2} \frac{\partial^4 w}{\partial x^4} + \sigma_x t \nabla^4 \frac{\partial^2 w}{\partial x^2} = 0 \quad (2.3)$$

For moderately long cylindrical shells, the critical stress can be obtained by solving equation (2.3):

$$\sigma_{cr} = \frac{E}{[3(1-\mu^2)]^{1/2}} (t/R) \quad (2.4)$$

According to St.Venant's principle, only the surface adjacent to the loaded edges of the cylinder is affected by the restraint along those edges. Hence the critical stress for a cylindrical shell of intermediate length, given by equation (2.4), is valid for clamped or built-in as well as simply supported edges.

The equation (2.4) is regarded as a classical solution. It was first obtained in 1910-1911 by Timoshenko, Lorentz and Southwell^{10,11} who applied the energy method in a cylindrical shell assuming axisymmetrical buckling. However, buckling experiments over the next 50 years were unable to attain much more than 50%

of this value. This discrepancy between theory and experiment has led to a great deal of research both theoretically and experimentally. The cause of this discrepancy is generally believed to be the unstable post-buckling behaviour of the shell, which causes the shell to be extremely sensitive to even small initial geometrical imperfections.

2.2 DEVELOPMENT OF LARGE-DISPLACEMENT THEORY

The first attempt to explain the discrepancy between theory and experiment was made in 1934 by Donnell^{8,9} who introduced a set of simplified non-linear equations for the large deflection analysis of cylindrical shells. Donnell's theory is based on the assumptions of the Kirchhoff-Love hypotheses and shallow shell approximations. The latter assumption restricts the validity of the theory to situations in which the normal deflection predominates over the in-plane displacements. Despite its limits of applicability, owing to its relative simplicity and practical accuracy for short and moderately long cylinders, Donnell's theory has been widely used for analysing both buckling and post-buckling problems of cylindrical shells. A more complete non-linear theory without the limitation of the shallow shell approximation was developed around the same time by Flugge⁵. Flugge's theory is considered to be more refined and is often employed to check the accuracy of Donnell's equations or in situations where the latter is not applicable. Both Donnell's and Flugge's non-linear theories

were followed by numerous theoretical and experimental investigations, which have led to a more complete understanding of the phenomenon of shell buckling and post buckling.

A major breakthrough to explain the discrepancy between theory and experiment was made in 1941 by Von Karman and Tsien¹²⁻¹⁵ who demonstrated that an analysis of the buckling of thin shells by means of the small-displacement linear theory is insufficient to establish the practical limits of the load-carrying capacity of thin shells. Instead, they used Karman-Donnell type large displacement equations and for the first time showed that the highly unstable post-buckling behaviour of axially compressed cylindrical shells was the main cause of the large discrepancy between theory and experiment. They found that, subsequent to reaching the critical load, the load that an initially perfect shell can support drops sharply with increasing deformations. As indicated in Figure 2.3, the post-buckling behaviour of the shell is in sharp contrast to the way a simple column buckles. Whereas the load that a column can support subsequent to the onset of buckling remains fairly constant before increasing again with large deflections, the load-carrying capability of the shell drops precipitously once buckling begins.

The unstable post-buckling behaviour of cylindrical shells discovered by Von Karman and Tsien indicates that equilibrium is possible in a deformed configuration at loads well below the critical load of the classical theory. It was recognized

that the presence of initial imperfections, or that of external disturbances, would cause the shell to jump to these lower equilibrium positions before reaching the critical load. As illustrated in Figure 2.3, the initially imperfect shell never reaches the critical load given by the linear theory for a perfect shell. Instead, the initially imperfect shell exhibits a maximum load that is considerably lower than the critical load of the perfect shell.

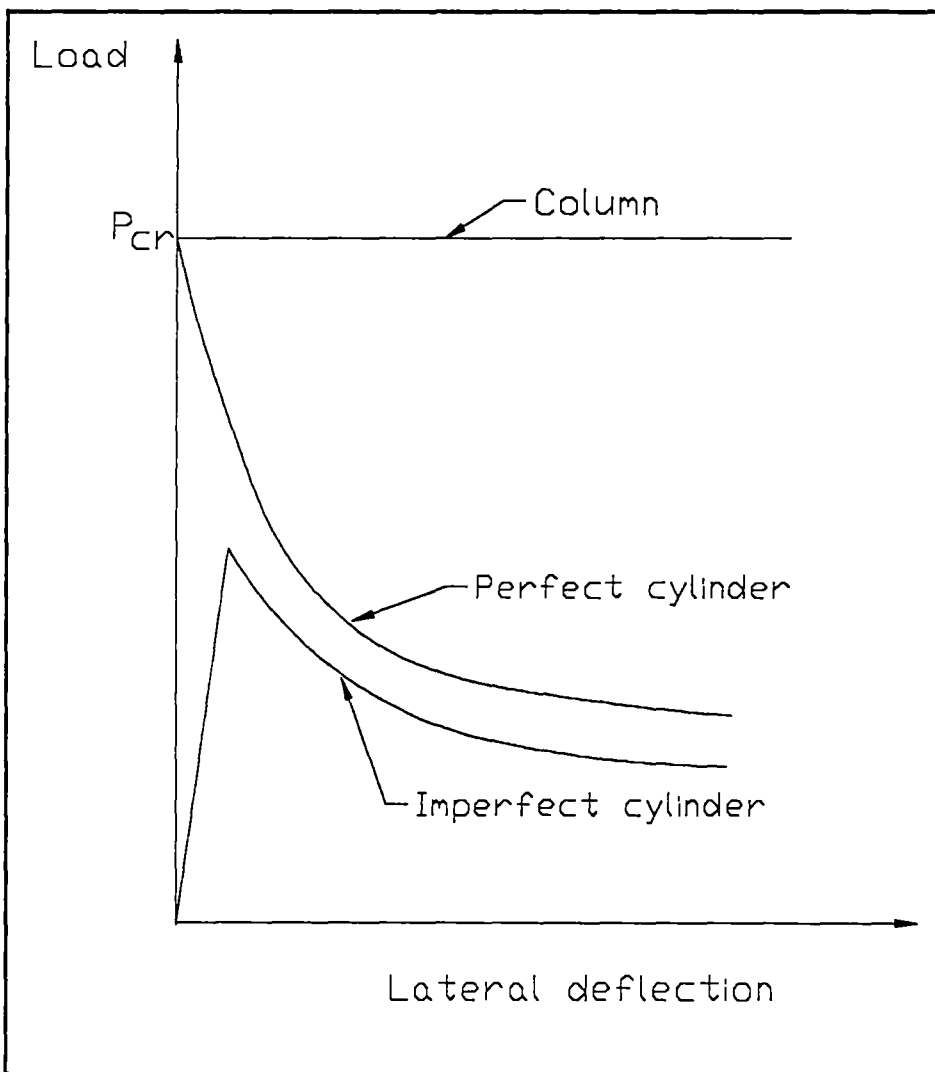


Figure 2.3
Post-buckling curves for column and axially compressed
cylindrical shell

Many investigators followed in the footsteps of Von Karman and Tsien. Most of them attempted to obtain more accurate results for the cylindrical shell under axial compression¹⁶⁻¹⁸, in particular finding the minimum load that the shell can support in the buckled state. It was then proposed that this minimum post-buckling load could be taken as the safe design load, on the grounds that the shell could always support at least this much load and that even imperfections would not reduce the postbuckling load below this value. However, by increasing the number of terms used to express the deflection and minimizing the total potential energy with respect to the thickness to radius ratio as well as the wave number parameter, lower and lower values of the minimum post-buckling load were produced; until Hoff, Madsen and Mayers¹⁹ showed that as the number of terms used to express the deflection is increased indefinitely, the minimum load required to maintain the post-buckled state approaches zero, the thickness to radius ratio of the shell tends to zero, and the deflection pattern approaches the exact Yoshimura pattern (a series of diamond shaped facets).

The Yoshimura pattern was attributed by Yoshimura²⁰ who described the buckled surface of the cylindrical shell in axial compression as a near developable surface. He suggested that the observed buckling pattern can be approximated by a concave polyhedron made up of triangular facets which can be obtained by an inextensional transformation from the original cylindrical surface, then explained the physical reason for the presence of

postbuckling equilibrium states with lower energy than the prebuckled state. Since the stiffness of the shell is proportional to the cube of its thickness, to a thin shell, the energy involved in bending is small, and the total strain energy contained in the buckled configuration is much smaller than the extensional strain energy in the compressed state just before buckling. This explains the sudden snapping with loud report caused by the release of energy and the small value of the load required to maintain the buckled shell. Obviously, if the thickness were vanishingly small, the resistance to bending would be negligible; hence the shell would buckle to the exact Yoshimura pattern, and no load would be required to maintain this shape.

2.3 EFFECT OF INITIAL IMPERFECTIONS

The effect of initial imperfections on the buckling behaviour of axially compressed cylindrical shells has posed baffling problems to engineering in the past several decades. Much research has been carried out on the subject and many review papers have been published²¹⁻²⁸.

When cylindrical shells are subjected to certain loads, the shells buckle at stresses lower than those predicted by classical theory. The reasons for this discrepancy are manifold; such as nonuniform shell thickness, nonuniform loading, inaccurately modelled boundary conditions, influence of prebuckling deformations (nonmembrane prebuckling stress), and deviations

from perfect shell geometry. The item that is most important is the last: geometric imperfections. This buckling behaviour was qualitatively displayed by Babcock²⁷. Figure 2.4 is reproduced from that source, where each influence is displayed for a cylindrical shell under axial compression. Elastic buckling is assumed. The horizontal axis is artificially scaled to reflect the reasonable magnitudes of the "imperfections". This figure demonstrates that geometric imperfections are extremely important.

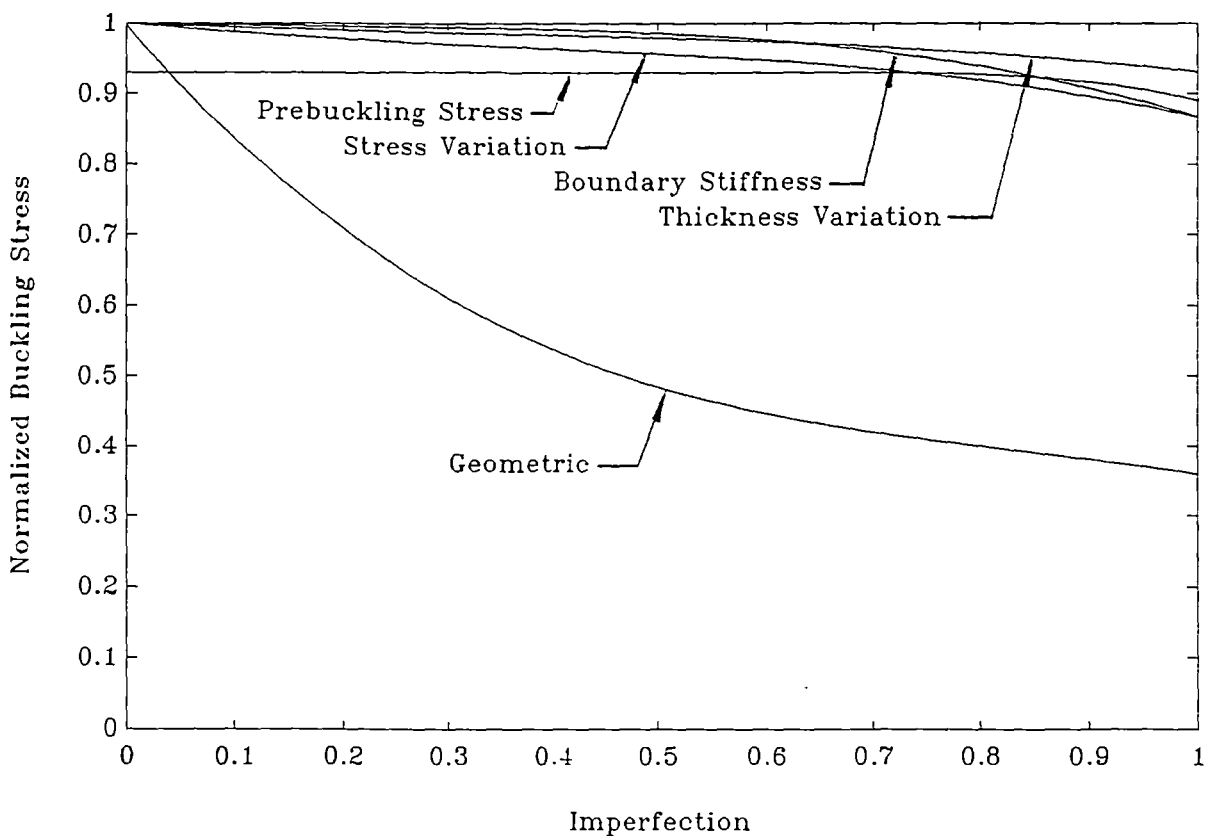


Figure 2.4
Effect of "imperfection" on critical stress
of cylindrical shells under axial compression (Babcock²⁷)

In 1945, Koiter²⁹ developed a general theory of post-buckling behaviour which confirms the conclusions aforementioned, i.e., initial geometric imperfections are responsible for the fact that failure loads are significantly lower than the classical buckling load. Classifying the bifurcation point into three types, stable symmetric, asymmetric and unstable symmetric, Koiter showed that imperfection sensitivity of a shell depends on the type of bifurcation point associated with it (See Figure 2.5, here reproduced from reference 21). The load corresponding to the bifurcation point of the perfect shell is commonly called the classical buckling load and is denoted here by P_{cl} . In each of the three cases, the prebuckling state of the perfect shell is stable for $P < P_{cl}$ and is unstable for $P > P_{cl}$ where it is shown as a dotted curve. Case one illustrates a shell with a stable postbuckling behaviour which can support loads in excess of the classical buckling load P_{cl} in the buckled state. The behaviour of a slightly imperfect version of the same shell is described by the dashed curve. Case two is an example of a shell which goes into a stable or unstable postbuckling behaviour depending on whether the load increases or decreases following bifurcation. An initial imperfection is all that is needed to influence the deflection one way or the other. If an imperfection causes a positive buckling deflection, the load-deflection curve of Case two has a limit load P_s , the buckling load of the imperfect shell, which is less than the bifurcation load of the perfect shell P_{cl} . Case two is an example of asymmetric branching behaviour, while Case three illustrates a shell whose buckling behaviour is symmetric with respect to the

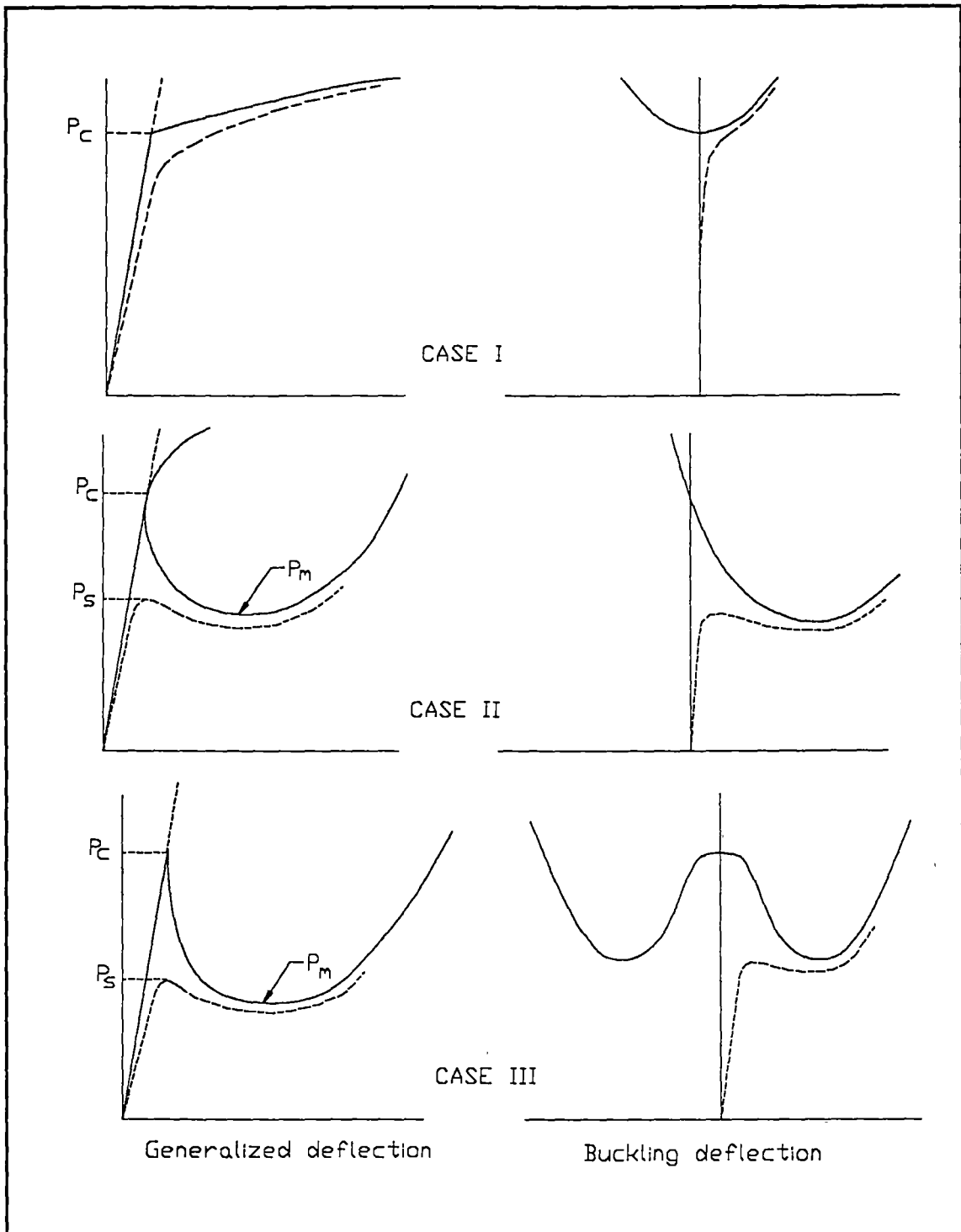


Figure 2.5
Load-deflection curves for single mode bifurcation behaviour

buckling deflection and in which initial postbuckling behaviour is always unstable under prescribed loading conditions.

Based on the work of Koiter and that of Budiansky and Hutchinson²¹⁻²³, the concept of imperfection sensitivity has been developed. In accordance with this theory, one is able to calculate a parameter which is a measure of the steepness of the post-buckling curve. This parameter can then be used to estimate the degree to which initial imperfections reduce the strength of a shell below its classical critical load. In other words, the deeper the post-buckling curve, the greater will be the imperfection sensitivity of the shell and the further below the critical load will be the maximum load that the shell can support. Using an analysis of this type, it can be shown that axially compressed cylindrical shells are highly imperfection sensitive. Even very small initial imperfections can cause these shells to fail at loads well below the critical load given by the linear theory. A quantitative measure of the sensitivity of the shell to axisymmetric geometric imperfections can be calculated.

A particular case of a cylindrical shell under compression was solved completely by Koiter³⁰ in 1963. He showed that small imperfections made in the shape of the classical axisymmetric buckling mode can significantly reduce the buckling load, and presented an analytically derived formula from which the ratio of the practical buckling stress to the theoretical critical stress can be computed when the magnitude of the deviation from

the exact cylindrical shape is known.

Koiter's asymptotic theory was later extended to the case of general random imperfections by Hansen³¹ using a probabilistic approach. Hansen's studies have indicated that on the buckling of axially loaded cylindrical shells, non-axisymmetric and general random imperfections can have a greater degrading effect than axisymmetric imperfections.

Experimental verification of Koiter's predictions on the effect of axisymmetric imperfections was obtained by Tennyson and Muggeridge³², who conducted an extensive testing program on accurately made spun-cast epoxy shells containing various types of axisymmetric imperfections. Their studies indicated that minimum buckling load is obtained when the wavelength of the axisymmetric imperfection is equal to that of the classical axisymmetric buckling mode.

The effect of actual imperfections was first investigated by Arbocz and Babcock³³⁻³⁶. Their theoretical predictions for the buckling load were obtained by representing the actual initial deviations of the shell wall as a Fourier series and were in reasonable agreement with observed test values.

The effect of local imperfections on cylindrical shells was investigated recently by Krishnakumar³⁷ using Foster's space frame analysis³⁸⁻⁴⁴ based on the geometry of the Yoshimura

pattern. The load carrying capacity of cylindrical shells with diamond-shaped defects similar to the facets of a buckled cylinder can be estimated. He also experimentally investigated the effect of changes in the defect size on the collapse load and the influence of more than one defect.

2.4 EFFECT OF PREBUCKLING DEFORMATION AND BOUNDARY CONDITIONS

Several researchers⁴⁵⁻⁵⁴ have investigated the effect of boundary conditions and the prebuckling bending deformation caused by edge restraints. The linear theory of cylindrical shells assumes that only membrane stresses and no bending stresses exist in the shell prior to buckling. In other words, the shell is free to expand laterally along its entire length prior to buckling and will consequently have the same shape. Actually, cylindrical shells are usually prevented from expanding at their ends by the supports and bending stresses do exist prior to buckling. However, it was shown by Stein⁴⁷ in 1962 that the effect of these prebuckling bending stresses is small and that their omission in the classical theory is therefore not a primary reason for the difference between the theoretical predictions and actual collapse loads.

The classical linear theory also assumes zero displacements at the edges, not only in a direction normal to the shell but also in the tangential direction. It has been shown by

Almroth⁵³ that cylinders whose edges are free to move in the tangential direction buckle at a stress one half as large as that given by equation (2.4). Since this edge condition rarely exists in actual shells, initial imperfections and not boundary conditions are believed to be responsible for the discrepancy between classical theory and test results.

2.5 EXPERIMENTS ON NEAR PERFECT SHELLS

Up to now, considerable advances have been made in experimental techniques. It is possible to subject the shell to uniform loading conditions without the problems of misalignment and eccentricity by using sophisticated testing equipment. With advanced manufacturing techniques such as electroplating^{55,56} and spincasting^{6,44,57,58}, geometrically "near-perfect" cylindrical shells could be made.

Prior to 1960, the conclusion that initial imperfections are responsible for the discrepancy between linear theory and actual buckling loads was based primarily on theoretical studies. However, experimental verification of the role that imperfections play has been obtained as well. Tennyson^{6,57,58} in 1963, by careful fabrication procedures, manufactured geometrically "near-perfect" circular cylindrical shells. Using these "near-perfect" circular cylindrical shells and clamped end constraints, he was able to obtain experimental buckling loads equal to $0.9\sigma_{cl}$, thus minimising the effect of initial imperfections. His test results are in close

agreement with the reduced theoretical value taking into account the edge restraints and prebuckling bending deformations and confirmed that the classical theory is valid for perfect cylindrical shells.

CHAPTER 3

BUCKLING

OF

ORTHOTROPIC

AND

ANISOTROPIC

CYLINDRICAL SHELLS

- A REVIEW OF CURRENT

LITERATURE

CHAPTER 3

BUCKLING OF ORTHOTROPIC AND ANISOTROPIC CYLINDRICAL SHELLS

- A REVIEW OF CURRENT LITERATURE

Aerospace structure design, by its very nature, requires the engineer to strive for minimum weight configurations. This in turn has led to the development of a variety of advanced thin-walled structures. These include stiffened thin-walled shell structures which are fabricated from a wide variety of light-weight materials, bonded constructions with honeycomb or foam cores, and laminated composite shells. The material behaviour of these shells can be considered as orthotropic.

Although for isotropic cylindrical shells in the elastic domain, the problem of buckling may now be considered to be solved completely. However, for orthotropic and anisotropic cylindrical shells, due to their complexity, both theoretical and experimental investigations still lag far behind those for isotropic shell structures.

Orthotropic shells have gained widespread usage because of the many unique advantages they offer. In advanced composite materials for instance, primarily because of their high stiffness/weight and strength/weight ratios, considerable weight

savings can be achieved. The designer has the advantage of being able to tailor his material and structure properties to meet specific requirements. It is necessary to develop an adequate background for analysing orthotropic structures that can result from the assembly of these material systems into various structural configurations.

A review of main developments in this field is presented in the following sections.

3.1 CLASSICAL BUCKLING THEORIES - PERFECT CYLINDRICAL SHELLS

In general, classical buckling theories assume linear relationships between stress/strain and strain/displacement. Furthermore, a membrane prebuckled shape is often considered in order to satisfy, either partially or completely, various end boundary conditions, although an "infinite" length shell model can also be employed. There have been many buckling analyses of orthotropic cylindrical shells.

Theoretical buckling analysis of homogeneous orthotropic cylindrical shells was started as early as in 1945 by March⁵⁹ in which torsional buckling of a plywood cylinder was studied. Studies of buckling under combined loading were performed by Thielemann et al.⁶⁰ and Hess⁶¹ at an early stage, in which simply supported boundary conditions were partially

satisfied. An early general buckling analysis of anisotropic cylindrical shells was presented by Cheng and Ho⁶² who derived the buckling characteristic equation for cylinders subjected to combined axial compression, external pressure, and torsion with arbitrary boundary conditions. Their general analysis was later applied to obtain numerical results for buckling under these kinds of loadings: external radial pressure⁶³ combined radial pressure and torsion⁶³, axial compression⁶⁴, combined axial compression and external radial pressure⁶⁴, torsion⁶⁵, combined torsion and axial compression⁶⁵, bending⁶⁵, combined bending and axial compression⁶⁵, combined bending, axial compression, external radial pressure and torsion⁶⁶.

It is worth noting that Cheng and Ho employed Flugge's linear theory which is considered to be more refined than the linear Donnell-type stability theory adopted by many authors such as Tasi⁶⁷, Martin and Drew⁶⁸, although considerable numerical analysis is required to obtain the critical loads. Tasi investigated in more detail the effect of heterogeneous composition on the axial compression buckling load of laminated composite cylinders, compared his results with data obtained for the same problem using Cheng and Ho's theory and found negligible difference. In Martin and Drew's analysis, a set of Donnell-type linear stability equations was used for the case of radial pressure. A comparison was made with Cheng and Ho's analysis. The difference between the two theories was negligible for the configurations considered. Another interesting comparison with Cheng and Ho's theory has been made

by Chao⁶⁹ using Timoshenko's buckling equilibrium equations. Combined loading of external pressure and torsion with different boundary conditions were considered. Similar agreement was also found. A modified form of Cheng and Ho's analysis was presented by Lei and Cheng⁶⁴ who investigated the buckling of orthotropic laminated shells including the effects of simply supported and clamped boundary conditions corresponding to the membrane prebuckled state. Buckling results were then obtained for various combinations of boundary conditions and varying length-to-radius ratios. Axial compression, radial pressure and combined loading were considered.

Other investigations of buckling of anisotropic cylindrical shells have also been published. Holston⁷⁰ studied the effect of the length-to-radius ratio on the axial compressive buckling load. By neglecting coupling between shearing and extensional strain, he showed that there are no significant effects on the buckling load for ratio values greater than 1.5. In buckling due to bending, Ugural and Cheng⁷¹ found that coupling between in-plane stretching and bending had an important effect on the buckling loads, while in Holston's analysis⁶⁶, which was based on Cheng and Ho's work, it was shown that the pure bending buckling stress was essentially equal to the uniform compression value. An interesting study was done by Pagano et al.⁷². They showed both theoretically and experimentally that buckling was possible in anisotropic cylinders subjected to axial tension. This seemingly

strange phenomenon is really a shear-type buckle due to the induced torque arising from the presence of end constraints.

For buckling of orthotropic cylindrical shells, two types of basic equations, corresponding either to Flugge-type or Donnell-type linear equations for isotropic shells, have been formulated in the literature. In either case, a resulting single eighth-order differential equation may be deduced. A common difficulty with these eighth-order equations in isotropic or orthotropic shell theory is that their general solutions remain unknown because of the algebraic complexities involved. However, the eighth-order equation for orthotropic shells is more complicated than the corresponding one for isotropic shells. Recently, Cheng and He⁷³ have proposed a pair of complex conjugate fourth-order partial differential equations that govern the deformation of orthotropic circular cylindrical shells. Subsequently, Xiao and Cheng⁷⁴ applied these equations to orthotropic cylinders loaded in local external pressure. This pair of equations is deduced from a set of basic equations that is based on the Kirchhoff hypothesis, that is:

- (a) The transverse normal stress is negligibly small, and
- (b) Sections normal to the middle surface of the shell remain normal to the middle surface and undergo no change in length during deformation.

The pair of equations is as accurate as equations can be within the scope of the Kirchhoff assumptions. From the pair of equations, a number of simplified fourth-order governing equations

can be systematically and explicitly deduced. These fourth-order equations for orthotropic cylindrical shells are of practical importance because they can be easily solved in closed forms and yet retain practically the same accuracy as the original eighth-order equation. Using these fourth-order equations, a particular problem of loss of stability of cylindrical shells due to pressure applied on part of their surfaces has been solved by Xiao and Cheng⁷⁴. The critical loads of orthotropic shells under this particular configuration were compared with those calculated from the corresponding equations given by Flugge⁵. Results show that the difference between the two equations is negligibly small.

3.2 LIMITATIONS IN THE CLASSICAL BUCKLING THEORIES

All of the theoretical works mentioned so far considered classical buckling theories undergoing small deflections in which several limitations were involved. Firstly, a linear stress and strain relation was used in basic equations. Secondly, membrane prebuckled shape is assumed, i.e., the effect of boundary conditions on the prebuckling stress state is ignored. Thirdly, the difference between the elastic moduli in tension and compression is ignored. Lastly, a geometrically "perfect" shell is always applied in classical buckling theories.

As far as the linear stress/strain relations are concerned, it is well known that for many composite materials, linearity may not exist for all types of stress and strain. Material

property tests on 'Scotchply' Type 1002 preimpregnated epoxy/glass were performed by Tennyson⁷⁵. His results show that although the axial tension and compression data in the main exhibit linearity, the shear behaviour is quite nonlinear. Hence some difficulty could arise in comparing torsional buckling loads with predicted values based on a constant shear modulus, although the initial load curve can be approximated reasonably well by a linear relation.

In the multitude of classical theories, prebuckling deformations caused by different boundary conditions are not included in the analysis, although buckling loads are affected by prebuckling deformations. However, for certain boundary conditions, such as the clamped case, the load reduction associated with the prebuckling displacements may only amount to 5%-10%.

One assumption generally made is that of a constant elastic modulus to describe both tension and compression. Jones⁷⁶ has shown that variations in these material coefficients can cause significant differences in buckling loads, at least for the case he considered.

However, similar to the behaviour of isotropic cylindrical shells, geometric imperfections play a major role in reducing the buckling loads of orthotropic cylindrical shells. A discussion of this is presented in the next section.

3.3 BUCKLING OF GEOMETRICALLY IMPERFECT ORTHOTROPIC CYLINDRICAL SHELLS

The effect of geometric shape imperfections on the buckling strength of isotropic cylindrical shells has been well known for some time. However, by comparison, relatively few studies have been done to investigate shape imperfection effects on the stability of orthotropic shells.

A theoretical analysis has been published by Khot⁷⁷⁻⁷⁹ based on the anisotropic shell theory for axial compression. A Donnell-type of analysis including nonlinear strain/displacement relations was employed using an initial shape imperfection having the form of the assumed buckling mode. The total potential energy was minimized to yield the buckling loads. Load/deflection curves were then obtained as a function of the imperfection amplitude. Khot's results indicated that any orthotropic cylindrical shell is less imperfection sensitive than an isotropic one. Experimental data on orthotropic cylindrical shells, which is presented in the next section, supported Khot's prediction.

Koiter's imperfection shell theory was first applied to anisotropic cylindrical shells by Card⁸⁰ in 1969. In his analysis, Koiter's theory was employed to examine the imperfection sensitivity of laminated orthotropic cylindrical shells based on a perturbation technique applied to a 'perfect' shell at the inception of instability. Furthermore, the prebuckling deformations

associated with simple and clamped boundary conditions were considered. Experimental data for filament-wound and glass-epoxy cylindrical shells under axial compression were carried out and compared with perfect shell prediction. The variation was 63% to 91%. Calculations of the imperfection sensitivity were made for qualitative comparison with the experiments, but since no measurements of actual imperfection distributions were done, a quantitative buckling loads comparison was not possible.

Also by using Koiter's theory, Tennyson et al.⁸¹ performed an axisymmetric imperfection analysis to determine the effect of imperfect amplitudes on the axial compression buckling load of anisotropic circular cylindrical shells as a function of fibre orientation. The effect of boundary conditions was neglected. Numerical results were presented only on orthotropic three-ply, glass-epoxy composite cylindrical shells. They indicated that the axisymmetric shape imperfection has a dominant effect on the axial compression buckling load of orthotropic composite cylindrical shells. For a perfect composite cylindrical shell, axial buckling load can be increased by changing the fibre orientation, but it will be accompanied by a corresponding increase in imperfection sensitivity. So from a design point of view, it was suggested that there is no significant advantage in selecting optimum fibre orientations that would give maximum buckling load for a perfect shell if there is some inherent axisymmetric shape imperfection introduced in the manufacture process. Subsequently, axial compression buckling tests were performed by Tennyson and

Muggeridge⁸² on three-ply, glass/epoxy cylindrical shells. Experimental results were compared with predicted values which was based on the analysis of Reference 81, and a good agreement was found.

Investigation of the effect of local shape defects on the buckling of orthotropic cylindrical shells was just started by Muir⁸³. He tested three sets of 4-ply carbon-fibre epoxy composite cylindrical shells in axial compression for lamina orientations of 30, 45 and 60 degrees. Diamond-shaped defects were imposed on the shell wall. However, because only a few shells were tested, no clear conclusions have arrived.

3.4 EXPERIMENTAL DATA ON ORTHOTROPIC CYLINDRICAL SHELLS

Preliminary experimental data on orthotropic plywood cylindrical shells under axial compression was published in 1943 by Norris and Kuenzi⁸⁴. Card and Peterson⁸⁵ and Card⁸⁶ reported on the results of 51 tests of filament-wound glass/epoxy circular cylindrical shells under axial compression. The experimental buckling loads averaged approximately 85% of analytical predictions based on a Donnell-type orthotropic analysis. Tasi et al.⁸⁷ have also investigated the buckling behaviour of filament-wound glass/epoxy cylindrical shells under axial compression and compared their test data with solutions obtained by using Cheng

and Ho's linear theory. Their experimental buckling loads were found to range from 66% to 85% of analytical predictions.

Buckling under external pressure of orthotropic fiberglass cylindrical shells has been studied by Schneider and Hofeditz⁸⁸. Test data on 53 glass fibre orthotropic cylindrical shells were reported and compared with theoretical buckling pressure. All of the experimental buckling external pressures were found to be more than 85% of theoretical predictions.

Torsional buckling of orthotropic filament-wound glass-epoxy cylinders was studied by Wall and Card⁸⁹ who compared their test data with the theoretical analysis by Chao⁶⁹. About 67% of the theoretical predictions were found in their experimental buckling results. Tennyson⁷⁵ has also conducted experiments on the torsional buckling of preimpregnated type wound glass-epoxy cylindrical shells. Experimental torsional loads were compared with the theoretical predictions which were based on the linear Donnell-type equations. A very good agreement was obtained; all of the experimental values were more than 80% of the theoretical predictions with an average of 90%.

For buckling under combined loading, an extensive study of filament-wound glass-epoxy cylindrical shells was undertaken by Hoston et al.⁹⁰ for various loading modes, including axial compression, torsion, bending, combined torsion and axial compression, and combined bending and axial compression. Using

linear buckling theory based on the work by Cheng and Ho, axial compression values were found to be 67%-90% of the theoretical predictions while bending critical loads were essentially equal to the axial compression values.

It should be pointed out that the experimental buckling results on orthotropic cylindrical shells mentioned above agrees with Khot's prediction, that is, any orthotropic cylindrical shell is less imperfection sensitive than an isotropic one.

CHAPTER 4

**THEORETICAL BUCKLING
ANALYSIS**

OF

**ORTHOTROPIC AND
CELLULAR-WALLED
CIRCULAR CYLINDRICAL
SHELLS**

CHAPTER 4

THEORETICAL BUCKLING ANALYSIS OF ORTHOTROPIC AND CELLULAR-WALLED CIRCULAR CYLINDRICAL SHELLS

As described in the last chapter, there have been many buckling analyses of orthotropic shells. Among them, Cheng and Ho's⁶³ theory was represented as a general theory of buckling of heterogeneous anisotropic cylinders under combined loading with arbitrary boundary conditions. Although it is based on a very accurate Flugge-type shell theory which is considered to be more refined than the linear Donnell-type stability theory, their analysis is rather lengthy; considerable numerical analysis is required to obtain the critical load.

The intention of this chapter is to develop simple formulae for buckling critical loads of orthotropic circular cylindrical shells under combined loading of axial compression and external pressure, so they can be used practically. This analysis is based on a Flugge-type linear shell theory. A simply supported boundary condition SS3: $w=0$, $M_\alpha=0$, $N_\alpha=0$, $v=0$ is considered. In practice, a clamped or built-in boundary is most commonly used which is represented by the following conditions: FF3: $w=0$, $w'_\alpha=0$, $N_\alpha=0$, $v=0$. As mentioned previously, boundary conditions have little effect on buckling loads compared to other factors such as shape imperfections. Some numerical results have shown⁶⁴ that

in moderately long cylindrical shells there is almost no difference in buckling loads between these two boundary conditions. Thus, the solution for buckling loads presented in this report has a practical significance.

First, a general orthotropic cylindrical shell was considered. Based on Flugge's linear theory for isotropic cylindrical shells, a general buckling solution under combined axial compression and external pressure was derived in this chapter. For moderate-length orthotropic cylindrical shells loaded in either external pressure or axial compression, buckling loads are formulated in a simple form.

Subsequently, the buckling criterion for a cellular-walled circular cylindrical shell under combined loading was developed. The cellular wall was modified to approximate a uniform orthotropic form. The modified wall was then treated as pseudo-orthotropic.

4.1 BUCKLING CRITERION OF AN ORTHOTROPIC CIRCULAR CYLINDRICAL SHELL UNDER COMBINED LOADING OF AXIAL COMPRESSION AND EXTERNAL PRESSURE

4.1.1 BASIC EQUATIONS

Consider an orthotropic cylindrical shell under combined loading of axial compression P and external pressure p .

Let R be the radius of the midsurface of the shell; x, y, z the axial, circumferential, and radial coordinates; and α, β, γ the dimensionless coordinates of x, y and z ($\alpha = x/R, \beta = y/R, \gamma = z/R$). The three displacement components u_α, u_β and u_γ of an arbitrary point of the shell can be expressed in terms of midsurface displacements u, v and w as follows⁵ :

$$\begin{aligned} u_\alpha &= u - \gamma \omega_\alpha, \\ u_\beta &= v - \gamma \omega_\beta, \\ u_\gamma &= w \end{aligned} \tag{4.1}$$

where

$$\begin{aligned} \omega_\alpha &= \frac{\partial w}{\partial \alpha}, \\ \omega_\beta &= \left(\frac{\partial w}{\partial \beta} - v \right), \end{aligned}$$

Now, let σ_α and σ_β be the normal stresses along α, β respectively; $\tau_{\alpha\beta}$ be the shear stress in the α, β plane; ε_α and ε_β be the normal strains and $\gamma_{\alpha\beta}$ be the shear strain. The stress-strain relations for orthotropic materials^{91,92} are

$$\begin{aligned} \sigma_\alpha &= \frac{E_1}{1 - \mu_1 \mu_2} (\varepsilon_\alpha + \mu_1 \varepsilon_\beta), \\ \sigma_\beta &= \frac{E_2}{1 - \mu_1 \mu_2} (\mu_2 \varepsilon_\alpha + \varepsilon_\beta), \end{aligned} \tag{4.2}$$

$$\tau_{\alpha\beta} = G_{12} \gamma_{\alpha\beta}$$

where E_1, E_2 are the moduli of elasticity along the principal directions α and β , respectively; G_{12} is the shear modulus that

characterizes the change of angles between principal directions α and β ; $\mu_1 = \mu_{\beta\alpha}$ is the Poisson's ratio that characterizes the decrease in α direction due to tension applied in β direction, and $\mu_2 = \mu_{\alpha\beta}$ is the Poisson's ratio that characterizes the decrease in β direction due to tension applied in the α direction. Among these material constants there exists a relation⁹¹:

$$E_1\mu_1 = E_2\mu_2 \quad (4.3)$$

The components of strain at any arbitrary point of the shell are related to the midsurface displacements by⁵

$$\begin{aligned} \varepsilon_\alpha &= \frac{1}{R} \left(\frac{\partial u}{\partial \alpha} - \gamma \frac{\partial^2 w}{\partial \alpha^2} \right), \\ \varepsilon_\beta &= \frac{1}{R} \left(\frac{\partial v}{\partial \beta} + w \right) - \frac{\gamma}{R(1+\gamma)} \left(\frac{\partial^2 w}{\partial \beta^2} + w \right), \\ \varepsilon_{\alpha\beta} &= \frac{1}{R(1+\gamma)} \left[\frac{\partial u}{\partial \beta} + \frac{\partial v}{\partial \alpha} + 2\gamma \left(\frac{\partial v}{\partial \alpha} - \frac{\partial^2 w}{\partial \alpha \partial \beta} \right) \right. \\ &\quad \left. + \gamma^2 \left(\frac{\partial v}{\partial \alpha} - \frac{\partial^2 w}{\partial \alpha \partial \beta} \right) \right] \end{aligned} \quad (4.4)$$

The bending (η_α, η_β) and twisting strains ($\eta_{\alpha\beta}$) are

$$\begin{aligned} \eta_\alpha &= -\frac{1}{R^2} \frac{\partial^2 w}{\partial \alpha^2}, \\ \eta_\beta &= -\frac{1}{R^2} \left(\frac{\partial^2 w}{\partial \beta^2} + w \right), \\ \eta_{\alpha\beta} &= -\frac{1}{2R^2} \left(\frac{\partial u}{\partial \beta} - \frac{\partial v}{\partial \alpha} + 2 \frac{\partial^2 w}{\partial \alpha \partial \beta} \right) \end{aligned} \quad (4.5)$$

Let t be the wall thickness; K_1, K_2 the extensional stiffnesses and D_1

and D_2 the bending stiffnesses along the principal directions α and β respectively,

$$\begin{aligned} K_1 &= \frac{E_1 t}{1 - \mu_1 \mu_2}, & K_2 &= \frac{E_2 t}{1 - \mu_1 \mu_2}, \\ D_1 &= \frac{E_1 t^3}{12(1 - \mu_1 \mu_2)}, & D_2 &= \frac{E_2 t^3}{12(1 - \mu_1 \mu_2)}, \end{aligned} \quad (4.6)$$

and we let

$$k = \frac{E_2}{E_1}, \quad k_1 = \frac{G_{12}(1 - \mu_1 \mu_2)}{E_1}, \quad (4.7)$$

Let N_α and N_β be the normal stress resultants, S_α and S_β the shear stress resultants, M_α and M_β the bending moments, $M_{\alpha\beta}$ and $M_{\beta\alpha}$ the twisting moments, and Q_α and Q_β the transverse stress resultants. Under the combined loading of axial compression P and external pressure p , the equations of static equilibrium are (see figure 4.1):

$$\begin{aligned} \frac{\partial N_\alpha}{\partial \alpha} + \frac{\partial S_\beta}{\partial \beta} - p \left(\frac{\partial^2 u}{\partial \beta^2} - \frac{\partial w}{\partial \alpha} \right) - \frac{P}{R} \frac{\partial^2 u}{\partial \alpha^2} &= 0, \\ \frac{\partial N_\beta}{\partial \beta} + \frac{\partial S_\alpha}{\partial \alpha} + Q_\beta - p \left(\frac{\partial^2 v}{\partial \beta^2} - \frac{\partial w}{\partial \beta} \right) - \frac{P}{R} \frac{\partial^2 v}{\partial \alpha^2} &= 0, \\ N_\beta - \frac{\partial Q_\alpha}{\partial \alpha} - \frac{\partial Q_\beta}{\partial \beta} + p \left(\frac{\partial u}{\partial \alpha} - \frac{\partial v}{\partial \beta} + \frac{\partial^2 w}{\partial \beta^2} \right) + \frac{P}{R} \frac{\partial^2 w}{\partial \alpha^2} &= 0, \quad (4.8) \\ \frac{\partial M_{\alpha\beta}}{\partial \alpha} - \frac{\partial M_\beta}{\partial \beta} - R Q_\beta &= 0 \\ \frac{\partial M_{\beta\alpha}}{\partial \beta} - \frac{\partial M_\alpha}{\partial \alpha} - R Q_\alpha &= 0 \end{aligned}$$

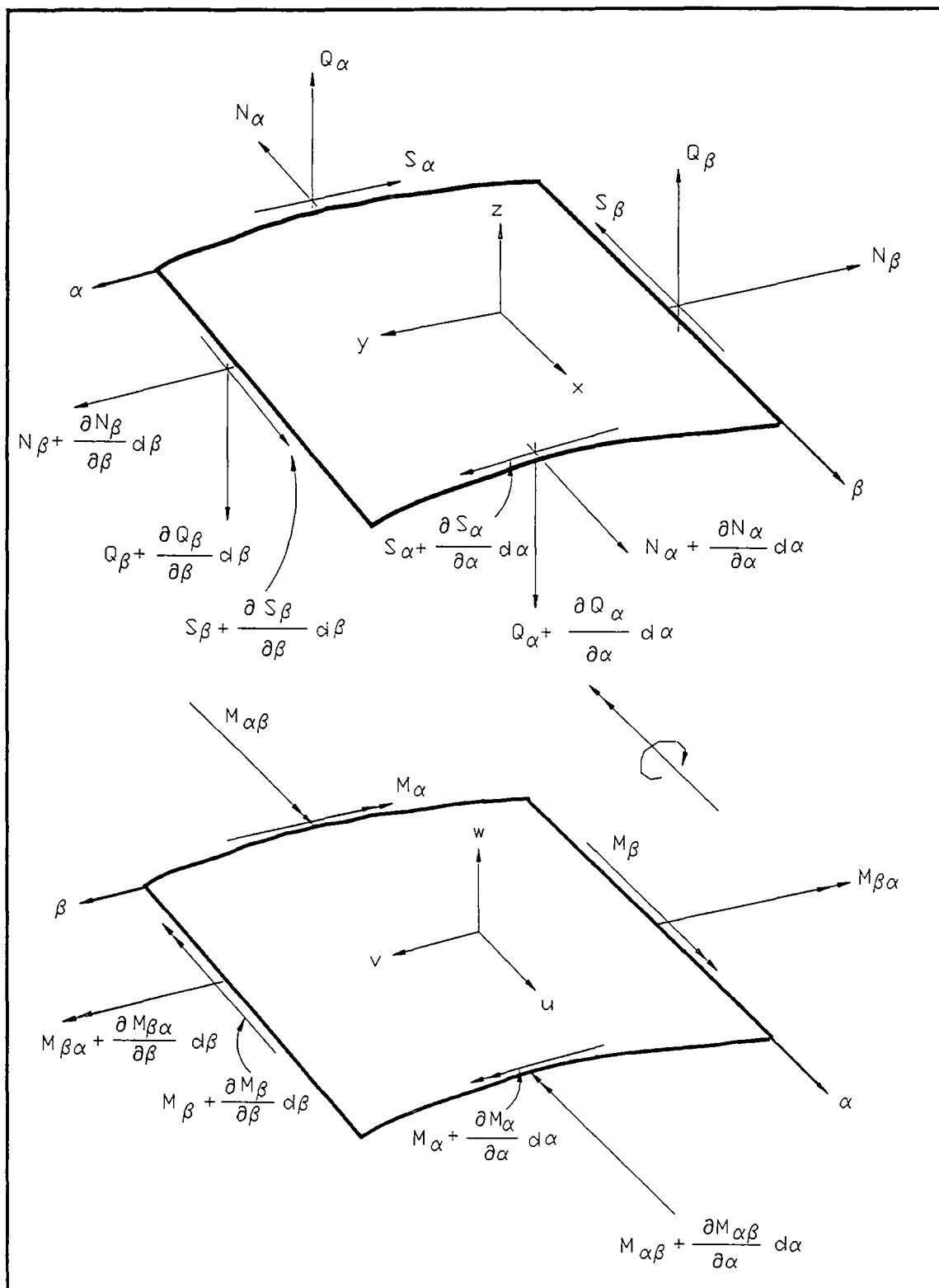


Figure 4.1 Shell element

In the equations (4.8), these stress resultants (N,S,Q) and couples (M) per unit length of the midsurface are related to the midsurface displacements through the stress-strain relations as:

$$\begin{aligned}
 [N_\alpha, S_\alpha, M_\alpha, M_{\alpha\beta}] &= \int_{-t/2}^{t/2} ([\sigma_\alpha, \tau_{\alpha\beta}, z\sigma_\alpha, z\tau_{\alpha\beta}]) [1 + z/R] dz \\
 [N_\beta, S_\beta, M_\beta, M_{\beta\alpha}] &= \int_{-t/2}^{t/2} ([\sigma_\beta, \tau_{\beta\alpha}, z\sigma_\beta, z\tau_{\beta\alpha}]) dz \\
 [Q_\alpha, Q_\beta] &= \int_{-t/2}^{t/2} ([\tau_{\alpha z}, \tau_{\beta z}]) dz
 \end{aligned} \tag{4.9}$$

which resulted in

$$\begin{aligned}
 N_\alpha &= \frac{K_1}{R} \left[\frac{\partial u}{\partial \alpha} + \mu_1 \left(\frac{\partial v}{\partial \beta} + w \right) - c^2 \frac{\partial^2 w}{\partial \alpha^2} \right] \\
 N_\beta &= \frac{K_2}{R} \left[\frac{\partial v}{\partial \beta} + \mu_2 \frac{\partial u}{\partial \alpha} + w + c^2 \left(\frac{\partial^2 w}{\partial \beta^2} + w \right) (1 + \delta) \right] \\
 S_\alpha &= \frac{G_{12}t}{R} \left[\frac{\partial u}{\partial \beta} + \frac{\partial v}{\partial \alpha} - c^2 \left(\frac{\partial^2 w}{\partial \alpha \partial \beta} - \frac{\partial v}{\partial \alpha} \right) \right] \\
 S_\beta &= \frac{G_{12}t}{R} \left[\frac{\partial u}{\partial \beta} + \frac{\partial v}{\partial \alpha} + c^2 \left(\frac{\partial^2 w}{\partial \alpha \partial \beta} + \frac{\partial u}{\partial \beta} \right) (1 + \delta) \right] \\
 M_\alpha &= - \frac{D_1}{R^2} \left[\frac{\partial u}{\partial \alpha} + \mu_1 \frac{\partial v}{\partial \beta} - \left(\frac{\partial^2 w}{\partial \alpha^2} + \mu_1 \frac{\partial^2 w}{\partial \beta^2} \right) \right] \\
 M_\beta &= \frac{D_2}{R^2} \left[\left(\frac{\partial^2 w}{\partial \beta^2} + w \right) (1 + \delta) + \mu_2 \frac{\partial^2 w}{\partial \alpha^2} \right] \\
 M_{\alpha\beta} &= \frac{G_{12}t^3}{6R^2} \left[\frac{\partial v}{\partial \alpha} - \frac{\partial^2 w}{\partial \alpha \partial \beta} \right]
 \end{aligned} \tag{4.10}$$

$$M_{\beta\alpha} = \frac{G_{12}t^3}{12R^2} \left[\frac{\partial u}{\partial \beta} - \frac{\partial v}{\partial \alpha} + 2\frac{\partial^2 w}{\partial \alpha \partial \beta} + \delta \left(\frac{\partial u}{\partial \beta} + \frac{\partial^2 w}{\partial \alpha \partial \beta} \right) \right]$$

$$Q_{\alpha} = \frac{D_1}{R^3} \left[\frac{\partial^2 u}{\partial \alpha^2} - k_1(1+\delta) \frac{\partial^2 u}{\partial \beta^2} + (k_1 + \mu_1) \frac{\partial^2 v}{\partial \alpha \partial \beta} - \frac{\partial^3 w}{\partial \alpha^3} - (2k_1 + \mu_1 + \delta k_1) \frac{\partial^3 w}{\partial \alpha \partial \beta^2} \right]$$

$$Q_{\beta} = \frac{D_2}{R^3} \left[2\frac{k_1}{k} \frac{\partial^2 v}{\partial \alpha^2} - (1+\delta) \left(\frac{\partial^3 w}{\partial \beta^3} + \frac{\partial w}{\partial \beta} \right) - \left(2\frac{k_1}{k} + \mu_2 \right) \frac{\partial^3 w}{\partial \alpha^2 \partial \beta} \right]$$

in which $c^2 = \frac{t^2}{12R^2}$, and

$$\begin{aligned} \delta &= \frac{(\tanh^{-1}\sqrt{3}c - \sqrt{3}c)}{\sqrt{3}.c^3} - 1 \\ &= 9c^2 \left[\frac{1}{5} + \frac{1}{7}(\sqrt{3}c)^2 + \frac{1}{9}(\sqrt{3}c)^4 + \dots \right] \end{aligned}$$

4.1.2 BUCKLING UNDER COMBINED LOADING

Substituting these stress resultants (N,S,Q) and couples (M) in equation (4.10) into the equation of static equilibrium (4.8), a system of three differential equations is obtained for the three basic displacement functions (u,v,w)

$$\begin{aligned} &[(1-q_2) \frac{\partial^2}{\partial \alpha^2} + \{k_1[1+c^2(1+\delta)] - q_1\} \frac{\partial^2}{\partial \beta^2}]u + (k_1 + \mu_1) \frac{\partial^2}{\partial \alpha \partial \beta} v \\ &+ \{(\mu_1 + q_1) \frac{\partial}{\partial \alpha} - c^2[\frac{\partial^3}{\partial \alpha^3} - k_1(1+\delta) \frac{\partial^3}{\partial \alpha \partial \beta^2}]\} w = 0, \end{aligned}$$

$$\begin{aligned} &[(k_1 + \mu_1) \frac{\partial^2}{\partial \alpha \partial \beta}]u + \{(k - q_1) \frac{\partial^2}{\partial \beta^2} + [k_1(1+3c^2) - q_2] \frac{\partial^2}{\partial \alpha^2}\} v \\ &+ [(k - q_1) \frac{\partial}{\partial \beta} - c^2(3k_1 + \mu_1) \frac{\partial^3}{\partial \alpha^2 \partial \beta}] w = 0, \end{aligned} \quad (4.11)$$

$$\begin{aligned}
& (\mu_1 + q_1) \frac{\partial}{\partial \alpha} - c^2 \left[\frac{\partial^3}{\partial \alpha^3} - k_1 (1 + \delta) \frac{\partial^3}{\partial \alpha \partial \beta^2} \right] u + \left[(k - q_1) \frac{\partial}{\partial \beta} - c^2 (3k_1 + \mu_1) \frac{\partial^3}{\partial \alpha^2 \partial \beta} \right] v \\
& + \left\{ k + q_1 \frac{\partial^2}{\partial \beta^2} + q_2 \frac{\partial^2}{\partial \alpha^2} + c^2 \left[\frac{\partial^4}{\partial \alpha^4} + (4k_1 + 2\mu_1 + \delta k_1) \frac{\partial^4}{\partial \alpha^2 \partial \beta^2} \right. \right. \\
& \left. \left. + k(1 + \delta) \left(\frac{\partial^2}{\partial \beta^2} + 1 \right)^2 \right] \right\} w = 0
\end{aligned}$$

in which q_1 and q_2 are dimensionless loads,

$$q_1 = \frac{pR}{K_1}, \quad q_2 = \frac{P}{K_1}, \quad (4.12)$$

It may be observed that these load parameters are small quantities. We introduce a solution for equation (4.11) of the form:

$$\begin{aligned}
u &= A \cos(\lambda \alpha) \cos(m \beta) \\
v &= B \sin(\lambda \alpha) \sin(m \beta) \\
w &= C \sin(\lambda \alpha) \cos(m \beta)
\end{aligned} \quad (4.13)$$

where

$$\lambda = \frac{n\pi R}{L},$$

and n is an integer. The solution describes a buckling mode with n half-waves along the length of the cylinder and with $2m$ half-waves around its circumference. We assume the edges of the cylinder to be at $\alpha = 0$ and $\alpha = L/R$. We can see that at the ends $v = w = 0$ and from the stress resultants that $N_\alpha = 0$, $M_\alpha = 0$. Thus, the solution represents the buckling of a shell whose edges are supported in

tangential and radial directions but are neither restricted in the axial direction nor clamped. (This has been classified as one of the simply-supported boundary conditions, namely SS3, by Lei & Cheng²).

When the solution (4.13) was introduced into the differential equations (4.11), the trigonometric functions drop out entirely and we are left with the following equations:

$$\begin{aligned}
& A [-\lambda^2(1-q_2) - m^2\{k_1[1+c^2(1+\delta)] - q_1\}] + B [\lambda m(k_1+\mu_1)] \\
& \quad + C [\lambda(\mu_1+q_1) - c^2\{-\lambda^3 + k_1(1+\delta)\lambda m^2\}] = 0, \\
& A [\lambda m(k_1+\mu_1)] + B [-m^2(k-q_1) - \lambda^2\{k_1(1+3c^2) - q_2\}] \\
& \quad + C [-m(k-q_1) - c^2(3k_1+\mu_1)m\lambda^2] = 0, \tag{4.14} \\
& A [\lambda(\mu_1+q_1) + c^2\{\lambda^3 - k_1(1+\delta)\lambda m^2\}] + B [-m(k-q_1) \\
& \quad - c^2(3k_1+\mu_1)m\lambda^2] + C [-k+q_1m^2+q_2\lambda^2 \\
& \quad - c^2\{\lambda^4 + (4k_1+2\mu_1+\delta k_1)m^2\lambda^2 + k(1+\delta)(m^2-1)^2\}] = 0
\end{aligned}$$

These are three linear equations with the buckling amplitudes A,B,C as unknowns and with the brackets as coefficients. These equations admit in general, since they are homogeneous, only the solution $A = B = C = 0$, indicating that the shell is not in neutral equilibrium. Only if the determinant of the nine coefficients equals zero is a nonvanishing solution A,B,C possible. Thus the vanishing of this determinant is the buckling condition of the shell. The coefficients of the above equations are linear functions of c^2 , q_1 and q_2 . The expanded determinant is,

therefore, a polynomial of the third degree in these parameters. Since they are very small quantities, it is sufficient to keep only the linear terms and to write the buckling condition as:

$$c_1 + c_2 \cdot c^2 = c_3 \cdot q_1 + c_4 \cdot q_2 \quad (4.15)$$

The coefficients $c_1 \dots c_4$ of equation (4.15) may be found by expanding the determinant of equation (4.14):

$$c_1 = (k - \mu_1^2) k_1 \lambda^4$$

$$\begin{aligned} c_2 = & \lambda^8 k_1 - \lambda^6 m^2 (\mu_1^2 - k - 4k_1^2) \\ & - 2 \lambda^4 m^4 (4k_1 \mu_1^2 + 4k_1^2 \mu_1 - 3kk_1 + \mu_1^3 - k\mu_1) \\ & - \lambda^2 m^6 k (\mu_1^2 - k - 4k_1^2) + m^8 k^2 k_1 - 2 \lambda^2 m^4 k (k - \mu_1^2 + 4k_1^2 - k_1 \mu_1) \\ & - 2 \lambda^4 m^2 (3kk_1 + k\mu_1 - 4k_1 \mu_1^2 - \mu_1^3 - 4k_1^2 \mu_1) \\ & - \lambda^2 m^2 k (\mu_1^2 - k - 4k_1^2 + 2k_1 \mu_1) - 2 \lambda^6 k_1 \mu_1 \\ & - 2m^6 k^2 k_1 - \lambda^4 k_1 (3 \mu_1^2 - 4k) + m^4 k^2 k_1 \end{aligned} \quad (4.16)$$

$$\begin{aligned} c_3 = & \lambda^2 m^4 (k - 2k_1 \mu_1 - \mu_1^2) + m^6 k k_1 + \lambda^2 m^2 (2k_1 \mu_1 + \mu_1^2 - k k_1 - k) \\ & - m^4 k k_1 + \lambda^4 m^2 k_1 + 2k_1 \mu_1 \lambda^4 \end{aligned}$$

$$\begin{aligned} c_4 = & \lambda^6 k_1 + \lambda^4 m^2 (k - 2k_1 \mu_1 - \mu_1^2) + \lambda^2 m^4 k k_1 \\ & + \lambda^2 m^2 k k_1 + \lambda^4 (k + k k_1 - \mu_1^2) \end{aligned}$$

Since c_1 turns out to be proportional to λ^4 , we may drop the term with λ^4 in all other coefficients. By using the relation $E_1 \mu_1 = E_2 \mu_2$, and an approximate relation⁹³

$$G_{12} = \frac{\sqrt{E_1 E_2}}{2(1 + \sqrt{\mu_1 \mu_2})} \quad (4.17)$$

in which $\sqrt{E_1 E_2}$ and $\sqrt{\mu_1 \mu_2}$ are geometric mean values for the Young's modulus E and Poisson's ratio μ , respectively, it may be shown that

$$\begin{aligned} (2k_1 + \mu_1)^2 &= 4k_1^2 + \mu_1^2 + 4k_1\mu_1 \\ &= 4 \frac{G^2(1 - \mu_1\mu_2)^2}{E_1^2} + \mu_1^2 + 4 \frac{G(1 - \mu_1\mu_2)}{E_1} \mu_1 \\ &= k(1 - \sqrt{\mu_1\mu_2})^2 + \mu_1^2 + \sqrt{k} 2\mu_1(1 - \sqrt{\mu_1\mu_2}) \\ &= [\sqrt{k}(1 - \sqrt{\mu_1\mu_2}) + \mu_1]^2 \\ &= k \end{aligned} \quad (4.18)$$

and

$$\frac{k - \mu_1^2}{k_1} = 4(k_1 + \mu_1) \quad (4.19)$$

By substituting the above equations (4.18) and (4.19) into equation (4.16), the four coefficients can be further simplified as:

$$c_1 = (k - \mu_1^2) k_1 \lambda^4$$

$$\begin{aligned} c_2 &= k_1(\lambda^2 + \sqrt{k}m^2)^4 - 2\lambda^6 k_1 \mu_1 - 6k k_1 \lambda^4 m^2 \\ &\quad - 2\lambda^2 m^4 k k_1 (4\sqrt{k} - \mu_1) - 2m^6 k^2 k_1 \\ &\quad + 2\lambda^2 m^2 k k_1 (2\sqrt{k} - \mu_1) + m^4 k^2 k_1 \end{aligned} \quad (4.20)$$

$$c_3 = k_1 m^2 (\lambda^2 + \sqrt{k} m^2)^2 - k_1 (2\sqrt{k} + k) \lambda^2 m^2 - m^4 k k_1$$

$$c_4 = \lambda^2 k_1 (\lambda^2 + \sqrt{k} m^2)^2 + \lambda^2 m^2 k k_1$$

These co-efficients are still relatively complicated. Under combined loading of axial compression and external pressure, the buckling condition, equation (4.15), not only depends on material properties (E_1 , E_2 , μ_1 , μ_2 , G_{12}) but also on the buckling mode (m,n) , i.e., number of waves along axial and circumferential directions.

4.1.3 BUCKLING UNDER EXTERNAL PRESSURE ONLY

Now, if an orthotropic cylindrical shell was loaded under external pressure alone, i.e. when $q_2=0$. Then the equation (4.15) yields

$$q_1 = \frac{c_1}{c_3} + \frac{c_2}{c_3} c^2 \quad (4.21)$$

where

$$\begin{aligned} \frac{c_1}{c_3} &= (k - \mu_1^2) k_1 \lambda^4 / \{ k_1 m^2 (\lambda^2 + \sqrt{k} m^2)^2 \\ &\quad - k_1 (2\sqrt{k} + k) \lambda^2 m^2 - m^4 k k_1 \} \\ \frac{c_2}{c_3} &= \{ k_1 (\lambda^2 + \sqrt{k} m^2)^4 - 2 \lambda^6 k_1 \mu_1 - 6 k k_1 \lambda^4 m^2 \\ &\quad - 2 \lambda^2 m^4 k k_1 (4\sqrt{k} - \mu_1) - 2 m^6 k^2 k_1 + 2 \lambda^2 m^2 k k_1 (2\sqrt{k} - \mu_1) \\ &\quad + m^4 k^2 k_1 \} / \{ k_1 m^2 (\lambda^2 + \sqrt{k} m^2)^2 - k_1 (2\sqrt{k} + k) \lambda^2 m^2 \\ &\quad - m^4 k k_1 \} \end{aligned} \quad (4.22)$$

It may be shown by analyzing equation (4.22) that a minimum value of q_1 is obtained when λ or n (the number of half-wavelengths in the axial direction) has its smallest value; namely $n=1$, hence $\lambda = \lambda_1 = \pi R/L$. As a consequence, a circular cylindrical shell under external pressure buckles into a single half-wavelength in the axial direction. For moderate-length cylinders, it may be assumed that

$$(\pi R/mL)^2 < \sqrt{k} \quad \text{and} \quad (1/m)^2 < 1, \quad (4.23)$$

as used by Gerard⁹⁴ for isotropic cylinders. Thus, equation (4.22) reduces to:

$$\begin{aligned} \frac{c_1}{c_3} &= (k - \mu_1^2) k_1 \lambda_1^4 / m^6 k k_1 \\ &= \left(1 - \frac{\mu_1^2}{k}\right) \lambda_1^4 / m^6 \\ &= (1 - \mu_1 \mu_2) \lambda_1^4 / m^6 \\ \frac{c_2}{c_3} &= km^2 - \lambda_1^2 (\mu_1^2 - k - 4k_1^2) / k_1 - 2k \\ &= km^2 \end{aligned} \quad (4.24)$$

So, equation (4.21) becomes

$$\begin{aligned} q_1 &= (1 - \mu_1 \mu_2) \lambda_1^4 / m^6 + (km^2) c^2 \\ &= H/x^3 + (kx) c^2, \end{aligned} \quad (4.25)$$

where

$$H = (1 - \mu_1 \mu_2) \lambda_1^4, \quad x = m^2,$$

and the minimum value of q_1 will occur when

$$\frac{\partial q_1}{\partial x} = 0, \quad (4.26)$$

which results in:

$$x = m^2 = \left[\frac{3R_1}{kc^2} \right]^{1/4}$$

So the critical load q_{cr} is:

$$\begin{aligned} q_{cr} &= \frac{p_{cr}R}{K_1} \\ &= H \left[\frac{kc^2}{3H} \right]^{3/4} + k \left[\frac{3H}{kc^2} \right]^{1/4} \cdot c^2 \\ &= \frac{4}{3} (3H)^{1/4} (kc^2)^{3/4} \end{aligned} \quad (4.27)$$

and the critical external pressure load for a moderate-length cylindrical shell is:

$$\begin{aligned} p_{cr} &= q_{cr} \cdot K_1 / R = \frac{q_{cr}}{R} \frac{E_1 t}{1 - \mu_1 \mu_2} \\ &= \frac{4\pi(1 - \mu_1 \mu_2)^{1/4} D_1 k^{3/4}}{3^{3/4} R^2 L c^{1/2}} \end{aligned} \quad (4.28)$$

This formula can be used as long as the condition of equation (4.23) for moderate-length cylinders is satisfied. This result exactly agrees with the result derived by Xiao and Cheng⁷⁴ using a quite different approach. In the case of isotropic cylinders under

uniform external pressure, the preceeding formula (4.28) becomes:

$$P_{cr} = \frac{2\pi Et^2}{3\sqrt{6}(1-\mu^2)^{3/4}RL} \sqrt{\frac{t}{R}} \quad (4.29)$$

4.1.4 BUCKLING UNDER AXIAL COMPRESSION ONLY

For an orthotropic cylindrical shell loaded with axial compression alone, the buckling condition of equation (4.15) becomes:

$$q_2 = \frac{c_1}{c_4} + \frac{c_2}{c_4} c^2 \quad (4.30)$$

In which

$$\begin{aligned} \frac{c_1}{c_4} &= (k - \mu_1^2) \lambda^4 / [\lambda^2 (\lambda^2 + \sqrt{k} m^2)^2 + \lambda^2 m^2 k] \\ \frac{c_2}{c_4} &= \{ (\lambda^2 + \sqrt{k} m^2)^4 - 2\lambda^6 \mu_1 - 6k \lambda^4 m^2 - 2 \lambda^2 m^4 k (4\sqrt{k} - \mu_1) \\ &\quad - 2m^6 k^2 + 2 \lambda^2 m^2 k (2\sqrt{k} - \mu_1) + m^4 k^2 \} \\ &\quad / [\lambda^2 (\lambda^2 + \sqrt{k} m^2)^2 + \lambda^2 m^2 k] \end{aligned} \quad (4.31)$$

In general, this buckling condition is again complicated. However, there are two special cases in which the condition can be further considered (or simplified). These cases are represented by λ^2 being either much less or much greater than unity.

Case 1: $\lambda^2 \ll 1$. i.e. $n\pi R/L \ll 1$, for very long

cylinders. We may neglect λ^2 compared with 1 or m^2 , but in the first term (c_1/c_4) we must do so separately for the term without the small factor c^2 . We thus obtain the approximate relation

$$\begin{aligned} q_2 &= \frac{(k-\mu_1^2)\lambda^4 + c^2 m^4 k^2 (m^4 - 2m^2 + 1)}{\lambda^2 m^2 k (m^2 + 1)} \\ &= \frac{(1-\mu_1\mu_2)\lambda^4 + c^2 m^4 k (m^4 - 2m^2 + 1)}{\lambda^2 m^2 (m^2 + 1)} \end{aligned} \quad (4.32)$$

from which we see that

$$\begin{aligned} \frac{q_2}{c\sqrt{(1-\mu_1\mu_2)k}} &= \frac{1}{m^2(m^2+1)} \cdot \frac{\lambda^2\sqrt{1-\mu_1\mu_2}}{c\sqrt{k}} \\ &\quad + \frac{m^2(m^2-1)^2}{m^2+1} \cdot \frac{c\sqrt{k}}{\lambda^2\sqrt{1-\mu_1\mu_2}} \end{aligned} \quad (4.33)$$

This is a unique expression describing the non-dimensional axial buckling load q_2 modified by the quantity $c\sqrt{(1-\mu_1\mu_2)k}$ in terms of $\frac{c\sqrt{k}}{\lambda^2\sqrt{1-\mu_1\mu_2}}$ and the number of circumferential waves in the buckling pattern. From the definitions of k, c and λ we find that

$$\begin{aligned} \frac{c\sqrt{k}}{\lambda^2\sqrt{1-\mu_1\mu_2}} &= \frac{1}{\pi^2\sqrt{12(1-\mu_1\mu_2)}} \frac{(1/n)^2}{R^2} \frac{t}{R} \sqrt{\frac{E_2}{E_1}} \end{aligned} \quad (4.34)$$

Case 2: $\lambda^2 \gg 1$, i.e. $n\pi R/L \gg 1$, cylinder length is short compared to the product of radius and number of axial half-waves. In this case, we may simplify equation (4.30) by neglecting 1

compared with λ^2 . This yields the formula

$$q_2 = \frac{(k-\mu_1^2)\lambda^4 + c^2(\lambda^2 - \sqrt{k}m^2)^4}{\lambda^2(\lambda^2 + \sqrt{k}m^2)^2} \quad (4.35)$$

which may be written as

$$\begin{aligned} \frac{q_2}{c\sqrt{(1-\mu_1\mu_2)k}} &= \frac{\lambda^2}{(\lambda^2 + \sqrt{k}m^2)^2} \cdot \frac{\sqrt{k(1-\mu_1\mu_2)}}{c} \\ &+ \frac{(\lambda^2 + \sqrt{k}m^2)^2}{\lambda^2} \cdot \frac{c}{\sqrt{k(1-\mu_1\mu_2)}} \end{aligned} \quad (4.36)$$

The left-hand term represents the non-dimensional axial buckling load, while on the right-hand side one term is the reciprocal of the other. We now must distinguish three further sub cases:

Case 2a: moderately long cylinders. In this case we have the condition of $m > 0$, and $(n\pi R/L)^2 < \frac{\sqrt{k(1-\mu_1\mu_2)}}{c}$ or $L/nR > \frac{\pi\sqrt{c}}{[k(1-\mu_1\mu_2)]^{1/4}}$. We may permit m to vary continuously and find the minimum value of q_2 by differentiating equation (4.36) with respect to $(\lambda^2 + \sqrt{k}m^2)^2$. The differentiation leads to the conclusion that

$$(\lambda^2 + \sqrt{k}m^2)^2 = \lambda^2 \frac{\sqrt{k(1-\mu_1\mu_2)}}{c} \quad (4.37)$$

Substituting in equation (4.36), we find

$$\frac{q_2}{c\sqrt{(1-\mu_1\mu_2)k}} = 2 \quad (4.38)$$

from which we get the critical axial compression load for moderately long cylinders

$$P_{cr} = K_1 q_2 = \frac{\sqrt{E_1 E_2} t^2}{\sqrt{3(1-\mu_1\mu_2)} R} \quad (4.39)$$

For isotropic cylinders, the above equation (4.39) can be reduced to the classical buckling load:

$$P_{cl} = \frac{Et^2}{\sqrt{3(1-\mu^2)} R} \quad (4.40)$$

Case 2b: very short cylinders, i.e., $m=0$ and $(n\pi R/L)^2 > \frac{\sqrt{k(1-\mu_1\mu_2)}}{c}$ or $L/nR < \frac{\pi\sqrt{c}}{[k(1-\mu_1\mu_2)]^{1/4}}$. Equation (4.38) is acceptable as long as equation (4.37) yields a reasonable value of m^2 . In this case, equation (4.37) no longer exists; thus equation (4.36) may be written as

$$\frac{q_2}{c\sqrt{(1-\mu_1\mu_2)k}} = \frac{1}{\lambda^2} \frac{\sqrt{(1-\mu_1\mu_2)k}}{c} + \lambda^2 \frac{c}{\sqrt{(1-\mu_1\mu_2)k}} \quad (4.41)$$

Thus the critical axial load modified by the quantity $c\sqrt{(1-\mu_1\mu_2)k}$ as before can be expressed in terms of either $\frac{1}{\lambda} \frac{[(1-\mu_1\mu_2)k]^{1/4}}{\sqrt{c}}$ or $\frac{L}{n\pi R} \left[\frac{12(1-\mu_1\mu_2)R^2 E_2}{2E_1} \right]^{1/4}$.

$$\text{Case 2c: } m = 0 \text{ and } (L/n\pi R)^2 = \frac{\sqrt{(1-\mu_1\mu_2)k}}{c}$$

For this case, equation (4.37) always exists and from equation (4.36) we get the same result as in equation (4.38), i.e.,

$$\frac{q_2}{c\sqrt{(1-\mu_1\mu_2)k}} = 2.$$

4.2 BUCKLING CRITERION OF A CELLULAR-WALLED CIRCULAR CYLINDRICAL SHELL UNDER COMBINED LOADING OF AXIAL COMPRESSION AND EXTERNAL PRESSURE

A cellular-walled circular cylindrical shell was considered in this section under the same loading conditions, i.e. axial compression and external pressure. In order to make use of those equations on orthotropic shells, the cellular-walled shell wall has to be approximated as an homogeneous orthotropic wall (or pseudo-orthotropic). All the basic equations developed in the section 4.1 for general orthotropic shells exist except that the bending stiffness of the shell wall D_1 and D_2 in the equation (4.6) have to be redefined while extensional stiffness K_1 and K_2 can still remain the same. They are expressed as follows:

$$\begin{aligned} K_1 &= \frac{E_1 t}{1 - \mu_1 \mu_2} & K_2 &= \frac{E_2 t}{1 - \mu_1 \mu_2} \\ D_1^* &= \frac{E_{b1} t^3}{12(1 - \mu_1 \mu_2)} & D_2^* &= \frac{E_{b2} t^3}{12(1 - \mu_1 \mu_2)} \end{aligned} \quad (4.42)$$

where E_{b1} and E_{b2} are effective Young's moduli of bending in the axial and hoop direction which are to be determined in the next chapter.

4.2.1 BUCKLING UNDER COMBINED LOADING

Since the cellular-walled shell wall is treated as pseudo-orthotropic, the buckling condition of a general orthotropic cylindrical shell, equation (4.15), may still be applied. We represent it as follows:

$$c_1 + c_2 \cdot c^2 = c_3 \cdot q_1 + c_4 \cdot q_2 \quad (4.43)$$

Coefficients $c_1 \dots c_4$ may be determined in the same way as in the last section:

$$c_1 = (k - \mu_1^2) k_1 \lambda^4$$

$$\begin{aligned} c_2 = & \lambda^8 k_1 \frac{E_{b1}}{E_1} + m^8 k k_1 \frac{E_{b2}}{E_1} \\ & - \lambda^6 m^2 [(\mu_1^2 - k) \frac{E_{b1}}{E_1} - 4k_1^2 + k_1 (\mu_1 \frac{E_{b1}}{E_1} - \mu_2 \frac{E_{b2}}{E_1})] \\ & - \lambda^4 m^4 [4k_1 \mu_1^2 + (2k_1 \mu_1 + \mu_1^2 - k) (\mu_1 \frac{E_{b1}}{E_1} + \mu_2 \frac{E_{b2}}{E_1}) + 8k_1^2 \mu_1 \\ & \quad - 4k k_1 - k_1 (k \frac{E_{b1}}{E_1} + \frac{E_{b2}}{E_1})] \\ & - \lambda^2 m^6 [(\mu_1^2 - k + 2k_1 \mu_1) \frac{E_{b2}}{E_1} - 4k k_1^2 - k k_1 (\mu_1 \frac{E_{b1}}{E_1} + \mu_2 \frac{E_{b2}}{E_1})] \\ & - \lambda^2 m^4 [(2k - k_1 \mu_1) \frac{E_{b2}}{E_1} - 2k \mu_1^2 + 8k k_1^2 - 3k k_1 \mu_1 \\ & \quad + k k_1 (\mu_1 \frac{E_{b1}}{E_1} + \mu_2 \frac{E_{b2}}{E_1})] \end{aligned}$$

$$\begin{aligned}
& -\lambda^4 m^2 [6kk_1 + (k - k_1\mu_1 - \mu_1^2)(\mu_1 \frac{E_{b1}}{E_1} + \mu_2 \frac{E_{b2}}{E_1}) - 6k_1\mu_1^2 - 8k_1^2\mu_1 \\
& \quad + k_1(k \frac{E_{b1}}{E_1} - \frac{E_{b2}}{E_1})] \\
& -2m^6 k^2 k_1 - \lambda^6 k_1 \mu_1 (1 + \frac{E_{b1}}{E_1}) \\
& -\lambda^2 m^2 [\frac{E_{b2}}{E_1} (k_1\mu_1 + \mu_1^2 - k) + k(k_1\mu_1 - 4k_1^2)] \\
& -\lambda^4 k_1 (3\mu_1^2 - 4k) + m^4 k k_1 \frac{E_{b2}}{E_1}
\end{aligned}$$

$$c_3 = k_1 m^2 (\lambda^2 + \sqrt{k} m^2)^2 - k_1 (2\sqrt{k} + k) \lambda^2 m^2 - m^4 k k_1$$

$$c_4 = \lambda^2 k_1 (\lambda^2 + \sqrt{k} m^2)^2 + \lambda^2 m^2 k k_1 \quad (4.44)$$

It may be noted that due to E_{b1} and E_{b2} being introduced, the buckling condition of a cellular-walled cylindrical shell is more complicated than the one of a general orthotropic cylindrical shell. The equation (4.43) describes a straight line in the q_1, q_2 plane, and the limit of the stable region is a polygon consisting of sections of straight lines for different pairs m, n (buckling mode). The details of the theoretical performance of a cellular-walled cylindrical shell will be discussed in Chapter Six.

4.2.3 BUCKLING UNDER EXTERNAL PRESSURE ONLY

Under external pressure alone ($q_2=0$), the buckling condition, equation (4.43), becomes

$$q_1 = \frac{c_1}{c_3} + \frac{c_2}{c_3} c^2 \quad (4.45)$$

where the coefficients c_1, c_2 and c_3 are represented by equation (4.44). For moderate-length cylindrical shells, assumptions defined by the equation (4.23) exist, i.e.,

$$(\pi R/mL)^2 < \sqrt{k} \quad \text{and} \quad (1/m)^2 < 1, \quad (4.23)$$

By using the above condition, the coefficients in the equation (4.45) can be simplified as:

$$\begin{aligned} \frac{c_1}{c_3} &= (k - \mu_1^2) \lambda_1^4 / (km^6) = (1 - \mu_1 \mu_2) \lambda_1^4 / m^6 \\ \frac{c_2}{c_3} &= m^8 k k_1 \frac{E_{b2}}{E_1} / (m^6 k k_1) = m^2 \frac{E_{b2}}{E_1} \end{aligned} \quad (4.46)$$

By using the same procedure of Section 4.1.3, i.e. substituting the equation (4.46) into the equation (4.45) then minimizing the function q_1 to m^2 , the following critical external pressure for moderate-length cellular-walled cylindrical shells may be derived:

$$P_{cr} = \frac{4\pi(1 - \mu_1 \mu_2)^{1/4} D_1^* \left(\frac{E_{b2}}{E_1}\right)^{3/4}}{3^{3/4} R^2 L c^{1/2}} \quad (4.47)$$

In the case of general orthotropic cylindrical shells, we have $E_{b1} = E_1$, $E_{b2} = E_2$ and $D_1^* = D_1$. Thus the above equation (4.47) reduces to the formula (4.28), i.e.,

$$P_{cr} = \frac{4\pi(1 - \mu_1 \mu_2)^{1/4} D_1 k_1^{3/4}}{3^{3/4} R^2 L c^{1/2}} \quad (4.28)$$

4.2.2 BUCKLING UNDER AXIAL COMPRESSION ONLY

Under axial compression load alone ($q_1=0$), the buckling condition, equation (4.43), becomes

$$q_2 = \frac{c_1}{c_4} + \frac{c_2}{c_4} c^2 \quad (4.48)$$

where the coefficients c_1, c_2 and c_4 are represented by equation (4.44). Due to complexity, equation (4.48) could not be further simplified.

NOTATION

A,B,C:	Amplitudes of a set of displacement functions u,v,w
c ² :	$= \frac{t^2}{12R^2}$
c ₁ ,c ₂ ,c ₃ ,c ₄ :	Coefficients in the buckling condition, refer to equations (4.15),(4.16),(4.20)
D:	Flexural rigidity of isotropic shells, $D = \frac{Et^3}{12(1-\mu_1\mu_2)}$
D ₁ ,D ₂ :	Bending stiffness of orthotropic shells; $D_1 = \frac{E_1 t^3}{12(1-\mu_1\mu_2)}, \quad D_2 = \frac{E_2 t^3}{12(1-\mu_1\mu_2)}$
D ₁ [*] ,D ₂ [*] :	Bending stiffness of cellular-walled shells; $D_1 = \frac{E_{b1} t^3}{12(1-\mu_1\mu_2)}, \quad D_2 = \frac{E_{b2} t^3}{12(1-\mu_1\mu_2)}$
E ₁ ,E ₂ :	Young's moduli of extension in axial and circumferential respectively
E _{b1} ,E _{b2} :	Young's moduli of bending in axial and circumferential respectively
G ₁₂ :	Orthotropic shear modulus that characterized the change of angles between principal directions α and β
K ₁ ,K ₂ :	Extensional stiffness, $K_1 = \frac{E_1 t}{1-\mu_1\mu_2}, \quad K_2 = \frac{E_2 t}{1-\mu_1\mu_2}$
k:	$= E_2/E_1$
k ₁ :	$= \frac{G(1-\mu_1\mu_2)}{E_1}$
L:	Length of a cylindrical shell
M _{α} ,M _{β} :	Bending moments per unit length of the middle surface of the shell
M _{$\alpha\beta$} ,M _{$\beta\alpha$} :	Twisting moments per unit length of the middle surface

	of the shell
$2m$:	Number of half waves along circumferential direction
N_α, N_β :	Normal stress resultants per unit length of the middle surface of the shell
n :	Number of half-waves along axial direction
P :	Axial compressive load
P_{cl} :	Classical axial buckling load
P_{cr} :	Critical axial buckling load
p :	External pressure
p_{cr} :	Critical external pressure load
Q_α, Q_β :	Transverse stress resultants per unit length of the middle surface of the shell
q_1 :	Non-dimensional axial compression load
q_2 :	Non-dimensional external pressure load
R :	Radius of the midsurface of the cylindrical shell
S_α, S_β :	Shear stress resultants per unit length of the middle-surface of the shell
t :	Shell wall thickness
u, v, w :	Midsurface displacements in x, y and z directions, respectively
u_α, u_β, u_z :	Displacement components of an arbitrary point of the cylindrical shell
x, y, z :	Axial, circumferential and radial coordinates of the cylindrical shell
ω_α :	$= \frac{\partial w}{\partial \alpha}$
ω_β :	$= (\frac{\partial w}{\partial \beta} - v)$

α, β, γ :	Dimensionless coordinates of x,y,z, $\alpha = x/R$, $\beta = y/R$, $\gamma = z/R$
$\varepsilon_\alpha, \varepsilon_\beta$:	Normal strains in α, β directions, respectively
$\varepsilon_{\alpha\beta}$:	Shear strain in α, β plane
δ :	$= \frac{(\tanh^{-1}\sqrt{3}c - \sqrt{3}c)}{\sqrt{3}.c^3} - 1$
η_α, η_β :	Bending strains
$\eta_{\alpha\beta}$:	Twisting strain
λ :	$= \frac{n\pi R}{L}$
μ :	Poisson's ratio of an isotropic shell
$\mu_1 = \mu_{\beta\alpha}$:	Poisson's ratio of Orthotropic shells that characterizes the decrease in α direction due to tension applied in β direction
$\mu_2 = \mu_{\alpha\beta}$:	Poisson's ratio of Orthotropic shells that characterizes the decrease in β direction due to tension applied in α direction
$\sigma_\alpha, \sigma_\beta$:	Normal stress in α, β directions, respectively
$\tau_{\alpha\beta}$:	Shear stress in $\alpha - \beta$ plane

CHAPTER 5

**NUMERICAL ESTIMATION
OF
AVERAGE CELLULAR-
WALLED SHELL
PROPERTIES**

CHAPTER 5

NUMERICAL ESTIMATION OF AVERAGE CELLULAR-WALLED SHELL PROPERTIES

In developing the buckling criterion of cellular-walled cylindrical shells in the last chapter, the following shell properties were used, and they are to be determined in this chapter:

- E_1 : Young's modulus of extension in axial direction,
- E_2 : Young's modulus of extension in hoop direction,
- E_{b1} : Young's modulus of bending in axial direction,
- E_{b2} : Young's modulus of bending in hoop direction,
- μ_1 : Poisson's ratio that characterizes the decrease in circumferential direction due to tension applied in axial direction,
- μ_2 : Poisson's ratio that characterizes the decrease in axial direction due to tension applied in circumferential direction,
- G_{12} : Shear modulus.

Where E_1 and E_2 are involved in extensional stiffnesses K_1 and K_2 :

$$K_1 = \frac{E_1 t}{1 - \mu_1 \mu_2} \quad K_2 = \frac{E_2 t}{1 - \mu_1 \mu_2} \quad (5.1)$$

and E_{b1} , E_{b2} are involved in the bending stiffnesses D_1 and D_2 :

$$D_1 = \frac{E_{b1}t^3}{12(1-\mu_1\mu_2)} \quad D_2 = \frac{E_{b2}t^3}{12(1-\mu_1\mu_2)} \quad (5.2)$$

The shear modulus (G_{12}) can be estimated from the following approximate relation:

$$G_{12} = \frac{\sqrt{E_1 E_2}}{2(1+\sqrt{\mu_1 \mu_2})} \quad (5.3)$$

A diagram of a shell model, a cellular-walled circular cylindrical shell, is shown in Figure 5.1. It has overall uniform wall thickness. Since the shell wall consists of a section containing a large number of circular, closely spaced longitudinal holes, the line of this investigation was to consider it in a similar fashion to a longitudinal stringer-stiffened shell with the stringers closely spaced. Thus the cellular wall construction was treated as homogeneous and pseudo-orthotropic. Local variations in wall properties were ignored in determining buckling loads. Average wall properties had to be established from a consideration of local wall geometry. Once these material properties were established, they could be used in the determination of buckling loads.

When a high fluid pressure is applied within the cells of the shell, it causes a similar effect as that of an internal pressure of the shell. In that sense, the cell pressure can be treated as equivalent to the internal pressure in the buckling analysis. The relation between the cell pressure and the internal pressure had to be determined before the shell properties were established.

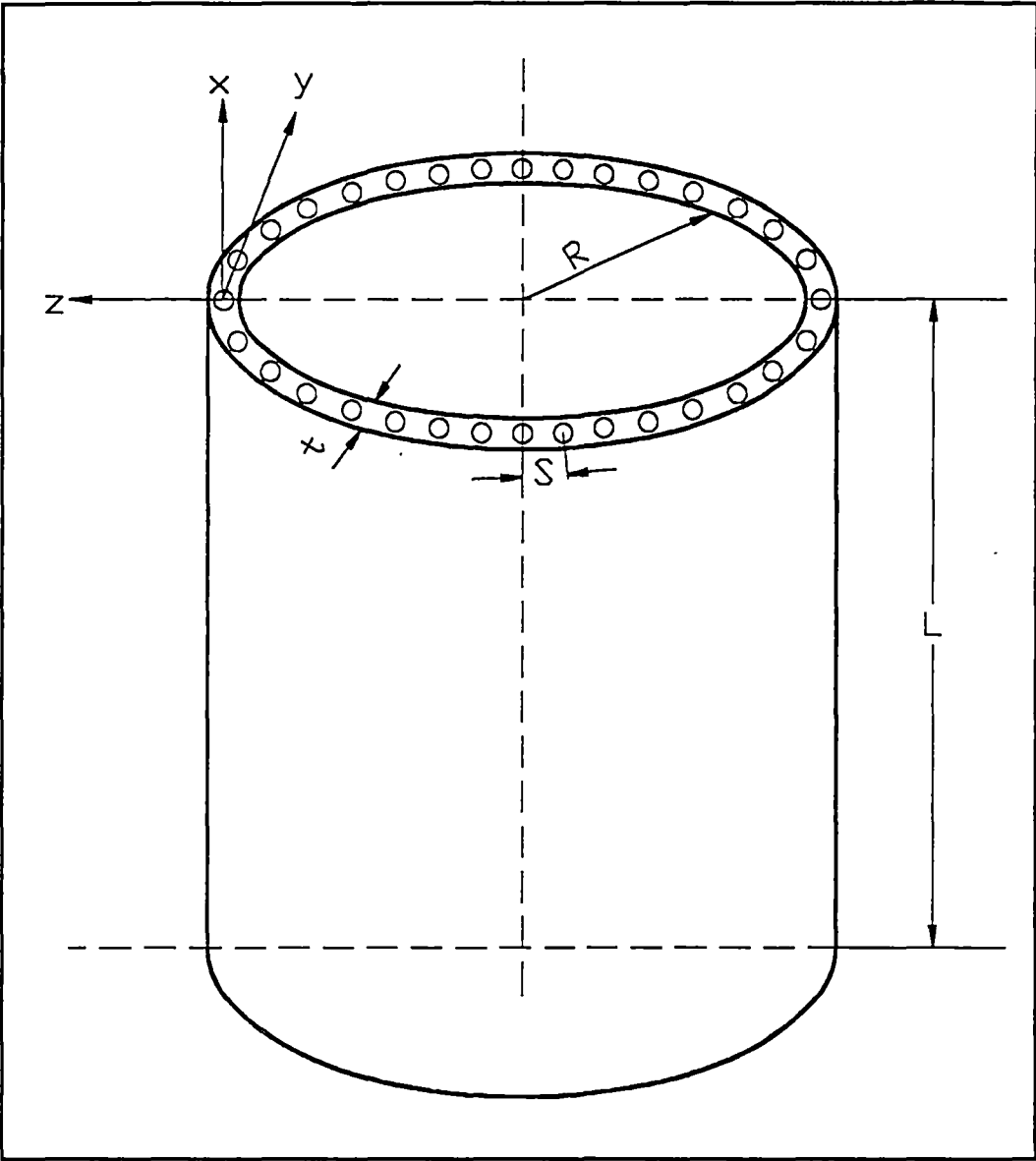


Figure 5.1

Diagram of shell model

5.1 DETERMINATION OF EQUIVALENT CELL PRESSURE TO INTERNAL PRESSURE

5.1.1 STRUCTURE ANALYSIS AND ELEMENTS

In the shell model of Figure 5.1, let L be the length of the shell, R the radius of the midsurface of the shell, t the wall thickness and S the hole spacing (measuring from the midsurface). Assume that the shell is loaded in axial compression, external pressure and pressure within the cells. Since cell pressure (pressure applied within the cells) would have the same effect as that of internal pressure of the shell, i.e., to cause expansion and produce positive radial displacement of the shell wall, the local load cell pressure can be treated as global load internal pressure. In that case the loading system of the shell is axially symmetric. It should also be noted that the cells are very closely spaced in the shell wall. If local geometric variations are ignored and the shell wall treated as homogeneous, then the shell is geometrically axial symmetric. Only an average shell wall unit which represents characteristics of the shell wall need to be considered in the structural analysis.

The finite element model illustrated in Figure 5.2 was used for the analysis. This model covered a section of the shell wall between the centre of the cell and the centre of the solid wall between adjacent cells, since these locations represented planes of symmetry in the circumferential sense. Thus the model was

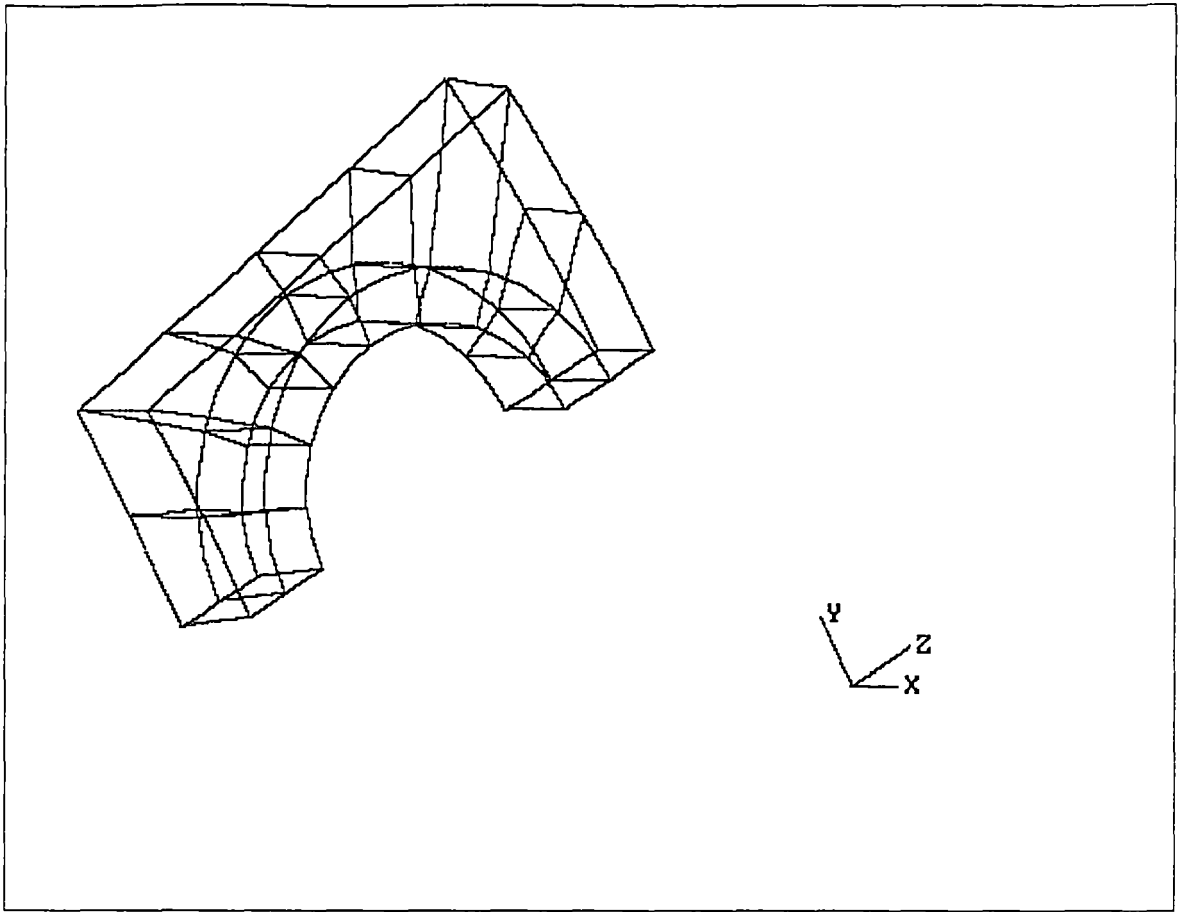


Figure 5.2
Finite element model of shell wall

essentially a wedge with a very small wedge angle, so small that the sides of the wedge are almost parallel. One side of the wedge had a semi-circular cut out which corresponded with the cell. A constraint was placed on the model in which the angle of the wedge remained constant and the model remained linear along the planes of symmetry. When the load was applied (cell pressure or internal pressure), the model moved outwards, and the width of the wedge

increased. Thus, small circumferential expansions corresponded with substantial outward radial displacements. The finite element model consisted of sixteen three dimensional 20-node isoparametric brick elements. A software package called STRAND-5⁹⁵ was used in the analysis.

5.1.2 THE EMPIRICAL RELATIONS OF THE EFFECT OF CELL PRESSURE TO THAT OF INTERNAL PRESSURE

In this analysis, the effect of cell pressure p_1 was considered to be the same as that of an internal pressure p_2 , when the radial displacements of the midsurface were the same in both cases. The radial displacements of the midsurface under unit cell pressure and internal pressure were calculated for different geometric configurations. The ratios of the radial displacements ($\frac{w_1}{w_s}$, $\frac{w_2}{w_s}$ and $\frac{w_1}{w_2}$) were plotted against the geometric variables (S/t , R/t and $2r/t$). By analysing the calculated data, the following empirical relations were established linking the effect of cell pressure to that of internal pressure

$$\begin{aligned}\frac{w_1}{w_s} &= [a_1 + b_1 \left\{ \frac{2r}{t} \right\} + c_1 \left\{ \frac{2r}{t} \right\}^2] * \left\{ \frac{R}{t} \right\} d_1 * \left\{ \frac{S}{t} \right\} f_1 \\ \frac{w_2}{w_s} &= [a_2 + b_2 \left\{ \frac{2r}{t} \right\} + c_2 \left\{ \frac{2r}{t} \right\}^2] * \left\{ \frac{R}{t} \right\} d_2 * \left\{ \frac{S}{t} \right\} f_2 \\ \frac{w_1}{w_2} &= [a_3 + b_3 \left\{ \frac{2r}{t} \right\}] * \left\{ \frac{R}{t} \right\} d_3 * \left\{ \frac{S}{t} \right\} f_3\end{aligned}\tag{5.4}$$

Table 5.1 Shell geometry for Calculation

S/t	R/t	2r/t
0.80	10	0.20 0.40 0.60
0.80	30	0.20 0.40 0.60
0.80	60	0.20 0.40 0.60
0.80	100	0.20 0.40 0.60
0.80	300	0.20 0.40 0.60
0.80	600	0.20 0.40 0.60
1.00	10	0.10 0.20 0.30 0.40 0.50 0.60 0.70 0.80
1.00	30	0.10 0.20 0.30 0.40 0.50 0.60 0.70 0.80
1.00	60	0.10 0.20 0.30 0.40 0.50 0.60 0.70 0.80
1.00	100	0.10 0.20 0.30 0.40 0.50 0.60 0.70 0.80
1.00	300	0.10 0.20 0.30 0.40 0.50 0.60 0.70 0.80
1.00	600	0.10 0.20 0.30 0.40 0.50 0.60 0.70 0.80
1.40	10	0.20 0.40 0.60
1.40	30	0.20 0.40 0.60
1.40	60	0.20 0.40 0.60
1.40	100	0.20 0.40 0.60
1.40	300	0.20 0.40 0.60
1.40	600	0.20 0.40 0.60
1.60	10	0.20 0.40 0.60
1.60	30	0.20 0.40 0.60
1.60	60	0.20 0.40 0.60
1.60	100	0.20 0.40 0.60
1.60	300	0.20 0.40 0.60
1.60	600	0.20 0.40 0.60

Where w_1 is the radial displacement due to a unit of cell pressure, w_2 is the radial displacement due to a unit of internal pressure and w_s is the radial displacement of a shell with a solid wall of the same thickness due to a unit of internal pressure.

The values of w_1 and w_2 are calculated for different geometric configurations by changing the variables S/t , R/t and $2r/t$. Five values of S/t were selected, i.e. $S/t=0.8, 1.0, 1.2, 1.4, 1.6$. For each value of S/t , different values of R/t were selected from 10 to 600, i.e. $R/t=10, 30, 60, 100, 300, 600$. Furthermore, for each case of R/t , different values of $2r/t$ were selected. Totally, 102 different geometric cases were calculated. The details of the calculated cases are listed in Table 5.1. The calculated data of $w_1, w_2, \frac{w_1}{w_s}, \frac{w_2}{w_s}$ and $\frac{w_1}{w_2}$ are presented in of Appendix A. Functions $\frac{w_1}{w_s}, \frac{w_2}{w_s}$ and $\frac{w_1}{w_2}$ were plotted against the three variables $S/t, R/t$ and $2r/t$. These plots are also contained in Appendix A.

The constants a_1, a_2, a_3 and b_1 etc. in the equation (5.4) were determined by least squares fitting to the calculated data. The program used in least squares fitting is listed in Appendix B. Values of the constants are given as follows, f_1, f_2 and f_3 are polynomials in $2r/t$

$a_1 = 0.0967$	$b_1 = -0.6933$
$c_1 = 2.8276$	$d_1 = -0.9960$
$a_2 = 0.9570$	$b_2 = -0.2720$

$$\begin{aligned}
c_2 &= 2.9360 & d_2 &= 0.0130 \\
a_3 &= -0.0907 & b_3 &= 0.7861 \\
d_3 &= -1.0160 \\
f_1 &= -0.3540 - 2.2400 (2r/t) + 1.7430 (2r/t)^2 \\
f_2 &= 0.3280 - 2.4660 (2r/t) + 2.5630 (2r/t)^2 \\
f_3 &= -0.1790 - 2.6160 (2r/t) + 2.5240 (2r/t)^2
\end{aligned}$$

Figure 5.3 summarises this data for the particular case of w_1/w_s with $S/t=1.0$ and is typical of these relations.

5.2 DETERMINATION OF AVERAGE PROPERTIES OF CELLULAR-WALLED CIRCULAR CYLINDRICAL SHELLS

5.2.1 DETERMINATION OF AVERAGE YOUNG'S MODULUS

E_1

Figure 5.4 shows an average wall unit, taken from the cellular-walled cylindrical shell. E is denoted as the Young's modulus of the materials. Then the extensional stiffness of the unit in the axial direction can be written as $EA_m = E(St - \pi r^2)$. On the other hand, when the unit is treated as homogeneous orthotropic and E_1 is denoted as the modified Young's modulus in the axial direction, then its extensional stiffness can be written in another form, $E_1 A = E_1(St)$. Obviously, these two extensional stiffnesses with different expressions must be the same, i.e.

$$E(St - \pi r^2) = E_1(St) \quad (5.5)$$

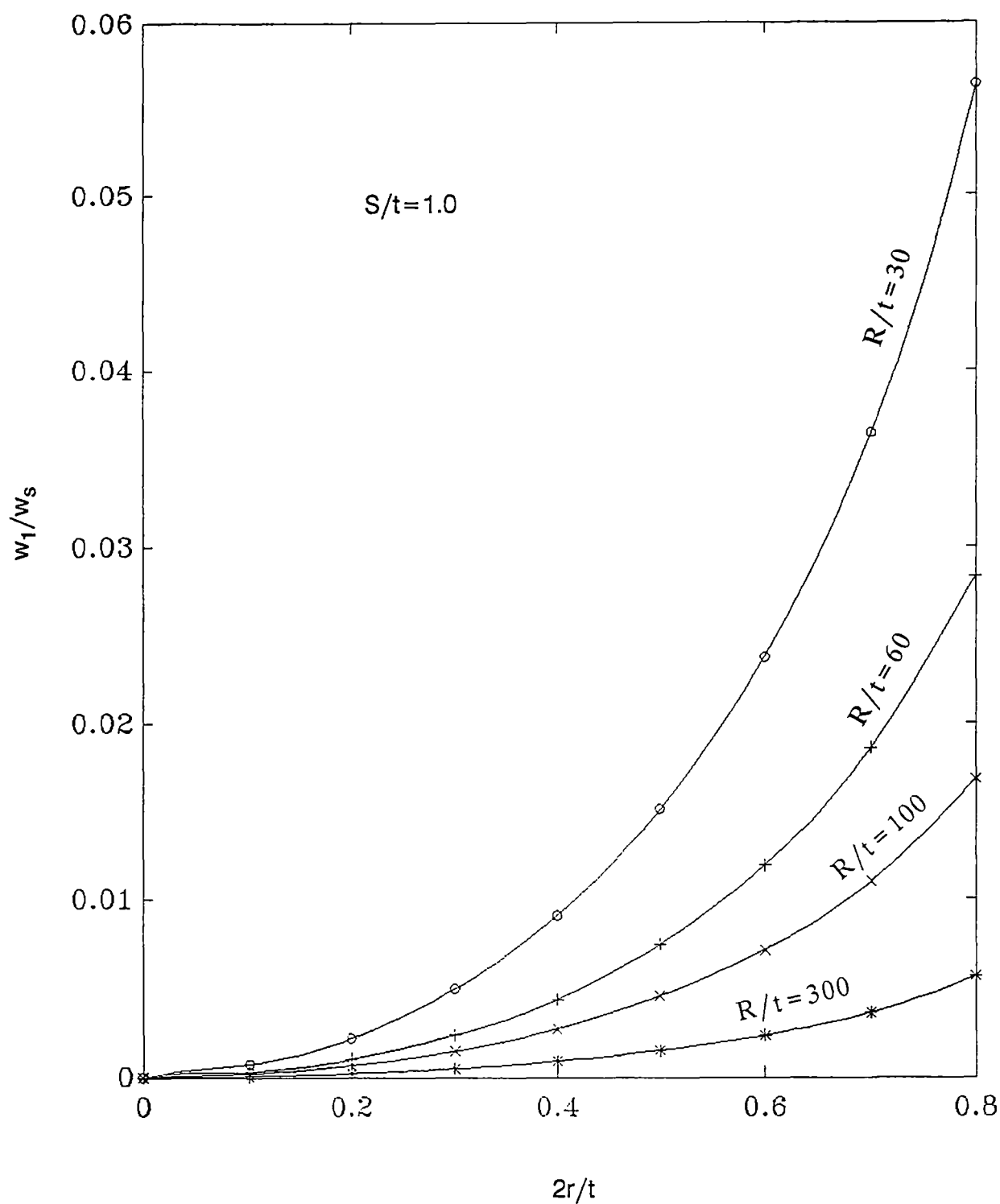


Figure 5.3

Ratios of deflections for internal pressure loading on cellular-walled and solid-walled shell of the same thickness ($S/t=1.0$)

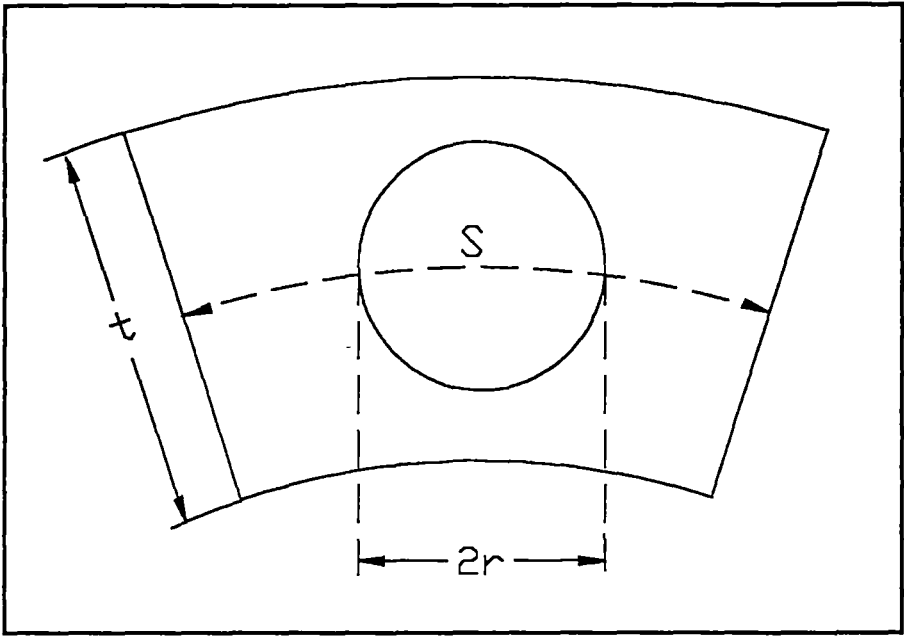


Figure 5.4 An average shell wall unit

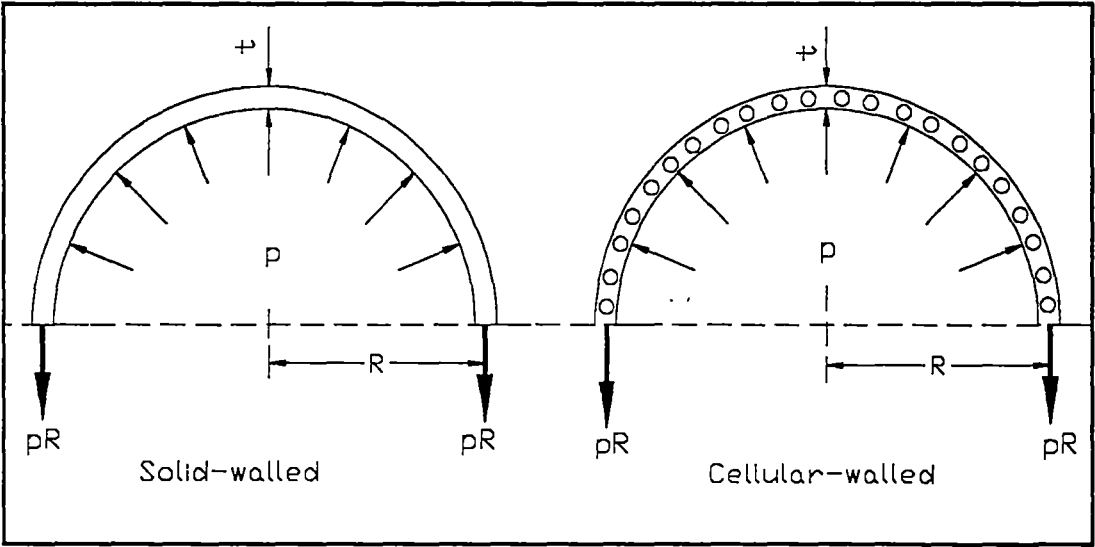


Figure 5.5 Diagram for shell under internal pressure

So, the modified Young's modulus in the axial direction of a homogeneous cellular-walled shell can be written as

$$E_1 = \frac{E(St-\pi r^2)}{St} \quad (5.6)$$

5.2.2 DETERMINATION OF AVERAGE YOUNG'S MODULUS

E_2

As shown in Figure 5.5, for a cellular-walled cylindrical shell under internal pressure p_2 , the radial displacement of the midsurface w_{p2} can be expressed as:

$$w_{p2} = \frac{p_2 R^2}{E_2 t} \quad (5.7)$$

while w_{p2} also can be expressed as

$$w_{p2} = w_2 p_2 = \frac{w_2}{w_s} w_s p_2 \quad (5.8)$$

where $w_s = R^2/Et$ is the radial displacement of a solid-walled shell due to unit internal pressure. Substituting it into the equation (5.8) and comparing the two equations of (5.7) and (5.8), we get:

$$E_2 = \frac{E}{w_2/w_s} \quad (5.9)$$

By substituting equation (5.4) into the equation (5.9), the modified Young's modulus of the cellular-walled shell in the circumferential direction can be finally expressed as

$$E_2 = \frac{E}{[a_2 + b_2\{\frac{2r}{t}\} + c_2\{\frac{2r}{t}\}^2] * \{\frac{R}{t}\}d_2 * \{\frac{S}{t}\}f_2} \quad (5.10)$$

5.2.3 DETERMINATION OF POISSON'S RATIOS μ_1 AND μ_2

As shown in Figure 5.6, by definition, Poisson's ratio μ_2 can be written as

$$\mu_2 = -\frac{\varepsilon_2}{\varepsilon_1}, \quad (5.11)$$

where ε_1 and ε_2 are the strains in 1 and 2 directions. Denoting S as the unit length in 2 direction, the deformation in 2 direction dS can be written as,

$$dS = -S\varepsilon_2 = S \mu_2 \varepsilon_1, \quad (5.12)$$

and also,

$$dS = dS_m + dS_h, \quad (5.13)$$

in which,

$$dS_m = S V_m \mu_m \varepsilon_1$$

$$dS_h = S V_h \mu_h \varepsilon_1$$

where V_m , V_h are the volume percentage occupied by m (mass) and h (hole), and they have $V_m + V_h = 1$; μ_m , μ_h are Poisson's ratios for m and h . Substituting the above dS_m and dS_h into equation (5.13), then using equation (5.12), we have:

$$\mu_2 = V_m \mu_m + V_h \mu_h, \quad (5.14)$$

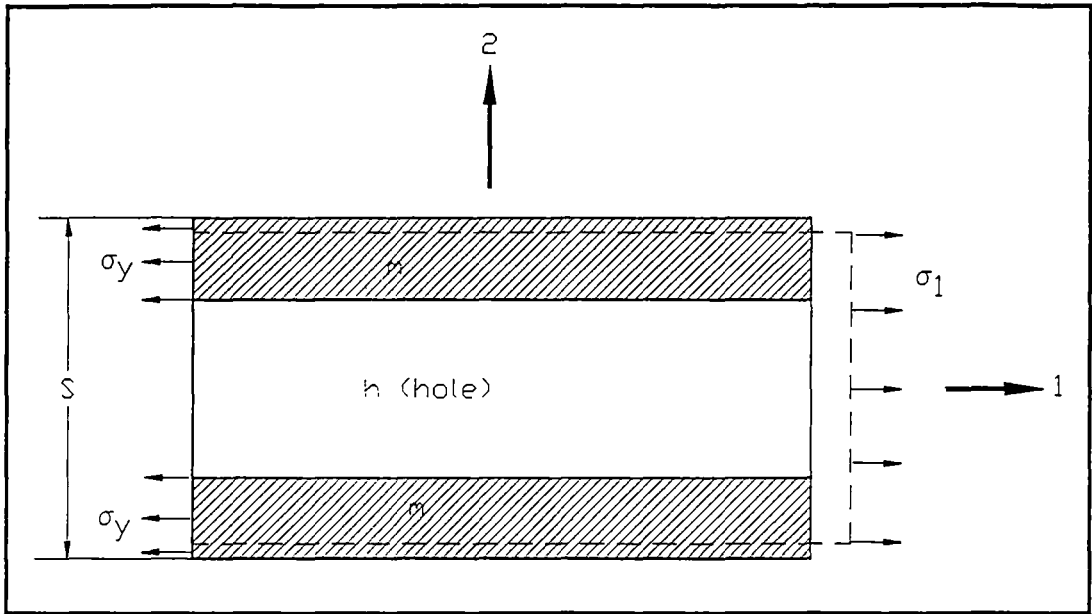


Figure 5.6 A shell wall unit under tension

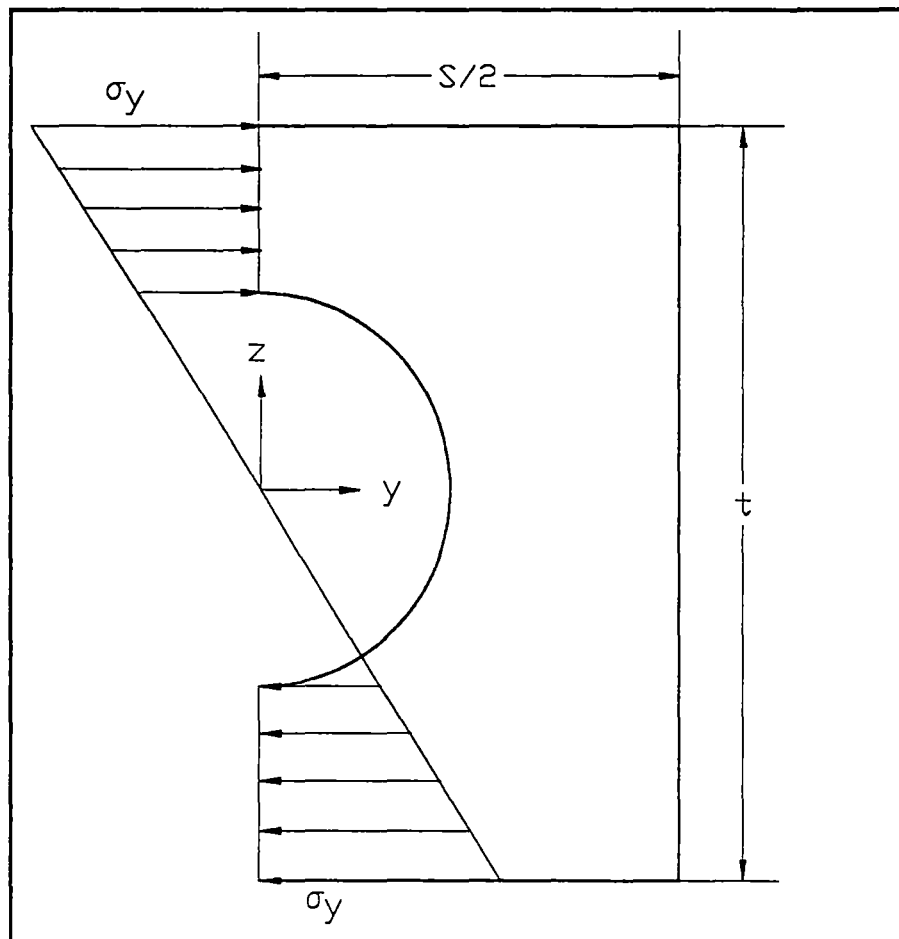


Figure 5.7 A shell wall unit under pure bending

During deformation $\mu_h = \mu_m = \mu$, so we have:

$$\mu_2 = \mu \quad (5.15)$$

From the relation of shell properties $\mu_1 E_1 = \mu_2 E_2$, we have

$$\mu_1 = \mu \frac{E_2}{E_1} \quad (5.16)$$

5.2.4 DETERMINATION OF AVERAGE YOUNG'S MODULUS E_{b1}

Consider again the average wall unit shown in Figure 5.4. First, if we consider a unit of a solid walled shell with a thickness t , its bending stiffness will be $\frac{E(St^3)}{12(1-\mu^2)}$. And the bending stiffness of a solid cylinder with diameter $2r$ is $\frac{E(3\pi r^4)}{12(1-\mu^2)}$. Combining the above two stiffnesses, the average bending stiffness of a cellular-walled cylindrical shell $\frac{E_{b1}(St^3)}{12(1-\mu^2)}$ can be obtained:

$$E_{b1}(St^3) = E(St^3) - E(3\pi r^4), \quad (5.17)$$

then

$$E_{b1} = \frac{E(St^3 - 3\pi r^4)}{St^3} \quad (5.18)$$

5.2.5 DETERMINATION OF AVERAGE YOUNG'S MODULUS E_{b2}

It should be noted that the shell we are considering is

thin walled, i.e., the shell radius R is very large compared to the shell thickness t and cell radius r . So curved-edges of the shell wall section can be approximately treated as straight lines, and the shell unit can be treated as a plate, as shown in Figure 5.7.

Under the pure bending moment M , we assume that only the stress σ_y exists and its distribution along z direction is linear, so it can be written as

$$\sigma_y = c(y)z \quad (5.19)$$

When $y < r$, at any section,

$$\begin{aligned} \frac{1}{2}M &= \frac{t/2}{\sqrt{r^2-y^2}} \int \sigma_y z dz = \frac{t/2}{\sqrt{r^2-y^2}} \int c(y) z^2 dz \\ &= \frac{c(y)}{24} [t^3 - 8(r^2-y^2) \sqrt{r^2-y^2}] \end{aligned} \quad (5.20a)$$

and when $y > r$, at any section

$$\begin{aligned} \frac{1}{2}M &= \int_0^{t/2} \sigma_y z dz = \int_0^{t/2} c(y) z^2 dz \\ &= \frac{c(y)}{24} t^3 \end{aligned} \quad (5.20b)$$

Thus, the distribution of stress σ_y in equation (5.19) can be determined:

$$c(y) = \frac{12M}{t^3 - 8(r^2 - y^2) \sqrt{r^2 - y^2}} \quad (\text{when } y < r) \quad (5.21a)$$

and,

$$c(y) = \frac{12M}{t^3} \quad (\text{when } y > r) \quad (5.21b)$$

The potential energy of this isotropic plate produced by the moment M can be written as:

$$U = \int_A \frac{\sigma_y^2}{2E} dA \quad (5.22)$$

Now, if we assume the plate consists of uniform orthotropic material, and its bending stiffness is E_{b2} , its potential energy produced by the moment M can be expressed as:

$$\begin{aligned} U_1 &= \int_A \frac{\sigma_y^2}{2E_{b2}} dA = \frac{1}{2E_{b2}} \int_0^{S/2} c^2(y) dy \int_0^{t/2} z^2 dz \\ &= \frac{1}{2E_{b2}} \int_0^{S/2} \left(\frac{12M}{t^3}\right)^2 dy \int_0^{t/2} z^2 dz \\ &= \frac{3M^2}{E_{b2}t^3} (S/2) \end{aligned} \quad (5.23)$$

Since they are produced by the same moment M , the above two potential energies U and U_1 of the equations (5.22) and (5.23) must be equal, i.e.:

$$\int_A \frac{\sigma_y^2}{2E} dA = \frac{3M^2}{E_{b2}t^3} (S/2) \quad (5.24)$$

From the above equation, we can get

$$E_{b2} = \frac{3ESM^2}{t^3} / \int_A \sigma_y^2 dA \quad (5.25)$$

where

$$\begin{aligned} \int_A \sigma_y^2 dA &= \int_0^r \int_{\sqrt{r^2-y^2}}^{t/2} c^2(y)z^2 dy dz + \int_r^{S/2} \int_0^{t/2} c^2(y)z^2 dy dz \\ &= \int_0^r \frac{6M^2}{t^3-8(r^2-y^2)\sqrt{r^2-y^2}} dy + \int_r^{S/2} \frac{6M^2}{t^3} dy \\ &= \int_0^r \frac{6M^2}{t^3-8(r^2-y^2)\sqrt{r^2-y^2}} dy + \frac{6M^2}{t^3} (S/2-r) \quad (5.26) \end{aligned}$$

In the above equation (5.26), the first term of the right hand side can not be evaluated. An approximation was made as follows:

$$\begin{aligned} \int_0^r \frac{6M^2}{t^3-8(r^2-y^2)\sqrt{r^2-y^2}} dy &\approx \int_0^r \frac{6M^2}{t^3-3\sqrt{3}r^3} dy \\ &= \frac{6M^2}{t^3-3\sqrt{3}r^3} r \quad (5.27) \end{aligned}$$

The above approximation could lead to a small error, for a shell configuration of $2r/t=0.50$ and $S/t=1.0$, may cause a possible error up to 3% of above equation. As the consequence, up to 1.5% error could be introduced in the equation (5.25) for the same shell configuration.

Finally, Young's modulus for bending in circumferential direction E_{b2} is obtained as:

$$\begin{aligned}
 E_{b2} &= \frac{3ESM^2}{t^3} / \left[\frac{6M^2}{t^3} (S/2-r) + \frac{6M^2}{t^3 - 3\sqrt{3}r^3} r \right] \\
 &= E / \left[1 - 2r/S + \frac{2r/S}{1 - \frac{3\sqrt{3}}{8} (2r/S)^3} \right] \quad (5.28)
 \end{aligned}$$

NOTATION

A_m :	Cross-section area of an average shell wall unit
a_i, b_i, c_i, d_i :	Coefficients ($i = 1, 2, 3$), refer to the equations (5.4)
D_1, D_2 :	Bending stiffness in axial and circumferential direction, respectively, $D_1 = \frac{E_{b1}t^3}{12(1-\mu_1\mu_2)}$, $D_2 = \frac{E_{b2}t^3}{12(1-\mu_1\mu_2)}$
E :	Young's Modulus of an isotropic solid-walled shell
E_1, E_2 :	Young's moduli of extension in axial and circumferential direction, respectively
E_{b1}, E_{b2} :	Young's moduli of bending in axial and circumferential direction, respectively
f_1, f_2, f_3 :	Polynomials in $2r/t$, refer to equation (5.4)
G_{12} :	Shear modulus
K_1, K_2 :	Shell extensional stiffness in axial and circumferential direction, $K_1 = \frac{E_1t}{1-\mu_1\mu_2}$, $K_2 = \frac{E_2t}{1-\mu_1\mu_2}$
L :	Length of cylindrical shell
p :	Lateral pressure, positive inward
p_c :	cell pressure
r :	cell radius
R :	Shell radius
S :	Cell spacing in circumferential direction
t :	Thickness of shell wall
U, U_1 :	Potential energies
w_1, w_2 :	Midsurface radial displacements due to unit cell pressure and unit lateral pressure, respectively
w_{p2} :	Midsurface radial displacement due to lateral pressure of p_2

w_s :	Midsurface radial displacement of a solid walled shell due to unit lateral pressure
x,y,z :	Axial, circumferential and radial coordinates of the shell
μ :	Poisson's ratio of an isotropic shell
μ_1 :	Poisson's ratio that characterizes the decrease in circumferential direction due to tension applied in axial direction
μ_2 :	Poisson's ratio that characterizes the decrease in axial direction due to tension applied in circumferential direction
σ_y :	Normal stress in circumferential direction, positive for compression

CHAPTER 6

**THEORETICAL
PERFORMANCE
OF
CELLULAR-WALLED
CIRCULAR CYLINDRICAL
SHELLS**

CHAPTER 6

THEORETICAL PERFORMANCE OF CELLULAR-WALLED CIRCULAR CYLINDRICAL SHELLS

6.1 BUCKLING UNDER AXIAL COMPRESSION AND EXTERNAL PRESSURE

The buckling criterion for a cellular-walled circular cylindrical shell under combined loading of axial compression and external pressure, i.e., equation (4.43), was developed in Chapter Four. For the sake of convenience, we rewrite it here:

$$c_1 + c_2 \cdot c^2 = c_3 \cdot q_1 + c_4 \cdot q_2 \quad (6.1)$$

In which q_1, q_2 are non-dimensional external pressure and axial compression loads, respectively, and c^2 is a non-dimensional geometric parameter,

$$q_1 = \frac{pR}{K_1}, \quad q_2 = \frac{P}{K_1}, \quad c^2 = \frac{t^2}{12R^2} \quad (6.2)$$

The coefficients $c_1 \dots c_4$ of the equation (6.1) were presented in the equation (4.44) of Chapter Four. They are related to the shell wall properties ($E_1, E_2, E_{b1}, E_{b2}, \mu_1, \mu_2, G_{12}$) and buckling mode (m, n). The shell wall properties have been determined in Chapter Five. Denoting p_{cr} as the critical external pressure and P_{cr} as the critical axial compression load (N/M), and by letting $q_1=0$ and $q_2=0$ in eqn. (6.1), we get:

$$P = \frac{(c_1 + c_2 c^2) K_1}{c_4} \quad (6.3)$$

$$p = \frac{(c_1 + c_2 c^2) K_1}{c_3 R} \quad (6.4)$$

The above functions have two variables, m and n . Any pair of m, n presents a load. The critical buckling loads P_{cr} and p_{cr} are the minimum values of the functions (6.3) and (6.4). Dividing equation (6.1) by $p_{cr} P_{cr}$, we obtain:

$$\frac{c_1 + c_2 c^2}{p_{cr} P_{cr}} = \frac{c_3 R}{K_1 P_{cr}} R_p + \frac{c_4}{K_1 p_{cr}} R_x \quad (6.5)$$

where R_p and R_x are the notations introduced as

$$R_p = \frac{P}{P_{cr}} \quad R_x = \frac{p}{p_{cr}} \quad (6.6)$$

We rewrite the eqn. (6.5) simply as

$$Q_1 R_p + Q_2 R_x = Q \quad (6.7)$$

In the above, we have introduced the notations

$$\begin{aligned} Q_1 &= \frac{c_3 R}{K_1 P_{cr}} & Q_2 &= \frac{c_4}{K_1 p_{cr}} \\ Q &= \frac{c_1 + c_2 c^2}{p_{cr} P_{cr}} \end{aligned} \quad (6.8)$$

Like $c_1 \dots c_4$, the coefficients Q_1, Q_2 and Q are also related only to material properties and buckling mode, i.e. the numbers of half-

waves in the axial direction (m) and the numbers of waves in the circumferential direction (n). From eqn. (6.7), we get:

$$R_p = (Q - Q_2 R_x) / Q_1 \quad (6.9)$$

It can be seen that R_p is a function of R_x and the buckling mode m,n. When the variable R_x is given, the value of R_p depends only on the buckling mode (m,n). The minimum value of R_p can be determined by minimizing the above function (6.9) to m,n. To do that, a small program was written which was prepared by calling a procedure named POWELL from the suit of programs "Numerical Recipes" ⁹⁶. The program is listed in Appendix C.

From the formula (6.9), the buckling interaction curve may be easily constructed. Some examples are given in Figure (6.1) to Figure (6.10) for different shell geometries. In Figure 6.1, the geometry parameters represent a shell close the shells to be tested which is described as follows:

$$\begin{aligned} L &= 200\text{mm}, & R &= 76.80\text{mm}, & t &= 1.15\text{mm}, \\ 2r &= 0.70\text{mm}, & S &= 1.34\text{mm} \end{aligned}$$

and the non-dimensional geometric parameters can be calculated:

$$\begin{aligned} R/t &= 66.7826, & L/R &= 2.6040. \\ S/t &= 1.1652, & 2r/t &= 0.6087, \end{aligned}$$

In Figure 6.2 to Figure 6.9, geometric parameters were modified from that of Figure 6.1. The following conclusions may be drawn from the figures:

(the coupled numbers in figures are buckling mode m,n)

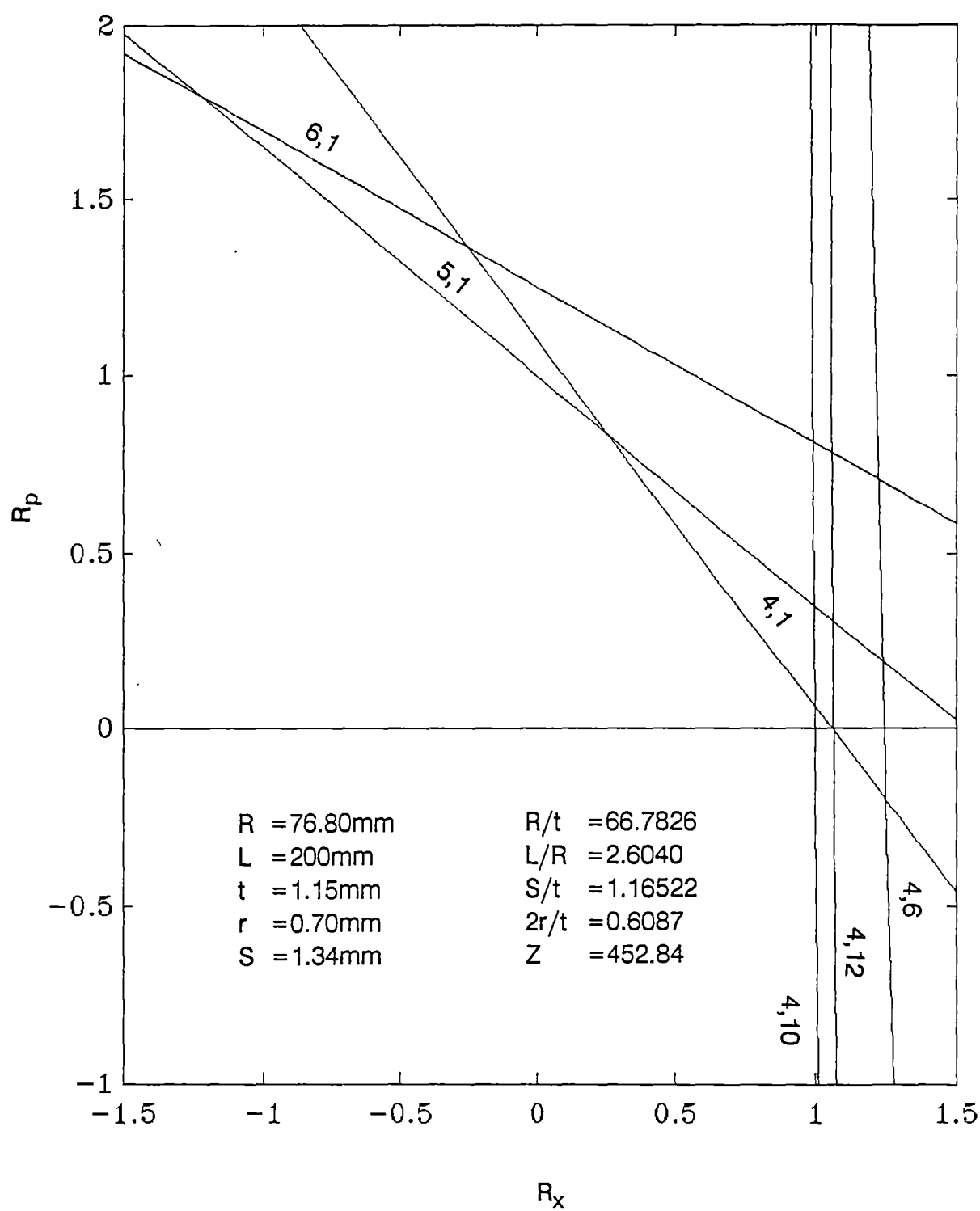


Figure 6.1
Buckling interaction curve

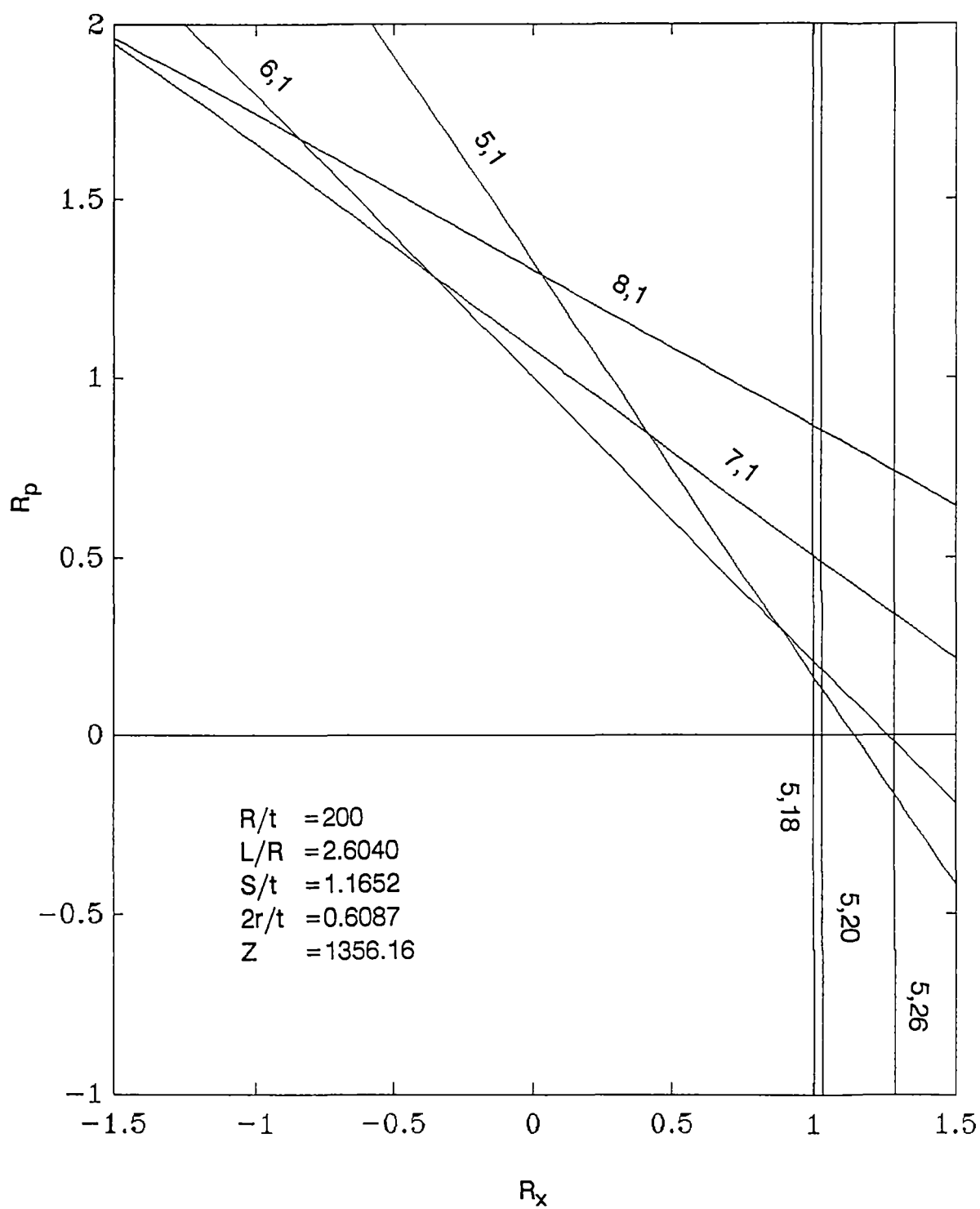


Figure 6.2
Buckling interaction curve

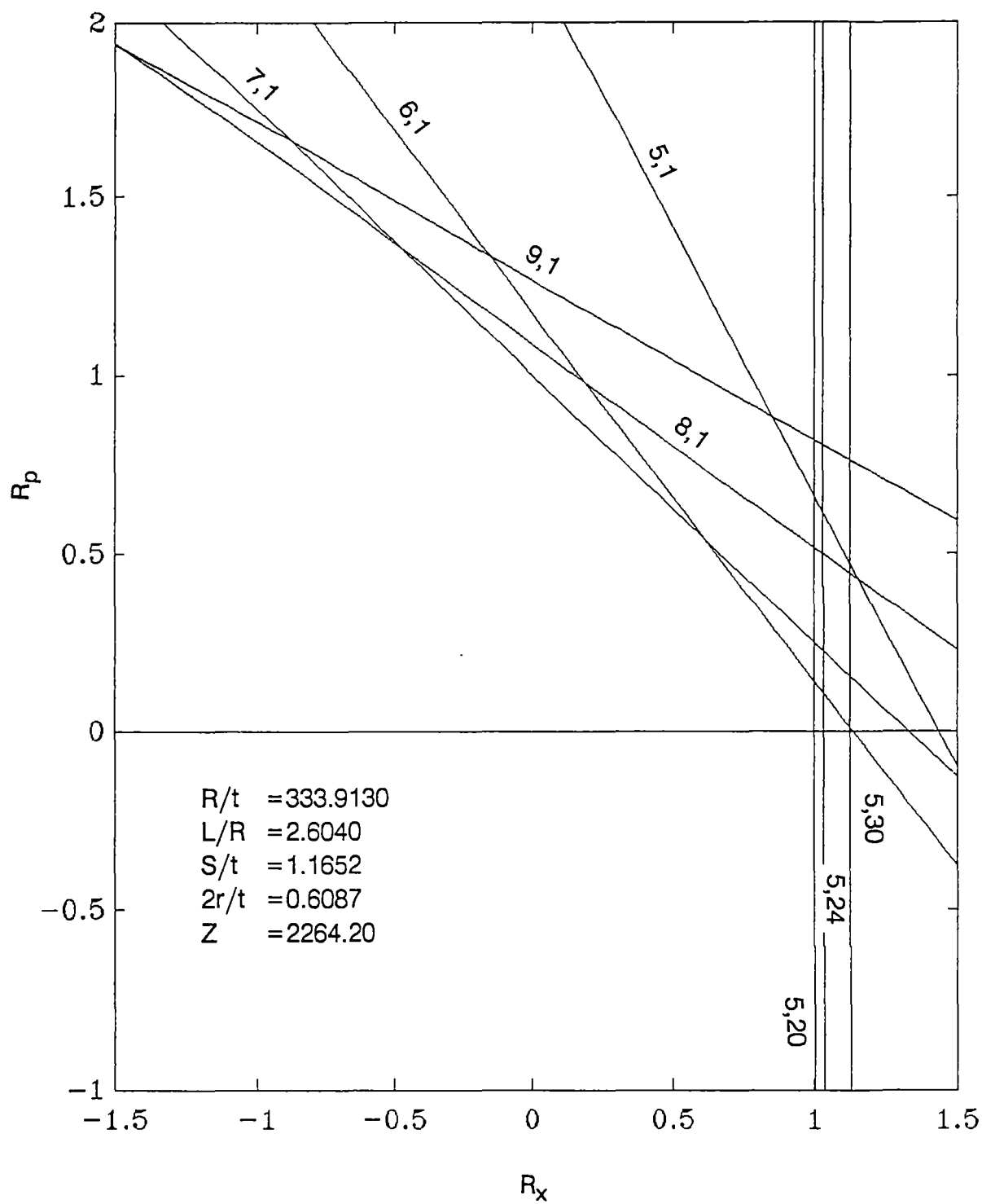


Figure 6.3
Buckling interaction curve

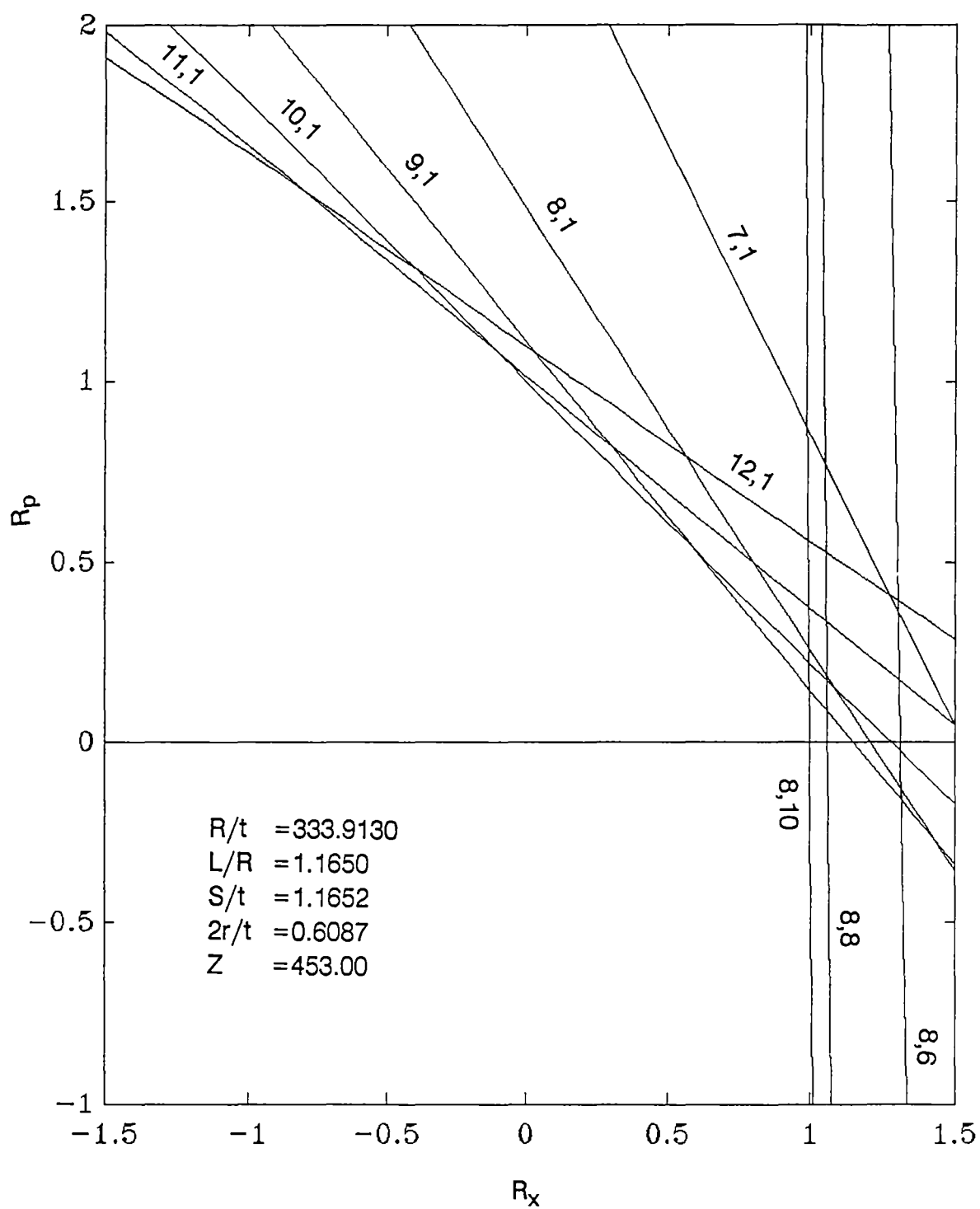


Figure 6.4
Buckling interaction curve

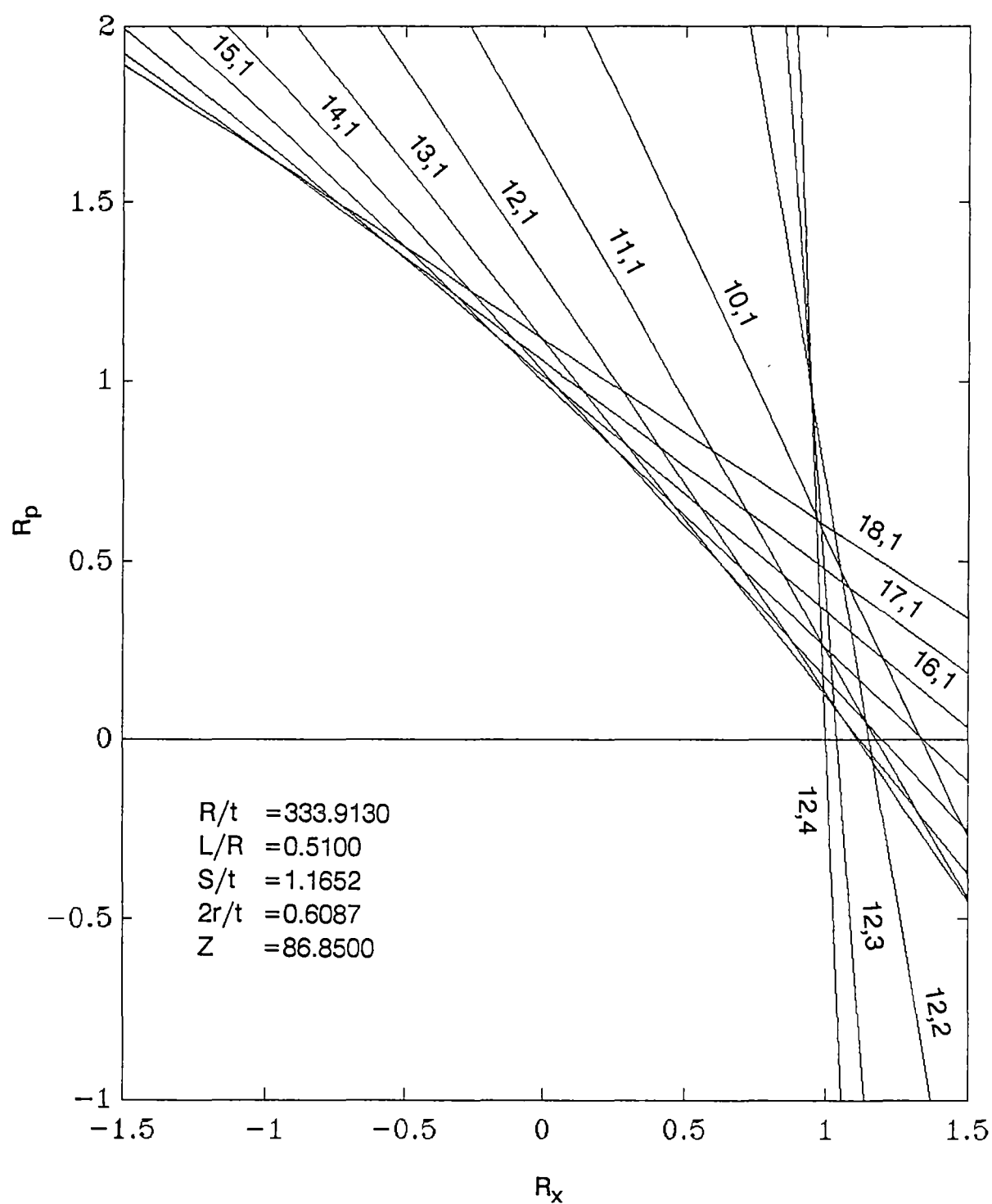


Figure 6.5
Buckling interaction curve

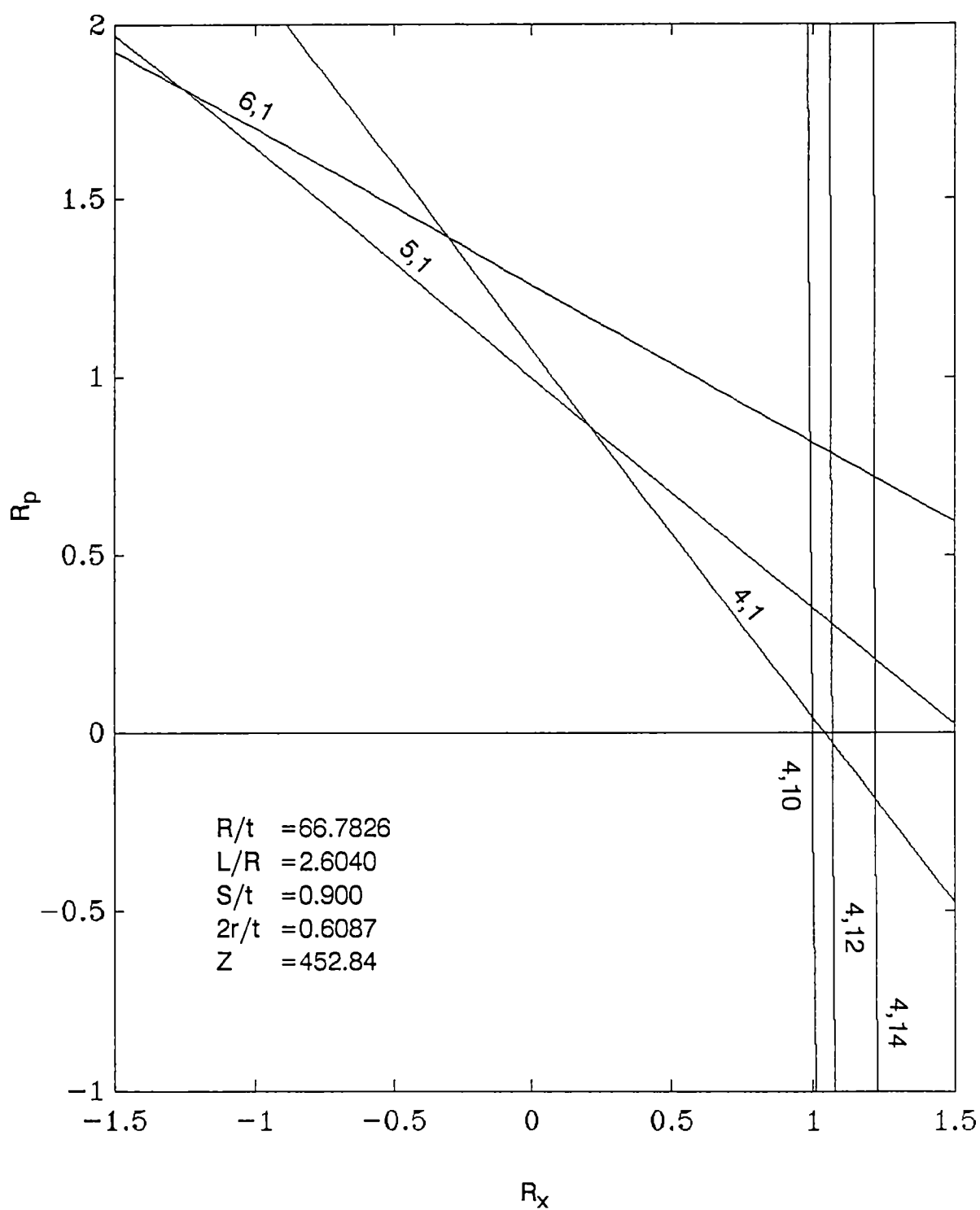


Figure 6.6
Buckling interaction curve

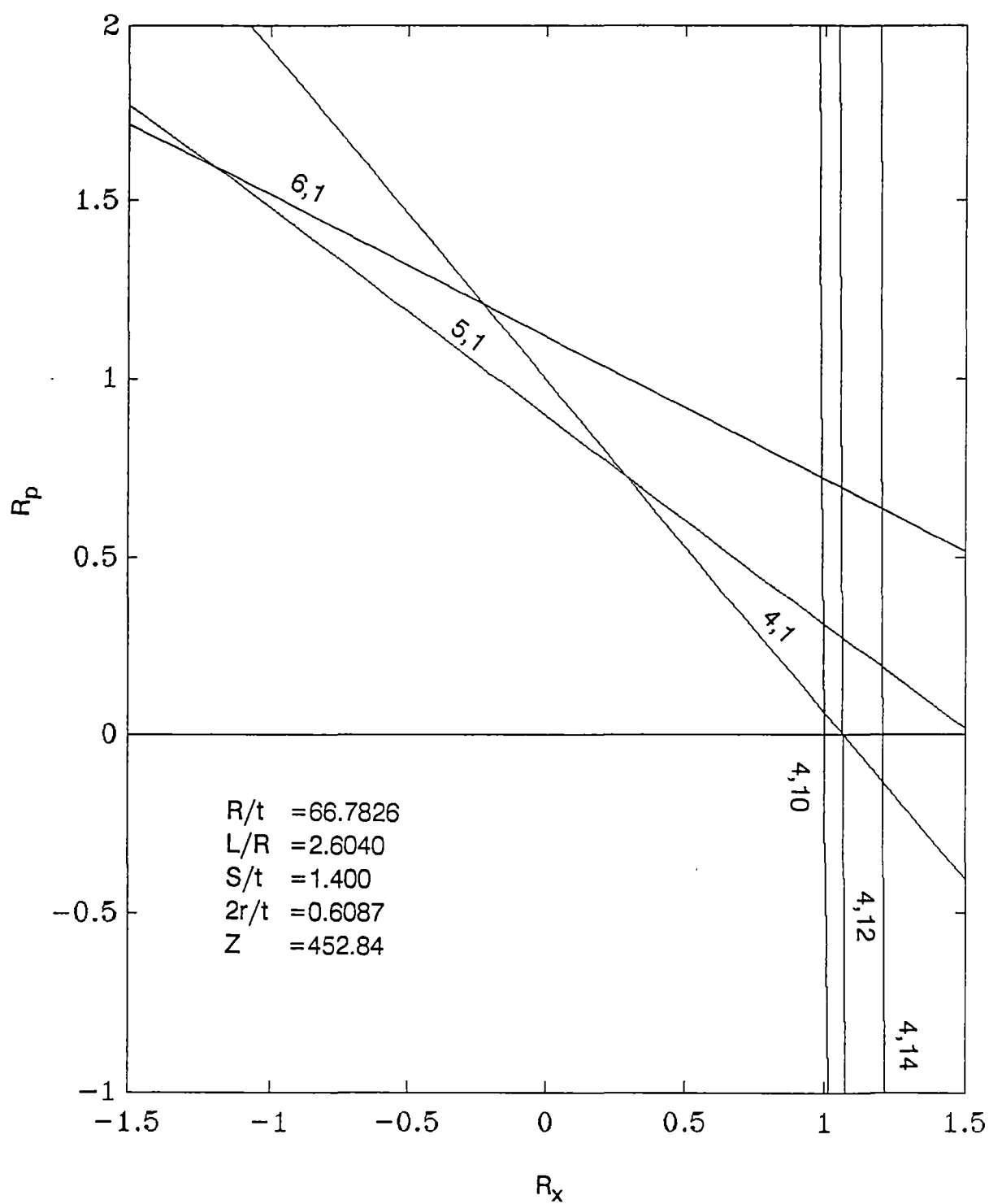


Figure 6.7
Buckling interaction curve

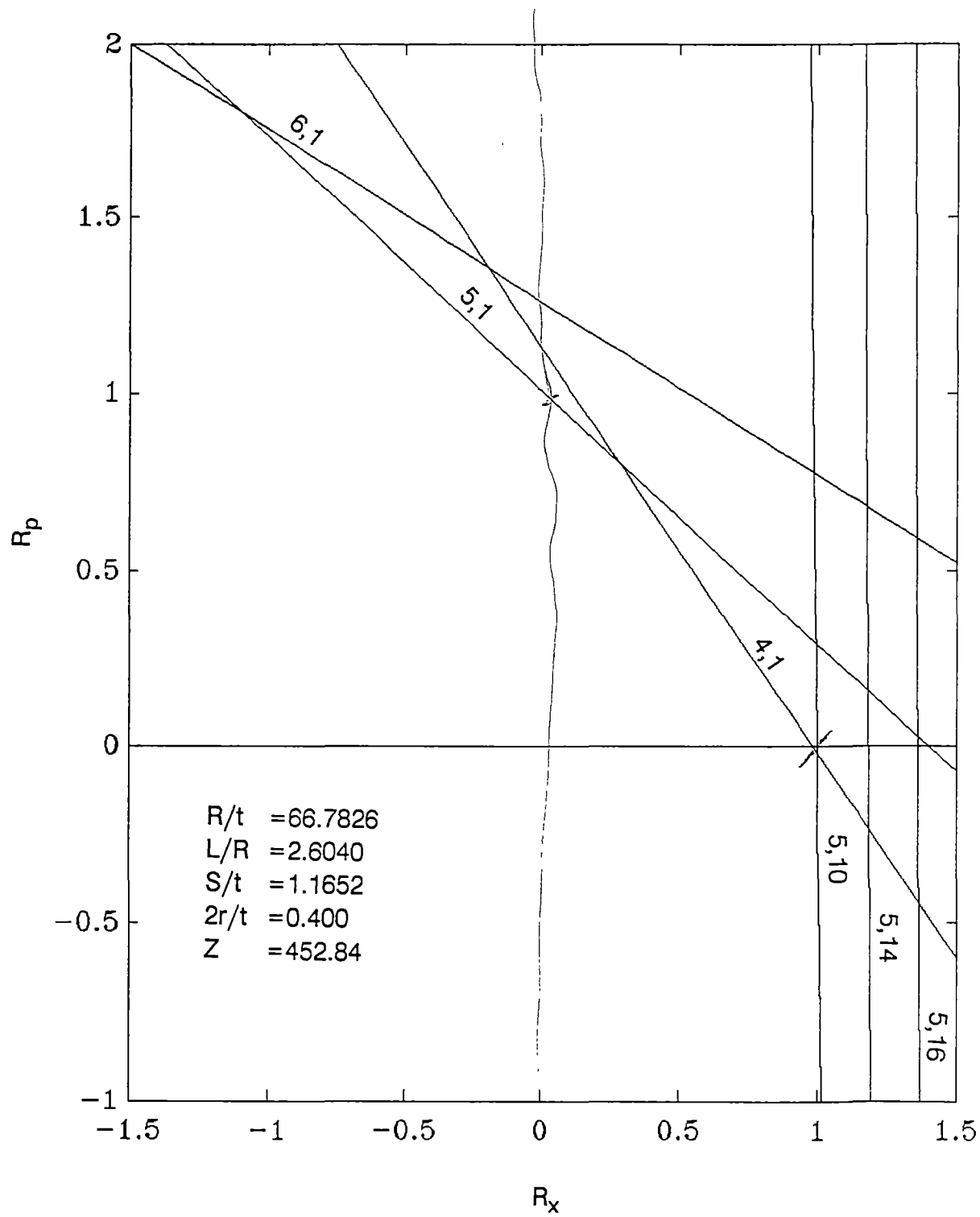


Figure 6.8
Buckling interaction curve

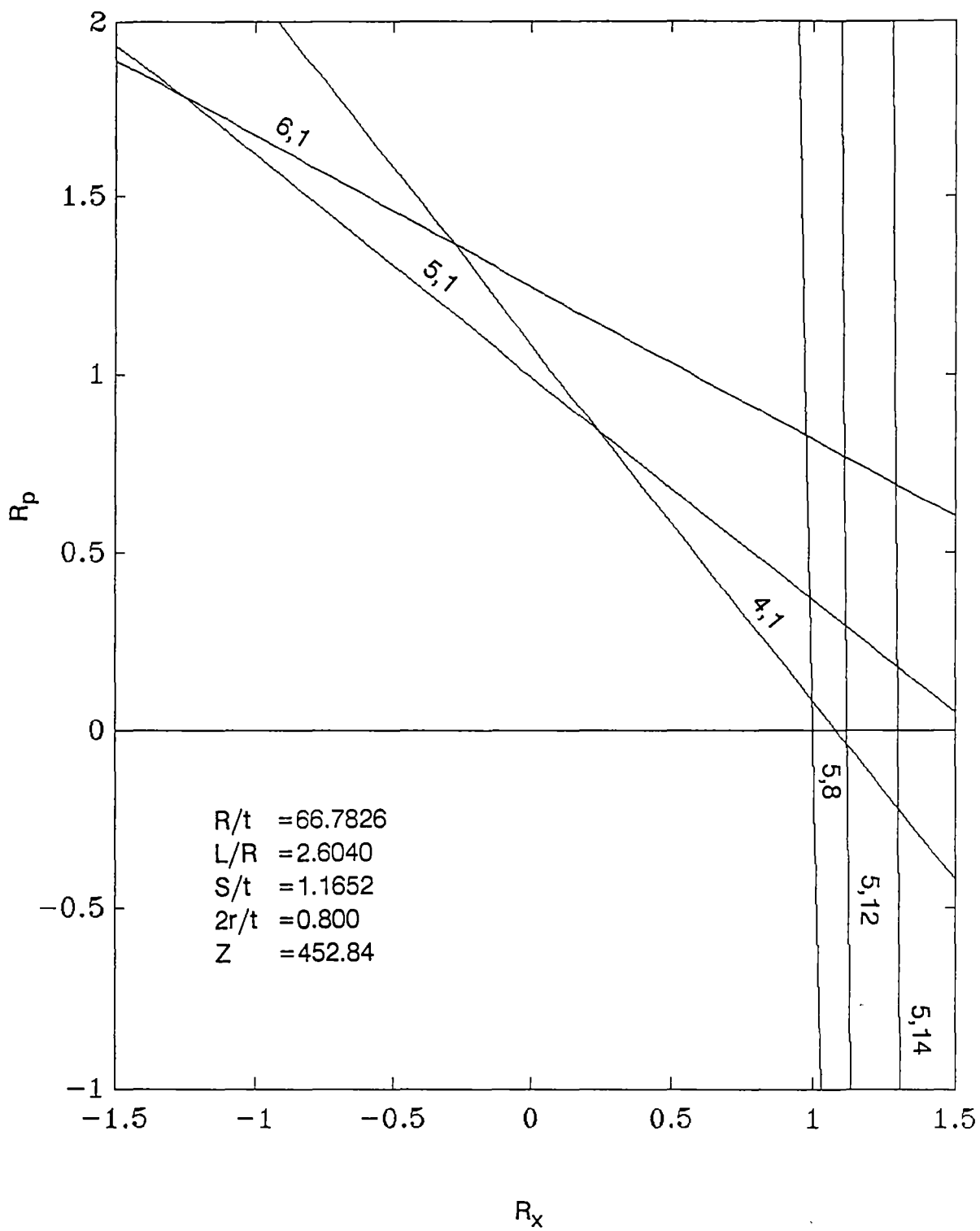


Figure 6.9
Buckling interaction curve

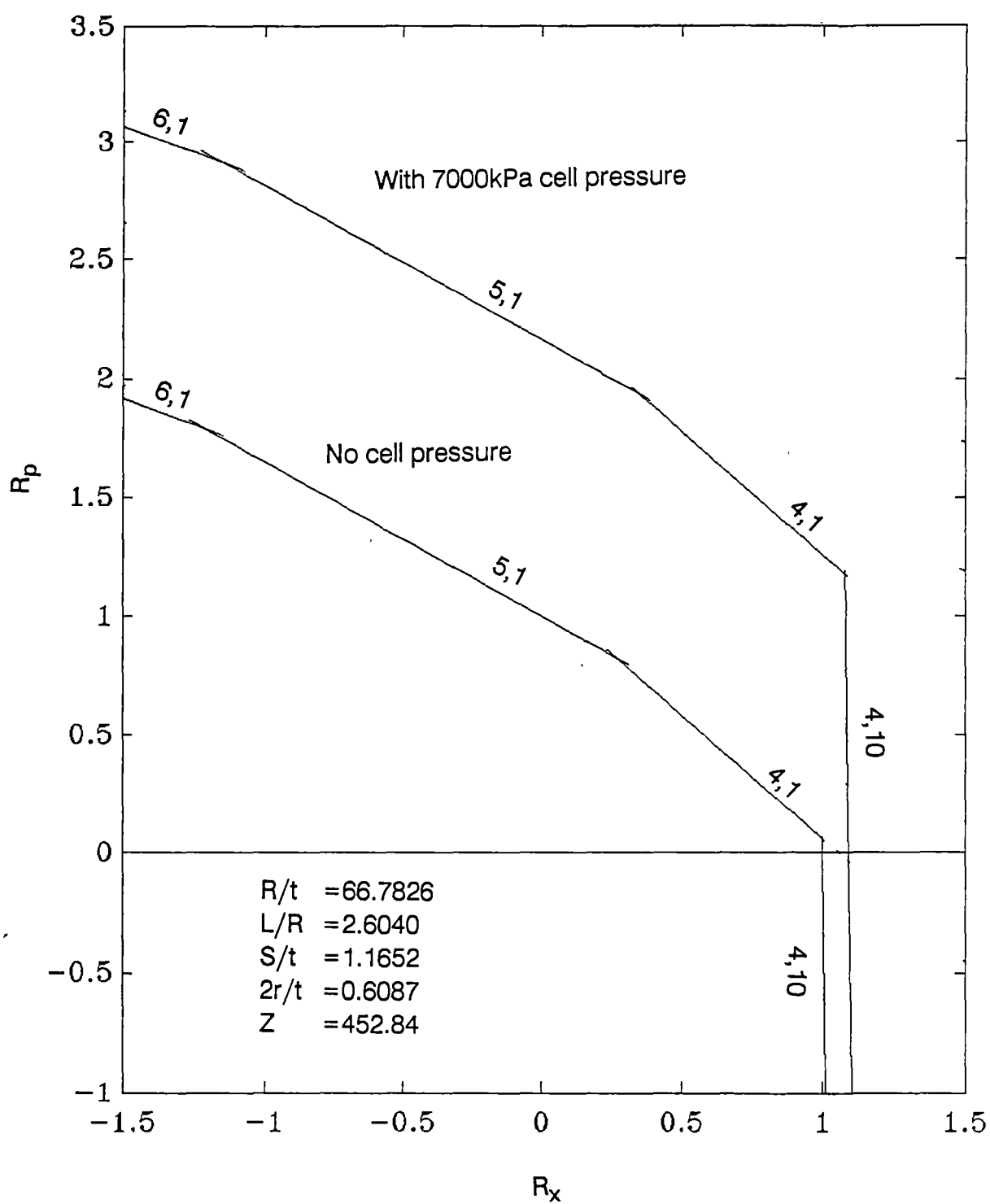


Figure 6.10
Buckling interaction curve with cell pressure

- a. Under axial compression load and external pressure, the limit of the stable region for the shell is a polygon consisting of sections of straight lines for different buckling modes.
- b. Although the load and the basic stress system have axial symmetry, the buckling mode does not ($m \neq 0$). The number of buckling modes increases as R_p increases and is higher for shorter or thinner shells.
- c. The buckling mode has a sudden change as curves approach $R_x = 1$, and the buckling curve becomes almost a straight line near the R_x axis. As a consequence, an internal pressure ($R_p < 0$) does not perceptibly increase the axial load R_x , while an axial tension ($R_x < 0$) increases considerably the resistance offered to an external pressure.
- d. The length parameter which is defined as $Z = L^2/(Rt)$, does not totally control the shell buckling mode. As can be seen, shells in Figure 6.1 and Figure 6.4 have the same length parameter $Z = 453$, but have very different buckling modes.
- e. The length of the shell has little effect on the axial buckling load, but it does affect buckling external pressure. As shell length decreases, the external buckling pressure increases.

6.2 BUCKLING INCLUDING CELL PRESSURE

The effect of cell pressure p_1 has been considered to be the same as that of an internal pressure p_2 , when the radial displacements of the midsurface produced by them were the same in both cases. In equation (5.4) of Chapter Five, the empirical relations were established linking the effect of the cell pressure to that of internal pressure

$$\frac{w_1}{w_2} = [a_3 + b_3 \left\{ \frac{2r}{t} \right\}] * \left\{ \frac{R}{t} \right\} d_3 * \left\{ \frac{S}{t} \right\} f_3 \quad (6.10)$$

where w_1, w_2 are radial displacements due to a unit cell pressure and unit internal pressure. r is the cell radius, R the shell radius, S the circumferential cell spacing and t the wall thickness. The coefficients a_3, b_3, d_3 and f_3 are as follows:

$$\begin{aligned} a_3 &= -0.0907 & b_3 &= 0.7861 \\ d_3 &= -1.0160 \\ f_3 &= -0.1790 - 2.6160 (2r/t) + 2.5240 (2r/t)^2 \end{aligned}$$

If we assume that the ends of the shell wall are sealed while applying cell pressure p_1 , then tension in the axial direction is created. The tension stress P' due to a cell pressure p_1 may be calculated:

$$P' = \frac{\pi r^2 p_1}{St}$$

$$= p_1 * \frac{\pi}{4} * (2r/t)^2 * (t/S) \quad (6.11)$$

and the equivalent internal pressure p' of pressure p_1 can be determined:

$$\begin{aligned} p' &= p_1 \frac{w_1}{w_2} \\ &= p_1 [a_3 + b_3 \{\frac{2r}{t}\}] * \{\frac{R}{t}\} d_3 * \{\frac{S}{t}\} f_3 \end{aligned} \quad (6.12)$$

From equation (6.7), the buckling condition of shells with cell pressure p_1 can be written as:

$$Q_1(R_p - \frac{p'}{p_{cr}}) + Q_2(R_x - \frac{P'}{P_{cr}}) = Q \quad (6.13)$$

The buckling interaction curve for the shell containing cell pressure may be generated from that of a shell without cell pressure: first moving the curve by $\frac{p'}{p_{cr}}$ along the R_p axis, then moving the curve by $\frac{P'}{P_{cr}}$ along the R_x axis. As demonstrated in Figure 6.10, as the cell pressure increases, the buckling interaction curve moves further outwards, and the critical buckling load increases.

To see the effects of cell pressure more clearly, buckling loads of a cellular-walled shell with and without cell pressure were calculated. An isotropic cylinder with the same mass as the cellular one, which has the same length and radius but

thinner in thickness was considered. Its critical buckling load also was calculated and compared.

6.3 CALCULATION OF BUCKLING LOADS

Taking the shell used in Figure 6.1 as an example, the geometric configurations of the shell are:

$$\begin{aligned} L &= 200\text{mm}, & R &= 76.80\text{mm}, & t &= 1.15\text{mm} \\ 2r &= 0.70\text{mm}, & S &= 1.34\text{mm} \end{aligned}$$

and the non-dimensional parameters:

$$\begin{aligned} R/t &= 66.7826, & L/R &= 2.6040, \\ S/t &= 1.1652, & 2r/t &= 0.6087 \end{aligned}$$

The shell is assumed to be made of epoxy: Young's modulus can be determined experimentally, here taking the average value of Young's modulus from a few tested shell models $E=3.45\text{GPa}$. The Poisson's ratio is given by $\mu=0.35$. By minimizing the equations (6.3) and (6.4) to m,n , critical buckling loads of both axial compression and external pressure were calculated as follows:

$$P_{cr}^* = 24.79 \text{ kPaM}, \quad p_{cr} = 30.74 \text{ kPa}$$

In order to make a comparison, let us now consider a solid-walled shell which has the same mass of the above cellular-

* P_{cr} is the force per unit length, the total axial compression load should be $2\pi R P_{cr}$.

walled shell by keeping the same length and radius of the shell but reducing the thickness:

$$L_s = 200 \text{ mm}, \quad R_s = 76.80 \text{ mm}, \quad t_s = 0.86 \text{ mm}$$

Its classical axial buckling load and external buckling pressure can be calculated by using equations (4.40) and (4.29) from Chapter Four:

$$P_{cl} = \frac{Et_s^2}{3\sqrt{1-\mu^2} R_s} = 20.48 \text{ kPaM},$$

$$P_{cl} = \frac{2\pi Et_s^2}{3\sqrt{6}(1-\mu^2)^{3/4} R_s L_s} \cdot \left(\frac{t_s}{R_s}\right)^{1/2} = 16.60 \text{ kPa}$$

Obviously, even without pressure applied within the cells, the cellular-walled shell has considerably higher buckling loads than a solid one with the same mass.

Now, let us apply the cell pressure $p_1 = 7,000 \text{ kPa}$ to the cellular-walled shell. The maximum cell pressure which could be applied to the epoxy cellular-walled shell model is $35,000 \text{ kPa}$. The equivalent internal pressure created by p_1 may be calculated from the equations (6.12).

$$p' = p_1 \frac{w_1}{w_2} = 34.08 \text{ kPa}$$

and the additional tension load from equation (6.11):

$$P' = \frac{\pi r^2 p_1}{S} = 2.01 \text{ kPaM}$$

By comparing the above calculations, the advantages of cellular-walled over solid walled shells are quite obvious. With no cell pressure applied, the buckling axial load of a cellular-walled shell with the same geometry as in Figure 5.1 can be increased by 21%, and the buckling external pressure by 85%. With one-fifth of the maximum potential cell pressure, the axial buckling compression load can be further increased by 8.1%, and the external buckling pressure can be more than doubled.

Therefore, from the theoretical performance of cellular-walled circular cylindrical shell demonstrated in this chapter, it may be concluded that by applying substantial pressure to the cells within the wall, the buckling load due to external pressure can be considerably increased and somewhat increased in axial compression. Thus the analysis supports the possibility of using this form of shell as an engineering structure, particularly in marine situations. To verify this theoretical prediction, appropriate tests on cellular-walled shell models had to be done. The experimental work including manufacture of the shell models, experiment set-up and the test results are presented in the next three chapters.

NOTATION

a_3, b_3, d_3 :	Coefficients, refer to equation 6.10
c^2 :	Non-dimensional geometric parameter, $c^2 = \frac{t^2}{12R^2}$
D :	Flexural rigidity of isotropic shells, $D = \frac{Et^3}{12(1-\mu_1\mu_2)}$
D_1, D_2 :	Bending stiffness, $D_1 = \frac{E_{b1}t^3}{12(1-\mu_1\mu_2)}$, $D_2 = \frac{E_{b2}t^3}{12(1-\mu_1\mu_2)}$
E_1, E_2 :	Young's moduli of extension in axial and circumferential respectively
E_{b1}, E_{b2} :	Young's moduli of bending in axial and circumferential respectively
G_{12} :	Shear modulus that characterized the change of angles between principal directions α and β
K_1, K_2 :	Extensional stiffness, $K_1 = \frac{E_1t}{1-\mu_1\mu_2}$, $K_2 = \frac{E_2t}{1-\mu_1\mu_2}$
k :	$= \frac{E_2}{E_1}$
k_1 :	$= \frac{G(1-\mu_1\mu_2)}{E_1}$
L :	Length of the cylindrical shell
m :	Number of waves around the shell circumferential
n :	Number of half-waves along the shell length
p :	Lateral pressure, positive inward
P :	Axial load, positive inward
p_c :	Cell pressure, pressure applied within the cells
P_{cl} :	Classical axial buckling load of an isotropic cylindrical shell

P_{cl} :	Classical external pressure buckling load of an isotropic cylindrical shell
P_{cr} :	Critical load of axial compression when no other load is applied
P_{cr} :	Critical load of external pressure when no other load is applied
q_1, q_2 :	Non-dimensional external pressure and axial compression load, respectively, $q_1 = \frac{pR}{K_1}$, $q_2 = \frac{P}{K_1}$
Q :	$(c_1 + c_2 c^2)/(p_{cr} P_{cr})$
Q_1 :	$c_3 R/(K_1 P_{cr})$
Q_2 :	$c_4/(K_1 P_{cr})$
r :	Radius of cells
R :	Shell radius
R_p :	External pressure ratio; ratio of external pressure present to critical external pressure when no other load is applied
R_x :	Axial compression load ratio; ratio of direct axial load present to critical axial compressive load when no other load is applied
S :	Cell spacing in the circumferential direction
t :	Thickness of shell wall
w_1, w_2 :	Midsurface radial displacements, due to unit cell pressure and unit lateral pressure
w_s :	Midsurface radial displacement of a solid walled shell due to unit lateral pressure

CHAPTER 7

**MANUFACTURE
OF
MODEL SHELLS**

CHAPTER 7

MANUFACTURE OF MODEL SHELLS

The model shells for the experimental work were manufactured by a spin-casting technique from an epoxy resin (Araldite LC 261 and LC 249, mass ratio 10:3). In order to make longitudinal cells in the shell wall, a special nylon line cage was used. The cage with nylon lines was first cast in the shell wall. After curing, the nylon lines were cut and removed from the shell wall, leaving a cellular-walled shell. The details of the manufacture process are described in the following sections.

7.1 NYLON LINE CAGE

The nylon line cage consisted of two brass rings with longitudinal spacers. Each of the rings held a number of short pegs near the circumference and a series of machined nicks on the external corner. Figure 7.1 shows an enlarged section of one of the rings before winding the lines. Nylon lines were wound around the pegs and guided by the nicks between the rings to form the cage. Nylon fishing lines* with 0.70mm diameter were used for the present work, which provide 22.6kg of guaranteed knot strength. It was noted that substantial forces were required to pull the nylon lines straight while winding. After the nylon lines were wound, a release agent (Klingerfon PTFE Lubricant) was sprayed evenly over

* Commercial fishing lines manufactured by Pro-Line.



Figure 7.1 Section of brass rings for nylon line cage

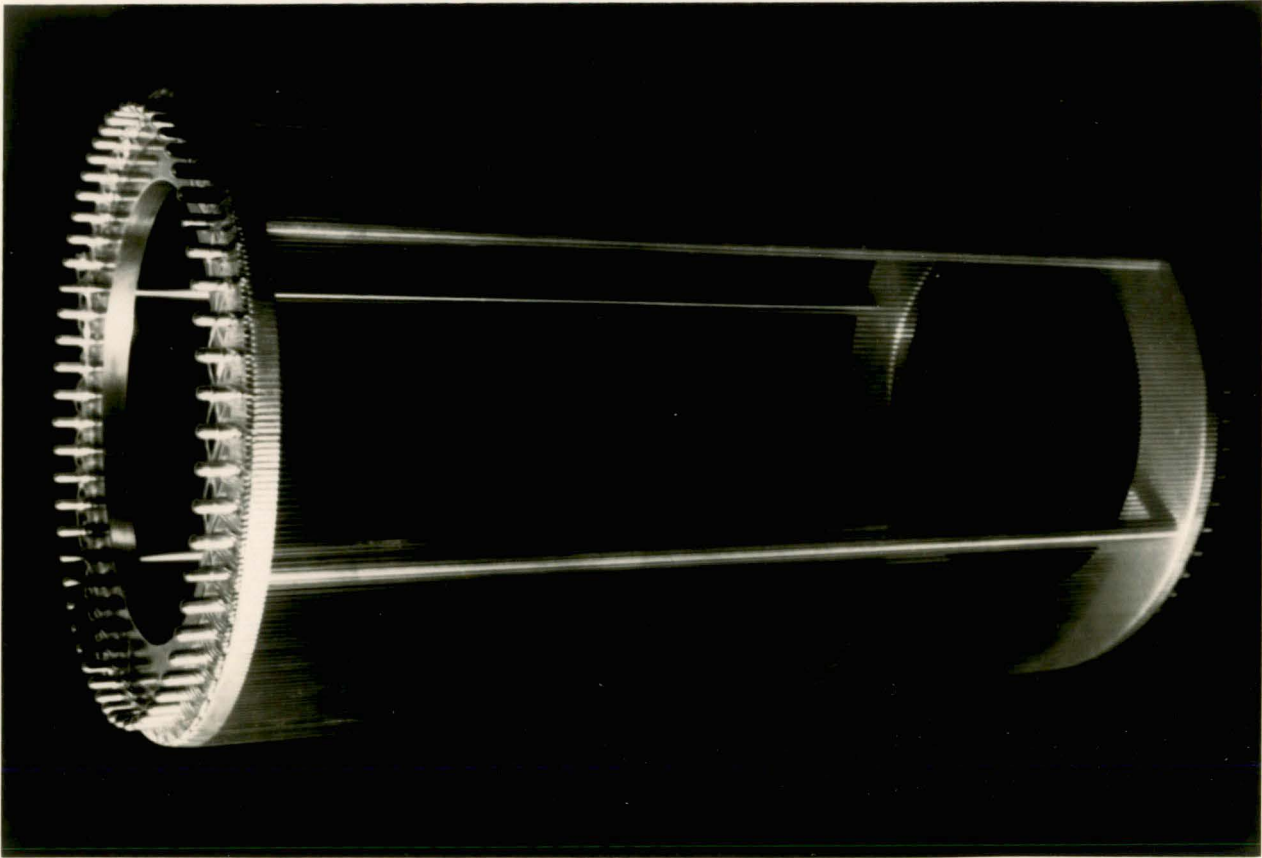


Figure 7.2 Cage of nylon line ready for insertion in former

the surface of the lines. Figure 7.2 shows a cage with nylon lines in place and ready for use.

7.2 MODEL SHELL CASTING

Once the nylon line cage was prepared, the shell was ready to be cast. A spin casting technique was used in this process, which was first developed by Tennyson⁶ who employed it successfully to manufacture near perfect shells with buckling loads close to the theoretical value. The equipment used in the present

work was developed by Foster⁴⁴, which is an improvement over that used by Tennyson.

Figure 7.3 shows this equipment. It consisted of a steel cylindrical former with an open end cantilevered from a rotating shaft which was supported on a rigid structure with bearing clearance minimised. The steel former was spun at a relatively high speed (about 1000rpm) approximately on the axis of the former. A liquid mixture of Dow Corning 20 Release Coating and Trichloroethylene (mass ratio 1:15) was applied as a release agent. An epoxy resin (Araldite LC 261 and LC 249, mass ratio 10:3) was warmed separately in an oven to about 65°C and placed in the spinning former to produce a true cylindrical surface concentric with the shaft axis. Once the liner was cured sufficiently, the liquid mixture of release agent was again poured into the former and allowed to dry for about one hour. The end cover of the former was removed and the previously prepared nylon line cage was inserted. Two strips of thin brass shim were inserted between the cage and the liner at both ends to help the cage concentric with the liner. When the cage was inserted in the former, epoxy was added to cover the nylon lines and cured while spinning. Any additional epoxy was added to the former to form a cylindrical shell of remarkably uniform shell thickness. Clearly the cage need to be well balanced or uneven wall thickness would result. This was achieved through care in machining the brass components and through a regular winding pattern for the nylon fishing line. To add the epoxy mix to the former, a hypodermic syringe was used so



Figure 7.3 Spin-casting equipment

that the volume of the epoxy could be measured accurately. During the first eight or nine hours of this casting process, a 2400 W domestic fan heater was used to heat the former to speed up the curing process and maintain low viscosity of the epoxy while being placed. The former was allowed to spin for another fifteen or sixteen hours without heating (making a total spinning time of the former about twenty-four hours). A typical spin-casting program is shown in Table 7.1. The shells manufactured by this technique had a reasonably smooth and highly reflective inner surface.

It should be pointed out that three different types of release agents have been used during the shell casting of this work. Initially, Klingerfon PTFE Lubricant was used as a release agent and was found to be the most effective one. However, this Klingerfon spray was soon banned for environmental reasons because it contained fluorocarbons. Since no other type of similar release agent was available, a new type of release agent was tried: a liquid mixture of Dow Corning 20 Release Coating and Trichloroethylene. Liquid mixtures with different compositions have been tested in making solid-walled shells. Satisfactory results were obtained when a mixture of Dow Corning 20 Release Coating and Trichloroethylene in a mass ratio of 1:15 was used between the liner and the shell. However, this mixture was less satisfactory on the surface of the fishing lines. Luckily, when the Klingerfon was banned, we still had four tins left: they were saved to use on the surface of the fishing lines. A small glass measuring cup was used to pour the liquid release agent mixture onto the surface of the

Table 7.1
A typical program of shell casting

Time	Program
9:00am	Former started spinning, fan heater turned on.
9:10am	Liquid release agent poured onto the former.
10:10am	Pre-warmed Araldite mixed then injected into the former with a syringe to form the liner.
11:10am	Release agent applied on the surface of the liner.
12:10pm	End cover of the former removed, previously prepared nylon line cage inserted.
12:30pm	Epoxy mixture injected to cover the nylon lines and to form the first layer of the shell.
2:00pm	Any additional epoxy mixture injected to form the rest of the shell.
6:00pm	Heater turned off; fan kept on. Spinning speed reduced to half.
9:00am (Next day)	Former stopped; fan turned off. The shell and cage were ready to be extracted.

liners. Later, a new spray release agent named Teflon TUF-E-COAT Lubricant which is considered ozone safe became available. However, this spray was found to decompose fairly readily when heated. Therefore, the fan heater had to be reduced to lower setting while casting, and a longer curing time was needed to ensure the shell cured sufficiently.

7.3 FINISHING WORK

After curing, the shell, the liner and the cage were removed from the former with the aid of an extractor. The extractor was basically a screw thread with a plate attached to it. The screw thread was positioned at the centre of the bottom of the former while the plate was placed against the end ring of the cage. The screw was turned slowly to extract the cage. After the cage was removed, the liner was carefully cut away. The fishing lines were cut at an angle of about 60 degrees to the line axis. Then the fishing lines were gently pulled through the shell wall. Because the shell wall is thin and fragile, great care had to be taken in cutting the fishing lines and pulling them through the shell wall. The thickness of the shell wall was only about 1.2 mm. After taking away the 0.7 mm diameter fishing line, the epoxy remaining outside of the hole is only about 0.25 mm in thickness. Any sudden pulling would easily break the shell wall or leave broken fishing line in the shell wall. After all of the fishing lines were pulled out, a cellular-walled shell remained. The edges of the shell were trimmed while the shell was positioned in a specially designed

circular support frame. The inner diameter of the frame was slightly larger than the outer diameter of the shell. Gummed paper was stuck on the surface of the shell so that the shell could be firmly positioned inside of the frame. A piercing saw was used to cut away the edges. In that manner, the edges were flat and cleanly cut. A photograph of part of a section of the cellular-walled cylindrical shell wall is shown in Figure 7.4. The cells were located at the centre of the middle surface of the shell within an accuracy of about 10% of the wall thickness.

Shells were consistently produced with an internal diameter of 153 mm, wall thickness 1.2 mm and length 245mm. These shells had 360 holes each of 0.7 mm diameter. The radius to thickness ratio for these shells ranged from 60 to 67. Thus they should be considered as relatively thick shells. Unfortunately, it does not appear possible to make model shells by our current technique (with the same former) with walls that are much thinner. The former used for the manufacture of the shells had a diameter of about 154 mm. The actual internal diameter of the shell was measured with vernier callipers before it was removed from the former. For measuring the wall thickness, the shell was placed on a machined steel mandrel to which a dial gauge with a resolution of 0.001 mm attached. By rotating the shell over the mandrel and moving it along the axis, thickness measurements were taken over the entire surface of the shell. Most of the shells manufactured had a thickness variation of less than 3.4%.

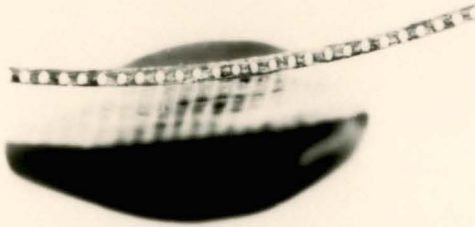


Figure 7.4 Section of shell wall

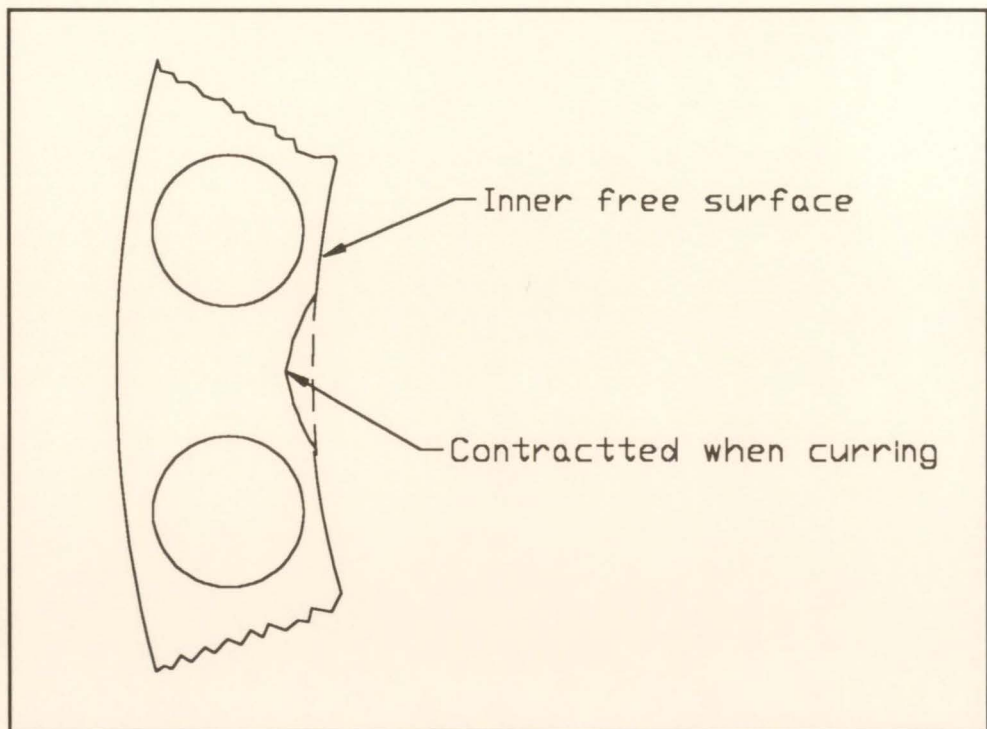


Figure 7.5 Ribbed appearance on free surface

Since the shells are cast with a free surface on the inside, they are internally reflective. However, epoxy contracts slightly on curing causing the thickness of the shell between the cells to be slightly less than that over the cells, as illustrated in Figure 7.5. This difference is not readily detected because it is small, but the inside surface has a ribbed appearance. The difference in thickness due to this contraction was of the order of 0.001mm.

CHAPTER 8

EXPERIMENTAL SET UP

CHAPTER 8

EXPERIMENTAL SET UP

Experimental data on the buckling behaviour of these cellular-walled cylindrical shells was obtained on a specially designed loading frame incorporating an optical examination system based on the reflective moire technique. The optical system and the loading frame used in the current work was that used by Foster^{38,97} and Krishnakumar³⁷ modified to accept the different type of shell. Pre-buckling data was digitised into a personal computer (PC), and was used to predict the axial critical load with the aid of a Southwell technique.

8.1 OPTICAL SYSTEM

Foster⁹⁷ developed a whole field optical technique for the measurement of radial deformations over the entire surface of a cylindrical shell. Central to the technique is the use of a conical mirror which provides a complete view of the internal surface of the shell. The reflection of a grid on the internal surface of the shell wall is viewed through this conical mirror, which essentially transforms the cylindrical surface of the shell to a plane surface (polar coordinates) to be photographed. Foster employed the inner surface of a large hollow cone to view the inside of the shell. He successfully obtained the whole field image of the surface of cylindrical shells. However, the manufacture of this hollow cone

and the polishing of its inner surface required considerable time and effort. The optical system was later modified by Krishnakumar³⁷ who replaced the large hollow cone by a compact solid conical mirror of shallow angle made from aluminium whose outer surface is used for reflecting the shell wall. The machining of the conical mirror and the polishing of its outer surface to mirror finish is relatively easy.

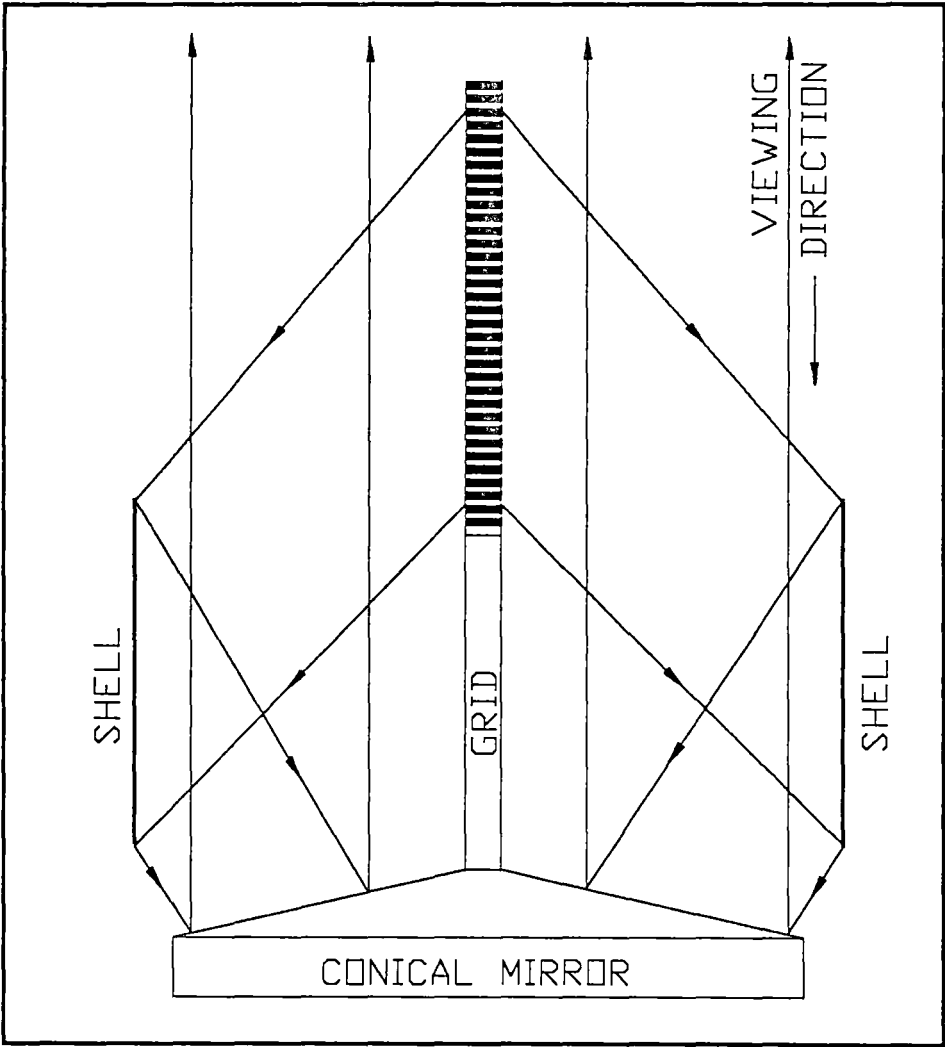


Figure 8.1 Schematic of optical system

The reflective inner surface of the shell models was used to monitor shell deformation. The optical system used in the current work for monitoring is shown in Figure 8.1. The image of a cylindrical grid placed at the centre along the shell axis was reflected from the shell wall and the conical mirror at the base of the shell, and viewed along the axis of the shell. Thus a whole field two dimensional image was obtained from which the deformations of the entire shell could be observed. Using the optical system, the image of the surface of cylindrical shells is formed in the conical mirror. It is photographed by a camera with a long focal length lens via a plane mirror positioned at the top and at a 45 degree angle to the grid axis.

Three types of grids were used in the present work, one axial grid (longitudinal lines) with a pitch of 2.50 mm, one circumferential grid consisting of equi-spaced circles with a pitch of 9.00 mm, and one spiral grid with equi-spaced helical lines having a normal pitch of 2.40 mm and a helix angle of 74.5 degrees. The grid with circumferential lines produces an image of concentric circles and the helical lines on the spiral grid appear as spiral lines on the image plane, while the axial grid is transformed to a set of radial lines. Deviations in line geometry represent changes in slope of the shell surface. The axial grid responds only to slope changes in the circumferential direction on the shell surface, while the circumferential grid is sensitive mainly to slope changes in the axial direction with some dependence on the circumferential slope. The spiral grid is sensitive to slope variations in both directions,

effectively combining the qualities of the other two. It is impossible to detect axisymmetric defects with the axial grid, difficult to see with the circumferential grid and usually easy to detect with the spiral grid. Thus all three grids are usually necessary for any investigation.

The grids were basically aluminium rods with black lines painted on a white background on the surface. All three grids were of the same size with a radius of 9.6 mm. The grid was illuminated by lights from a circular light source positioned on the top of the shell. The light source consisted of two circular arrays of lights (24 V vehicle tail lights). Each light was placed in an aluminium panel. The panels were so arranged that the grid was able to be illuminated by the light sources directly and the light was baffled so that it did not shine on the surface of the shell itself. This arrangement provided good contrast, making the grid lines sharp and clear in the photographs.

The camera* used to photograph the image reflected by the plane mirror at the top of the loading frame was placed at a distance of about 4300 mm from the conical mirror. The photographs were recorded on 35 mm black and white film** using a F16 aperture and an exposure period of 6 seconds. The negatives

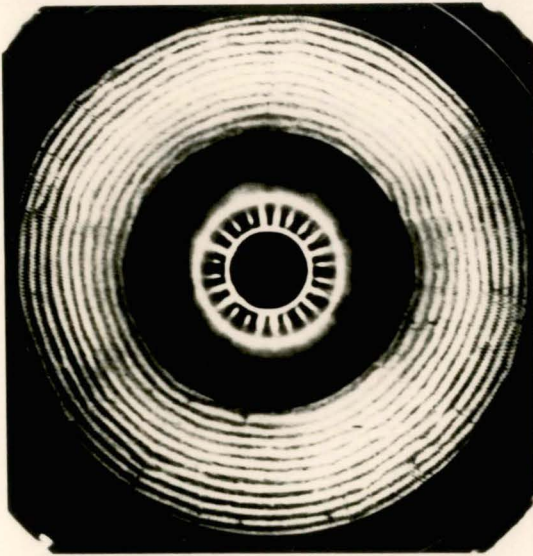
* Pentax K1000 camera (35 mm format) attached with a 400 mm focal length telephoto lens.

** Kodak Technical Pan 2415 (125 ASA).

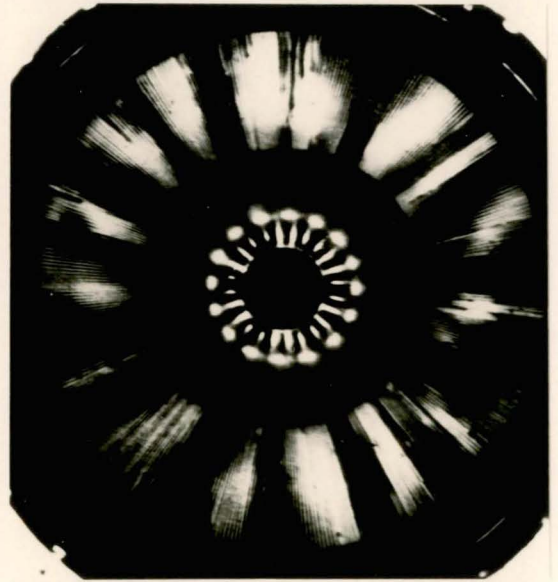
were developed for 5 minutes using Kodak D-19 developer and fixed for 5 minutes with Kodak X-ray fixer.

One of the main applications of the optical system was to record the presence of initial imperfections in the shell. The location as well as its size, i.e., that of the area on the shell surface covered by the imperfection, could be gauged from the extent of the distortion of the lines in the recorded photographs. Figure 8.2 shows typical images obtained with this system on an unloaded shell. None of the images shown in Figure 8.2 clearly shows the effect of the waviness on the internal surface, but careful examination of the image recorded with the spiral grid shows a certain fuzziness on the edge of the lines. This fuzziness is due to the surface waviness and is not normally observed in images of either of the other grids. At about the 3 o'clock position in the images made with the circumferential and spiral grids there is some deviation of the grid lines near the shell mid length. This line deviation is best seen in the image with the axial grid.

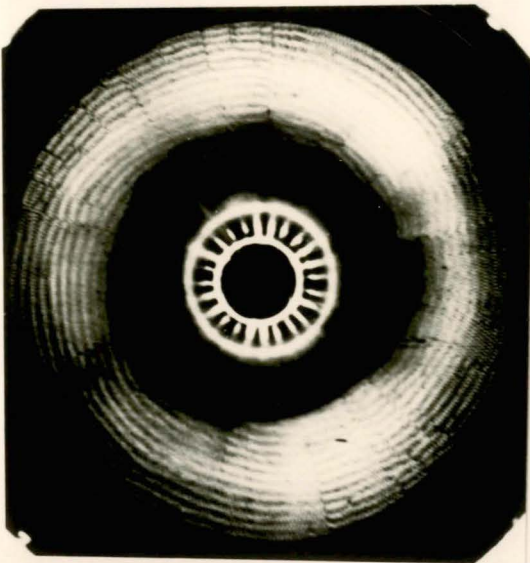
The optical system is remarkably sensitive to small deformations so that defect growth could be observed during the loading process. Because the shells are likely to shatter on buckling, collapse of the shells was avoided. The axial buckling loads were predicted by employing Southwell plots based on the axial pre-buckling loads and deformations which were logged in the PC during loading (the Southwell plot is described in Section 8.5). The maximum load applied to the shell was often very critical in



(a)



(b)



(c)

- (a) Circumferential grid lines
- (b) Axial grid lines
- (c) Spiral grid lines

Figure 8.2 Photographic images taken from unloaded shell

predicting the buckling load. Thus the optical system was found particularly useful in monitoring the growth of deformations and hence to determine when to stop loading.

On the few occasions when the shell buckled without shattering, the optical system was used to record the buckled patterns over the entire surface of the collapsed shell. From these photographs the number of facets around the circumference as well as the size and regularity of the facets could be observed. Figure 8.3 shows an image of a buckled shell taken with the circumferential grid in place. Clearly this shell had buckled into 5 circumferential lobes with one single tier of lobes at the centre of the shell's length.

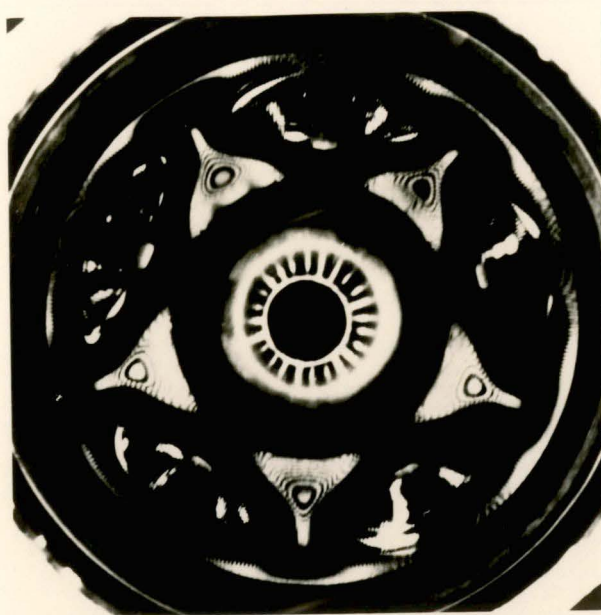


Figure 8.3 Photographic images of buckled shell

8.2 END RINGS

The design of the rings supporting the ends of the shell proved a challenging task. It was the most time consuming part of the testing programme. For quite a long time no progress in testing was possible because of failures of various forms of end rings. The failed end rings were made from steel. A typical design is that shown in Figure 8.4. The system consisted of two steel rings. The grooves were made in the steel rings to transfer the load between the epoxy and the ring. It was realized that the bond between epoxy and steel was not adequate to prevent leakage of pressurising fluid. A seal had to be placed under the epoxy filling. The seal was provided by a band of silicon sealant which was placed with the aid of a solvent to ensure it covered the complete width of the groove. The major problem with this system was one of obtaining a satisfactory seal to contain the relatively high pressure encountered within the cells. This seal had to be incorporated within the end rings providing the built in support. The system was abandoned when it was found that silicon sealant could not form an adequate seal. In fact when the silicon sealant was cured, it contracted leaving a void. Because the space between the shell wall and steel rings is very small, it was very difficult to observe the silicon sealant when it was cured.

The system that was successfully used in the shell models testing is shown in Figure 8.5. The system is basically made of three parts: the bottom steel ring and two epoxy rings. The steel

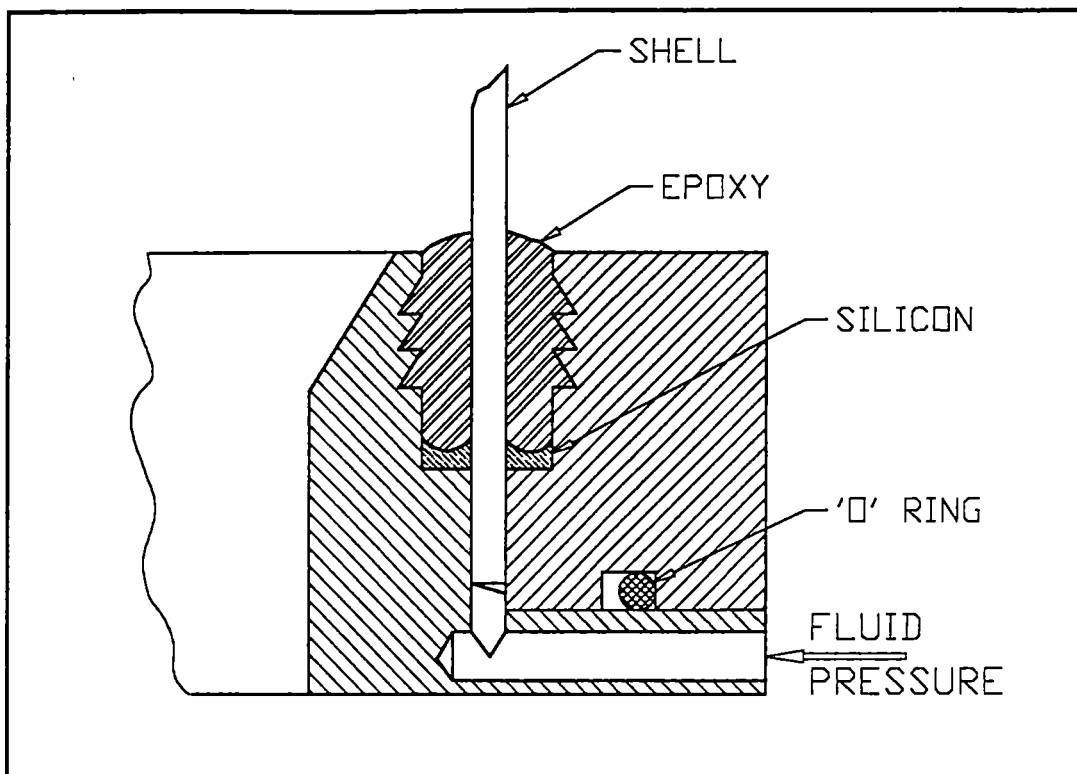


Figure 8.4 A typical design of failed end ring

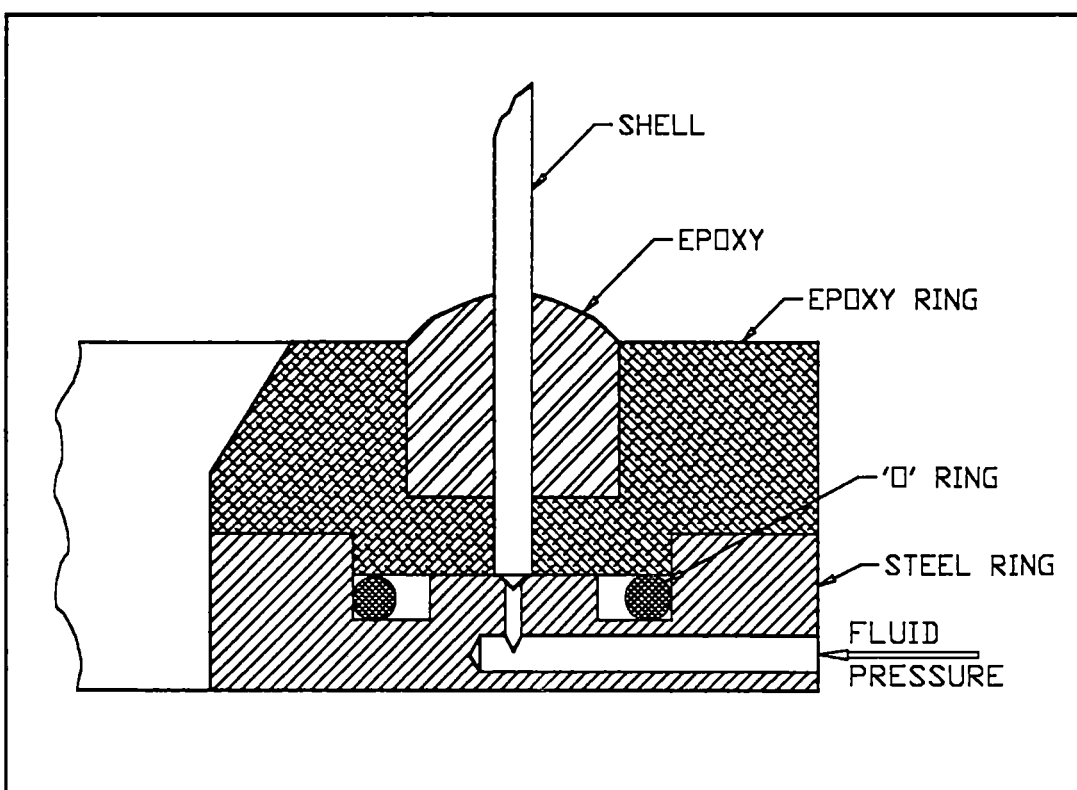


Figure 8.5 The end rings successfully used

ring and each of the two epoxy rings were connected by using a set of 24 equi-spaced locating screws. Between the steel ring and the epoxy rings, two "O" rings are used as mechanical seals. The steel ring contained a channel. Fluid was conveyed through the channel to the end of the shell, and this channel was connected to a hand operated hydraulic pump. Circular grooves between the shell wall and the rings were filled with the same LC 261/249 epoxy mixture as that used for making the shells. Thus once the epoxy in the grooves were cured, a unique epoxy ring was formed at the top part of the end rings. Since the three parts, i.e., the shell wall, epoxy rings and epoxy filling in the grooves were all made from epoxy, they bonded well to each other.

The epoxy rings were cast from comprising "west system" epoxy and micro-fibre cotton. The epoxy and the hardener were warmed to about 65° C and mixed thoroughly. Then the micro-fibre cotton was gradually added and mixed gently with the epoxy mix. The micro-fibre cotton was added to improve the stiffness of the end rings. As much of the micro-fibre cotton was added as the epoxy mixture could absorb. Small amounts of epoxy were used each time, to ensure the micro-fibre cotton was mixed thoroughly with the epoxy. The mixture of micro-fibre cotton and epoxy was poured into a previously prepared disk-shaped container. After the epoxy was properly cured, the disk was ready for machining. Complete curing of the epoxy required about 48 hours at room temperature.

In mounting the shells, the following procedure was adopted to ensure that the ends of the shell were parallel: with the end rings fitted, the shell was first placed upside down in the loading frame, i.e., with the top end ring resting on the base plate. After aligning the shell properly, the end of the shell was "potted" into this end ring using the epoxy mix. When the epoxy was cured the shell was inverted with the bottom end ring fitted. The cross-head of the loading frame was then lowered and the top end ring secured to the loading plate under the cross-head using a set of eight equi-spaced locating screws while the other end of the shell was sitting in the bottom end ring and located centrally over the conical mirror. The bottom end was then potted with the epoxy mix. It should be noted that complete curing of the epoxy in the end rings at room temperature normally required 48 hours. After the tests were completed on each shell, the epoxy from the grooves of the end rings was machined out, and they were further cleaned by hand before using them again on the next shell.

8.3 LOADING FRAME

The apparatus used for the testing is shown in Figure 8.6. The rigid loading frame had a capacity of 20 kN. The 30 mm thick cross-head was supported by a pair of linear bearing on two 32 mm diameter parallel guide rods fixed between the 30 mm thick base plate and the 20 mm thick top plate of the machine. The 32 mm diameter loading screws, having a 5 mm pitch, were driven by a hand wheel via a 50:1 worm reduction unit and a chain and

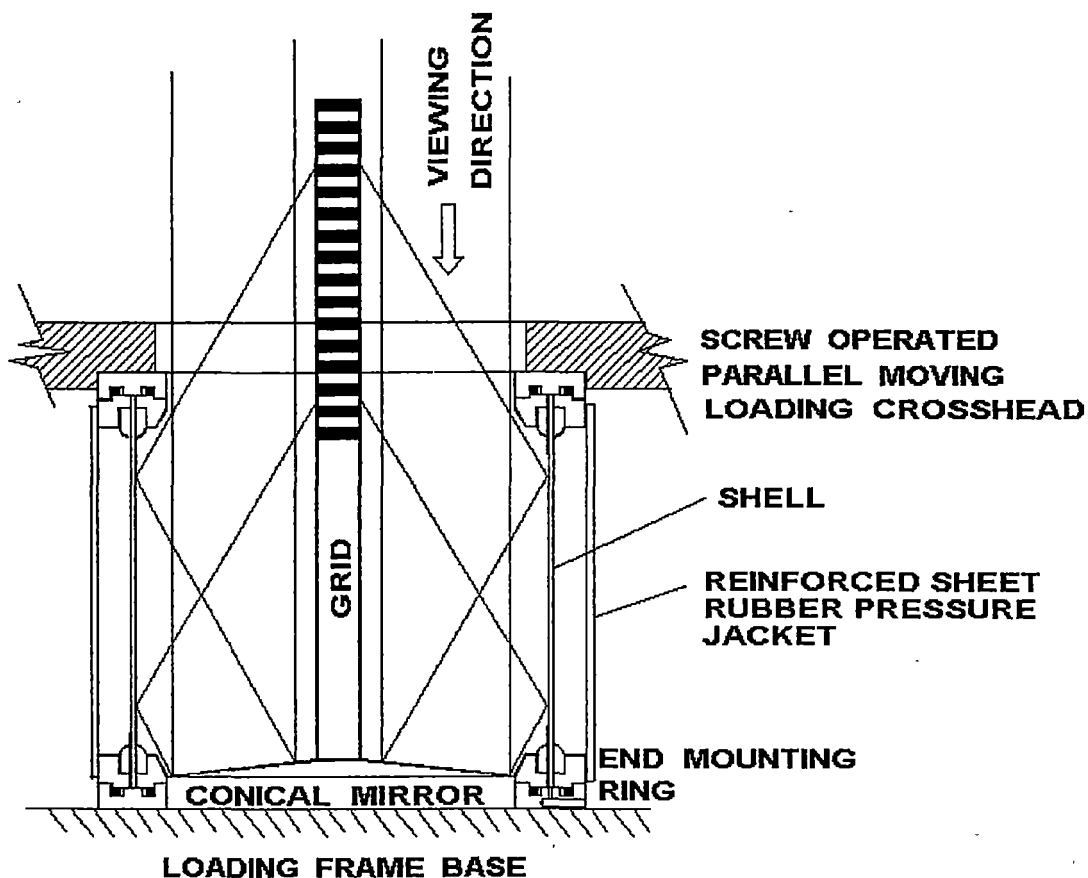


FIGURE 8.6A
GENERAL ARRANGEMENT OF SHELL TESTING FACILITY

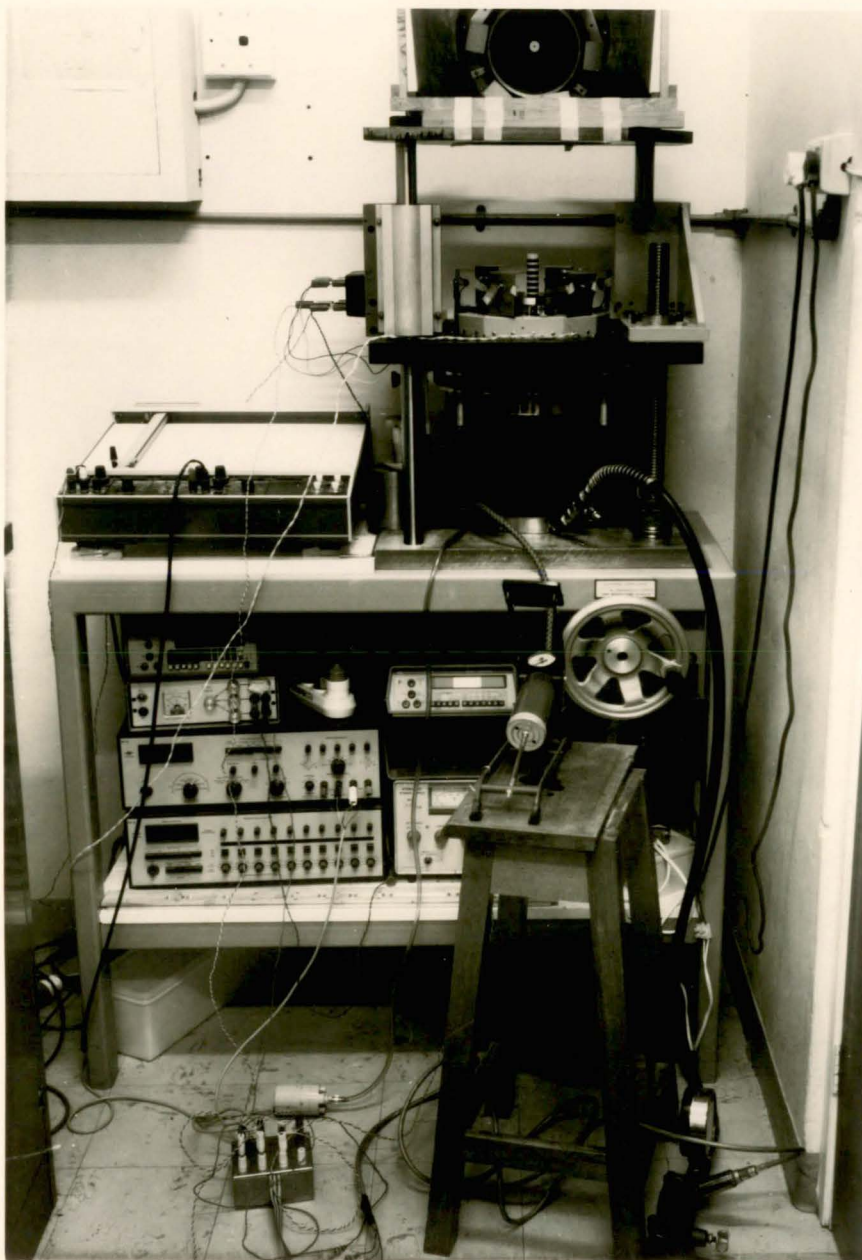


Figure 8.6 The experimental set-up

sprocket arrangement. A motor was also attached to the hand wheel for quicker movement in raising and lowering the cross-head. However the loading of the shells was always done manually by turning the hand wheel. The drive motor had insufficient torque to collapse a shell.

The calibration plot for the loading system is shown in Figure E1 of Appendix E. The system provided a sensitivity of 0.007147 N/Microstrain. The strains were measured on a strain indicator*. The end-shortening was measured by means of a Differential Current Displacement Transducer** with a sensitivity of 1.3115 V/mm. The calibration plot of the transducer is shown in Figure E2 of Appendix E. The outputs from the strain indicator and the Displacement Transducer were connected with an analog-to-digital interface in a PC to record the axial load and deformation during the tests. At the same time they were fed directly into an X-Y plotter*** to record load-deflection curves.

To apply external pressure to the shell, a rubber jacket was made and fitted over the end rings. A silicon sealant was used on the contact surface of the rubber jacket. A pair of hose clamp fasten the rubber jacket to the end rings. A hand operated air pump (car tyre pump) was used to supply the air pressure. A low

* Bruel and Kjaer, type 1526.

** Hewlett Packard, Model 7 DCDT-050, Serial No. EM.

*** Hewlett Packard, 7004 B.

range pressure transducer* with a sensitivity of 0.02488 Volt per kPa was used to record the external pressure in the analog-to-digital interface in the PC. The calibration plot of the external pressure transducer is shown in Figure E3 of Appendix F. A volt-meter was used to read the external pressure. Cell pressure was supplied via a channel in the end ring by a hand operated hydraulic pump attached to a high range pressure transducer**. The calibration plot of the cell pressure transducer is shown in Figure E4 of Appendix E. The sensitivity of the transducer is 2.9323E-04 Volt per kPa. A second volt-meter was used to read the cell pressure. Two stabilised power supplies*** were used for the two pressure transducers. All four channels, i.e., the axial compression load measured by the strain indicator, the end-shortening measured by the displacement transducers, external pressure and cell pressure measured by the pressure transducers were connected to the data logging interface in the PC.

8.4 DATA LOGGING

A Data Translation DT2818 analog-to-digital interface board in a 386PC was used for data logging. The DT2818 uses a simultaneous sample and holds a A/D converter, which permits up to four A/D channels to be sampled simultaneously. The A/D (analog to digital) converter system of the DT2818 has 12 bits of

* Robinson-Halpan, Model 155A-130G, Serial No. 973.
** M.B. Electronics, Model 510A, Serial No. 52516.
*** B.W.D Electronics, Model 272A.

resolution, i.e., 0.024% resolution. The calibration of the DT2818 board was done by inputting voltage to the four channels simultaneously. Calibration data from the DT2818 board is presented in Figure E5 of Appendix E. The sensitivity of DT2818 was found to be 204.1 per Volt.

The four channels used in the current work were designated as channel 0 to channel 3. The arrangement for data logging is shown in Table 8.1. Channel 0 was used for recording axial load (N). The axial load was initially measured by strain gauges attached on the load cell and recorded by a strain indicator in microstrain. The strain indicator was then connected to the DT2818 board. So the converting factor of Channel 0 had to be calculated by considering all the steps involved: N \leftrightarrow microstrain (load cell), microstrain \leftrightarrow Volts (strain indicator), Volts \leftrightarrow digit number (DT2818 board). The converting factor was found to be 16.67 N/Digit number. The calibration plot of the strain indicator is shown in Figure E.6 of Appendix E. Channel 1 was used for recording end shortening of the shell as measured by the displacement transducer. Channel 2 was used for recording cell pressure from the high range pressure transducer. Channel 3 was used for external pressure recording measured by the low range pressure transducer.

A small program was written to log data. The program allowed data collection in two modes, either by single point in which the sampling was manually controlled by hitting a key or

Table 8.1
The Arrangement for Data Logging

CHANN.	MEASURING	TRANSDUCER	CONVERSION FACTOR
0	Axial load (N)	Electric resistance strain gauge	16.67 (N/Digit num)
1	End shortening (mm)	Displacement transducer	3.73E-03 (mm/Digit num)
2	External pressure (kPa)	Low pressure transducer	0.1969 (kPa/Digit num)
3	Cell pressure (kPa)	High pressure transducer	16.71 (kPa/Digit num)

continuously in which the data was collected automatically at a specified rate. The program listing is presented in Appendix D. Data from the acquisition program was placed in a file, which was then transferred to the MAT-LAB software package⁹⁸, where the calibrations were applied and axial buckling loads were predicted using the Southwell plot.

8.5 SOUTHWELL PLOT

The Southwell plot⁹⁹ is a well known technique used to predict the collapse load of a structure. The technique was originally applied to columns, the load-deformation curve for a column is basically a rectangular hyperbola with an asymptote at the classical buckling load. The Southwell technique changes this hyperbola into a straight line by plotting the parameter CHANGE OF DEFORMATION/LOAD against DEFORMATION. For this technique any measurable deformation may be used, and the critical load is the reciprocal of the slope of the straight line. The intercept of the abscissa is often used as an estimate of the initial crookedness of the column. Theoretically, the Southwell's technique can be used with any other structure as long as the load-deformation curve is an hyperbola. However, no real structure will behave in this manner. Even columns exhibit a stiffening beyond the Euler load when very large deformations are encountered. The technique works for columns because when these large deformations are ignored the load-deformation curve is very nearly hyperbolic. Foster¹⁰⁰ investigated the validity of Southwell's technique on buckling of stringer stiffened epoxy cylindrical shells. He employed the technique to estimate buckling loads of non-linear collapse of cylindrical shells, the estimated were compared with the actual collapsed loads and satisfactory results was obtained. His study shown that non-linear effects associated with large deformations in shells can be tolerated. For the cellular-walled shells tested in this study, it was found that provided only those deformations are considered which are associated with loads considerably less than the buckling load, the load-deformation

curve is sufficiently close to hyperbolic to render the technique satisfactory.

The use of a Southwell plot is illustrated in Figure 8.7. The solid straight lines represent the behaviour of a perfect elastic cylindrical shell, while the thinner curve represents the behaviour of a real shell, i.e., a shell with defects. P and δ are axial load and axial deformation of the shell respectively, P_c is the classical buckling load of the perfect elastic cylindrical shell and $d\delta$ is the difference of the deformations. The expression of $d\delta$ is

$$d\delta = \frac{P/P_c}{1-P/P_c} a, \quad (8.1)$$

where a is the initial crookedness. From equation (8.1), we obtain

$$\frac{d\delta}{P} = \frac{1}{P_c} d\delta + \frac{a}{P_c} \quad (8.2)$$

Equation (8.2) represents a straight line in the coordinates of $d\delta$ - $d\delta/P$. The plot shown in Figure 8.8 is known as the Southwell plot on measured axial deformation.

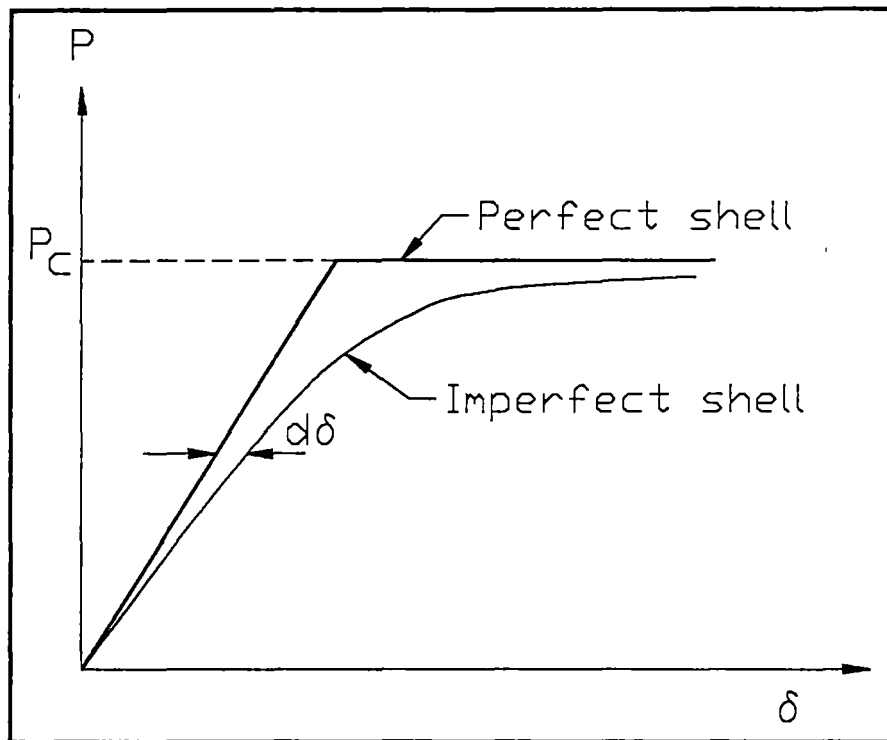


Figure 8.7 A typical load-deformation curve

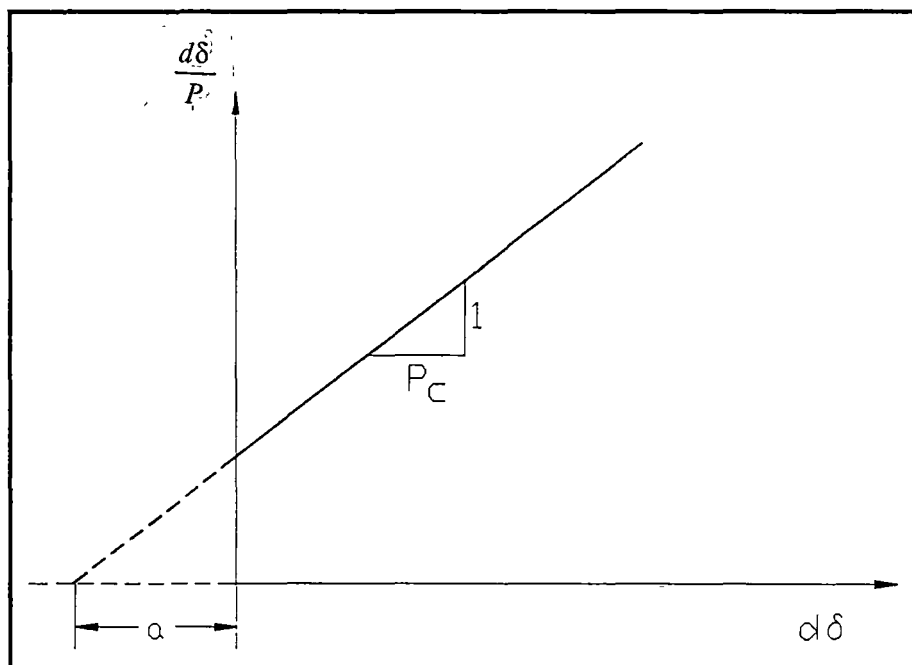


Figure 8.8 Southwell plot

CHAPTER 9

MEASURED BEHAVIOUR

OF

MODEL SHELLS

CHAPTER 9

MEASURED BEHAVIOUR OF MODEL SHELLS

The geometric data of the shells tested are presented in Table 9.1. The radius to thickness ratio for these shells ranged between 60 and 67. Thus they should be considered as relatively thick shells. Unfortunately, with our current technique and equipment, it does not appear possible to make the walls of model shells much thinner. Each shell had the same cell diameter of 0.70 mm. However, shells 6 to 14 had 400 cells each and the rest of the shells had only 360 cells each. Five model shells (1-5) were tested under combined loading of axial compression, external pressure and cell pressure with new end rings as shown in Figure 8.5. Twelve model shells (6-17) were tested with the initial design end rings as shown in Figure 8.4. Because the end rings leaked at very low pressures, only axial compression buckling loads were measured. However, all shells were mounted into end-rings as described in Chapter 8, so the boundary conditions were considered to be built-in support.

A full set of experimental results (including axial compression, external pressure and cell pressure at three cell pressures - 0 kPa, 25.38 kPa and 50.76 kPa) was obtained from shells 1 to 5.

Table 9.1
Geometric Data of Shells Tested

Shell No.	R mm	t mm	Max. $\Delta t/t$	L mm	2r mm	R/t	2r/t	S/t	L/R
1	76.68	1.25	0.8%	200	0.70	61.34	0.56	1.07	2.61
2	76.72	1.19	7.5%	200	0.70	63.47	0.59	1.12	2.61
3	76.67	1.20	3.4%	160	0.70	63.89	0.58	1.12	2.15
4	76.69	1.20	2.1%	200	0.70	63.91	0.58	1.12	2.61
5	76.67	1.28	2.3%	200	0.70	59.90	0.55	1.05	2.61
6	76.73	1.25	1.0%	125	0.70	61.40	0.56	0.97	1.63
7	76.83	1.15	1.1%	125	0.70	66.81	0.61	1.05	1.63
8	76.78	1.15	1.1%	125	0.70	66.77	0.61	1.05	1.63
9	76.83	1.15	1.1%	125	0.70	66.81	0.61	1.05	1.63
10	76.77	1.16	1.1%	125	0.70	66.18	0.60	1.04	1.63
11	76.77	1.16	1.2%	125	0.70	66.18	0.60	1.04	1.63
12	76.60	1.23	2.4%	125	0.70	62.28	0.57	0.98	1.63
13	76.54	1.23	2.4%	125	0.70	62.23	0.57	0.98	1.63
14	76.70	1.20	2.0%	125	0.70	63.92	0.58	1.00	1.63
15	76.69	1.22	2.5%	200	0.70	62.86	0.57	1.10	2.61
16	76.69	1.23	2.4%	200	0.70	62.35	0.57	1.09	2.61
17	76.71	1.28	1.6%	200	0.70	60.88	0.56	1.06	2.61

9.1 TEST PROCEDURE

The test procedure used can be summarized as follows:

- (1) The shell was set up in the testing system (including loading frame, optical system, end-rings and data logging which were described in Chapter 8).
- (2) Three photographs of the shell image (with axial, circumferential and spiral oriented grids) were taken to record any initial imperfections of the unloaded shell.
- (3) Initial data from all four channels were logged into the PC (single point mode).
- (4) A cell pressure followed by an external pressure was applied.
- (5) Data was logged again using single point mode to record the initial pressures.
- (6) Axial load on the shell was continuously increased and the data was logged into the PC. At the same time, the image of the shell was being observed to monitor the development of deformations. Axial load was increased until the pre-cursor to the buckling pattern appeared.
- (7) Another three photographs of the image were taken to record the final deformation pattern.

Because epoxy creeps under compression load, it was necessary that each test be conducted fairly quickly. Eight hours were allowed between successive tests permitting the shell to recover since immediate retesting would give a lower buckling load. This recovery period appeared to be adequate as the test results

were always repeatable after this interval and no permanent damage was detected.

After the data logging was complete, the data was transferred to the MAT-LAB software package for analysis, and the axial buckling load was predicted by the Southwell technique. The series of transformations applied with MAT-LAB is listed in Appendix F. Figure 9.1 shows a typical load-deformation curve for a shell with very small initial defects (shell 1, without cell-pressure and external-pressure). The asymptote to the load-deformation curve was determined by linear regression on the selected points marked with "o". The slope* of the asymptote was used to determine Young's modulus for the shell. At low loading, the shell may not have been fully supported by the end rings or the end rings may not have been completely in contact with the base, so the slope of that part of the curve is much smaller. Those points were ignored in deriving the Southwell plot. The point at which the shell became fully supported was estimated, and the points beyond that were used to fit a straight line in the Southwell plot as shown in Figure 9.2. This line did not pass through the origin but had an intercept on the deformation axis of about 6.0×10^{-6} m, which indicates the magnitude of the shell axial deformation defect.

It must be pointed out that the measured Young's modulus of the shell depends on the number of points (with "o")

* Deviations from the fitted straight line were mainly due to vibration of the displacement transducer.

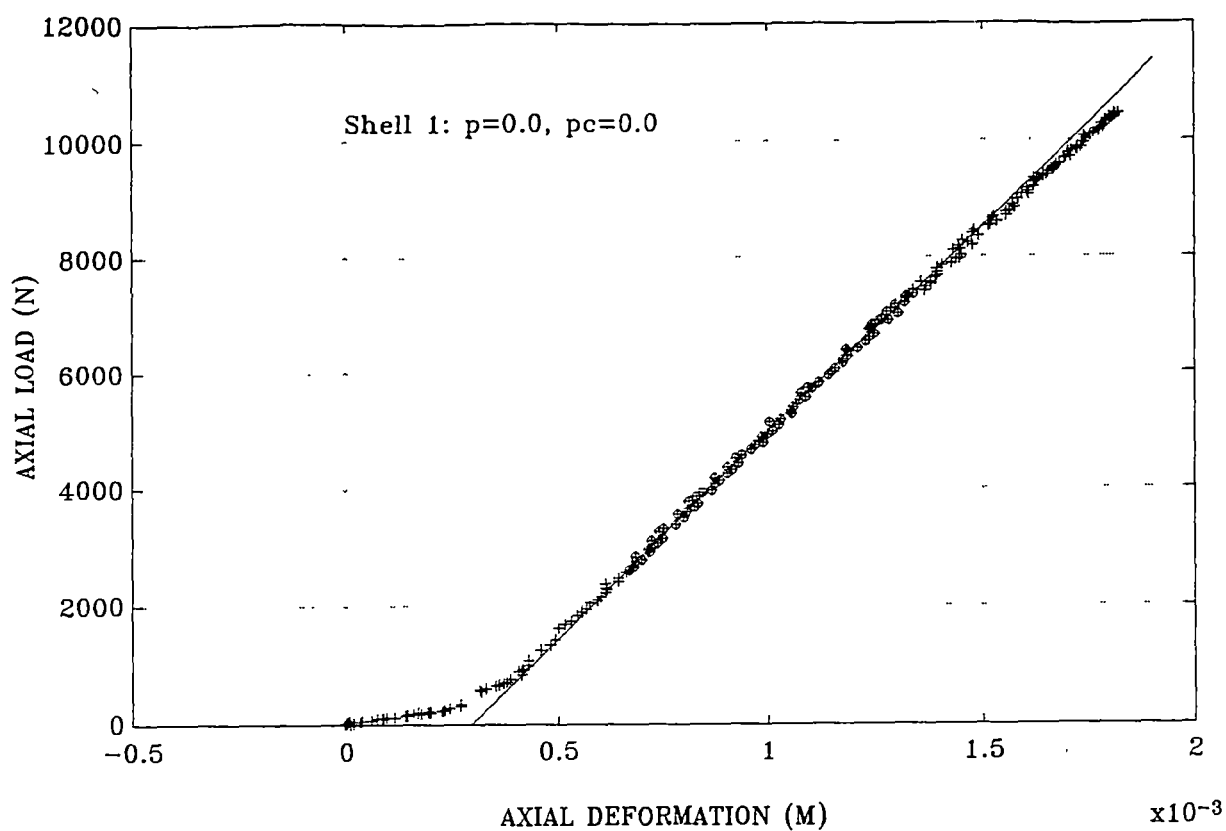


Figure 9.1 Load-deformation curve

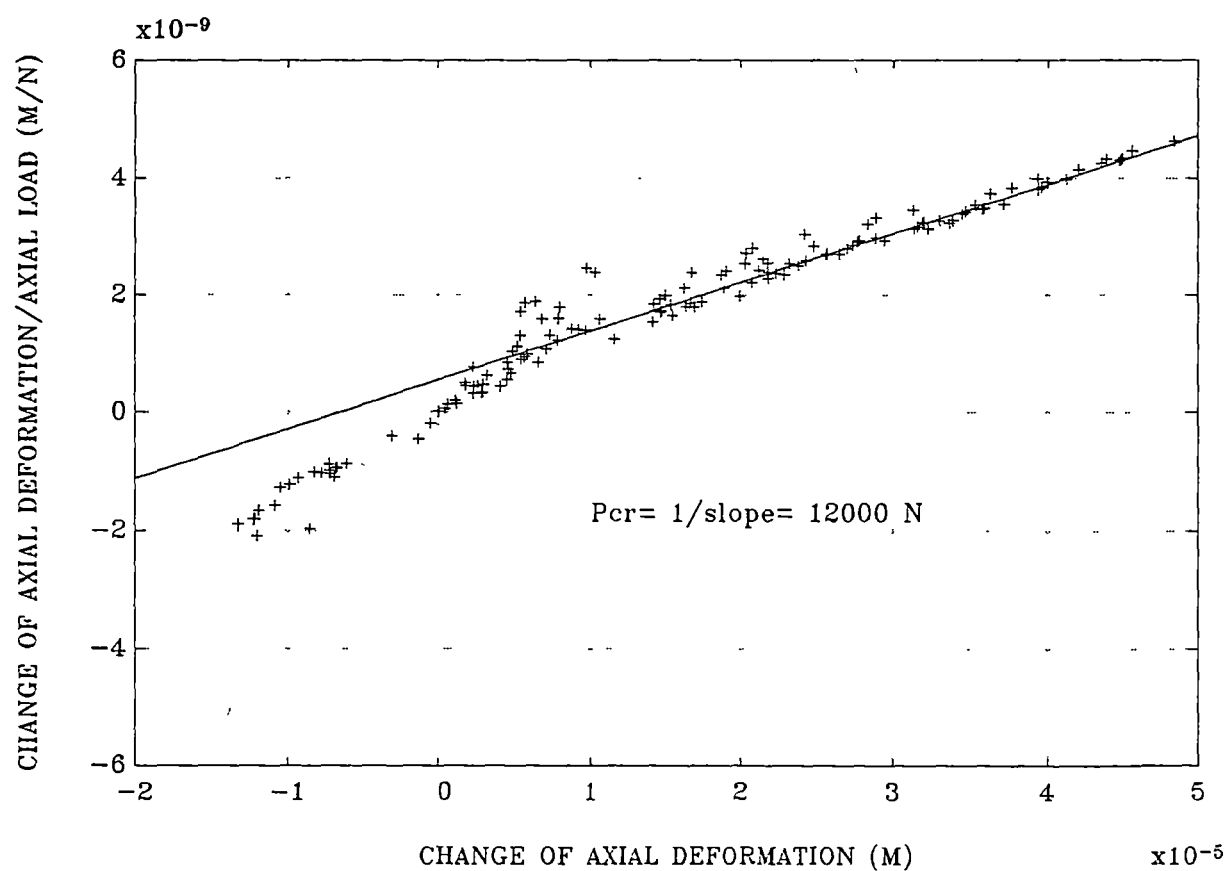


Figure 9.2 Southwell plot corresponding to Figure 9.1

marked) taken. A certain amount of judgement was involved in selecting the points. A common way was to try different number of points and to find the maximum value of the Young's modulus. Figure 9.3 illustrated how Young's modulus changed through fitting a straight line to a different number of the points of the load-deformation curve in Figure 9.1. In this case, the maximum value of Young's modulus was found to be 3.06 GPa when 75 points were taken.

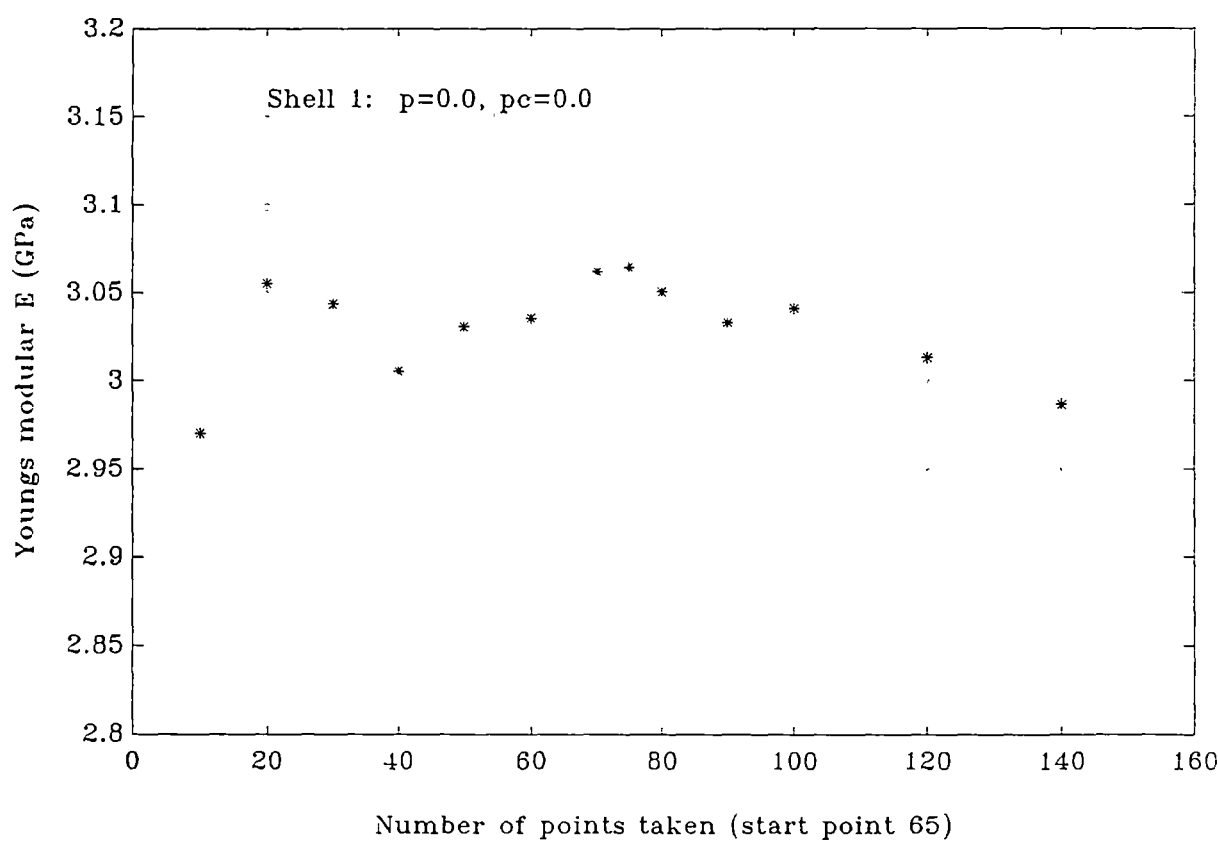


Figure 9.3 Effects on Young's modulus with different points taken

9.2 SHELL PERFORMANCE UNDER COMBINED LOADING: AXIAL COMPRESSION, EXTERNAL PRESSURE AND CELL PRESSURE

The results from shells under combined loading of axial compression, external pressure and cell pressure are summarised in Figures 9.4 to 9.8, where the predictions of Southwell plots are compared with calculations using equation (6.13). Each shell has a buckling load which is used to compare the Southwell plot prediction and theoretical predictions. In the figures, p_c represents cell pressure; and "*", "o" and "+" represent the test results at cell pressure of 0.0 Mpa, 1.2 Mpa and 2.4 Mpa respectively.

Shell 1 finally collapsed at $p_c = 2.4 \text{ Mpa}$, $p = 28 \text{ kPa}$ and $P = 6520 \text{ N}$. The predicted axial buckling load from Southwell plot was $P = 6680 \text{ N}$ - a discrepancy of 2.5%. Shell 2 collapsed at $P = 8500 \text{ N}$ under axial load alone, compared with the Southwell plot value of 8720 N - a 2.6% discrepancy. Shell 3 collapsed at $P = 9860 \text{ N}$ under axial compression load alone compared with the predicted 10000 N of Southwell plot - a discrepancy of 1.4%. Shell 4 and 5 collapsed under external pressure loading with no cell pressure or axial load applied.

Compared with other shells tested, the performance of shell 1 (Fig. 9.4) was remarkably good. The shell had a very uniform thickness - the deviation of overall thickness being as low as 0.8%. The three interaction curves of axial-load and external-pressure are very distinct. The higher the cell pressure applied, the

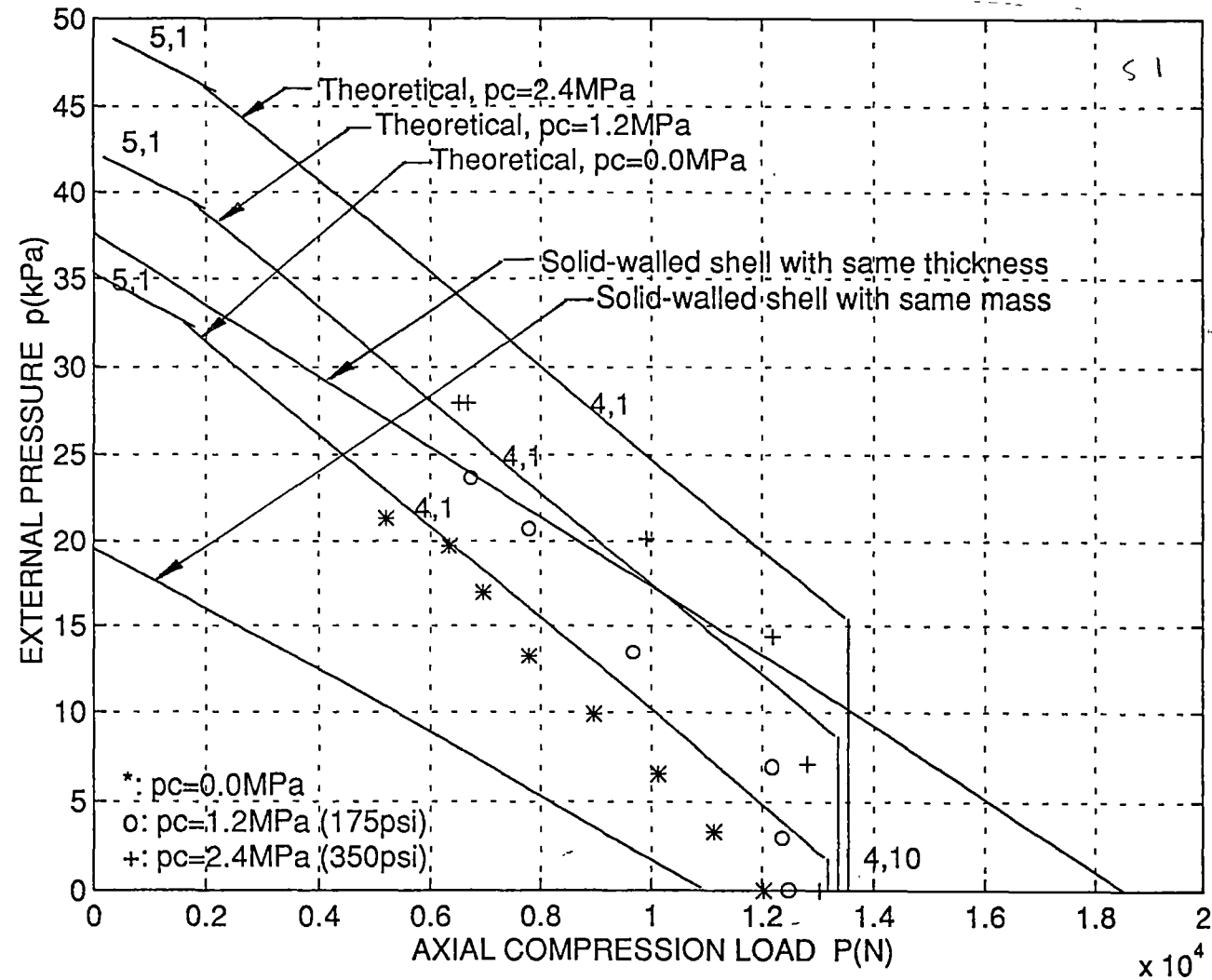


Figure 9.4 Measured Performance of Shell 1

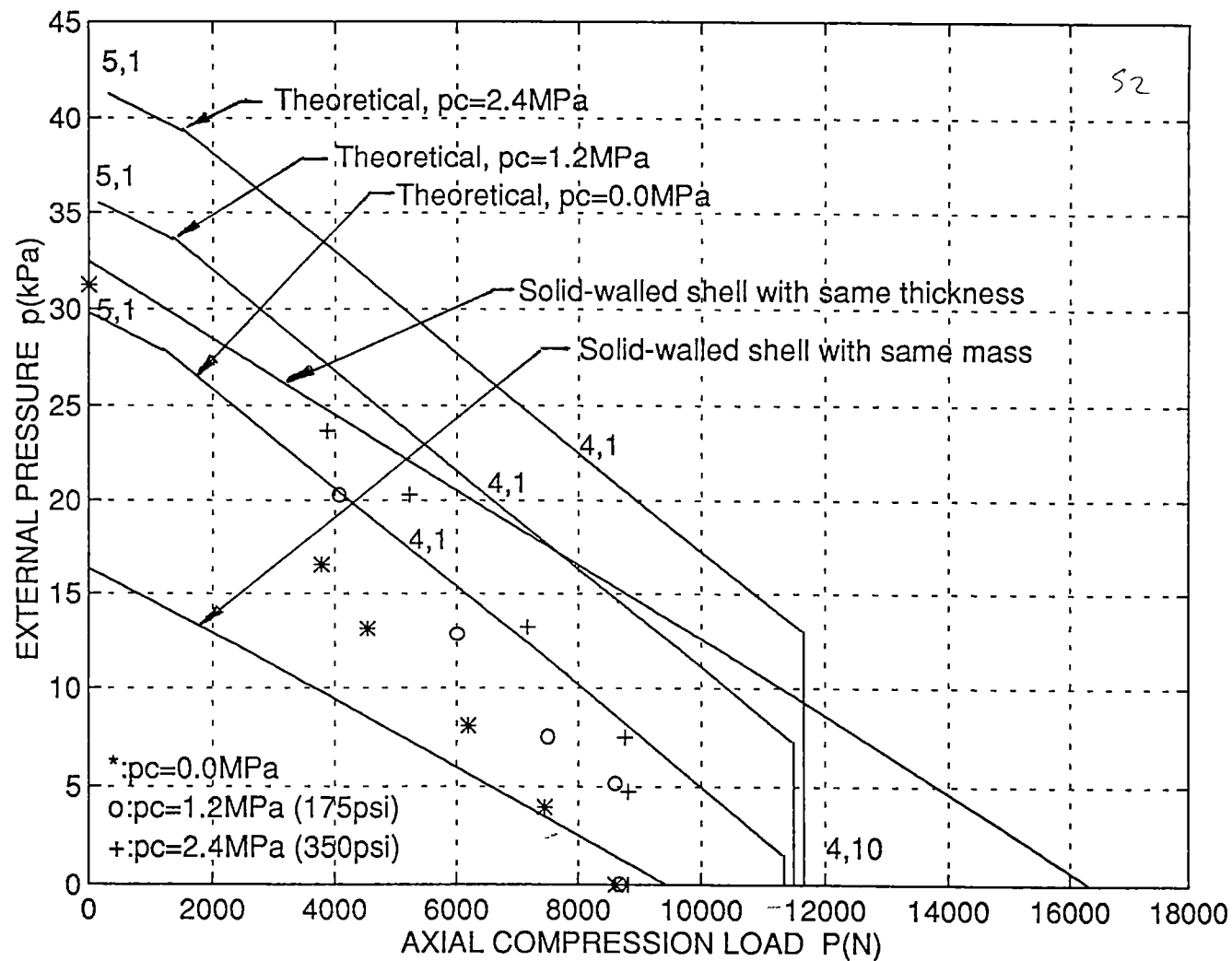


Figure 9.5 Measured Performance of Shell 2

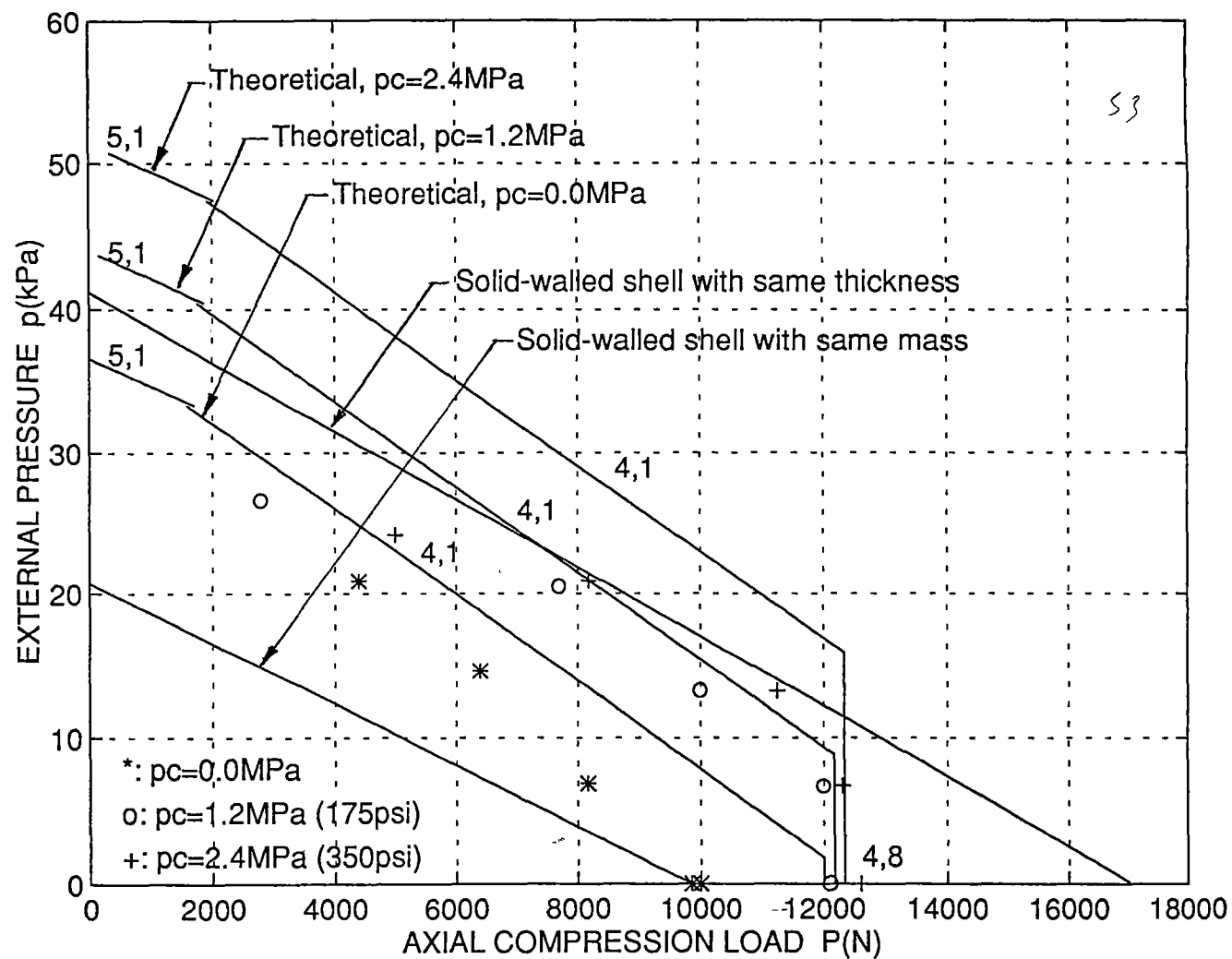


Figure 9.6 Measured Performance of Shell 3

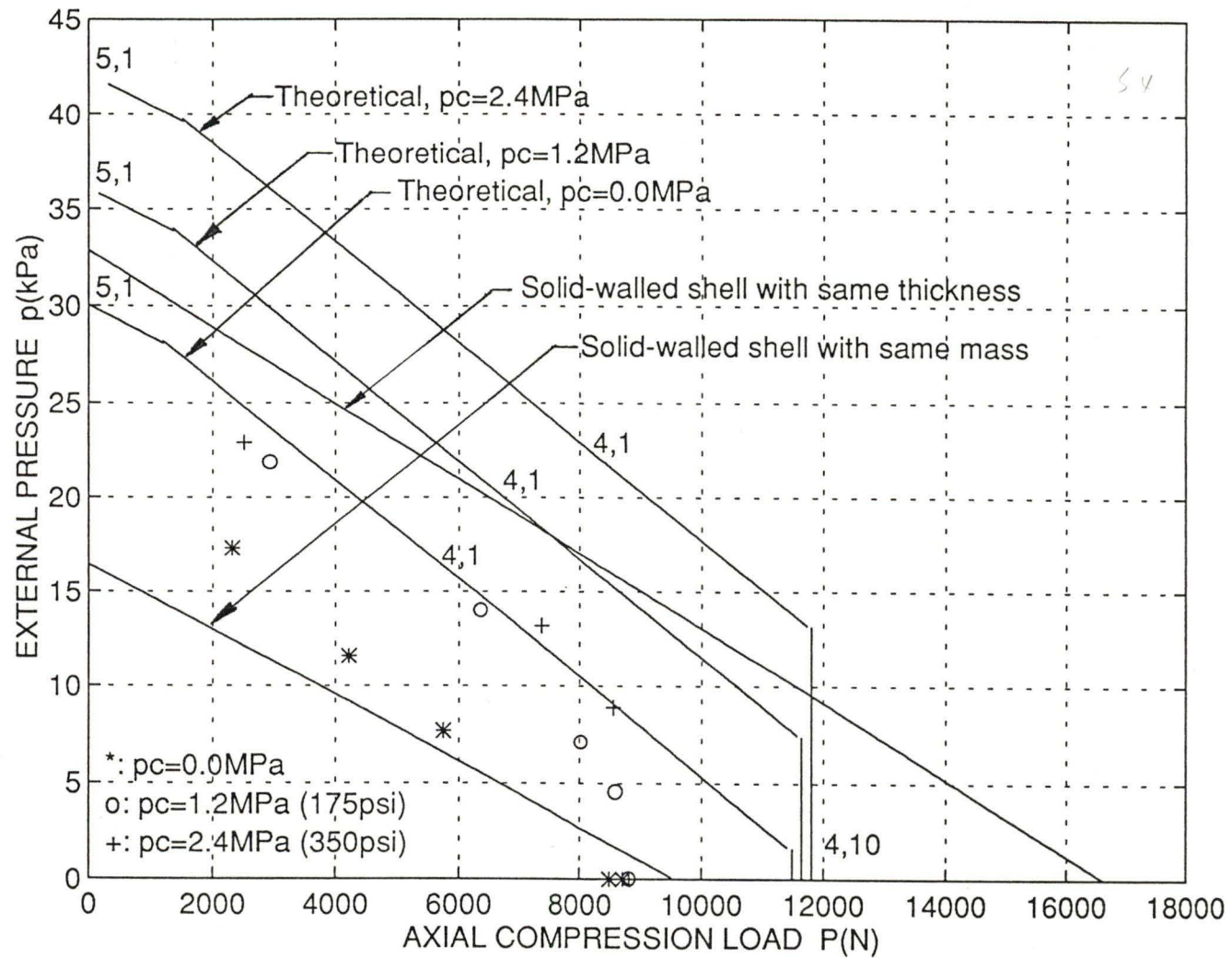


Figure 9.7 Measured Performance of Shell 4

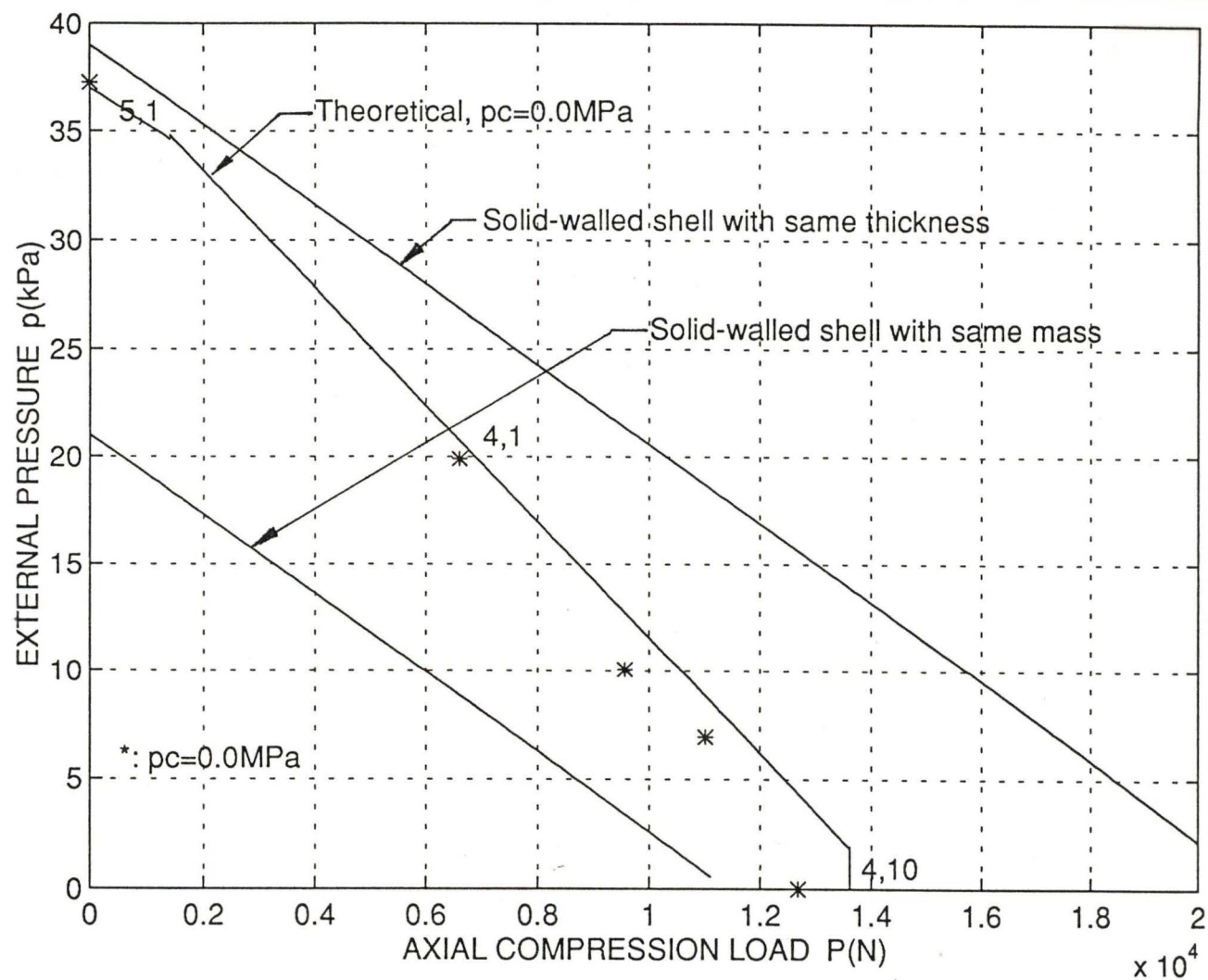
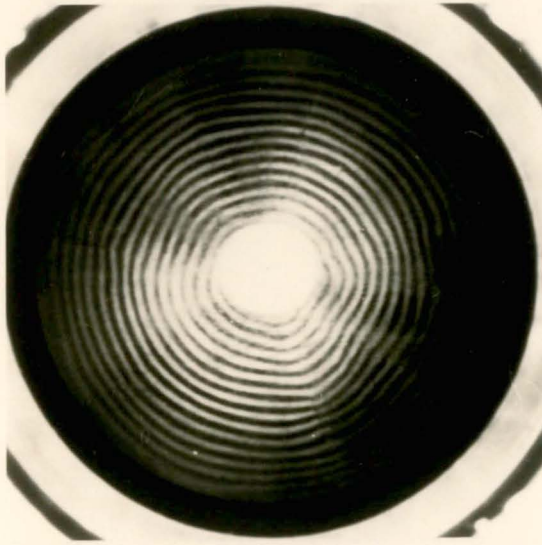


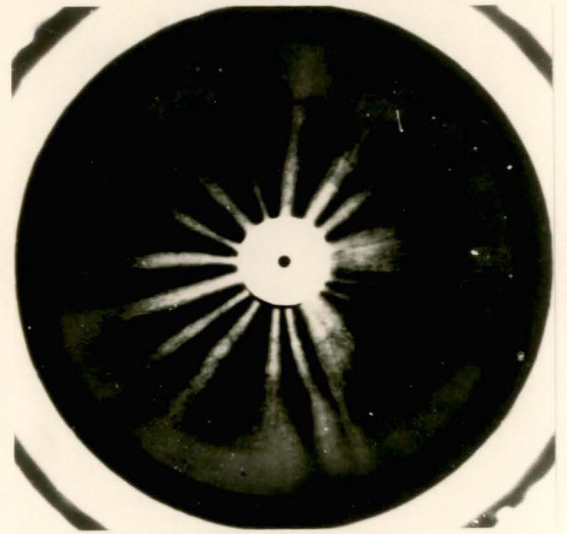
Figure 9.8 Measured Performance of Shell 5

more stable the shell becomes. This clearly shows that an increase of the cell pressure results in an increase of stiffness and consequently an increase of buckling load of the shell. The shell benefits in gaining stability from the application of cell pressure in the shell wall, particularly under low external pressure loading conditions. For the $p_c = 1.2 \text{ Mpa}$ curve, when the external pressure increases from 0 to about 10 kPa the axial buckling load retains a value of 12400 N. Similar behaviour appears in the curve of $p_c = 2.4 \text{ Mpa}$ when the external pressure increases from 0 to 15 kPa, the axial buckling load remains almost constant (13000 N).

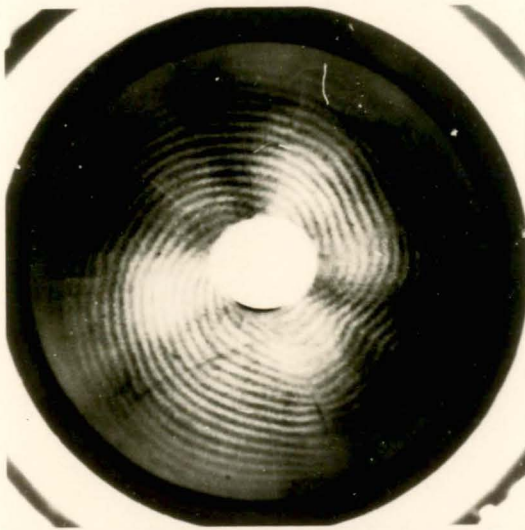
By contrast, shell 2 (Fig. 9.5), the thinnest of the 5 shells, showed a poor performance. There was a considerable discrepancy between the measured buckling loads and theoretical predictions. In such a case, even increasing the cell pressure minimally improved the stability of the shell. The reason for such a poor performance may be found in the record of the geometric data of the shell. Shell 2 has a thickness deviation of 7.5% which should be considered as very non-uniform. Because of this non-uniformity, the shell showed a marked tendency to buckle locally, which can be clearly identified in images of the shell deformation under loading. Figure 9.9 shows the images of shell 2 under loading of $p_c = 2.151 \text{ Mpa}$, $p_{cr} = 8.85 \text{ kPa}$ and $P_{cr} = 8560 \text{ N}$. The shell tended to buckle locally in the lower part of the images: this is particularly easy to identify in Figure 9.9(a), the image taken with the circumferential grid.



(a)



(b)



(c)

- (a) Circumferential grid lines
- (b) Axial grid lines
- (c) Spiral grid lines

Figure 9.9 Photographic images of Shell 2
(Load condition: $p_c=2.1 \text{ Mpa}$, $p_{cr} = 8.85 \text{ kPa}$, $P_{cr} = 8560 \text{ N}$)

For shells 3 and 4, it was found that some of the holes were not centrally located in the shell wall. Shell 4 actually leaked through the shell wall when the cell pressure increased to 3.4 Mpa. Defects of the shells obviously weaken the measured stability. However, the patterns with different levels of cell pressure were still identifiable. They clearly demonstrated that the cellular-walled shell is stronger than the solid-walled one with the same mass and that the stability can be significantly improved by applying substantial cell pressure within the shell wall.

For shell 5, only one curve was measured with $p_c = 0.0 \text{ kPa}$. One of the end rings leaked at a low cell pressure of 25 kPa. It was found later that the screws on the end ring had not been tightened, so the "O" ring in the end ring did not seal properly.

The Young's modulus E for each shell was measured based on the slope of the load-deformation curve of the shell under axial compression load alone. The Poisson's ratio μ for each shell was assumed to be 0.35. The Young's modulus and Poisson's ratio were used in the theoretical predictions.

From Figures 9.4 to 9.8, it can be seen that all the measured buckling loads are lower than the corresponding theoretical predictions. The difference became more significant when the cell pressure was higher. This is mainly because in the theory the effects of the end-rings were ignored; in other words, the

shell was allowed to expand freely while the cell pressure was applied. Expanding due to cell pressure would make the shell stronger in standing against axial compression and especially external pressure. However, during model shell testing both ends of the shell was largely constrained by the end-rings. It is reasonable to expect that if the constraint from the end-rings vanished during testing, the measured buckling loads would be further increased, and the agreement between theoretical predictions and measured buckling loads would be significantly improved.

Comparisons between buckling conditions for cellular-walled shells and solid-walled circular cylindrical shells were made for shells 1 to 4. One solid-walled shell had the same mass as the cellular-walled one. Another had the same thickness and, of course, increased mass. Both solid-walled shells had the same length and radii as the cellular-walled shells. In the figures, it is clearly seen that the cellular-walled shell is much stronger than the solid-walled shell with the same mass even with no cell pressure applied. Although the cellular-walled shell without cell pressure is weak compared with the solid-walled shell with the same thickness, much greater stability can be achieved by applying substantial cell pressure. For instance, shell 1 became stronger than a solid-walled shell with considerably greater mass when 2.4 Mpa cell pressure was applied. It should be pointed out that for this epoxy shell, the maximum cell pressure that could be applied within the cells is 35 Mpa

— In that sense, the cellular-walled shells have a considerable

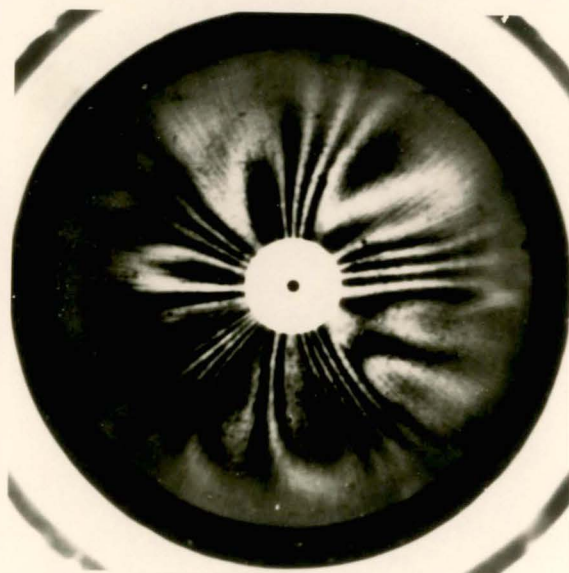
potential to increase stability. The limitation was mainly due to end fixity. If this problem could be overcome even better performance should be anticipated.

The buckling modes from theoretical predictions are marked in the figures. Unfortunately, not one buckled image of the 5 shells tested under combined loading was recorded, because all the shells shattered immediately after buckling. However, images very close to the buckled pattern were recorded. Figure 9.10 shows the images of shell 1 under a loading of $p_c = 2.4 \text{ Mpa}$, $p_{cr} = 21.10 \text{ kPa}$ and $P_{cr} = 9915 \text{ N}$. It is easy to see that a buckling pattern with 5 circumferential lobes and a single lobe at the centre of the shell's length was about to form; In other words, the measured buckling mode will be (5,1) for the shells tested, while the theoretical predicted buckling mode under the same loading condition was (4,1), which also indicates that the measured behaviour of the shells agrees fairly well with the theoretical predictions.

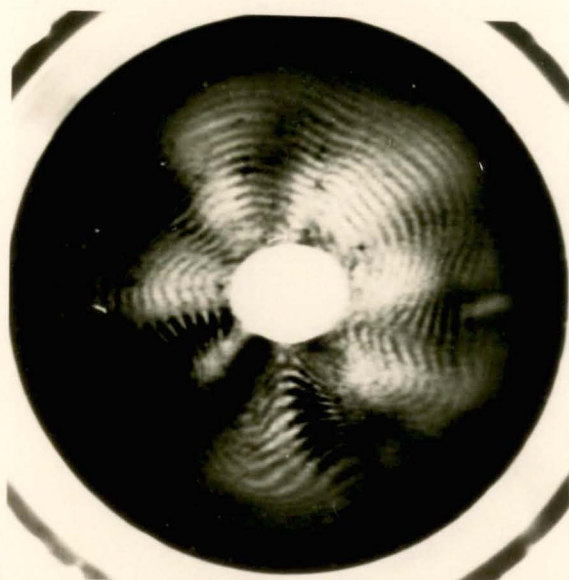
Details of the test data for shells 1 to 5 are listed in Tables 9.2 to 9.6.



(a)



(b)



(c)

- (a) Circumferential grid lines
- (b) Axial grid lines
- (c) Spiral grid lines

Figure 9.10 Photographic images of Shell 1
(Load condition: $p_c=2.4 \text{ Mpa}$, $p_{cr}= 21.10\text{kPa}$, $P_{cr}= 9915\text{N}$)

Table 9.2 Test Data for Shell 1 (6187)
($E = 3.06 \text{ GPa}$, $\mu = 0.35$)

Cell Pressure $p_c(\text{kPa})$	External Pressure $p_{cr}(\text{kPa})$	Critical Axial Load $P_{cr}(\text{N})$	Remarks
0.00	0.00	12000	The shell had a remarkably uniform thickness; No detectable initial imperfections were found.
0.00	3.35	11140	
0.00	6.50	10140	
0.00	9.85	8970	
0.00	13.20	7800	
0.00	16.95	6970	
0.00	19.70	6350	
0.00	21.30	5200	
25.38	0.00	12480	
25.38	2.95	12370	
25.38	6.90	12190	
25.38	13.40	9690	
25.38	20.70	7800	
25.38	23.60	6740	
50.76	0.00	13040	
50.76	7.10	12810	
50.76	14.40	12190	
50.76	21.10	9915	
50.76	28.00	6680	
50.76	28.00	6520*	* The collapsed load condition

Table 9.3 Test Data for Shell 2 (6168)

($E = 3.03\text{GPa}$, $\mu = 0.35$)

Cell pressure $p_c(\text{kPa})$	External pressure $p_{cr}(\text{kPa})$	Critical Axial Load $P_{cr}(\text{N})$	Remarks
0.00	0.00	8720	* Collapsed load condition.
0.00	7.70	8500*	
0.00	7.70	5750	
0.00	11.60	4230	
0.00	17.33	2330	
25.38	0.00	8830	The shell had large thickness deviations.
25.38	4.55	8600	
25.38	7.10	8020	
25.38	14.00	6365	
25.38	21.90	2950	
50.76	0.00	8830	Oil leaked from one of the end rings when the cell pressure reached 72.5 kPa.
50.76	8.85	8560	
50.76	13.20	7355	
50.76	22.90	2515	

Table 9.4 Test Data for Shell 3 (6165)

($E = 3.06\text{GPa}$, $\mu = 0.35$)

Cell Pressure $p_c(\text{kPa})$	External Pressure $p_{cr}(\text{kPa})$	Critical Axial Load $P_{cr}(\text{N})$	Remarks
0.00	0.00	10000	* Collapsed load condition.
0.00	0.00	9860*	
0.00	6.90	8160	
0.00	14.60	6400	
0.00	20.90	4400	
25.38	0.00	12000	
25.38	6.70	12000	
25.38	13.20	10000	
25.38	20.50	7700	
25.38	26.60	2800	
50.76	0.00	12600	Some holes were not centrally located in the shell wall.
50.76	6.70	12300	
50.76	13.20	11250	
50.76	20.90	8180	
50.76	24.15	5000	

Table 9.5 Test Data for Shell 4 (6179)

($E = 2.93\text{GPa}$, $\mu = 0.35$)

Cell Pressure $p_c(\text{kPa})$	External Pressure $p_{cr}(\text{kPa})$	Critical Axial Load $P_{cr}(\text{N})$	Remarks
0.00	0.00	8610	* Collapsed load condition
0.00	3.95	7450	
0.00	8.10	6200	
0.00	13.10	4550	
0.00	16.55	3790	
0.00	31.20	0.00*	
25.38	0.00	8680	
25.38	5.12	8610	
25.38	7.48	7510	
25.38	12.80	6030	
25.38	20.27	4080	
50.76	0.00	8815	Oil leaked through the shell wall when the cell pressure reached 72.5 kPa. A few holes were found too close to the inner surface.
50.76	4.75	8815	
50.76	7.50	8760	
50.76	13.20	7160	
50.76	20.28	5230	
50.76	23.60	3870	

Table 9.6 Test Data for Shell 5 (6192)

($E = 2.98 \text{ GPa}$, $\mu = 0.35$)

Cell Pressure $p_c(\text{kPa})$	External Pressure $p_{cr}(\text{kPa})$	Critical Axial Load $P_{cr}(\text{N})$	Remarks
0.00	0.00	12700	Oil leaked through one of the end rings when the cell pressure reached 25 kPa.
0.00	6.90	11020	
0.00	10.00	9580	
0.00	19.90	6610	
0.00	37.20	0.00*	* Collapsed load condition.

9.3 TESTS ON AXIAL COMPRESSION

A summary of the buckling loads for the 12 model shells in axial compression buckling is given in Table 9.7. The measured critical loads for each shell presented in the table are the actual buckling loads rather than that predicted from a Southwell plot. The measured critical loads were compared with theoretical predictions calculated from equation (6.3). The Young's modulus of each shell was determined from the slope of the load-deformation curve and was used in the theoretical calculations. The Poisson's ratio used in calculations for all shells was again assumed to be 0.35. Values of maximum $\Delta t/t$ represent thickness

deviations and values in the range of 1.0% - 2.5% indicate that the shells had very uniform thicknesses.

However, localized buckling was found in the tests of shells 11 and 12, and both had very low buckling loads. For shell 11, when the end rings were opened, it was found that the shell had been loosely fitted on the guide spigot of the end ring during testing. In other words, the shell was partially supported by the ends, and this uneven loading caused localized buckling. For shell 12, the end rings were not properly seated on the base and caused uneven loading. Figure 9.11 shows deformation images at an advanced pre-buckling stage (Fig. 9.11a) and buckled stage (Fig. 9.11b) of shell 11, from which the localized deformations or buckling pattern can be clearly seen. Figure 9.12 shows the localized buckling patterns of shell 12.

Apart from shells 11 and 12, measured critical buckling loads were in good agreement with theoretical predictions. The obtained knock down factors were high, ranging from 0.78 to 0.86. This indicates that the shells were of high quality and had small imperfection sizes.

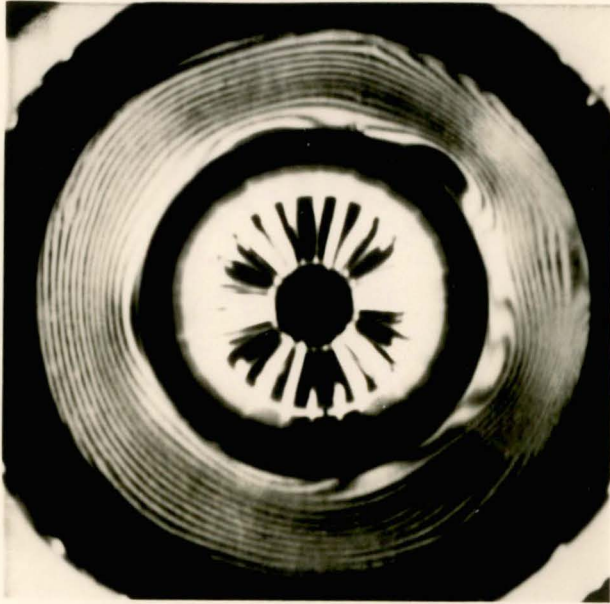
Table 9.7 Test Data of Axial Buckling

($\mu = 0.35$)

Shell No.	Max. $\Delta t/t$	E (GPa)	Measured Critical load $P_{cr}(N)$	Calculated Critical load $P_{cr}(N)$	Knock Down Factor
6	1.0%	3.52	12540	15050	0.83
7	1.1%	3.35	10000	11600	0.86
8	1.1%	3.55	10360	12290	0.84
9	1.1%	3.60	10670	12640	0.84
10	1.1%	3.48	10310	12320	0.84
11*	1.2%	---	6320	12390	0.51
12**	2.4%	---	1870	14370	0.13
13	2.4%	3.05	10770	12500	0.86
14	2.0%	3.50	10670	13500	0.79
15	2.5%	3.08	10660	12450	0.86
16	2.4%	3.10	11430	12790	0.89
17	1.6%	3.06	10500	13400	0.78

* It was found later that the ends of the shell were improperly seated in the end-rings, i.e., the shell was not fully supported by the end-rings. The calculated P_{cr} was based on the average Young's modulus $E=3.50\text{GPa}$.

** The end rings were not square with the base, i.e., the shell was unevenly loaded.



a. Advanced pre-buckling deformation image



b. Localized buckled image

Figure 9.11 Deformation images in uneven loading (shell 11)

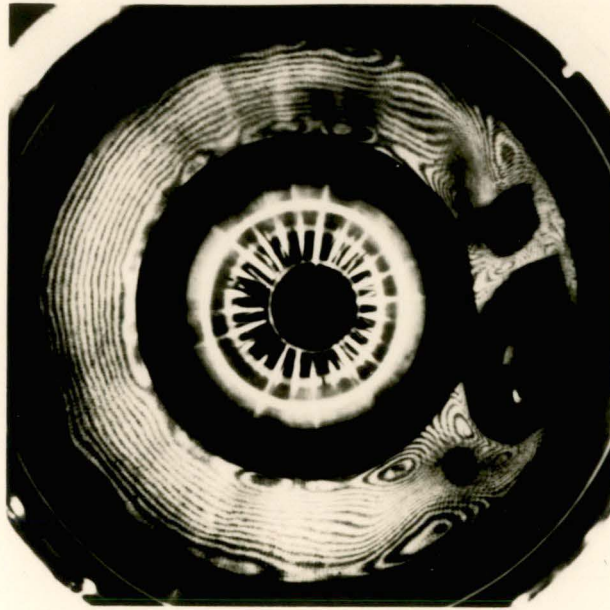


Figure 9.12 Localized buckling patten of shell 12

CHAPTER 10

CONCLUSIONS

AND

RECOMMENDATIONS

CHAPTER 10

CONCLUSIONS AND RECOMMENDATIONS

9.1 CONCLUSIONS

The results of this investigation constitute the first known theoretical and experimental investigation of buckling of cellular-walled cylindrical shells under simultaneous loading of axial compression, external pressure and cell pressure.

Theoretically, the cellular-walled shell was characterized as a pseudo-orthotropic cylindrical shell with the principal directions axially and circumferentially oriented. Different effective Young's moduli were used for tension and bending. Reliable interaction formulas for cellular-walled cylindrical shells under axial compression and external pressure including the effects of cell pressure have been derived from a buckling analysis based on Flugge's linear buckling theory. The effect of high fluid pressure within the cells on the buckling loads was considered to be the same as that of an internal pressure when the radial displacements of the midsurface were the same in both cases. Although the buckling formulas are based on a conventional simply-supported boundary condition which is different from the one commonly used in practice, i.e., a clamped or built-in boundary, they are, nevertheless, quite useful since in moderately long cylindrical shells Lei and Cheng⁶⁴ showed that there is very little difference in buckling loads between these two boundary conditions.

Cellular-walled model shells were made out of epoxy by an adaptation of the spin casting process developed by Tennyson⁶. These shells

had 360 longitudinal holes each of 0.7mm diameter, shell internal diameter 153mm, wall thickness 1.2mm and length up to 245mm. The tests of the model shells were carried out on a rigid test machine with parallel platens.

Based on theoretical and experimental results for cellular-walled cylindrical shells, it is evident that high fluid pressure within the cells can significantly increase the buckling loads, in particular external pressure. Hence, shells of this type appear to have potential in engineering applications, particularly in submarine structures.

9.2 DISCUSSIONS AND RECOMMENDATIONS

Because this investigation was based on a naturally occurring - though extinct - animal structure, it was thought that this study may shed some light on the reasons for the animal's demise. It seems possible that one reason may have been brittleness in bending in the circumferential direction. On several occasions, isotropic shells made of the same material were dropped on a concrete floor and in every case they have bounced without damage. However, on the one occasion that one of the cellular-walled shells was dropped with the axis tilted the shell shattered. It is clear that the existence of the cells reduces the local bending stiffness, so that concentrated or dynamic loads may lead to catastrophic failure. However, the bending stiffness can be improved by reinforcing around holes, e.g. by adding circumferential fibres around the holes. It is also possible to use so called "smart" materials to fill in the holes, which would expand after passage of a electric current to pressurise the holes.

It is suggested that future work in this field should study the effect of local loading and dynamic loading. Different ways of constructing shells should be studied to improve the local bending stiffness around the holes and to improve the method of pressurization. Finally, it is also suggested that tests on large model shells should be conducted, since only small model shells were tested in this investigation.

REFERENCES

REFERENCES

1. Banks, M.R., Private communication.
2. Hsu, Lo, Harold Crate and Edward B. Schwartz, "Buckling of thin-walled cylinder under compression and internal pressure". NACA TN 2021, Jan. 1950, pages 1-29.
3. Harris, L.A., Suer H.S. and Skene W.T., "The stability of thin walled unstiffened circular cylinders under compression including the effects of internal pressure" Journal of the Aeronautical Sciences, V.24, No.8, Aug. 1957, pages 587-596.
4. Fung, Y.C. and Sechler, E.E., "Buckling of thin-walled circular cylinders under compression and internal pressure" Journal of the Aeronautical Sciences, V.24, No.5, May 1957, pages 351-356.
5. Flugge, W., "Stresses in shells", Third printing, Springer-Verlag, Berlin, 1966.
6. Tennyson, R.C., "A note on the classical buckling load of circular cylindrical shells under compression", AIAA Journal, V.1, No.2, Feb. 1963, pages 475-476.
7. Batdorf, S.B., "A simplified method of elastic stability analysis for thin cylindrical shells," NACA Rept No.874, 1947, pages 1-25.
8. Donnell, L.H., "A new theory for the buckling of thin cylinders under axial compression and bending". Trans. ASME, Vol.56, No.11, November 1934, pages 795-806.
9. Donnell, L.H., "Stability of thin-walled tubes under torsion", NACA Rept No.479, 1933, pages 95-116.

10. Timoshenko, S.P. and Gere, J.M., "Theory of elastic stability", McGraw-Hill international book company, 2nd edition, 1963.
11. Southwell, R.V., "An introduction to the theory of elasticity for engineers and physicists", Oxford university press, 2nd edition, 1941.
12. Karman, Th. Von, and Tsien, H.S., "The buckling of spherical shells by external pressure," Journal of the Aeronautical Sciences, Vol.7, 1939, pages 43-50.
13. Karman, Th. Von, Dunn, L.G., and Tsien, H.S., "The influence of curvature on the buckling characteristics of structures," Journal of the Aeronautical Sciences, Vol.7, 1940, page 276.
14. Karman, Th. Von, and Tsien, H.S., "The buckling of thin cylindrical shells under axial compression", Journal of the Aeronautical Sciences. Vol.8, No.8, June 1941, pages 303-312.
15. Tsien, H.S., "A theory for the buckling of thin shell", Journal of the Aeronautical Sciences, Vol.9, No.10, August 1942, pages 373-384.
16. Michielsen, H.F., "The behaviour of thin cylindrical shells after buckling under axial compression", Journal of the Aeronautical Sciences, Vol.15, No.12, December 1948, pages 738-744.
17. Kempner, J., "Postbuckling behaviour of axial compressed circular cylindrical shells", Journal of the Aeronautical Sciences, Vol.21, No.5, May 1954, pages 329-335.

18. Almroth, B.O., "Postbuckling behaviour of axially compressed circular cylinders", AIAA Journal, Vol.1, No.3, March 1963, pages 630-633.
19. Hoff, N.J., Madsen, W.A., and Mayers, J., "Postbuckling equilibrium of compressed circular cylindrical shells", AIAA Journal, Vol.4, No.1, January 1966, pages 126-133.
20. Yoshimura, Y., "On the mechanism of buckling of a circular cylindrical shell under compression", NACA TN 1390, 1955.
21. Hutchinson, J.W. and Koiter, W.T., "Postbuckling theory," ASME Applied Mechanics Reviews, Vol.23, NO.12, September 1970, pages 1353-1366.
22. Budiansky, B. and Hutchinson, J.W., "A survey of some buckling problems," AIAA Journal, Vol.4, No.9, September 1966, page 1505.
23. Budiansky, B. and Hutchinson, J.W., "Buckling: progress and challenge," Trends in solid mechanics 1979, Proceeding of the Symposium Dedicated to the 65th Birthday of W.T.Koiter, Delft University of Technology June 13-15, 1979, Besseling, J.F., and van der heijden, A.M.A., eds, Delft University press, 1979, pages 93-116.
24. Tvergaard, V., "Buckling behaviour of plate and shell structures," Theoretical and Applied Mechanics, W.T.Koiter, ed., North-Holland, 1976, pages 233-247.
25. Citerley, R.L., "Imperfection sensitivity and post-buckling behaviour of shells," Pressure vessels and piping: Design Technology-1982, A Decade of Progress, Zamrik, S.Y. and Ditrich, D., eds, ASME, New York, pages 27-45.

26. Chaies, A., "Stability and collapse analysis of axially compressed cylindrical shell," *Shell Structures: Stability and Strength*, edited by R. Narayanan, 1985, pages 1-17.
27. Babcock, C.D., "Shell stability," *Journal of Applied Mechanics*, Vol.50, December 1983, pages 935-940.
28. Hoff, N.J., "Some recent studies of the buckling of thin shells," *The Aeronautical Journal of the Royal Aeronautical Society*, December 1969, pages 1057-1070.
29. Koiter, W.T., "On the stability of elastic equilibrium", Thesis, Technical High School Delft, J.H. Paris, Amsterdam, The Netherlands, 1945.
30. Koiter, W.T. "The effect of axisymmetric imperfections on the buckling of cylindrical shells under axial compression." *Proceeding of the Royal Netherlands Academy of Science*, Amsterdam, Series B., Vol 66, No5, 1963.
31. Hansen, J.S., "Influence of general imperfections in axially loaded cylindrical shells," *Intern. Journal of Solid Structures*, Vol.11, No.11, November 1975, pages 1223-1233.
32. Tennyson, R.C., and Muggeridge, D.B., "Buckling of axisymmetric imperfect circular cylindrical shells under compression", *AIAA Journal*, Vol.7, No.11, November 1969, pages 2127-2131.
33. Arbocz, J., and Babcock, C.D., "Effect of general imperfections on the buckling of cylindrical shells", *ASME Journal of Applied Mechanics*, March 1969, pages 28-38.
34. Arbocz, J., and Babcock, C.D., "Prediction of buckling loads based on experimentally measured initial imperfections",

- Buckling of Structures, IUTAM Symposium, Cambridge/USA, 1974, Budiansky, B. ed., Springer-verlag, Berlin, 1976, pages 291-311.
35. Arbocz, J., and Babcock, C.D., "Utilization of stags to determine knockdown factors from measured initial imperfections," Report LR-275, Delft University of Technology, Department of Aerospace Engineering, Delft, The Netherlands, 1978.
 36. Arbocz, J., "Shell stability analysis: Theory and Practice," The buckling of structures in theory and practice, Thompson, J.M.T., and Hunt, G.W., eds., Cambridge University Press, Cambridge, 1983. Proceeding of the IUTAM Symposium, University College, London, August 1982.
 37. Krishnakumar, S., "Buckling of axially compressed cylindrical shells with local imperfections," Ph.D Thesis, University of Tasmania, November 1988.
 38. Foster, C.G., "Deflections in thin cylindrical shells," Ph.D. Thesis, University of Tasmania, September 1979.
 39. Foster, C.G., "Some observations on the Yoshimura buckle pattern for thin-walled cylinders," ASME Journal of Applied Mechanics, Vol.46, No.2, June 1979, pages 377-380.
 40. Foster, C.G., "Estimation of the collapse loads of thin-walled cylinders in compression," ASME Journal of Applied Mechanics, Vol.46, No.2, June 1979, pages 381-385.
 41. Foster, C.G., "On the buckling of thin walled cylinders loaded in compression," Journal of Strain Analysis, Vol.16, No.3, July 1981, pages 205-210.

42. Foster, C.G., "Buckling of very thin, nearly perfect axially loaded circular cylindrical shells," *AIAA Journal*, Vol.21, No.5, May 1983, pages 794-796.
43. Foster, C.G., and Krishnakumar, S., "A class of transportable demountable structures," *Space Structures*, Vol.2, 1986/87, pages 129-137.
44. Foster, C.G., "Axial compression buckling of conical and cylindrical shells," *Experimental Mechanics*, Vol.27, No.3, September 1987, pages 255-261.
45. Hoff, N.J., "The perplexing behaviour of thin circular cylindrical shells in compression," *Israel Journal of Technology*, Vol.4, No.1, 1966, pages 1-28.
46. Almroth, B.O. "Influence of edge conditions on the stability of axially compressed cylindrical shells," *AIAA Journal*, Vol.4, No.1, 1966, pages 134-140.
47. Stein, M. "The effect on the buckling of perfect cylinders of prebuckling deformations and stresses induced by edge support", NASA TN D-1510, December 1962, pages 217-227.
48. Fischer, G., "Influence of boundary conditions on stability of thin-walled cylindrical shells under axial load and internal pressure", *AIAA Journal*, Vol.3, No.4, April 1965, pages 736-738,
49. Hoff, N.J., "Low buckling stresses of axially compressed circular cylindrical shells of finite length", *ASME Journal of Applied Mechanics*, Vol.32, No.3, September 1965, pages 533-541.

50. Hoff, N.J., and Rehfield, L.W., "Buckling of axially compressed circular cylindrical shells at stresses smaller than the classical critical value," ASME Journal of Applied Mechanics, Vol.32, No.3, September 1965, pages 542-546.
51. Hoff, N.J., and Soong, T.C., "Buckling of circular cylindrical shells in compression", Intern. Journal of Mechanical Sciences, Vol.7, No.7, July 1965, pages 489-520.
52. Simmonds, J.G. and Danielson, D.A., "New results for the buckling loads of axially compressed cylindrical shells subject to relaxed boundary conditions", ASME Journal of Applied Mechanics, Vol. 37, No.1, March 1970, pages 93-100.
53. Almroth, B.O., "Influence of edge conditions on the stability of axially compressed cylindrical shells", AIAA Journal, Vol.4, No.1, pages 134-140, January 1966; also NASA CR-161, February 1965.
54. Yamaki, N., "Elastic stability of circular cylindrical shells", North-Holland series in Appl. Math and Mechanics, Vol.27, 1984.
55. Babcock, C.D., and Sechler, E.E., "The effect of initial imperfections on the buckling stress of cylindrical shells," NASA TN D-1510, December 1962, pages 135-142.
56. Sendelbeck, R.S., and Hoff, N.J., "Loading rig in which axially compressed thin cylindrical shells buckle near theoretical values," Experimental Mechanics, Vol.12, No.8, August 1972, pages 372-376.

57. Tennyson, R.C., "Buckling of circular cylindrical shells in compression," AIAA Journal, Vol.2, No.7, July 1964, pages 351-353.
58. Tennyson, R.C., "An experimental investigation of the buckling of circular cylindrical shells in axial compression using the photoelastic technique," Institute of Aerospace Science, University of Toronto, Report No.102, Toronto, Canada, 1964.
59. March, H.W. et al., "Buckling of thin-walled plywood cylinders in torsion", Forest Products Lab, Madison, Wisc Report 1529, June 1945.
60. Thielemann, W.F., Schnell, W. and Fischer, G., "Buckling and post-buckling behaviour of orthotropic circular cylindrical shells subjected to combined and internal pressure", Zeitschrift Flugwiss 8 Heft 10/11, 1960.
61. Hess, T.E., "Stability of orthotropic cylindrical shells under combined loading", J. American Rocket Society, Vol.31, No.2, Feb. 1961, page 237.
62. Cheng, S. and Ho, B.P.C., "Stability of heterogeneous aeolotropic cylindrical shells under combined loading", AIAA Journal, Vol.1, No.4, April 1963, pages 892-898.
63. Ho, B.P.C. and Cheng, S., "Some problem in stability of Heterogeneous aeolotropic cylindrical shells under combined loading". AIAA Journal, Vol.1, No.7, July 1963, pages 1603-1607.
64. Lei, M.M. and Cheng, S., "Buckling of composite and Homogeneous isotropic cylindrical shells under and radial

- loading," Transactions of the ASME, Journal of Applied Mechanics, Vol. 54, December 1969, pages 791-798.
65. Holston, A., Jr., Feldman, A. and Stang, D.A., "Theoretical and experimental buckling loads of filament wound cylinders under combined loading," AIAA paper 68-107, New York, 1968
 66. Holston, A., Jr., "Buckling of inhomogeneous anisotropic cylindrical shells by bending," AIAA Journal, Vol.6, No.10, October 1968, pages 1837-1841.
 67. Tasi, J., "Effect of heterogeneity on the stability of composite cylindrical shells under compression", AIAA Journal, Vol.4, No.6, June 1966, page 1058.
 68. Martin, R.E. and Drew, D.D., "A batdorf type modified equation for the stability analysis of anisotropic cylindrical shells", Texas A&M University, Tech Report, No.10, March 1969.
 69. Chao, T.L., "Minimum weight design of stiffened fibre composite cylinders", USAFB Tech Report AFML-TR-69-251, Sept. 1969.
 70. Hoston, A. Jr., "Buckling of filament-wound cylinders by compression", AIAA Journal, Vol.6, No.5, May 1968, pages 935-936.
 71. Ugural, A.C. and Cheng S., "Buckling of composite cylindrical shells under pure bending", AIAA Journal, Vol.6, No.2, Feb. 1968, pages 349-354.

72. Pagano, N.J., Halpin, J.C. and Whitney, J.M., "Tension buckling of anisotropic cylinders", J. Composite Materials, Vol.2, No.2, April 1968, pages 154-167.
73. Cheng, S. and He, F.B., "Theory of orthotropic and composite cylindrical shells, accurate and simple fourth-order governing equations," Journal of Applied Mechanics, Vol.51, December 1984, pages 736-744.
74. Xiao, W. and Cheng, S., "Buckling of locally loaded isotropic, orthotropic, and composite cylindrical shells," Journal of Applied Mechanics, Vol.55, June 1988, pages, 425-429.
75. Tennyson, R.C., "Buckling of laminated composite cylinders: a review", Composite, January 1975, pages 12-24.
76. Jones, R.M., "Buckling of circular cylindrical shells with different moduli in tension and compression", USAF, Air Force Report No. SAMSO-TR-70-55, Dec. 1969.
77. Khot, N.S., "On the influence of initial geometric imperfections on the buckling and postbuckling behaviour of fibre-reinforced cylindrical shells under uniform axial compression", USAF, WPAFB, Tech Report AFFDL-TR-68-136, October 1968.
78. Khot, N.S., "Buckling and postbuckling behaviour of composite cylindrical shells under axial compression", AIAA Journal, Vol.8, No.2, February 1970, pages 229-235.
79. Khot, N.S., "Postbuckling behaviour of geometrically imperfect composite cylindrical shells under axial compression", AIAA Journal, Vol.8, No.3, March 1970, pages 579-581.

80. Card, M. F., "The sensitivity of buckling of axially compressed fibre-reinforced cylindrical shells to small geometric imperfections", NASA TMX-61914, June 1969.
81. Tennyson, R.C., Chan, K.H. and Muggeridge, D.B., "The effect of axisymmetric shape imperfections on the buckling of laminated anisotropic circular cylinders", Trans Canadian Aeronautics and Space Inst., Vol.4, No.2, Sept. 1971, pages 131-139.
82. Tennyson, R.C. and Muggeridge, D.B., "Buckling of laminated anisotropic imperfect circular cylinders under axial compression", J. Spacecraft & Rockets, Vol.10, No.2, Feb. 1973, pages 143-148 .
83. Muir, R.G., "The behaviour of thin-walled 4-ply carbon fibre epoxy composite cylindrical shells in axial compression", University of Tasmania, Research Report No. CM 92/15, November 1992.
84. Norris, C.B. and Kuenzi, E.W., "Buckling of long, thin plywood cylinders in compression - experimental treatment", US Forest products Lab Report 1322-B, 1943.
85. Card, M.F. and Peterson, J.P., "On the stability of orthotropic cylinders", NASA TN D-1510 ('Collected papers on instability of shell structures', Dec. 1962).
86. Card, M.F., "Experiments to determine the strength of filament-wound cylinders loaded in compression", NASA TN D-3522, Aug. 1966.

87. Tasi, J., Feldman, A. and Stang, D.A., "The buckling strength of filament-wound cylinders under compression", NASA CR-266, July 1965.
88. Schneider, M.H. and Hofeditz, J.T., "Buckling of fiberglass cylinders under external pressure", Proceeding of the winter annual meeting, American Soc. of Mechanical Engineering, New York, 1964, Paper No. 64-WA/UNT-12.
89. Wall, L.D., Jr. and Card, M.F., "Torsional shear strength of filament-wound glass-epoxy tubes", NASA TN D-6140, August 1970.
90. Holston, A., Jr., Feldman, A. and Stang, D.A., "Stability of filament-wound cylinders under combined loading", UFAF, WPAFB, Tech Report AFFDL-TR-67-55, May 1967.
91. Lekhnitskii, S. G., "Theory of elasticity of an anisotropic body", translated by Fern, P., and Brandstatter, J. J., Holden-Day, San Francisco, Calif., 1963.
92. Lekhnitskii, S. G., "Anisotropic plates", translated by Tsai, S. W., and Cheron, T., Gordon and Breach, New York, 1968.
93. Panc, V., "Theories of elastic plates", Noordhoff International, The Netherlands, 1975.
94. Gerard, G., "Introduction to structural stability theory", McGraw-Hill Book Co., Inc., 1962, pages 129-131.
95. "STRAND 5" User's Manual, September 1989.
96. Press, W.H., et., "Numerical recipes" - the art of scientific computing, Cambridge University press, 1988.

- 97 Foster, C.G., "Measurement of radial deformations in thin-walled cylinders", *Experimental Mechanics*, Vol.18, No.11, November 1978, pages 426-430.
- 98 Moler C., Little J. and Bangert S., "PC-Matlab for MS-DOS personal computers", Version 3.2-PC, June 8, 1987.
99. Southwell, R.V., "An introduction to the theory of elasticity for engineers and physicists", Oxford university press, 2nd edition, 1941, pages 428-429.
100. Foster, C.G. and Tennyson, R.C., "Use of the Southwell method to predict buckling strengths of stringer stiffened cylindrical shells", *Strain*, May 1983, pages 63-67.

APPENDIX A

**CALCULATED DATA
OF
RADIAL DISPLACEMENTS
 w_1 AND w_2 FOR VARIOUS
GEOMETRIC
CONFIGURATIONS**

TABLE A:

**CALCULATED DATA OF RADIAL DISPLACEMENTS w_1 AND w_2
FOR VARIOUS GEOMETRIC CONFIGURATIONS**

$$S/t = 1.0, R/t = 10$$

$$w_s = R^2/(Et) = 0.05 \text{ mm}$$

$2r/t$	w_1	w_1/w_s	w_2	w_2/w_s	w_1/w_2
0.10	0.800E-04	0.160E-02	0.495E-01	0.990	1.620E-03
0.20	0.350E-03	0.700E-02	0.525E-01	1.050	0.670E-02
0.30	0.750E-03	0.150E-01	0.580E-01	1.160	1.290E-02
0.40	0.140E-02	0.280E-01	0.670E-01	1.340	2.090E-02
0.50	0.240E-02	0.470E-01	0.785E-01	1.570	2.990E-02
0.60	0.350E-02	0.700E-01	0.965E-01	1.930	3.630E-02
0.70	0.550E-02	0.1100	0.1250	2.500	4.400E-02
0.80	0.850E-02	0.1700	0.1780	3.560	4.780E-02

TABLE A CONTINUE

$$S/t = 1.0, R/t = 30$$

$$w_s = R^2/(Et) = 0.45 \text{ mm}$$

$2r/t$	w_1	w_1/w_s	w_2	w_2/w_s	w_1/w_2
0.10	0.340E-03	0.760E-03	0.452	1.004	0.752E-03
0.20	0.100E-02	2.220E-03	0.483	1.037	2.070E-03
0.30	0.226E-02	5.000E-03	0.534	1.187	4.213E-03
0.40	0.410E-02	9.110E-03	0.615	1.367	6.670E-03
0.50	0.680E-02	1.510E-02	0.725	1.611	9.380E-03
0.60	0.107E-01	2.380E-02	0.890	1.978	1.202E-02
0.70	0.164E-01	3.640E-02	1.155	2.567	1.420E-02
0.80	0.254E-01	5.640E-02	1.644	3.653	1.545E-02

TABLE A CONTINUE
 $S/t = 1.0$, $R/t = 60$
 $w_s = R^2/(Et) = 1.80 \text{ mm}$

$2r/t$	w_1	w_1/w_s	w_2	w_2/w_s	w_1/w_2
0.10	0.540E-03	0.300E-03	1.850	1.028	0.298E-03
0.20	0.190E-02	0.106E-02	1.945	1.080	0.977E-03
0.30	0.432E-02	0.240E-02	2.220	1.233	1.950E-03
0.40	0.800E-02	0.440E-02	2.480	1.378	3.230E-03
0.50	1.350E-02	0.750E-02	3.010	1.672	4.485E-03
0.60	2.150E-02	1.190E-02	3.590	1.994	5.980E-03
0.70	3.350E-02	1.861E-02	5.210	2.894	6.430E-03
0.80	5.100E-02	2.83E-02	6.590	3.661	7.740E-03

TABLE A CONTINUE
 $S/t = 1.0$, $R/t = 100$
 $w_s = R^2/(Et) = 5.00 \text{ mm}$

$2r/t$	w_1	w_1/w_s	w_2	w_2/w_s	w_1/w_2
0.10	0.111E-02	0.222E-03	5.100	1.020	0.218E-03
0.20	0.340E-02	0.680E-03	5.420	1.084	0.627E-03
0.30	0.750E-02	0.150E-02	6.000	1.200	0.125E-02
0.40	0.138E-01	0.276E-02	6.900	1.380	0.200E-02
0.50	0.230E-01	0.460E-02	8.135	1.627	0.283E-02
0.60	0.358E-01	0.716E-02	10.020	2.004	0.357E-02
0.70	0.548E-01	0.110E-01	12.840	2.568	0.427E-02
0.80	0.840E-01	0.168E-01	18.320	3.664	0.459E-02

TABLE A CONTINUE
 $S/t = 1.0$, $R/t = 300$
 $w_s = R^2/(Et) = 45 \text{ mm}$

$2r/t$	w_1	w_1/w_s	w_2	w_2/w_s	w_1/w_2
0.10	0.364E-02	0.768E-04	46.050	1.023	0.750E-04
0.20	1.045E-02	2.320E-04	49.080	1.090	2.120E-04
0.30	2.278E-02	5.060E-04	54.450	1.210	4.184E-04
0.40	4.155E-02	9.230E-04	62.220	1.380	6.680E-04
0.50	6.880E-02	1.530E-03	73.600	1.636	9.350E-04
0.60	0.1068	2.370E-03	90.150	2.003	1.185E-03
0.70	0.1640	3.640E-03	116.800	2.596	1.400E-03
0.80	0.2555	5.680E-03	165.800	3.680	1.541E-03

TABLE A CONTINUE
 $S/t = 1.0$, $R/t = 600$
 $w_s = R^2/(Et) = 180 \text{ mm}$

$2r/t$	w_1	w_1/w_s	w_2	w_2/w_s	w_1/w_2
0.10	0.560E-02	0.310E-04	184.130	1.023	0.168E-04
0.20	0.204E-01	0.113E-03	196.210	1.090	1.038E-04
0.30	0.453E-01	0.252E-03	216.450	1.203	2.093E-04
0.40	0.816E-01	0.453E-03	249.100	1.384	3.270E-04
0.50	0.1371	0.762E-03	294.100	1.634	4.660E-04
0.60	0.2132	0.118E-02	360.200	2.001	5.920E-04
0.70	0.3255	0.181E-02	468.200	2.601	6.950E-04
0.80	0.5105	0.284E-02	664.000	3.689	7.690E-04

TABLE A CONTINUE
 $S/t = 0.80$, $R/t = 10$
 $w_s = R^2/(Et) = 0.05 \text{ mm}$

$2r/t$	w_1	w_1/w_s	w_2	w_2/w_s	w_1/w_2
0.20	0.430E-03	0.860E-02	0.535E-01	1.070	0.804E-02
0.40	1.700E-03	3.400E-02	0.685E-01	1.370	2.480E-02
0.60	4.500E-03	9.000E-02	0.991E-01	1.982	4.540E-02

TABLE A CONTINUE
 $S/t = 0.80$, $R/t = 30$
 $w_s = R^2/(Et) = 0.45 \text{ mm}$

$2r/t$	w_1	w_1/w_s	w_2	w_2/w_s	w_1/w_2
0.20	0.127E-02	0.282E-02	0.4890	1.0867	0.260E-02
0.40	0.505E-02	1.122E-02	0.6330	1.4067	0.800E-02
0.60	1.350E-02	3.000E-02	0.9170	2.0380	1.470E-02

TABLE A CONTINUE
 $S/t = 0.80$, $R/t = 60$
 $w_s = R^2/(Et) = 1.80 \text{ mm}$

$2r/t$	w_1	w_1/w_s	w_2	w_2/w_s	w_1/w_2
0.20	0.255E-02	0.142E-02	1.978	1.099	0.129E-02
0.40	1.020E-02	0.567E-02	2.555	1.419	0.399E-02
0.60	2.700E-02	1.500E-02	3.698	2.055	0.730E-02

TABLE A CONTINUE
 $S/t = 0.80$, $R/t = 100$
 $w_s = R^2/(Et) = 5.0 \text{ mm}$

$2r/t$	w_1	w_1/w_s	w_2	w_2/w_s	w_1/w_2
0.20	0.430E-02	0.860E-03	5.495	1.0990	0.783E-03
0.40	1.700E-02	3.400E-03	7.078	1.4156	2.402E-03
0.60	4.520E-02	9.000E-03	10.160	2.0320	4.450E-03

TABLE A CONTINUE
 $S/t = 0.80$, $R/t = 300$
 $w_s = R^2/(Et) = 45 \text{ mm}$

$2r/t$	w_1	w_1/w_s	w_2	w_2/w_s	w_1/w_2
0.20	0.125E-01	0.277E-03	49.470	1.099	0.252E-03
0.40	0.510E-01	1.133E-03	63.950	1.421	0.797E-03
0.60	1.338E-01	2.973E-03	93.030	2.067	1.438E-03

TABLE A CONTINUE
 $S/t = 0.80$, $R/t = 600$
 $w_s = R^2/(Et) = 180 \text{ mm}$

$2r/t$	w_1	w_1/w_s	w_2	w_2/w_s	w_1/w_2
0.20	0.02575	0.143E-03	201.100	1.117	0.128E-03
0.40	0.13000	0.569E-03	259.200	1.440	0.382E-03
0.60	0.26650	1.480E-03	372.300	2.068	0.716E-03

TABLE A CONTINUE
 $S/t = 1.4$, $R/t = 10$
 $w_s = R^2/(Et) = 0.05 \text{ mm}$

$2r/t$	w_1	w_1/w_s	w_2	w_2/w_s	w_1/w_2
0.20	0.28E-03	0.560E-02	0.515E-01	1.030	0.544E-02
0.40	0.95E-03	1.900E-02	0.625E-01	1.250	1.520E-02
0.60	2.40E-03	4.800E-02	0.890E-01	1.780	2.700E-02

TABLE A CONTINUE
 $S/t = 1.4$, $R/t = 30$
 $w_s = R^2/(Et) = 0.45 \text{ mm}$

$2r/t$	w_1	w_1/w_s	w_2	w_2/w_s	w_1/w_2
0.20	0.850E-03	0.189E-02	0.4735	1.0522	0.180E-02
0.40	3.000E-03	0.667E-02	0.5780	1.2844	0.519E-02
0.60	7.350E-03	1.633E-02	0.8250	1.8333	0.890E-02

TABLE A CONTINUE
 $S/t = 1.4$, $R/t = 60$
 $w_s = R^2/(Et) = 1.80 \text{ mm}$

$2r/t$	w_1	w_1/w_s	w_2	w_2/w_s	w_1/w_2
0.20	0.169E-02	0.939E-03	1.913	1.063	0.883E-03
0.40	0.600E-02	3.333E-03	2.315	1.286	2.592E-03
0.60	1.485E-02	8.250E-03	3.300	1.833	4.500E-03

TABLE A CONTINUE
 $S/t = 1.4$, $R/t = 100$
 $w_s = R^2/(Et) = 5.00 \text{ mm}$

$2r/t$	w_1	w_1/w_s	w_2	w_2/w_s	w_1/w_2
0.20	0.283E-02	0.566E-03	5.315	1.063	0.532E-03
0.40	1.001E-02	2.002E-03	6.455	1.291	1.551E-03
0.60	2.470E-02	4.940E-03	9.202	1.840	2.684E-03

TABLE A CONTINUE
 $S/t = 1.4$, $R/t = 300$
 $w_s = R^2/(Et) = 45 \text{ mm}$

$2r/t$	w_1	w_1/w_s	w_2	w_2/w_s	w_1/w_2
0.20	0.856E-02	0.190E-03	47.940	1.065	0.179E-03
0.40	3.000E-02	0.667E-03	58.150	1.292	0.516E-03
0.60	7.430E-02	1.651E-03	83.020	1.845	0.895E-03

TABLE A CONTINUE
 $S/t = 1.4$, $R/t = 600$
 $w_s = R^2/(Et) = 180 \text{ mm}$

$2r/t$	w_1	w_1/w_s	w_2	w_2/w_s	w_1/w_2
0.20	0.160E-01	0.890E-04	191.700	1.065	0.680E-04
0.40	0.602E-01	3.344E-04	233.000	1.294	2.583E-04
0.60	1.488E-01	8.266E-04	331.900	1.844	4.483E-04

TABLE A CONTINUE
 $S/t = 1.6$, $R/t = 10$
 $w_s = R^2/(Et) = 0.05 \text{ mm}$

$2r/t$	w_1	w_1/w_s	w_2	w_2/w_s	w_1/w_2
0.20	0.265E-03	0.530E-02	0.0510	1.020	0.520E-02
0.40	0.888E-03	1.780E-02	0.0610	1.220	1.456E-02
0.60	2.250E-03	4.400E-02	0.0840	1.680	2.620E-02

TABLE A CONTINUE
 $S/t = 1.6$, $R/t = 30$
 $w_s = R^2/(Et) = 0.45 \text{ mm}$

$2r/t$	w_1	w_1/w_s	w_2	w_2/w_s	w_1/w_2
0.20	0.760E-03	0.169E-02	0.470	1.044	0.162E-02
0.40	2.650E-03	0.589E-02	0.560	1.244	0.473E-02
0.60	6.550E-03	1.456E-02	0.775	1.722	0.845E-02

TABLE A CONTINUE
 $S/t = 1.6$, $R/t = 60$
 $w_s = R^2/(Et) = 1.80 \text{ mm}$

$2r/t$	w_1	w_1/w_s	w_2	w_2/w_s	w_1/w_2
0.20	0.156E-02	0.867E-03	1.895	1.053	0.823E-03
0.40	0.533E-02	2.960E-03	2.245	1.247	2.374E-03
0.60	1.320E-02	7.333E-03	3.145	1.747	4.197E-03

TABLE A CONTINUE
 $S/t = 1.6$, $R/t = 100$
 $w_s = R^2/(Et) = 5.0 \text{ mm}$

$2r/t$	w_1	w_1/w_s	w_2	w_2/w_s	w_1/w_2
0.20	0.258E-02	0.516E-03	5.280	1.056	0.489E-03
0.40	0.890E-02	1.780E-03	6.280	1.256	1.417E-03
0.60	2.170E-02	4.340E-03	8.750	1.750	2.480E-03

TABLE A CONTINUE
 $S/t = 1.6$, $R/t = 300$
 $w_s = R^2/(Et) = 45 \text{ mm}$

$2r/t$	w_1	w_1/w_s	w_2	w_2/w_s	w_1/w_2
0.20	0.776E-02	0.172E-03	47.560	1.057	0.163E-03
0.40	2.700E-02	0.600E-03	56.820	1.263	0.475E-03
0.60	6.590E-02	1.464E-03	78.850	1.752	0.836E-03

TABLE A CONTINUE
 $S/t = 1.6$, $R/t = 600$
 $w_s = R^2/(Et) = 180 \text{ mm}$

$2r/t$	w_1	w_1/w_s	w_2	w_2/w_s	w_1/w_2
0.20	0.01550	0.860E-04	190.400	1.0578	0.814E-04
0.40	0.05335	2.963E-04	226.700	1.2594	2.353E-04
0.60	0.13060	7.255E-04	315.500	1.7528	4.139E-04

FIGURES

DISPLACEMENT RATIO
 w_1/w_2 AND w_1/w_s AGAINST
GEOMETRIC PARAMETERS
 $2r/t$, R/t AND S/t

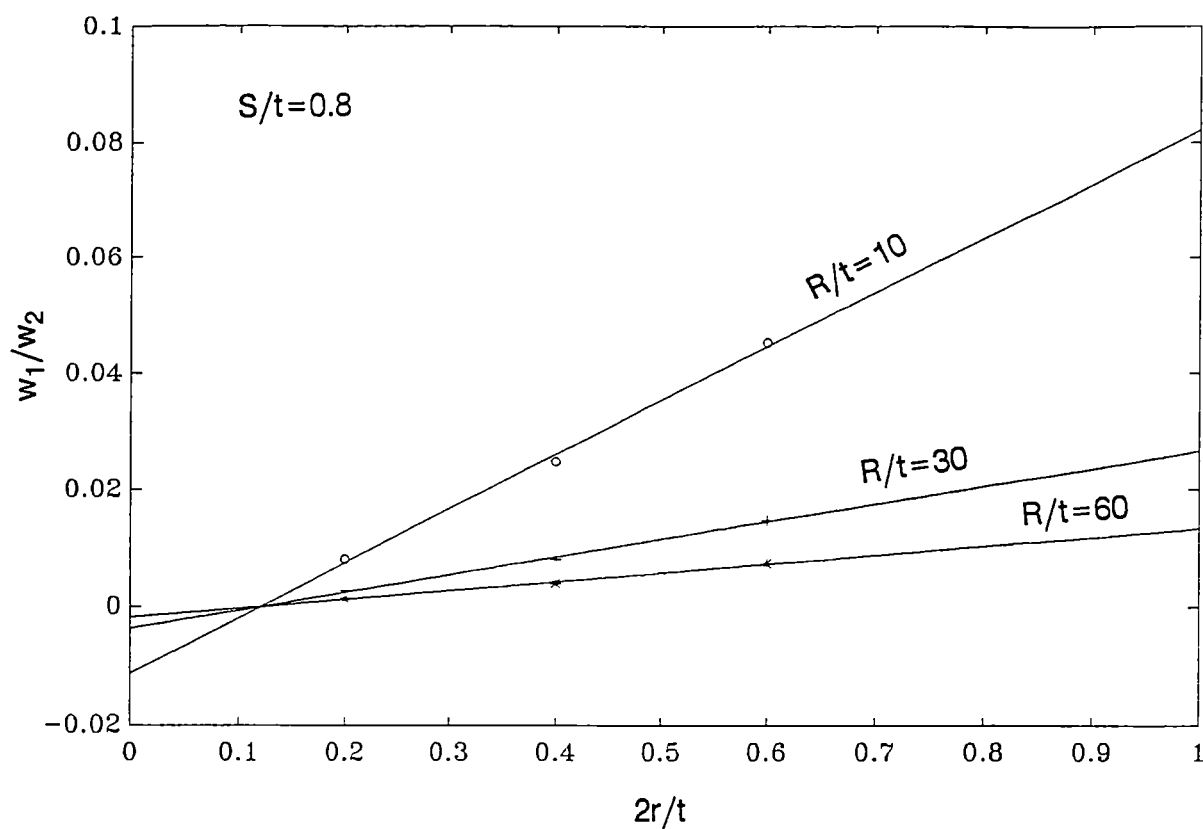


Figure A1 Ratio of displacements w_1/w_2

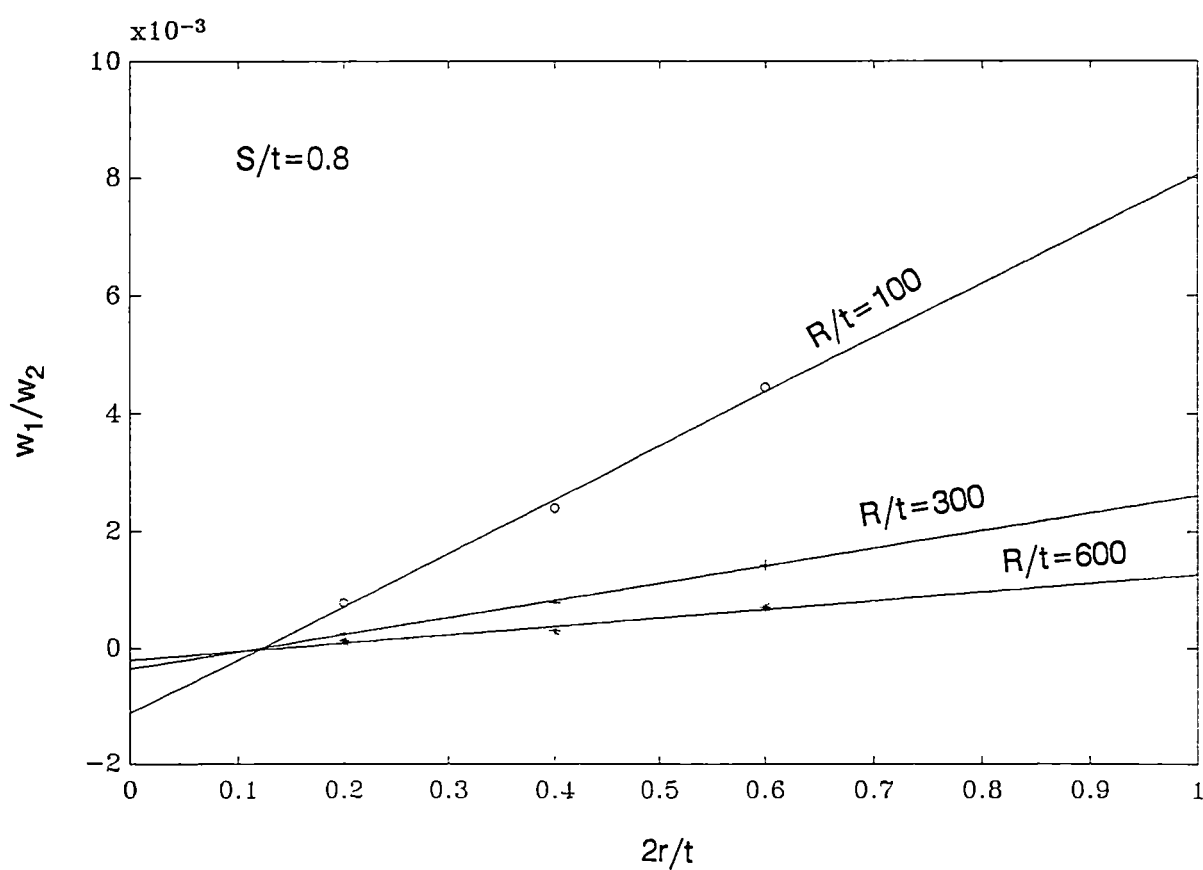


Figure A2 Ratio of displacements w_1/w_2

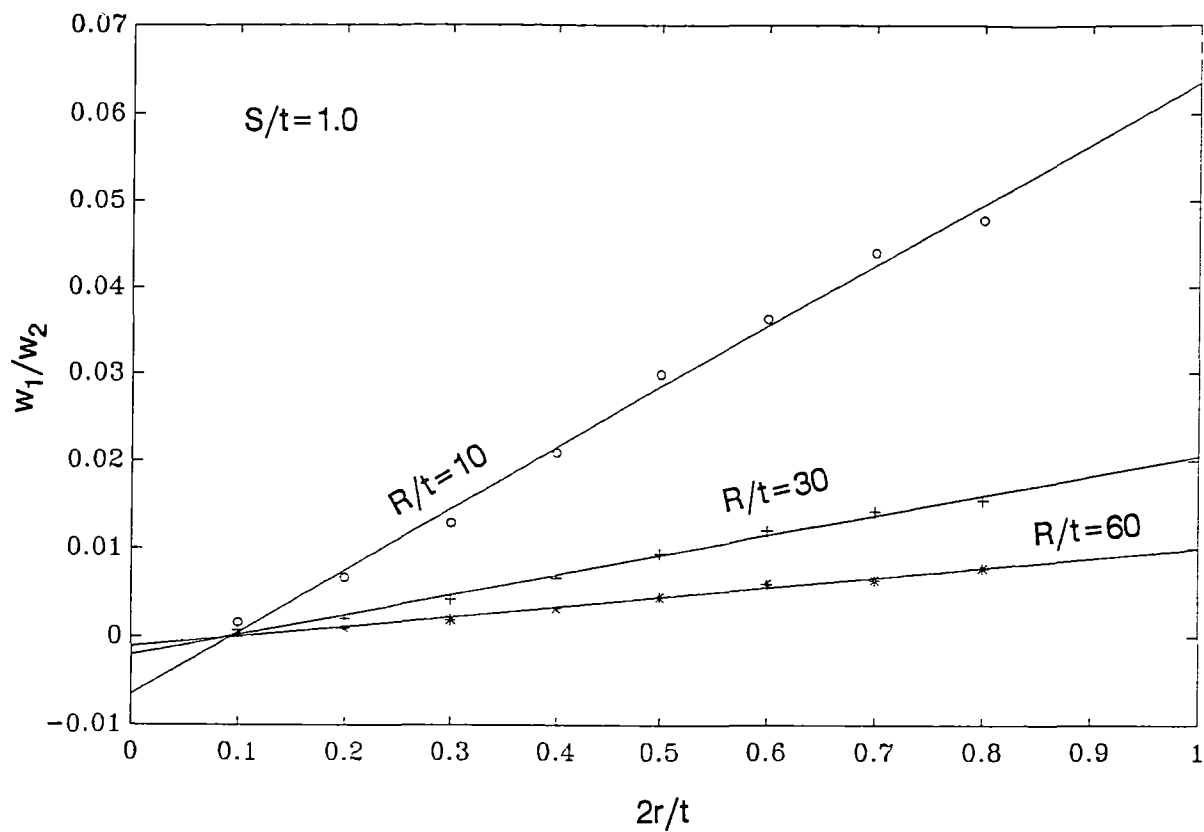


Figure A3 Ratio of displacements w_1/w_2

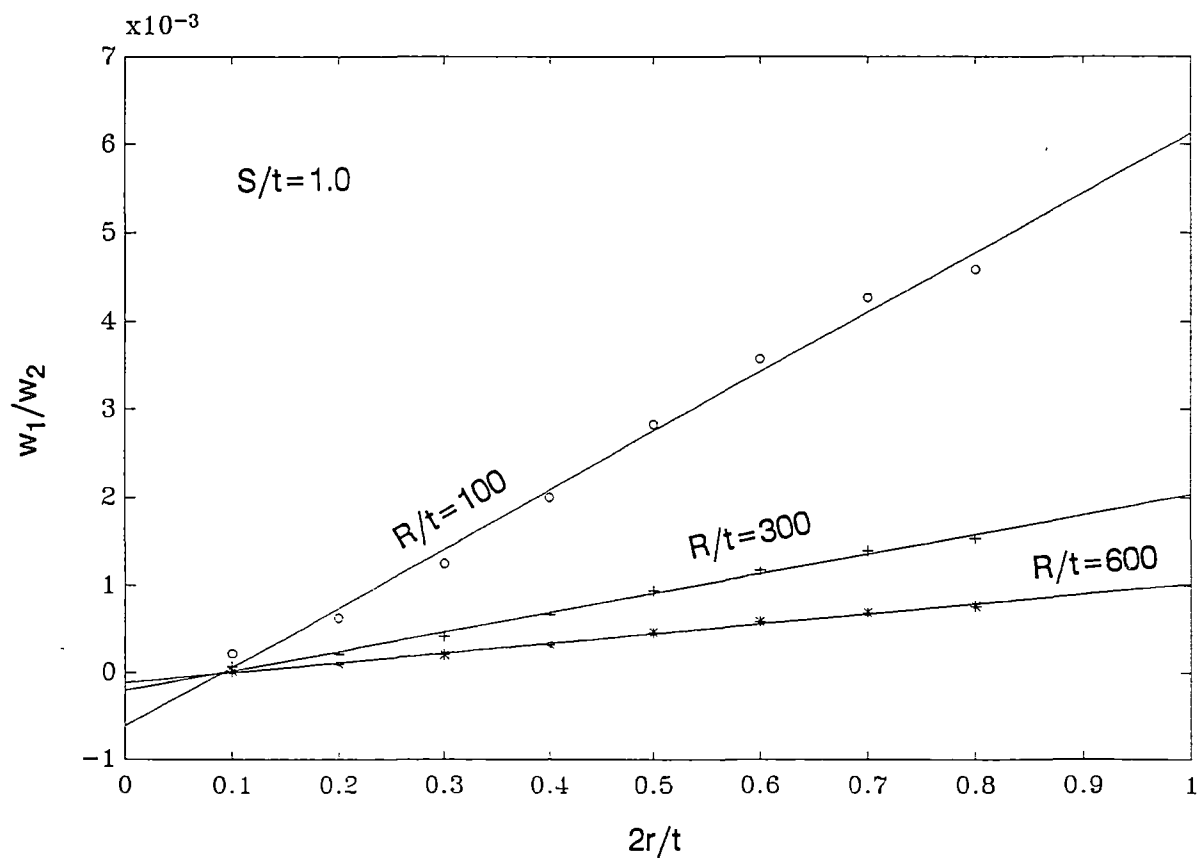


Figure A4 Ratio of displacements w_1/w_2

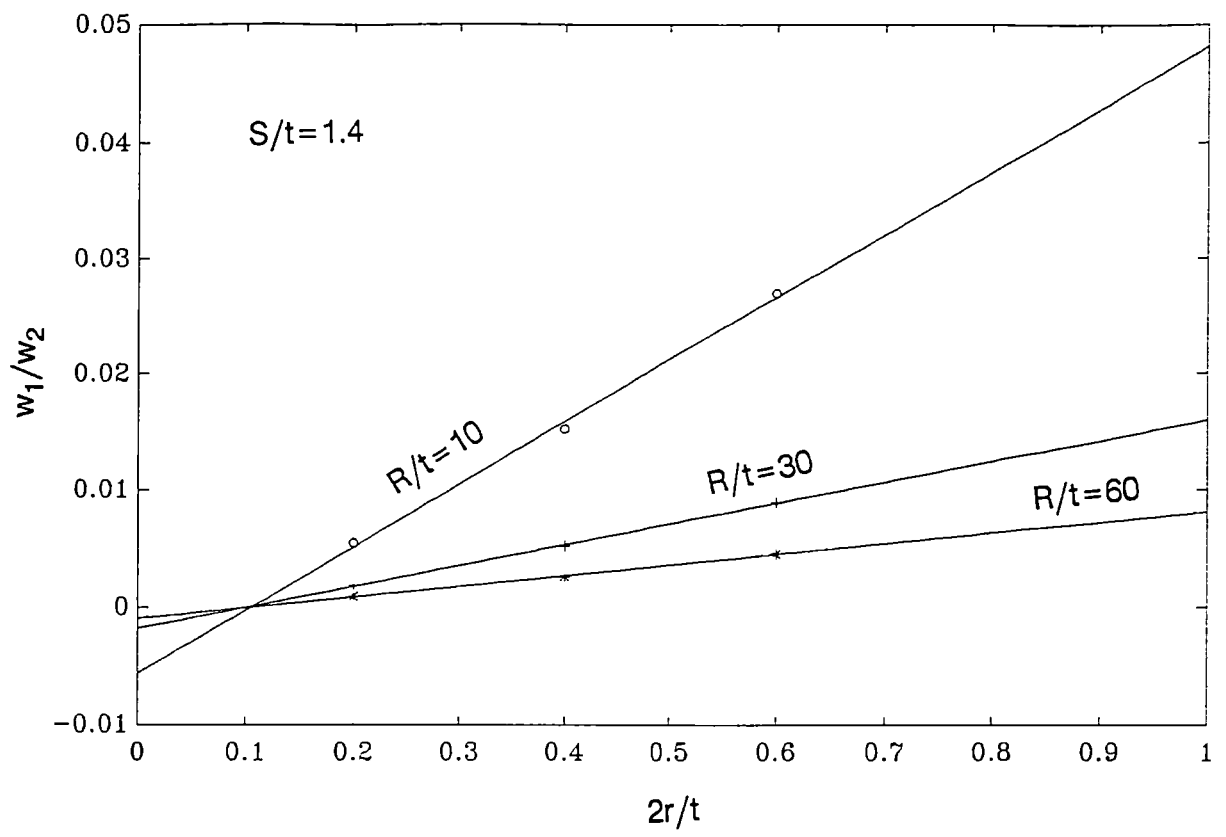


Figure A5 Ratio of displacements w_1/w_2

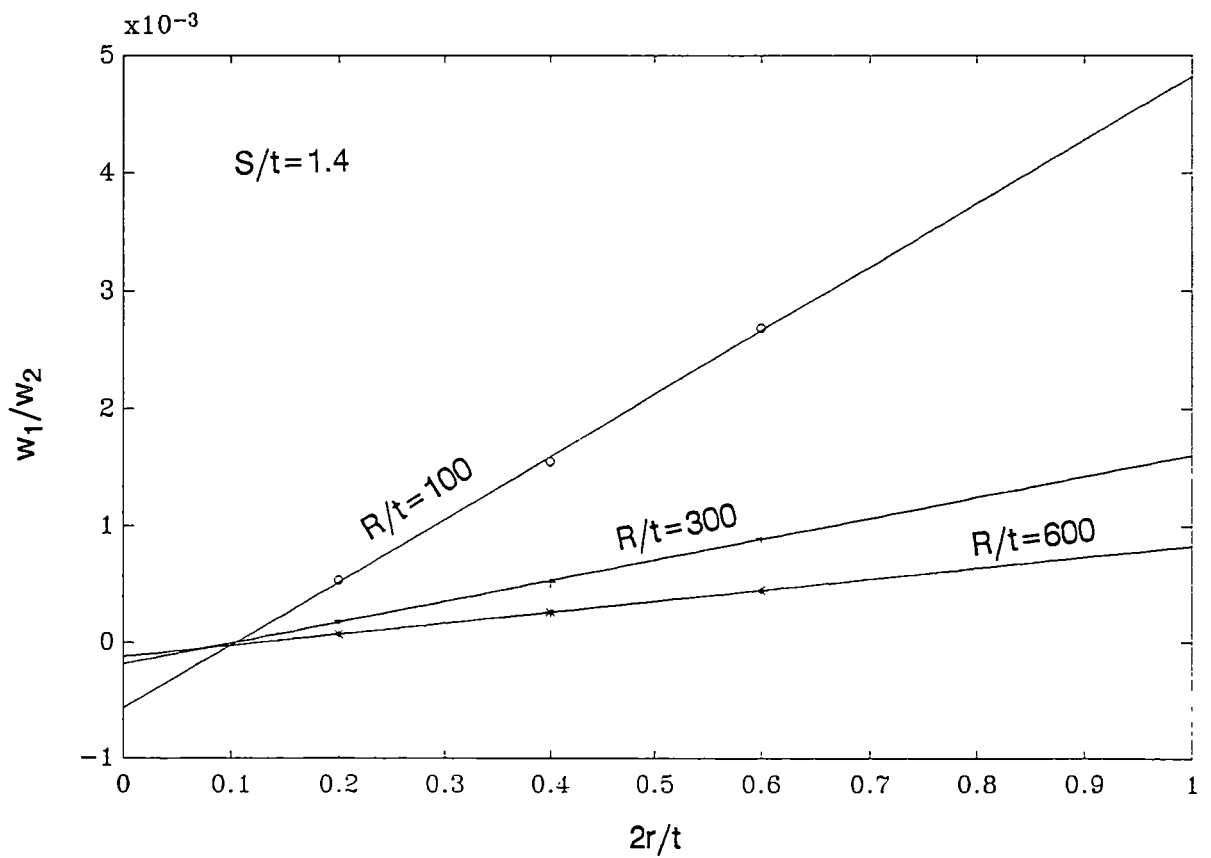


Figure A6 Ratio of displacements w_1/w_2

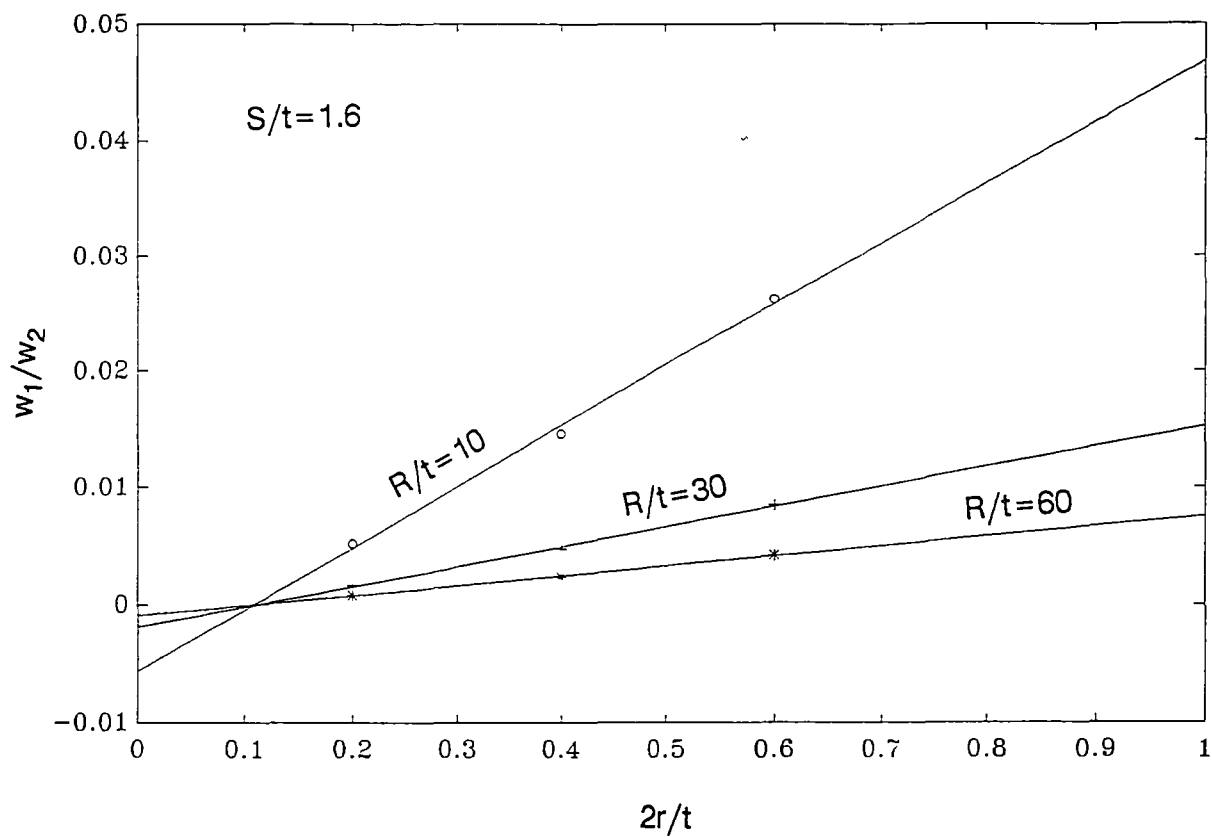


Figure A7 Ratio of displacements w_1/w_2

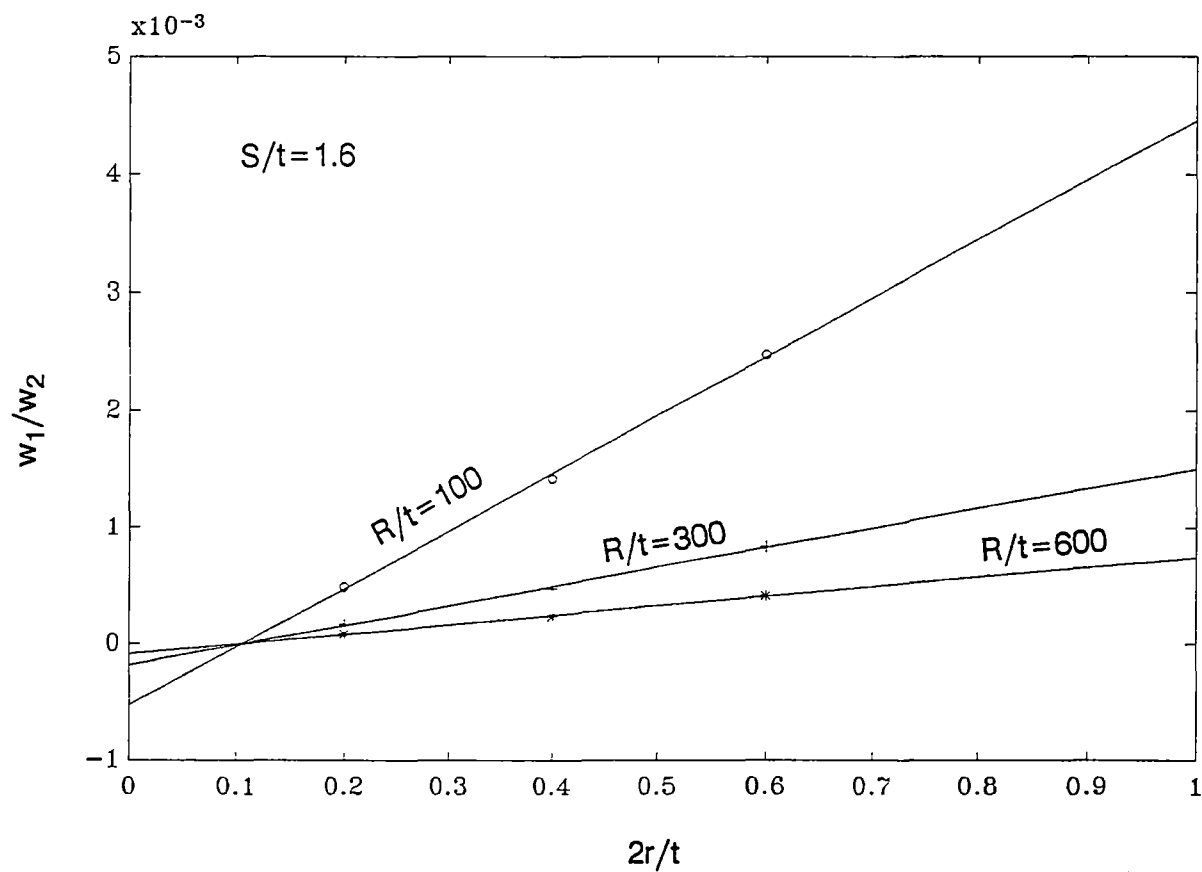


Figure A8 Ratio of displacements w_1/w_2

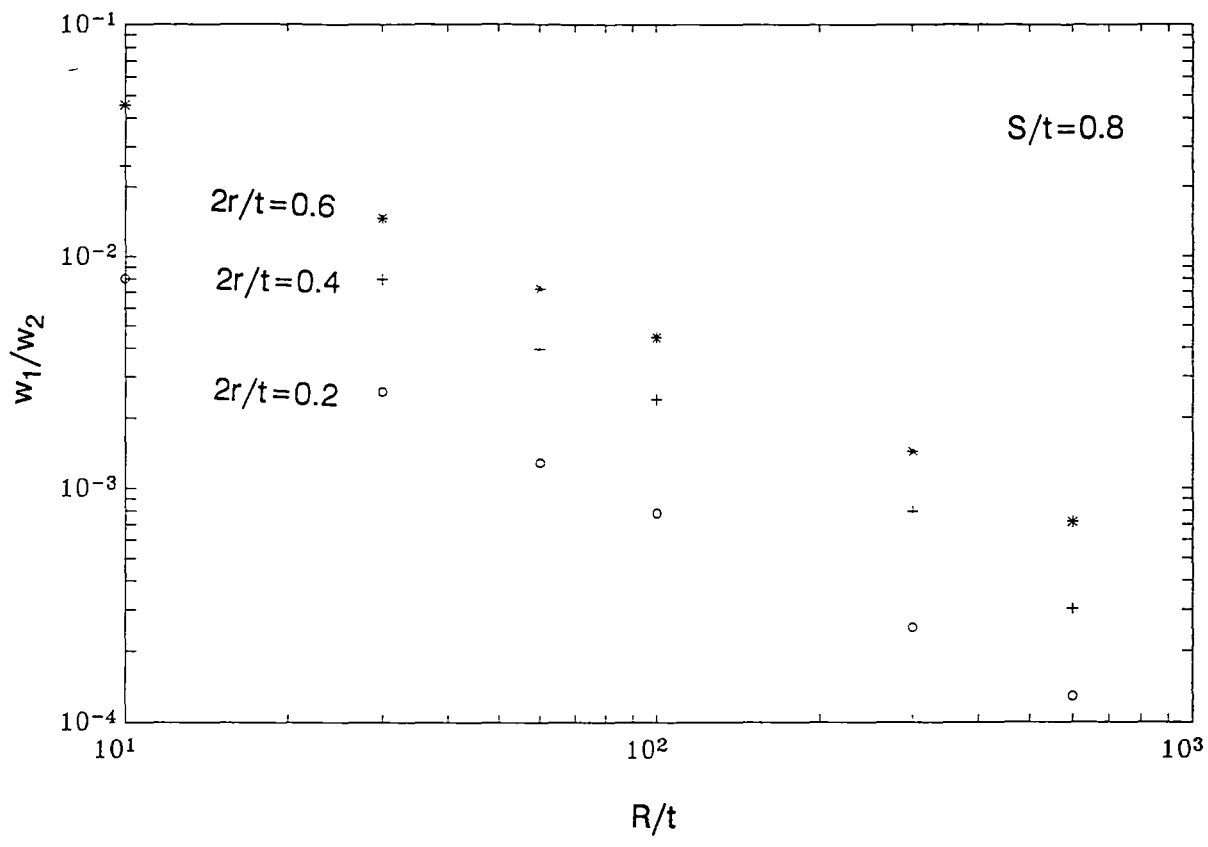


Figure A9 Ratio of displacements w_1/w_2

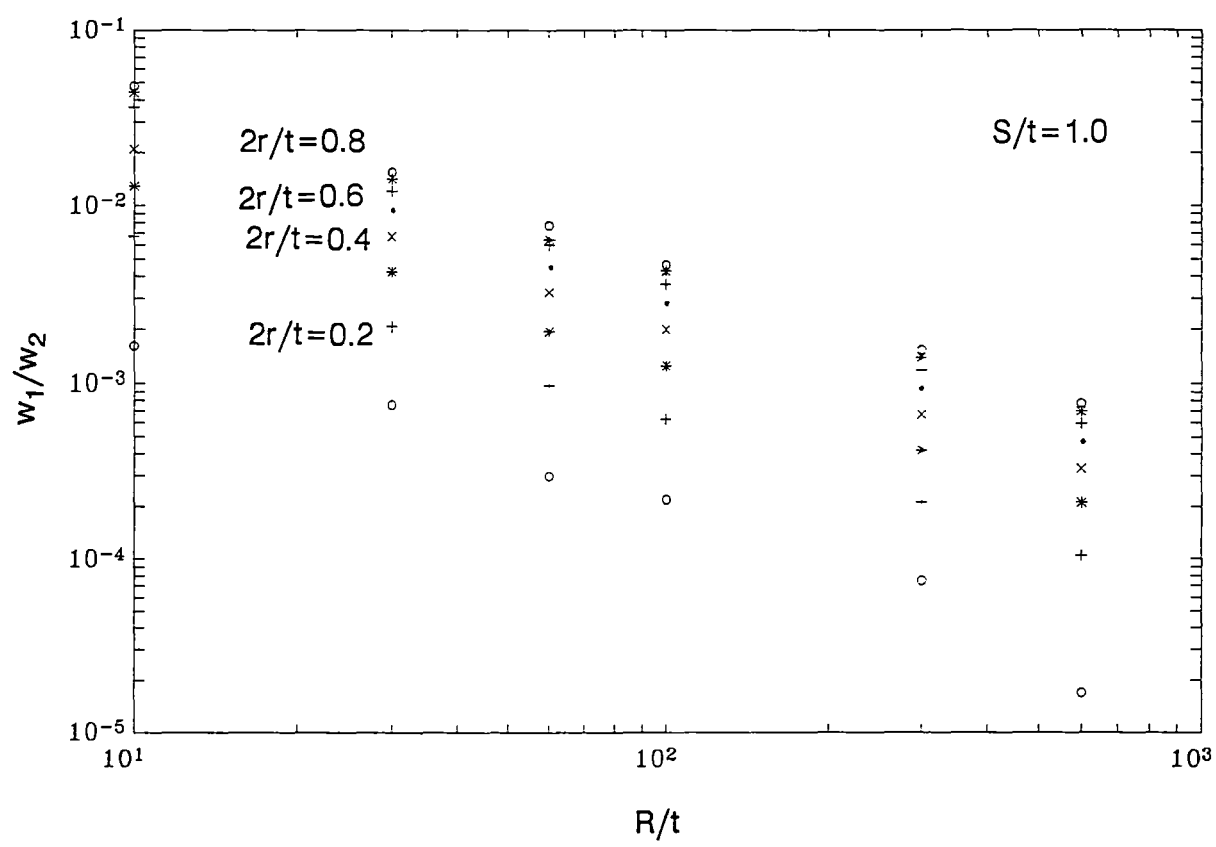


Figure A10 Ratio of displacements w_1/w_2

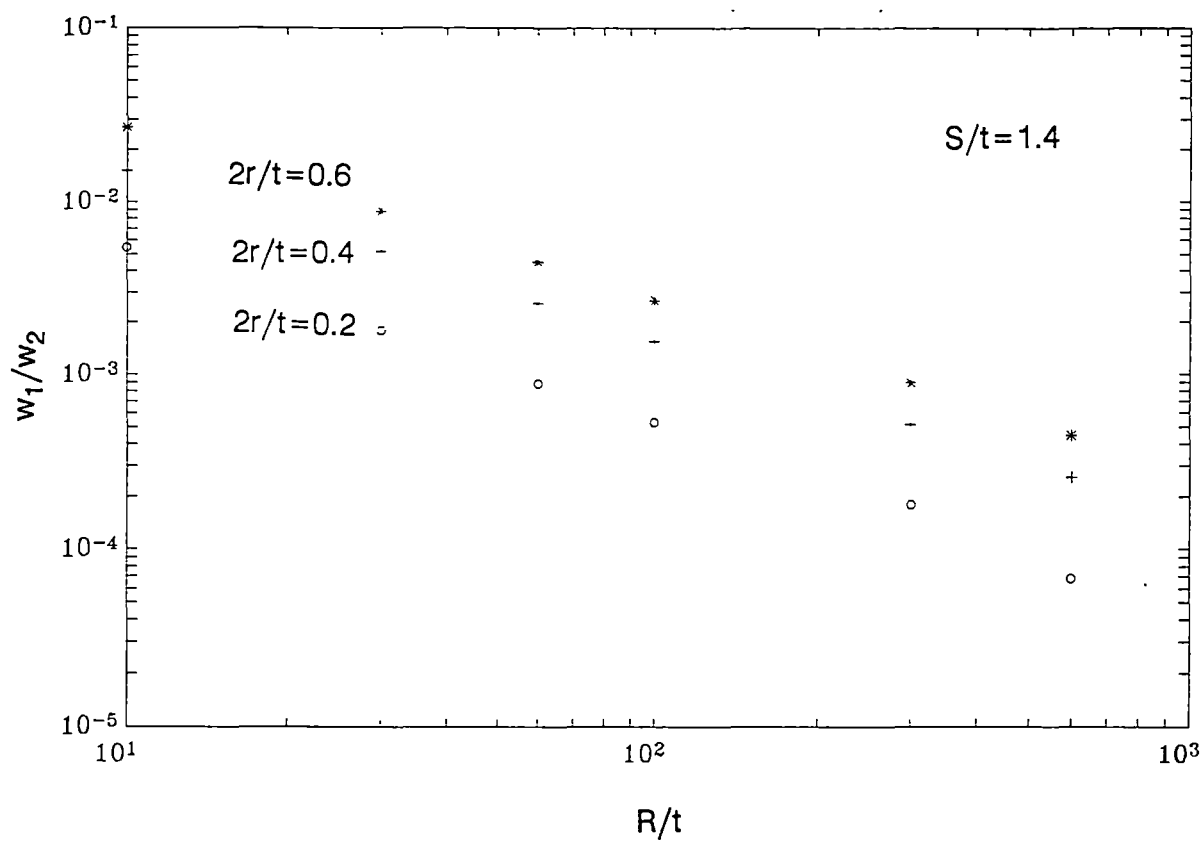


Figure A11 Ratio of displacements w_1/w_2

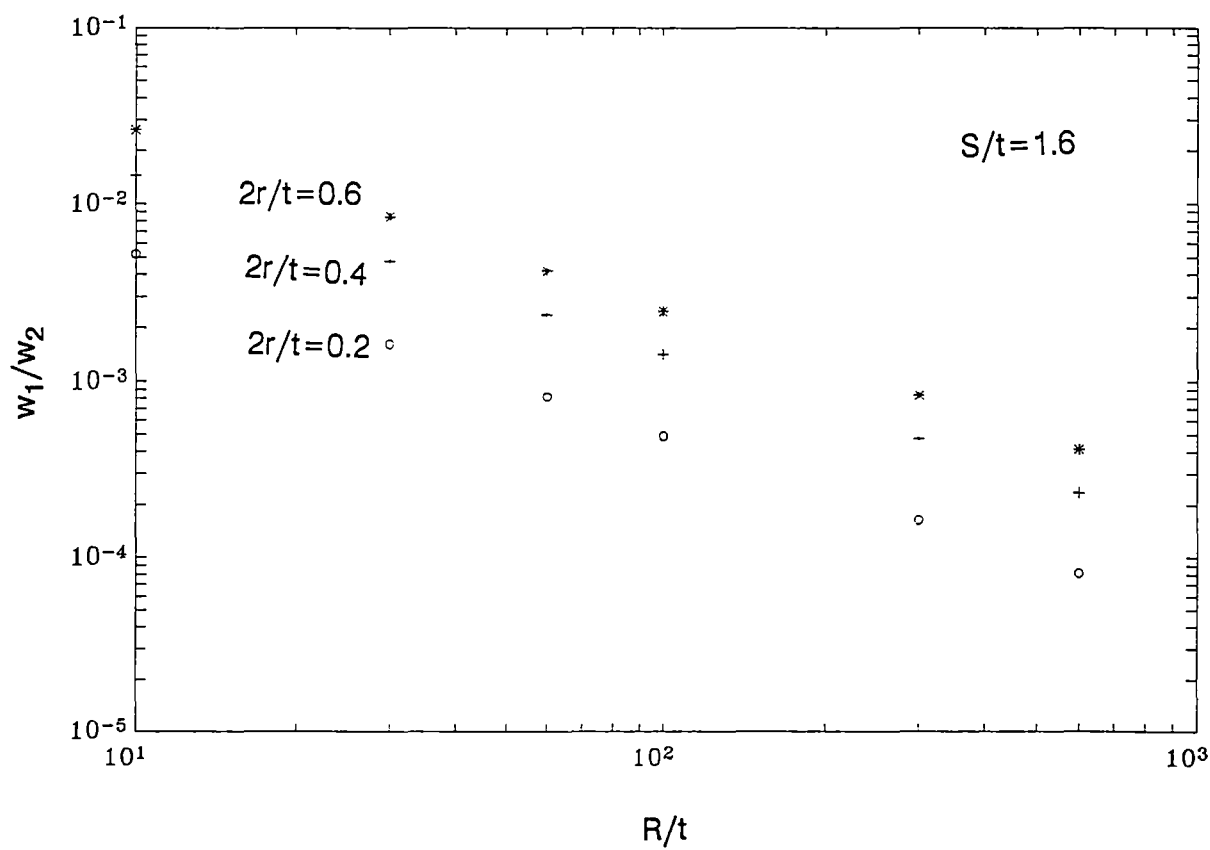


Figure A12 Ratio of displacements w_1/w_2

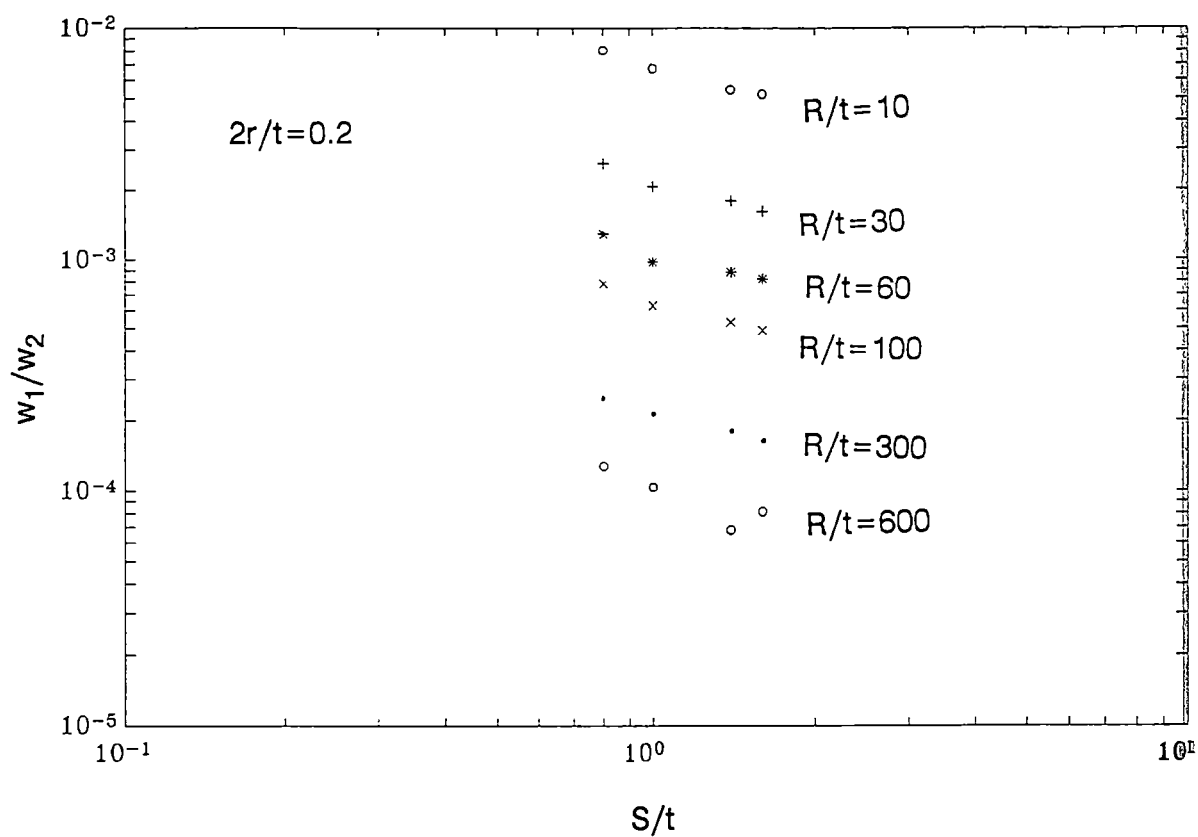


Figure A13 Ratio of displacements w_1/w_2

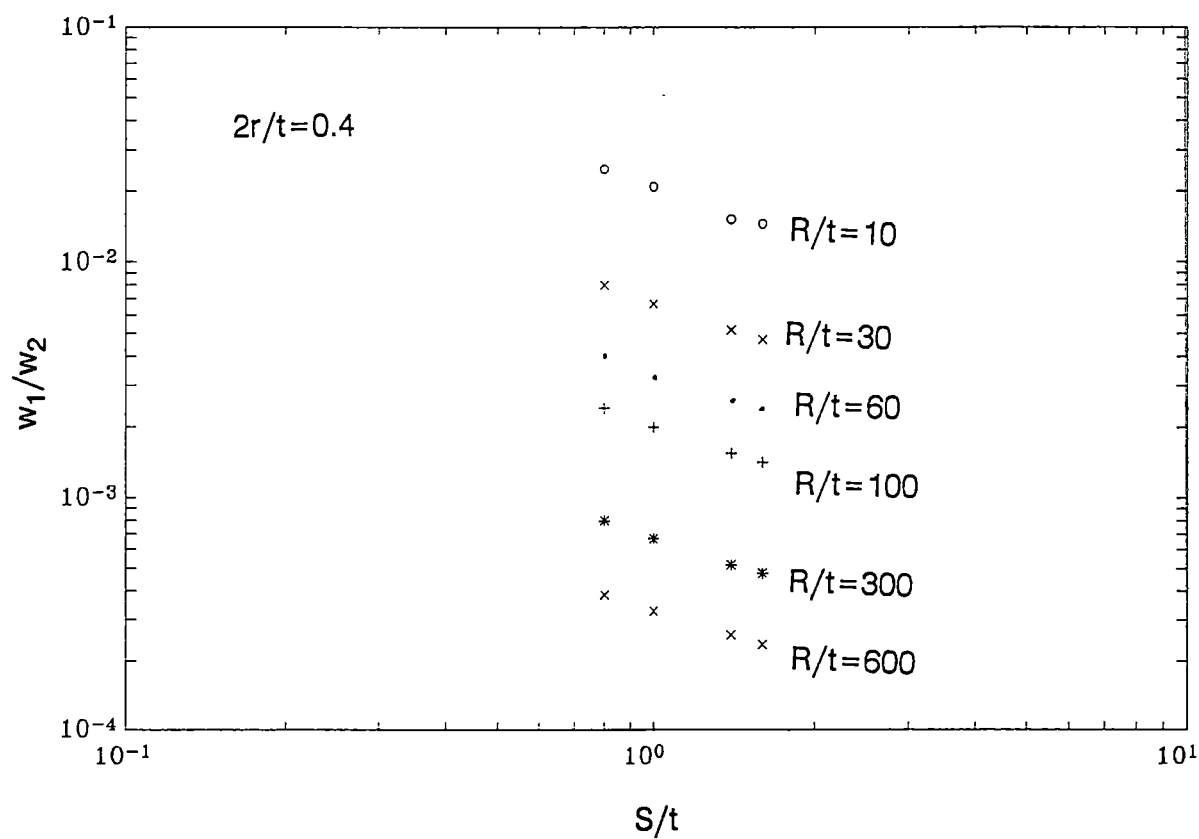


Figure A14 Ratio of displacements w_1/w_2

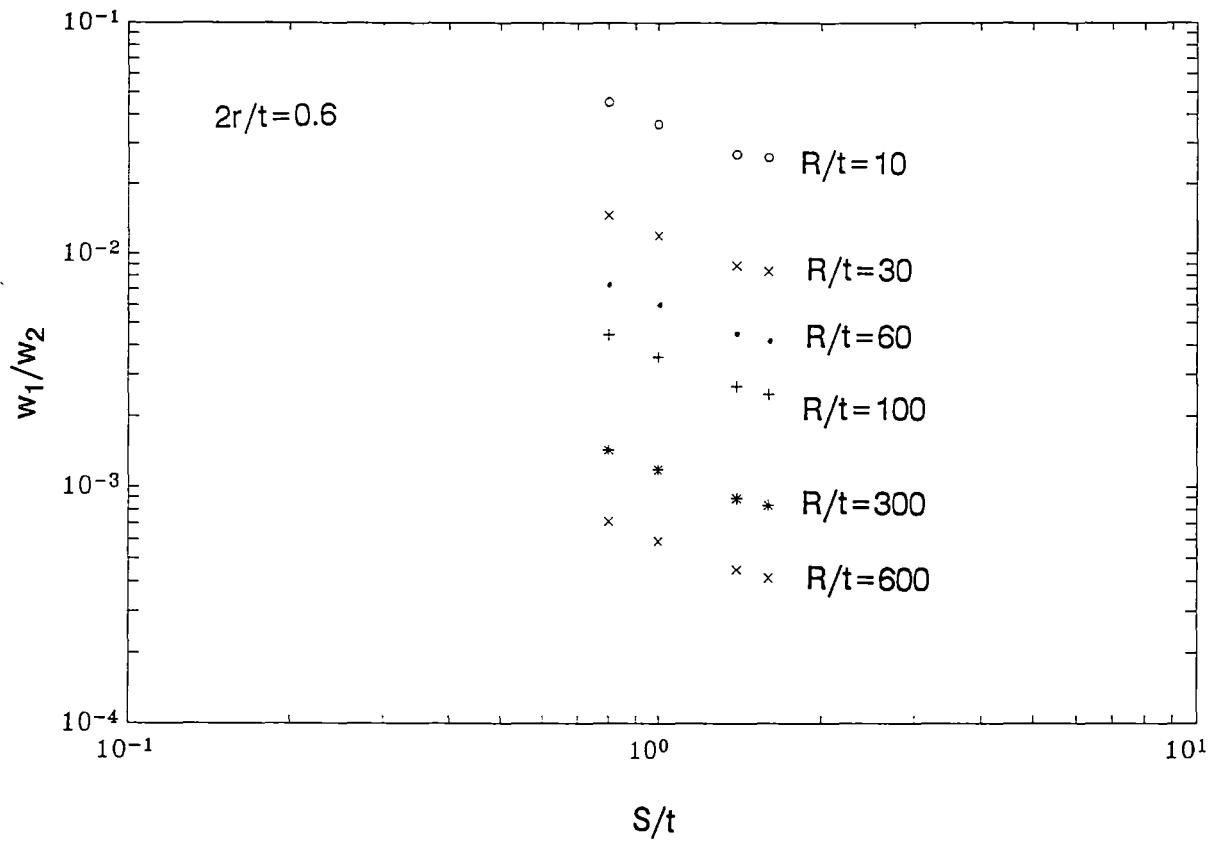


Figure A15 Ratio of displacements w_1/w_2

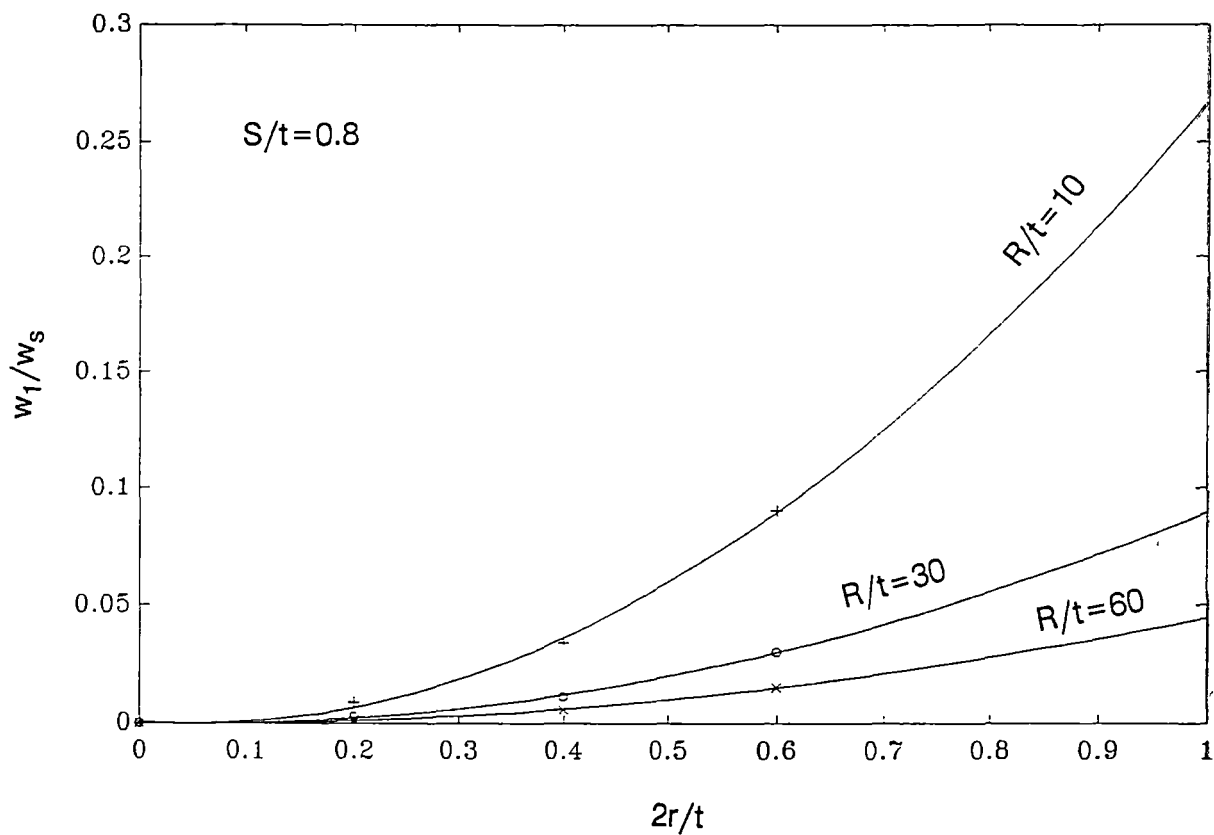


Figure A16 Ratio of displacements w_1/w_s

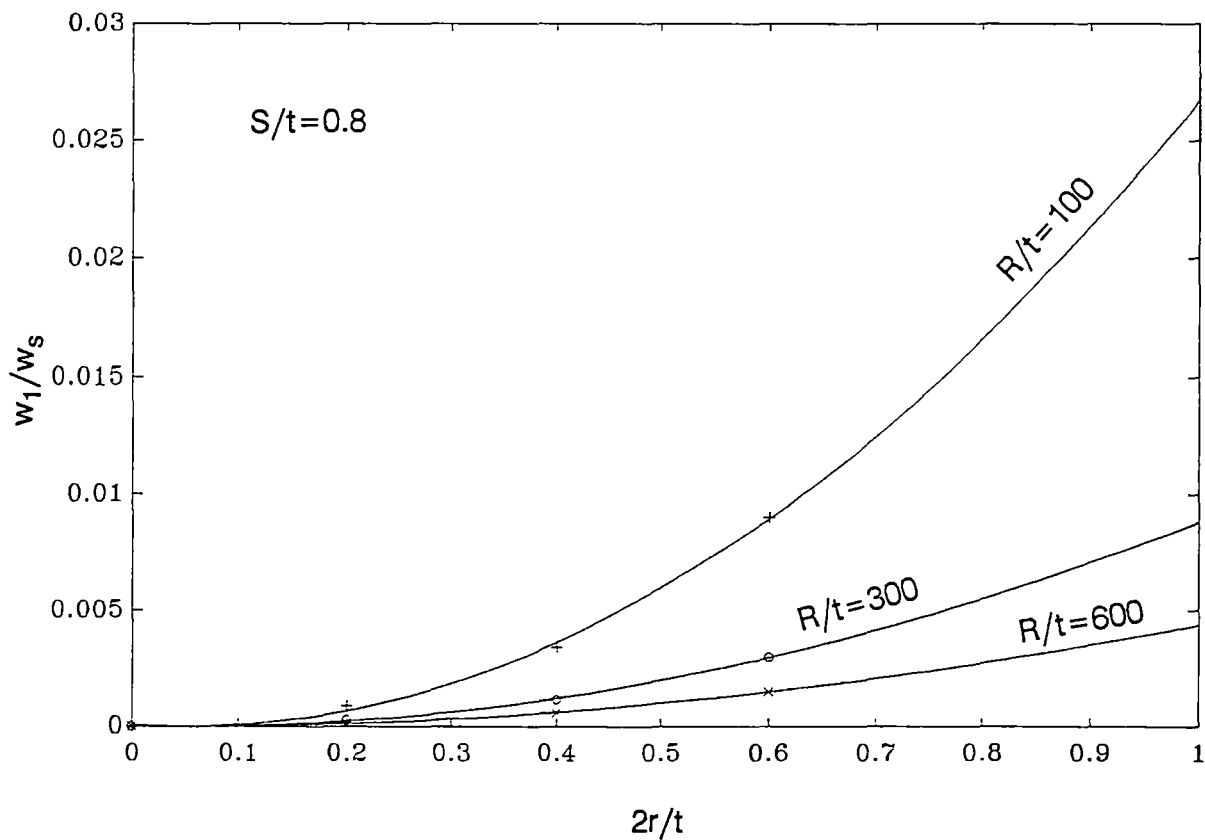


Figure A17 Ratio of displacements w_1/w_s

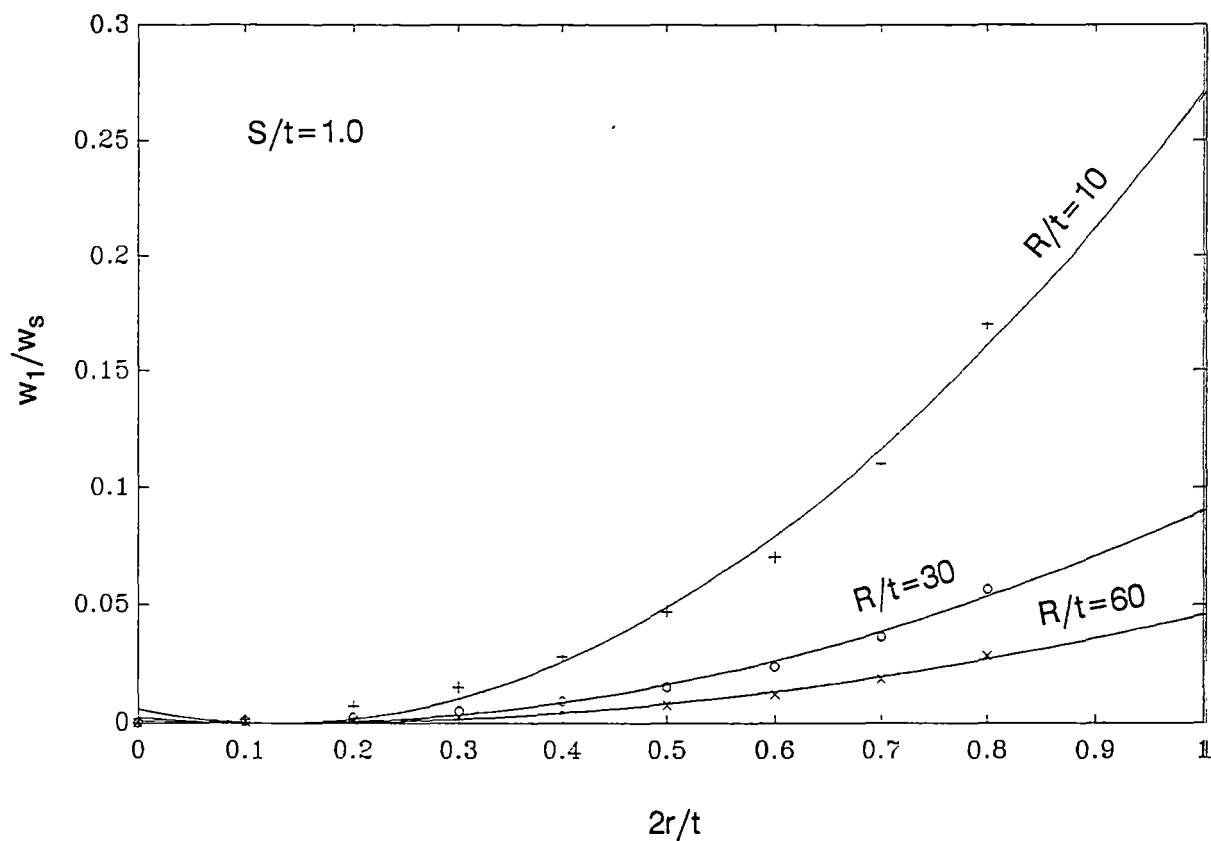


Figure A18 Ratio of displacements w_1/w_s

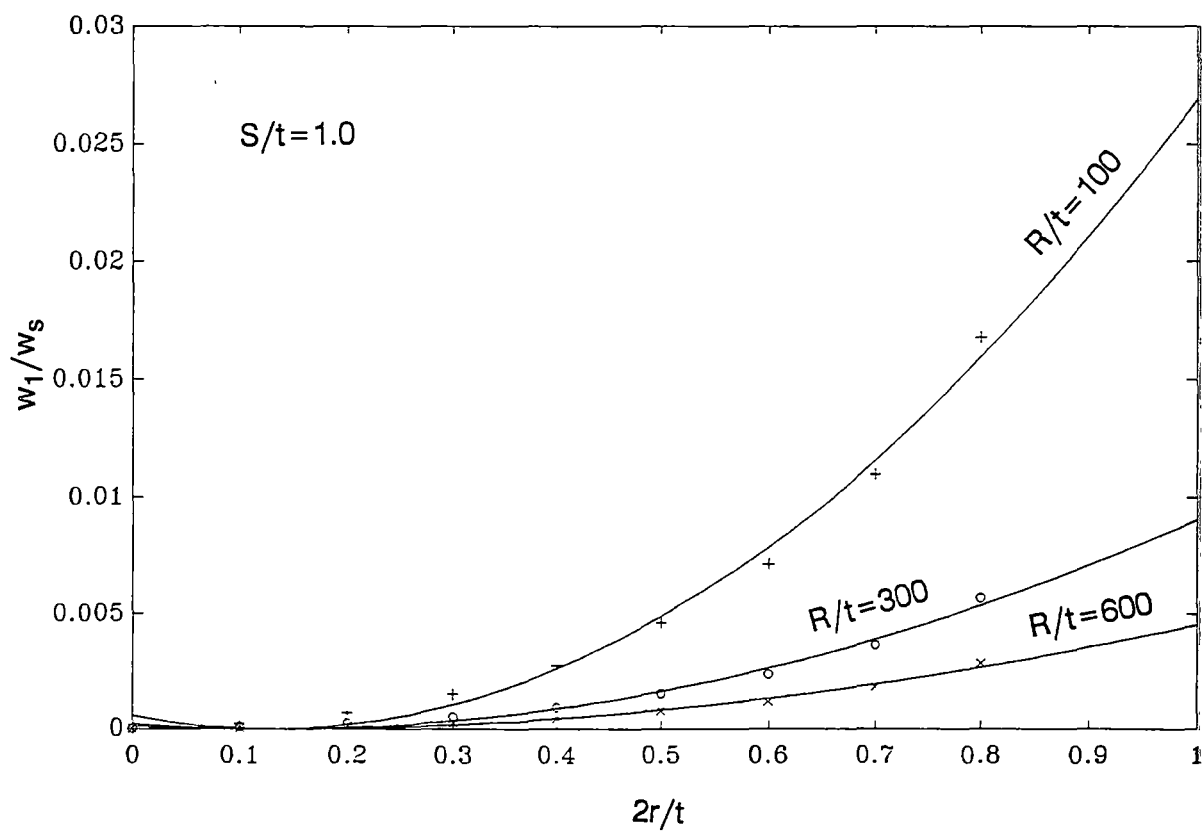


Figure A19 Ratio of displacements w_1/w_s

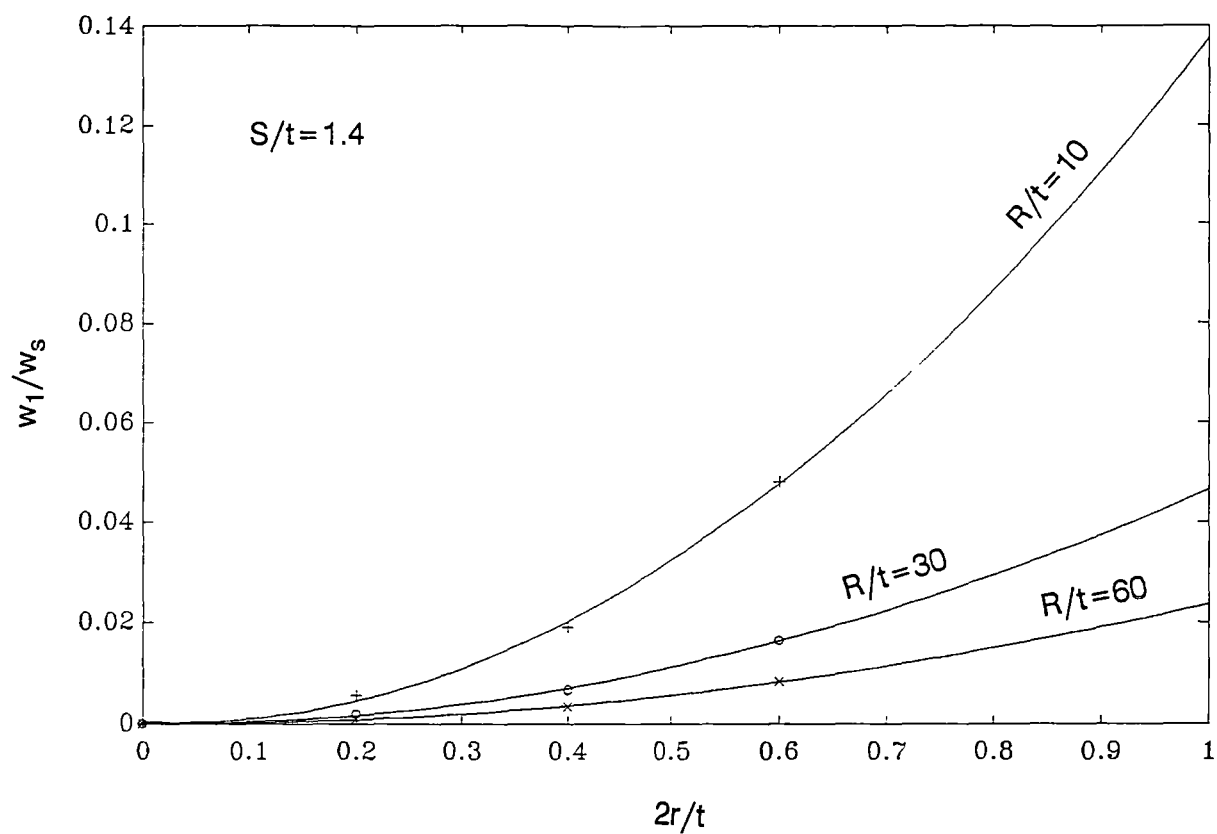


Figure A20 Ratio of displacements w_1/w_s

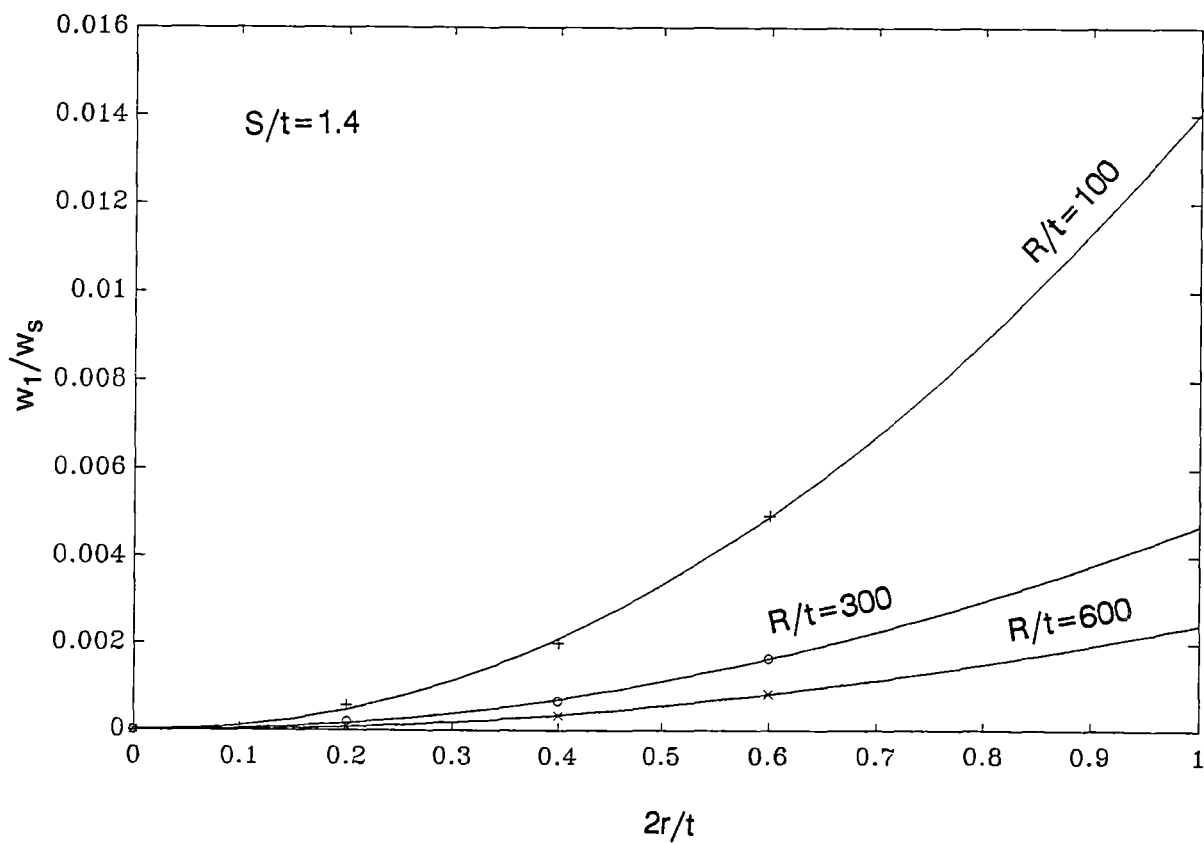


Figure A21 Ratio of displacements w_1/w_s

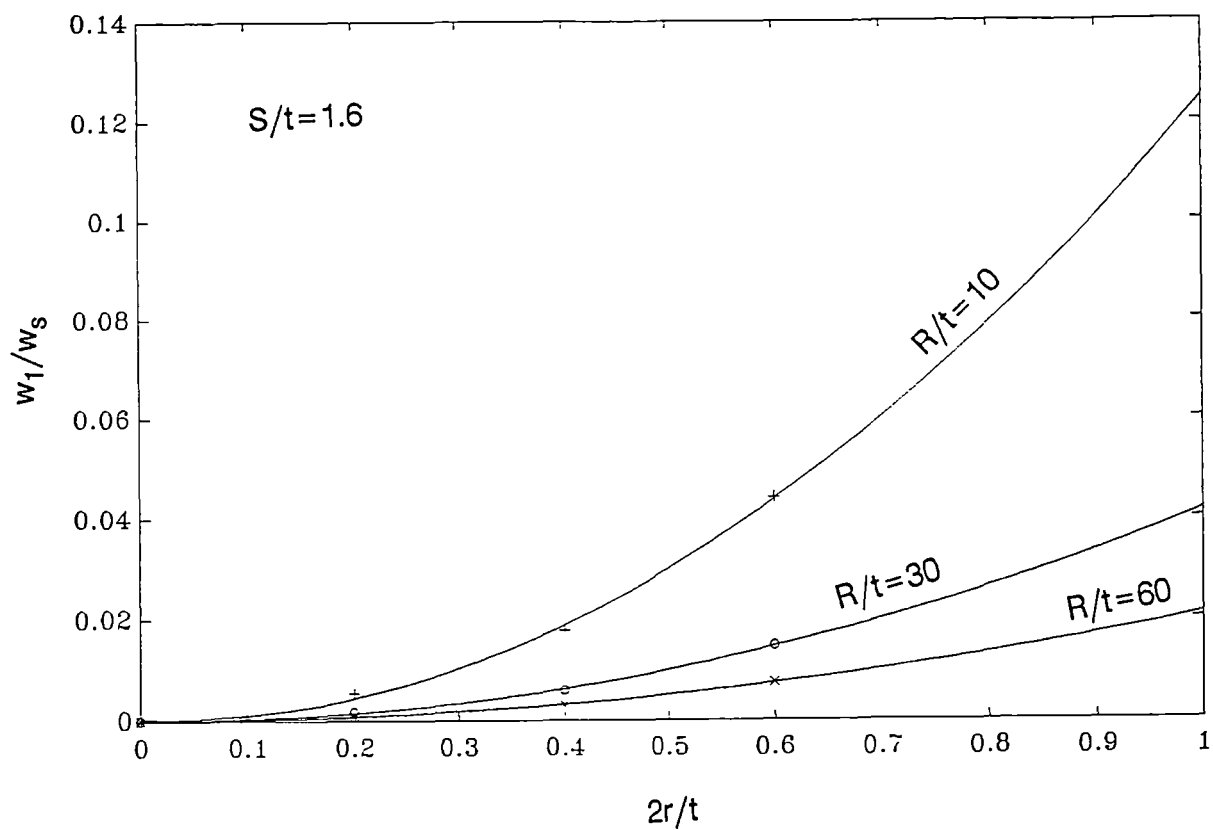


Figure A22 Ratio of displacements w_1/w_s

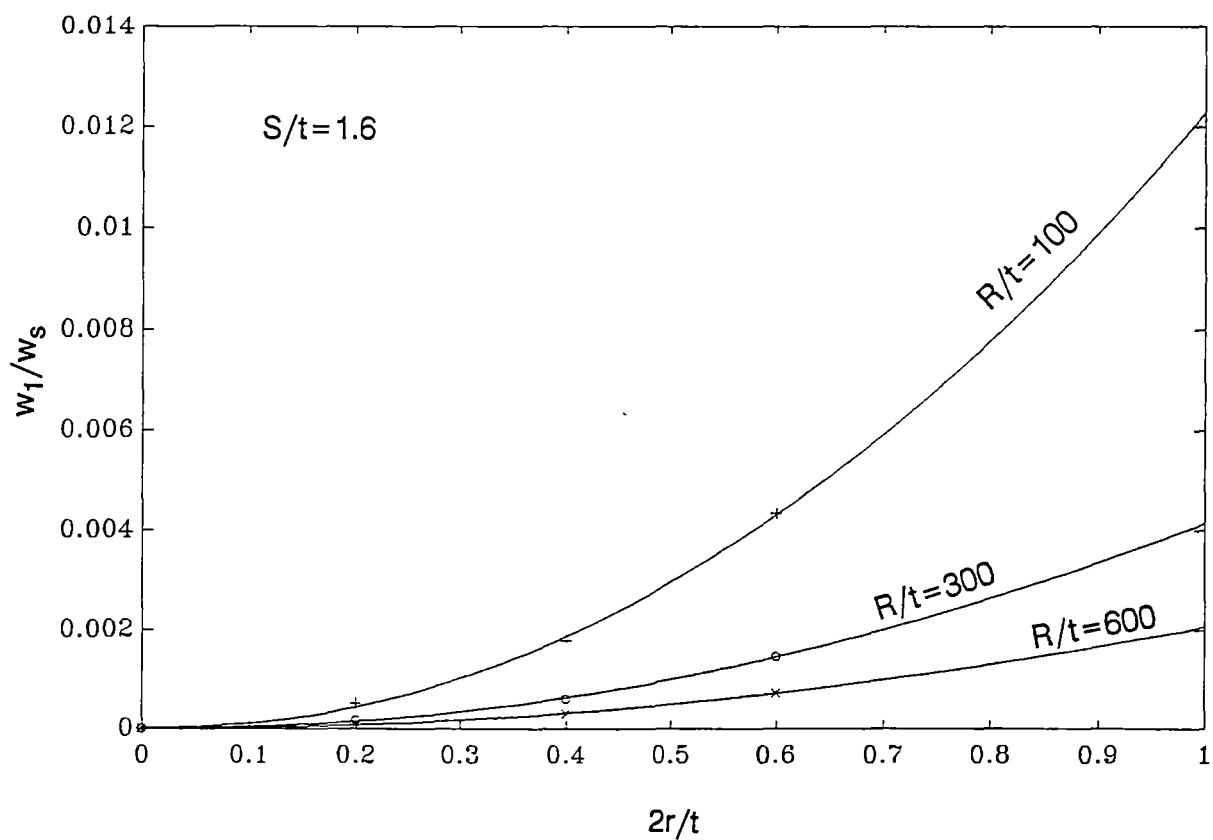


Figure A23 Ratio of displacements w_1/w_s

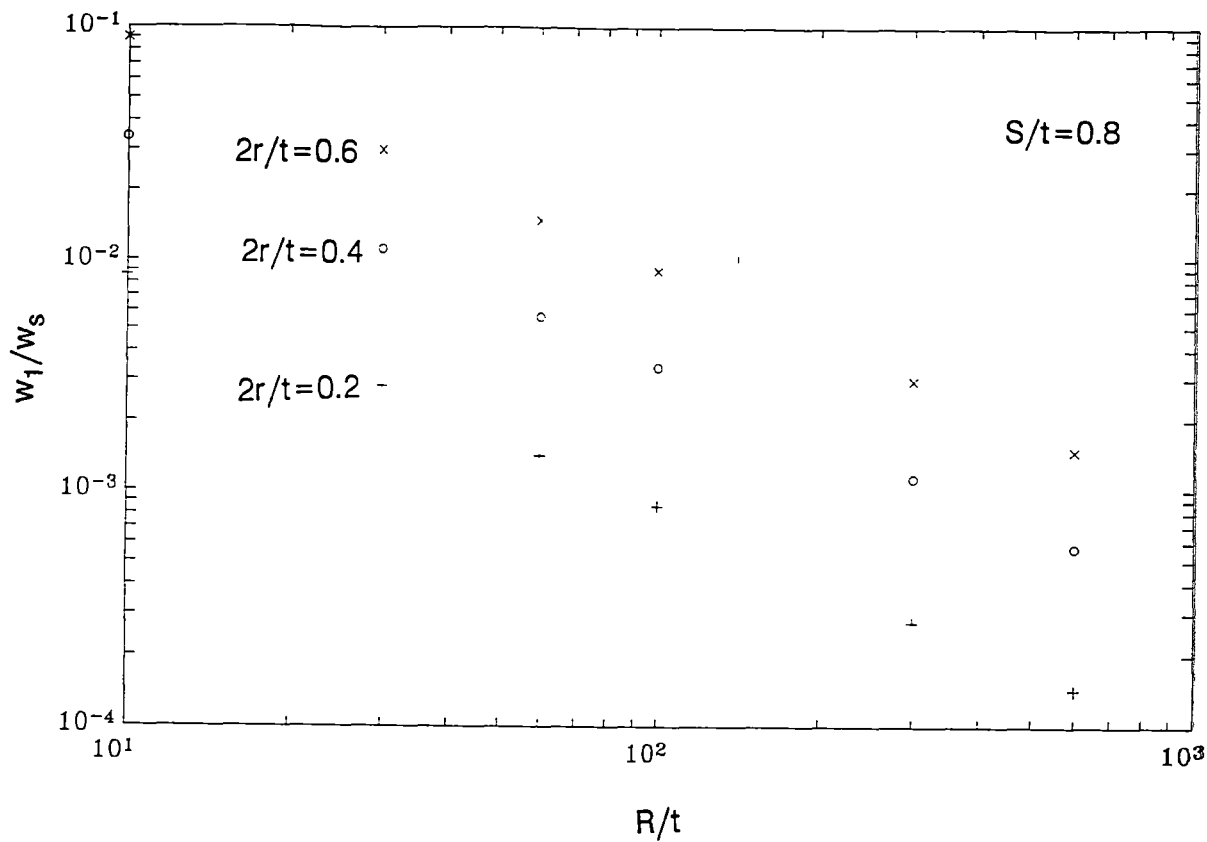


Figure A24 Ratio of displacements w_1/w_s

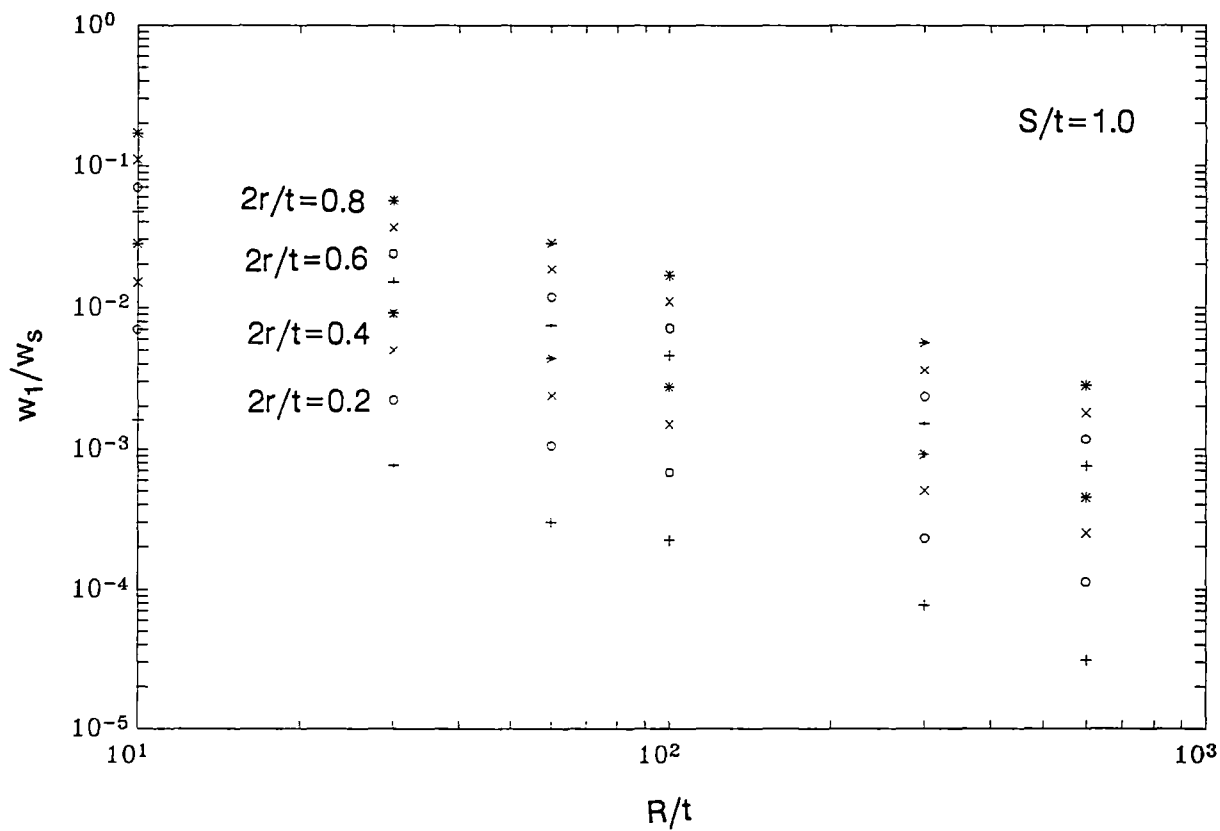


Figure A25 Ratio of displacements w_1/w_s

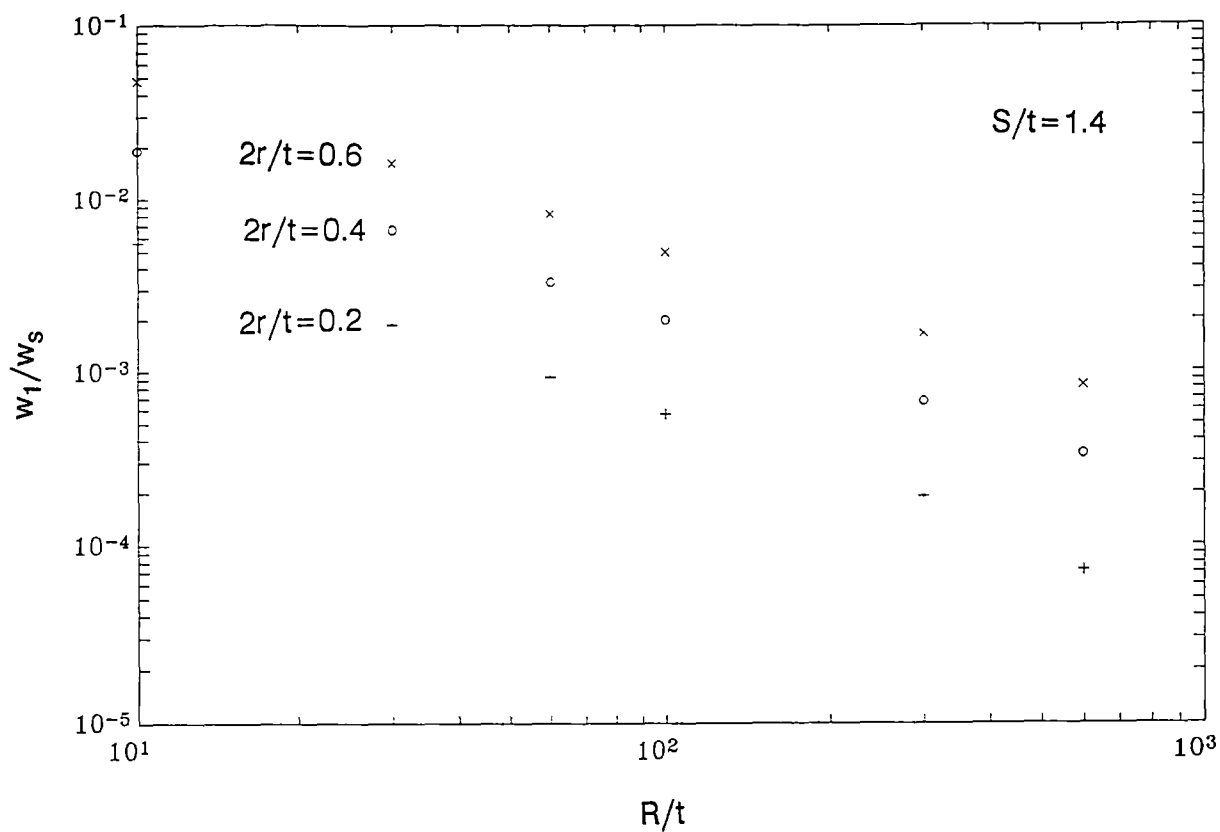


Figure A26 Ratio of displacements w_1/w_s

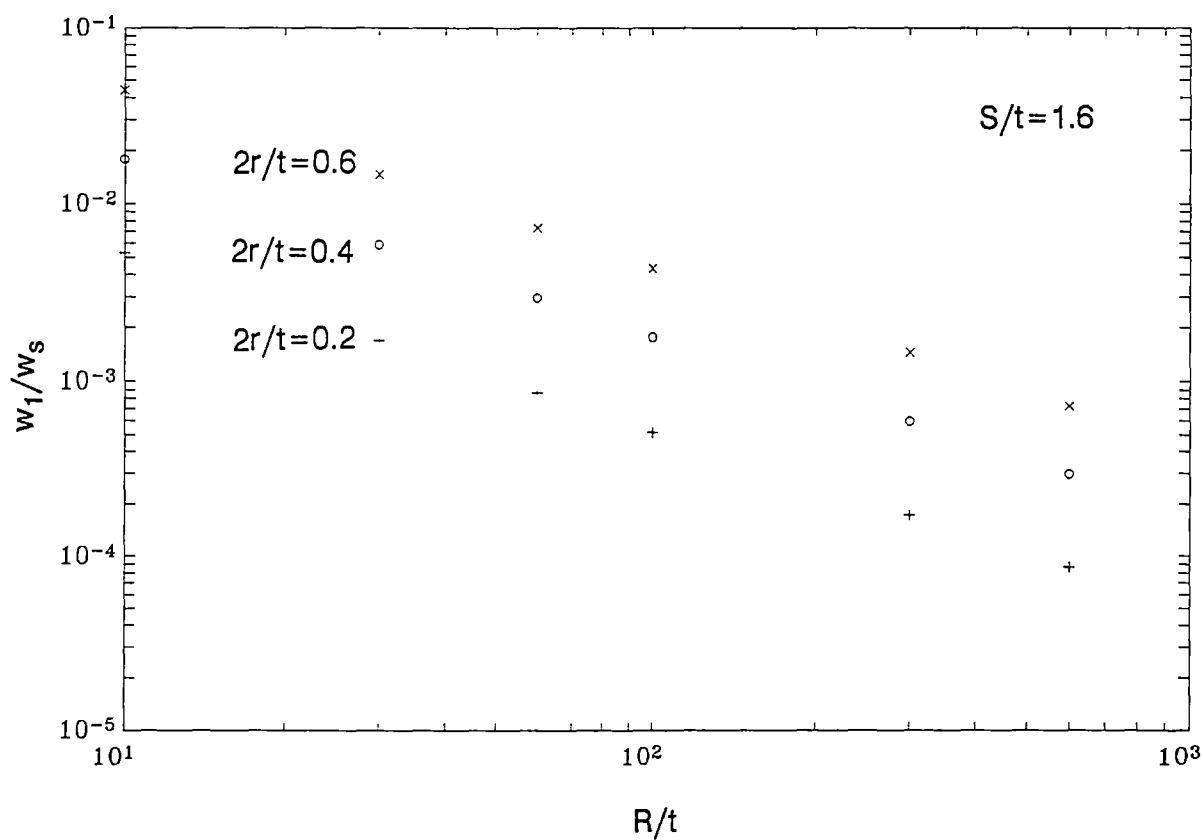


Figure A27 Ratio of displacements w_1/w_s

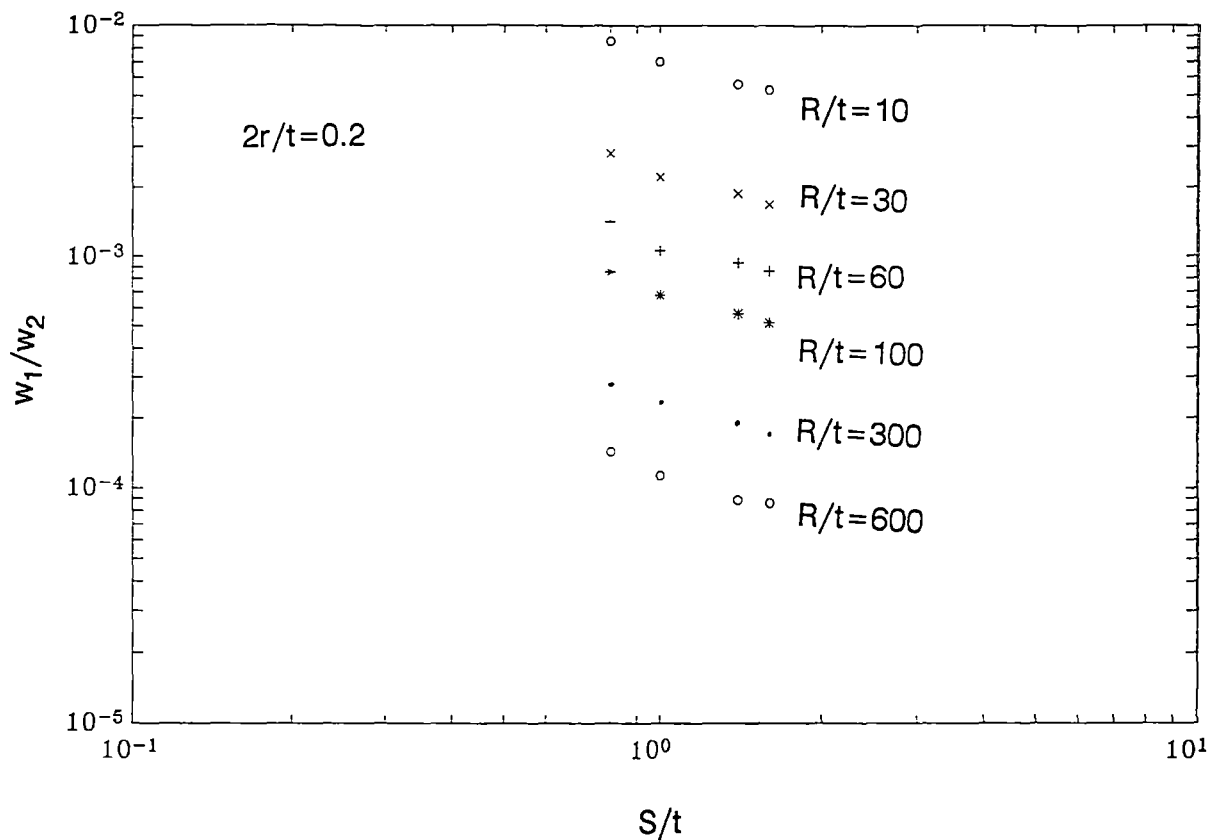


Figure A28 Ratio of displacements w_1/w_s

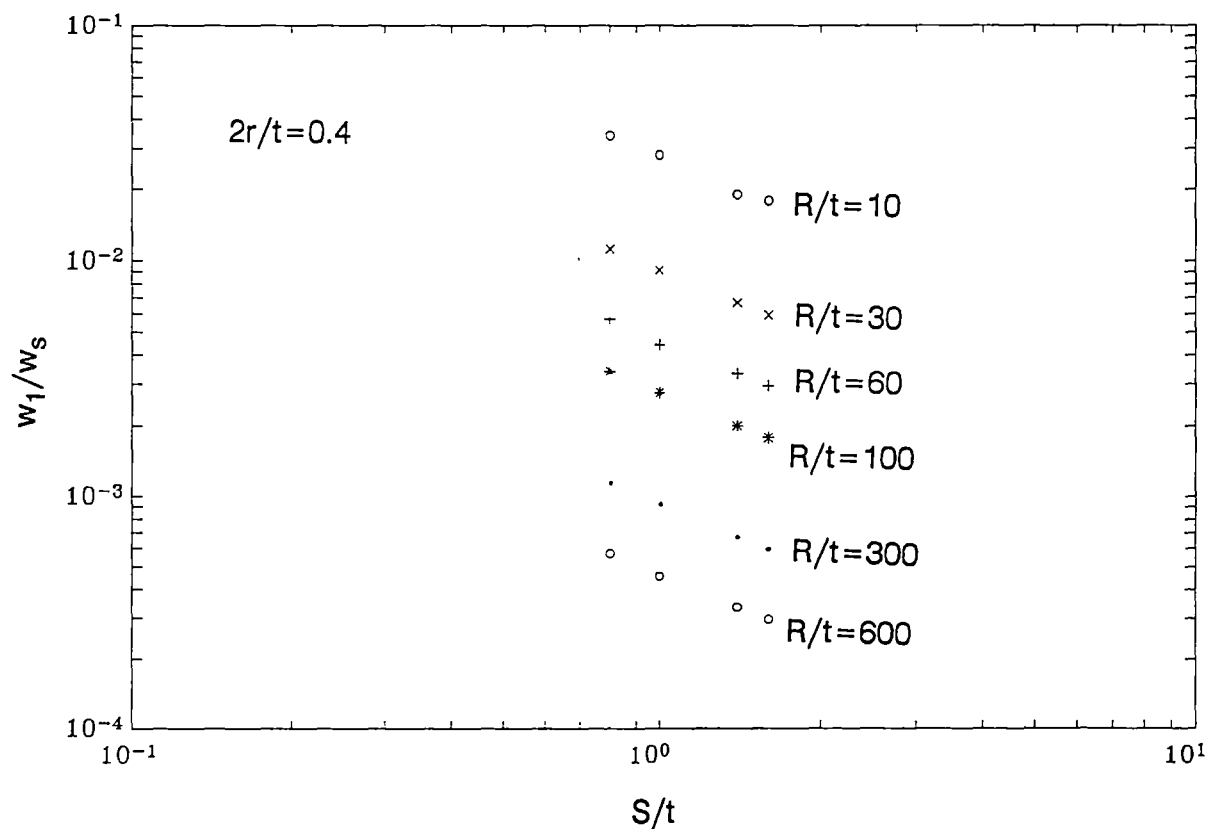


Figure A29 Ratio of displacements w_1/w_s

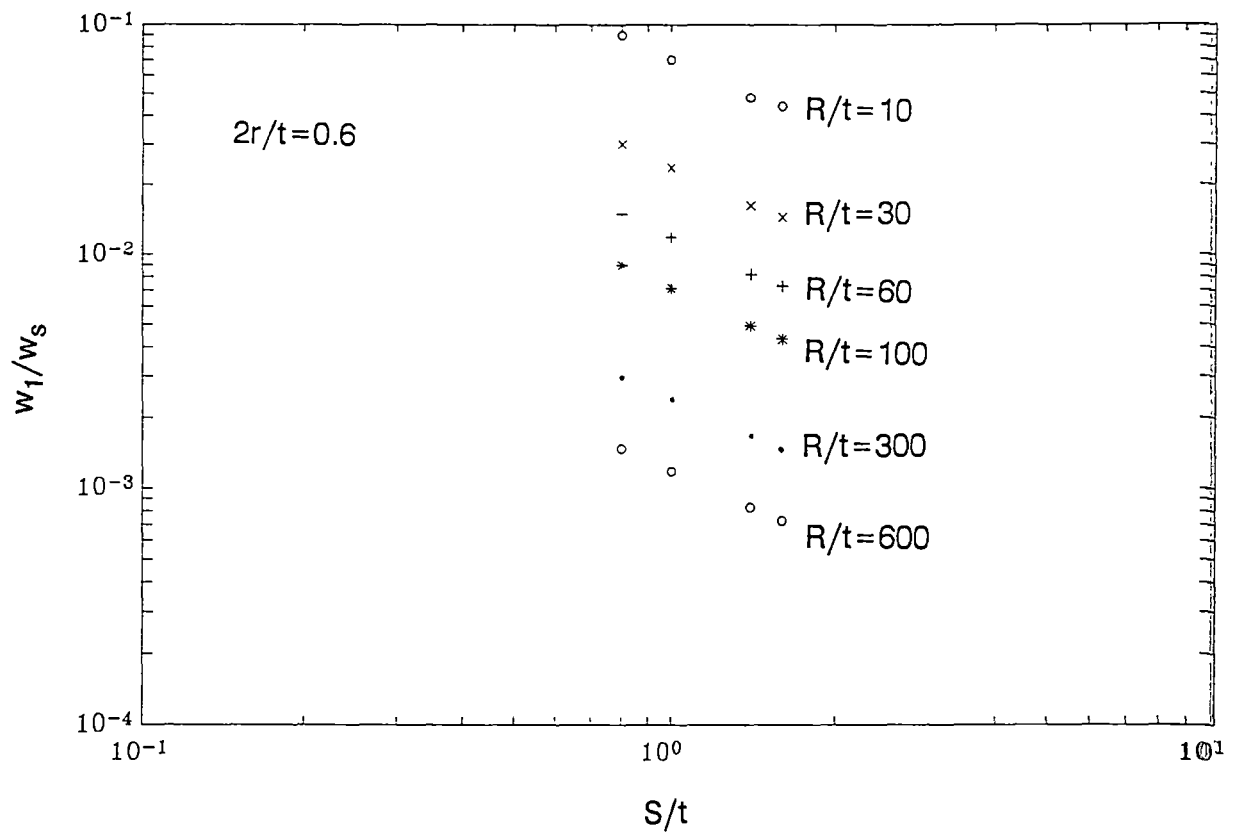


Figure A30 Ratio of displacements w_1/w_s

APPENDIX B

PROGRAM LISTING

USED IN
THE NON-LINEAR LEAST-
SQUARES FITTING

PROGRAM LISTING

USED IN THE NON-LINEAR LEAST-SQUARES FITTING

B.1 PROCEDURE POWELL¹

```
FUNCTION f1dim( x: real ): real;
  VAR
    j: integer;
    xt: glnarray;
  BEGIN
    {$ifdef diag }
    writeln( 'f1dim ', x:10:4 );
    {$endif }
    FOR j := 1 TO n DO
      BEGIN
        xt[j] := pcom[j] + x * xicom[j];
      END;
    f1dim := func( xt );
  END;

PROCEDURE mnbrak( VAR ax, bx, cx, fa, fb, fc: real );
  LABEL 1;
  CONST
    gold  = 1.618034;
    glimit = 100.0;
    tiny  = 1.0e-20;
  VAR
    ulim, u, r, q, fu, dum: real;
  FUNCTION max( a, b: real ): real;
    BEGIN
      IF (a > b) THEN max := a ELSE max := b
    END;
  FUNCTION sign( a, b: real ): real;
    BEGIN
      IF (b >= 0.0) THEN sign := abs(a) ELSE sign := -abs(a)
    END;
  BEGIN
```

¹ This procedure is written by William H. Press, et. in the book of "Numerical recipes" - the art of scientific computing [Cambridge university press 1988]. The procedure was also used in determine theoretical critical loads. It is listed here for the sake of convenience in reading .

```

fa := f1dim( ax );
fb := f1dim( bx );
IF ( fb > fa ) THEN
  BEGIN
    dum := ax;
    ax := bx;
    bx := dum;
    dum := fb;
    fb := fa;
    fa := dum;
  END;
cx := bx + gold * (bx - ax);
fc := f1dim( cx );
1:  IF (fb >= fc) THEN
  BEGIN
    r := (bx-ax)*(fb-fc);
    q := (bx-cx)*(fb-fa);
    u := bx - ( (bx-cx)*q - (bx-ax)*r )
           / ( 2.0*sign( max(abs(q-r),tiny), q-r ) );
    ulim := bx+glimit * (cx-bx);
    IF ((bx-u)*(u-cx) > 0.0) THEN
      BEGIN
        fu := f1dim(u);
        IF (fu<fc) THEN
          BEGIN
            ax := bx;
            fa := fb;
            bx := u;
            fb := fu;
            GOTO 1
          END
        ELSE
          IF (fu > fb) THEN
            BEGIN
              cx := u;
              fc := fu;
              GOTO 1
            END;
          u := cx+gold*(cx-bx);
          fu := f1dim(u)
        END
      ELSE
        IF ((cx-u)*(u-ulim) > 0.0) THEN

```

```

      BEGIN
      fu := f1dim( u );
      IF (fu < fc) THEN
        BEGIN
          bx := cx;
          cx := u;
          u := cx+gold*(cx-bx);
          fb := fc;
          fc := fu;
          fu := f1dim( u )
        END
      ELSE
        IF (u-ulim)*(ulim-cx) >= 0.0 THEN
          BEGIN
            u := ulim;
            fu := f1dim(u)
          END
        ELSE
          BEGIN
            u := cx+gold*(cx-bx);
            fu := f1dim(u)
          END;
          ax := bx; bx := cx; cx := u;
          fa := fb; fb := fc; fc := fu;
          GOTO 1
        END
      END;
END;

```

Function brent(ax, bx, cx, tol: real; VAR xmin: real): real;

```

  LABEL 1,2,3;
  CONST
    itmax=100; cgold=0.3819660;
    { zeps = 1.0e-10; }
    zeps = 1e-8;
  VAR
    a, b, d, e, etemp: real;
    fu, fv, fw, fx: real;
    iter: integer;
    p, q, r, tol1, tol2: real;
    u, v, w, x, xm: real;
  FUNCTION sign(a,b: real): real;
    BEGIN

```

```

        IF (b >= 0.0) THEN sign:= abs(a) ELSE sign :=-abs(a)
        END;
    BEGIN
    IF ax < cx THEN a := ax ELSE a := cx;
    IF ax > cx THEN b := ax ELSE b := cx;
    v := bx; w := v; x := v; e := 0.0;
    fx := f1dim(x); fv := fx; fw := fx;
    FOR iter := 1 TO itmax DO
        BEGIN
        xm := 0.5*(a+b);
        tol1 := tol*abs(x)+zeps;
        tol2 := 2.0*tol1;
    {$ifdef diag }
        writeln('BRENT', iter, ':', x:10:3, xm:10:3,
            tol1:10:3, tol2:10:3 );
    {$endif }
        IF (abs(x-xm) <= (tol2-0.5*(b-a))) THEN GOTO 3;
        IF (abs(e) > tol1) THEN
            BEGIN
            r := (x-w)*(fx-fv);
            q := (x-v)*(fx-fw);
            p := (x-v)*q-(x-w)*r;
            q := 2.0*(q-r);
            IF (q > 0.0) THEN p := -p;
            q := abs(q);
            etemp := e; e := d;
            IF ((abs(p) >= abs(0.5*q*etemp)) OR (p <= q*(a-x))
                OR (p >= q*(b-x))) THEN GOTO 1;
            d := p/q;
            u := x+d;
            IF (((u-a) < tol2) OR ((b-u) < tol2)) THEN
                d := sign(tol1, xm-x);
            GOTO 2
            END;
1:      IF (x >= xm) THEN e := a - x
        ELSE      e := b - x;
        d := cgold*e;
2:      if (abs(d) >= tol1) THEN u := x + d
        ELSE      u := x + sign(tol1,d);
        fu := f1dim(u);
        IF (fu <= fx) THEN
            BEGIN
            IF (u >= x) THEN a := x

```

```

        ELSE          b := x;
        v := w; fv := fw; w := x;
        fw := fx; x := u; fx := fu
    END
ELSE
    BEGIN
    IF (u < x) THEN a := u ELSE b := u;
    IF ((fu <= fw) OR (w=x)) THEN
        BEGIN
            v := w; fv := fw; w := u; fw := fu;
        END
    ELSE
        IF ((fu <= fv) OR (v = x) OR (v = w)) THEN
            BEGIN
                v := u; fv := fu;
            END
        END;
    { write('End of iteration'); readln; }
    END;
    writeln( 'pause in routine BRENT - too many iterations' );
3:  xmin := x;
    brent := fx
    END;

PROCEDURE linmin( VAR p, xi: glarray; n: integer; VAR fret: real );
CONST
    tol= 1.0e-04;
VAR
    j: integer;
    xx, xmin, fx, fb, fa, bx, ax: real;
BEGIN
    ncom := n;
    FOR j := 1 TO n DO
        BEGIN
            pcom[j] := p[j];
            xicom[j] := xi[j]
        END;
    ax := 0.0; xx := 1.0; bx := 2.0;
    mnbrak( ax, xx, bx, fa, fx, fb );
    fret := brent( ax, xx, bx, tol, xmin );
    FOR j := 1 TO n DO
        BEGIN
            xi[j] := xmin * xi[j];

```

```

        p[j] := p[j] + xi[j];
    END
END;

PROCEDURE powell( VAR p: glnarray;
    VAR xi: glnpbynp;
    n, np: integer;
    ftol: real;
    VAR iter: integer;
    VAR fret: real );
    LABEL 1,99;
    CONST
        itmax = 200;
    VAR
        j, ibig, i: integer;
        t, fptt, fp, del: real;
        pt, ptt, xit: glnarray;
    BEGIN
    {$ifdef diag }
        writeln ('procedure powell start: ftol = ', ftol );
    {$endif }
        fret := func( p );
        FOR j := 1 TO n DO
            BEGIN
                pt[j] := p[j]
            END;
            iter := 0;
            { while.....do }
1:      iter := iter + 1;
    {$ifdef diag }
        writeln ( 'Iteration number ', iter );
    {$endif }
        fp := fret;
        ibig := 0;
        del := 0.0;
        for i := 1 TO n DO
            BEGIN
                FOR j := 1 TO n DO
                    BEGIN
                        xit[j] := xi[j,i]
                    END;
                fptt := fret;
                linmin( p, xit, n, fret );

```

```

        IF (abs( fptt-fret ) > del) THEN
            BEGIN
                del := abs( fptt-fret );
                ibig := i
            END
        END;
    IF (2.0*abs(fp-fret) <= ftol*(abs(fret))) THEN
        begin
            writeln('Converge at fp = ', fp:10:4, ' fret = ', fret:10:4 );
            GOTO 99;
        end;
    IF (iter = itmax ) THEN
        BEGIN
            write( 'pause in routine POWELL ');
            write( ' too many iterations'); readln;
            GOTO 99;
        END;
    FOR j := 1 TO n DO
        BEGIN
            ptt[j] := 2.0*p[j] - pt[j];
            xit[j] := p[j] - pt[j];
            pt[j] := p[j]
        END;
    fptt := func(ptt);
    IF (fptt >= fp) THEN GOTO 1;
    t := 2.0*( fp - 2.0*fret+fptt ) *
        sqr( fp-fret-del ) - del*sqr( fp-fptt );
    IF (t >= 0.0) THEN GOTO 1;
    linmin( p, xit, n, fret );
    FOR j := 1 TO n DO
        BEGIN
            xi[ j, ibig ] := xit[ j ];
        END;
    GOTO 1;
99:
    END;

```

B.2 MAIN PROGRAM LISTINGS

PROGRAM MAIN;

CONST

```

n=7;
np=7;
m=72;
ftol : real= 1.0E-06;
XDATA='XDATA';
YDATA='YDATA';
ZDATA='ZDATA';
FIDATA='FIDATA';
TYPE
  glncarray=ARRAY[1..n] OF real;
  glncbynp=ARRAY[1..np,1..np] OF real;
  dataarray= ARRAY[1..m] OF real;
VAR
  i,j,iter,ncm: integer;
  p,pcom,xicom: glncarray;
  x,y,z,fi: dataarray;
  xi: glncbynp;
  fret: real;
  filename, ident: string;
  f, fout: text;

FUNCTION func(VAR p: glncarray): real;
  VAR
    j: integer;
    xj,xx:real;
    fx,fy,fz,sum: real;
    p1,p2,p3,p4,p5,p6,p7: real;
  BEGIN
    p1 :=p[1];
    p2 :=p[2];
    p3 :=p[3];
    p4 :=p[4];
    p5 :=p[5];
    p6 :=p[6];
    p7 :=p[7];
    sum :=0.0;
    writeln( 'func p4 ', p4 );
    FOR J := 1 TO m DO BEGIN
      xj := x[j];
      xx := xj*xj;
      fx := p1+p2*xj + p3*xx;
      fy := p4 * ln( y[j] );
      { write('func j :', j:2, 'y', y[j]:4:1, ln( y[j] )); }

```



```

        fy := exp( fy );
        fz := exp( (p5+p6*xj+p7*xx)*ln(z[j]));
        sum := sum + sqr(fi[j]-fx*fy*fz);
    END;
writeln; writeln( fout, 'func', sum );
    func := sum;
    END;

{$i powell.pas}

```

```

FUNCTION READARRAY (VAR x : dataarray; m : integer; ident : string ):
    boolean;
    var s : string;
        i : integer;
    begin
        repeat
            readln( f, s);
        until s = ident;
        writeln( fout, ident, ' array' );
        for i := 1 to m do
            begin
                read( f, x[i] );
                write( fout, x[i]:10:3 );
                if (i mod 8) = 0 then write( fout );
            END;
        writeln( ident, 'data read OK' );
        ReadArray := true;
    END;

```

```

BEGIN {Main program}
    writeln( 'LEAST SQUARE FITTING' );
    write( 'INPUT DATA FILE NAME: ' );
    read ( filename );
    assign( f, filename + '.dat' );
    reset( f);
    assign( fout, filename + '.out' );
    rewrite (fout );
    if READARRAY( x, m, XDATA ) THEN
        IF READARRAY ( z, m, ZDATA ) THEN
            IF READARRAY ( fi, m, FIDATA ) THEN
                BEGIN

```

```

        writeln ( ' ALL DATA READ OK' );
    END;
writeln( fout, 'Initial values of p[j], j = 1, ', n);
FOR j:= 1 TO n DO BEGIN
    read(f, p[j]);
    write(f, p[j]:9 );
    if (j mod 8) = 0 then writeln;
    END;
writeln( fout );
writeln( fout, 'Initial values of xi[i,j], i=1..', n, ', j=1..', n);
FOR i := 1 TO n DO
    BEGIN
        FOR j:= 1 TO n DO
            begin
                read(f, xi[i,j]);
                write( fout, xi[i,j]:9 );
            end;
        writeln( fout );
    END;
writeln( 'DATA INPUT COMPLETE');
writeln( fout, 'DATA INPUT COMPLETE' );
close( f );
write( 'Convergence tolerance ( ', ftol, ' )');
readln ( ftol );
writeln( fout, 'Convergence tolerance ', ftol );
powell ( p, xi, n, np,ftol, iter, fret);
writeln;
writeln('Minimum function value = ',fret);
writeln;
writeln(' Minimum found at: ');
writeln;
writeln( fout, 'Iterations:', iter);
writeln( fout );
writeln(fout, 'Minimum function value = ', fret);
writeln( fout );
writeln( fout, 'Minimum found at: ');
writeln( fout );
FOR i := 1 TO n DO
    BEGIN
        write( p[i]:10 );
        write (fout, p[i]:10:4);
    END;
{ FOR j := 1 TO m DO

```

```
BEGIN
WRITE( fw[]:10 );
write( fout, fw[]:10:4);
END; }
CLOSE( fout );
END.
```

APPENDIX C

**PROGRAM LISTING USED IN
DETERMINE
THEORETICAL BUCKLING
LOAD AND MODE**

PROGRAM LISTING USED IN DETERMINE THEORETICAL BUCKLING LOAD AND MODE

PROGRAM MAIN;

LABEL 1;

CONST

 n=2;
 np=2;
 ftol : real=1.0e-003;
 dt=0.6087;
 Rt=333.913;
 St=1.1652;
 LR=1.165;
 pcr=3.5026E-07;
 Ncr=1.42236E-03;
 pi=3.1415926535;
 fu1s=0.008857;
 fu2s=1.4286;

TYPE

 glnarray=ARRAY[1..n] of real;
 glnpbynp=ARRAY[1..np,1..np] of real;

VAR

 ppcr, NNcr, ZOU, func1: real;
 i,j,iter,ncom: integer;
 mwa,nwa,pcom,xicom: glnarray;
 xi: glnpbynp;
 fret: real;
 filename, ident: string;
 f, fout: text;

FUNCTION func(VAR mwa: glnarray): real;

 CONST

 E = 1.00;
 mu=0.35;
 a1=0.09671;
 b1=-0.6933;
 c1=2.8276;
 d1=-0.9960;

```

a2=0.9570;
b2=-0.2720;
c2=2.9360;
d2=0.0130;
a3=-0.0907;
b3=0.78614;
d3=-1.016;
VAR
mw,nw: real;
f1, f2, f3: real;
AfA, AmA: real;
fw1s, fw2s: real;
E1, E2, Eb1, Eb2, mu1, mu2: real;
k, ks, k1, namda, lnamda: real;
k1s, mws, namdas, mu1s : real;
mum, mumu, e11, e21 : real;
cp1, cp2, cp3, cp4, cp5, cp6, cp7 : real;
cc1, cc2, cc3, cc4: real;
G1, G2, Q1, Q2, Q3, Q4: real;
BEGIN
mw :=abs(mwa[1]);
nw :=abs(mwa[2]);
IF ( mw < 1 ) THEN mw := 1;
IF ( nw < 1 ) THEN nw := 1;
f1 :=-0.3540-2.240*dt+ 1.7430*dt*dt;
f2 :=0.3280-2.4660*dt+ 2.5630*dt*dt;
f3 :=-0.1790-2.6160*dt+ 2.5240*dt*dt;
AfA :=pi*dt*dt/(4*St);
AmA :=1-AfA;
fw1s := (a1+b1*dt+c1*dt*dt)*exp(d1*ln(Rt))*exp(f1*ln(St));
fw2s := (a2+b2*dt+c2*dt*dt)*exp(d2*ln(Rt))*exp(f2*ln(St));
E1 :=E*AmA;
E2 :=E/fw2s;
G1 :=dt/St*1/(1-0.6495*exp(3*ln(dt)))+ 1-dt/St;
Eb2:=E/G1;
Eb1:=E*(1-3*pi/16*exp(4*ln(dt))/St);
mu1 :=mu*fu2s/fw2s;
mu2 :=mu;
mu1s:=mu1*mu1;
k :=E2/E1;
ks :=sqrt(k);
k1 :=0.5*ks*(1-sqrt(mu1*mu2));
k1s:=k1*k1;

```

```

mws :=mw*mw;
namda :=pi*nw/LR;
namdas:=namda*namda;
lnamda :=ln(namda);
e11 :=Eb1/E1;
e21 :=Eb2/E1;
mum :=mu1*e11-mu2*e21;
mumu:=mu1*e11+mu2*e21;
cc1 := (k-mu1*mu1)*k1*exp(4*lnamda);
cp1 := k1*e11*exp(8*lnamda)-exp(6*lnamda)*mws*((mu1s-k)*e11
-4*k1s +k1*mum);
cp2 := -exp(4*lnamda)*exp(4*ln(mw))*(4*k1*mu1s + (2*k1*mu1
+mu1s-k) *mumu + 8*k1s*mu1-4*k1*k-k1*(k*e11+e21));
cp3 := -namdas*exp(6*ln(mw))*((mu1s-k+2*k1*mu1)*e21-4*k*k1s
-k*k1*mumu) +exp(8*ln(mw))*k*k1*e21;
cp4 := -namdas*exp(4*ln(mw))*((2*k-k1*mu1)*e21-2*k*mu1s
+4*k*k1s -3*k*k1*mu1 +k*k1*mumu);
cp5 := -exp(4*lnamda)*mws*(6*k*k1+ (k-k1*mu1-mu1s)*mumu
-6*k1*mu1s -8*k1s*mu1+k1*(k*e11-e21));
cp6 := -2*exp(6*ln(mw))*k*k*k1-exp(6*lnamda)*k1*mu1*(1+e11)
-namdas*mws*(e21*(k1*mu1+mu1s-k)+k*(k1*mu1-4*k1s));
cp7 := -exp(4*lnamda)*k1*(3*mu1s-4*k)+exp(4*ln(mw))*k*k1*e21;
cc2 := cp1 + cp2 + cp3 + cp4 + cp5 + cp6 + cp7;
cc3 := k1*mw*mw*sqr(namda*namda+ks*mw*mw)
+k1*(2*ks+k)*namda*namda*mw*mw-exp(4*ln(mw))*k*k1;
cc4 := namda*namda*k1*sqr(namda*namda+ks*mw*mw)
+namda*namda*mw*mw*k*k1;
Q1 := (cc1+cc2/(12*Rt*Rt))/(pcr*Ncr);
Q3 := (cc3*Rt*(1-mu1*mu2))/(E1*Ncr);
Q4 := cc4*(1-mu1*mu2)/(E1*pcr);
NNcr := (Q1-Q3*ppcr)/Q4;
func := NNcr;
END;

```

{ \$i powell.pas }

```

BEGIN {MAIN PROGRAM}
ZOU :=Rt*sqr(LR);
writeln( 'FINDING BUCKLING MODE' );
write ( 'INPUT DATA FILE NAME: ' );
read ( filename );
assign (f, filename + '.dat' );
reset ( f );

```

```

assign( fout, filename + '.out' );
rewrite (fout );
writeln (fout, 'BUCKLING INTERCURVE OF A CELLULAR WALLED
SHELL' );
WRITELN (FOUT);
WRITELN (fout, 'S/t = ', St);
writeln (fout, '2r/t = ', dt);
writeln (fout, 'R/t = ', Rt);
writeln (fout, 'L/R = ', LR);
writeln (fout, 'Z = ', ZOU );
writeln (fout, 'ppcr = ', ppcr);
writeln (fout, 'Ncr = ', Ncr);
writeln (fout);
writeln (fout, 'INITIAL VALUE OF mwa[j], j=1, ', n );
FOR j := 1 TO n DO BEGIN
    read(f, mwa[j]);
    write(fout, mwa[j]:9);
    if (j mod 8) = 0 then writeln;
    END;
writeln( fout );
writeln( fout, 'Initial value of xi[i,j], i=1..', n, ', j=1..', n);
FOR i := 1 TO n DO
    BEGIN
        FOR j := 1 TO n DO
            BEGIN
                read (f, xi[i,j]);
                write( fout, xi[i,j]:9 );
            END;
        writeln( fout );
    END;
writeln( 'DATA INPUT COMPLETE' );
writeln (fout, 'DATA INPUT COMPLETE' );
close( f);
write ('Convergence tolerance ( ', ftol, ' ');
readln( ftol );
writeln(fout, 'Convergence tolerance ', ftol );
ppcr := 1.10;
1:  ppcr := ppcr - 0.10;
powell ( mwa, xi, n, np, ftol, iter, fret );
writeln;
writeln('ppcr = ', ppcr);
writeln;
writeln('Minimum function value (NNcr) = ', fret);

```



```

writeln;
writeln('Minimum found at (m, n): ');
writeln( fout );
writeln( fout );
writeln( fout, 'ppcr = ', ppcr);
writeln( fout );
writeln( fout, 'Iterations:', iter);
writeln( fout );
{ writeln( fout, 'Minimum function value NNcr = ', fret);
  writeln( fout );
  writeln( fout, 'Minimum found at m, n: ');
  writeln( fout );
  FOR i := 1 TO n DO
    BEGIN
      write( mwa[i]: 10 );
      write( fout, mwa[i]: 10:4);
      writeln( fout );
    END;
  }
  nwa[1] := Int(mwa[1] + 0.5);
  if ( mwa[2] <= 1.0 ) then nwa[2] := 1.0
    else nwa[2] := Int(mwa[2] + 0.5);
  func1 := func ( nwa );
  writeln( fout );
  writeln( fout, 'Minimum function value NNcr = ', func1);
  writeln( fout );
  writeln( fout, 'Minimum found at m, n (buckling mode): ');
  writeln( fout );
  FOR i := 1 TO n DO
    BEGIN
      write( nwa[i]: 10:4 );
      write( fout, nwa[i]: 15:9);
      writeln( fout );
    END;
  if ( ppcr > -1.0 ) Then goto 1;
  close ( fout );
END.

```

APPENDIX D

PROGRAM LISTING
USED IN
DATA LOGGING

PROGRAM LISTING USED IN DATA LOGGING

```
PROGRAM READDATA;

USES PCLDEFS, PCLERRS, CRT;

const N = 2000;

VAR

    i,j,error : INTEGER;
    data : ARRAY[1..N] OF WORD;
    DDATA : STRING [20];
    OK : BOOLEAN;
    DFILE : TEXT;

function ConverterSetup : boolean;
    var error : integer;
    begin
        error := Initialize;
        if error < > 0 then
            begin
                writeln('Initialize returns ', error );
            end;
        (*      ConverterSetup := error = 0; *)
    converterSetup := true;
    end;

var outfile : text;

function OpenFile : boolean;
    var
        shell_id : integer;
        id, fn : string[20];
    begin
        write('Shell Number? '); readln( shell_id );
        str( shell_id, id );
        fn := 'c:\lab\sh' + id + '.dat';
        assign ( outfile, fn );
```

```

rewrite ( outfile );
writeln( 'Your data will be in file [, fn, ']' );
OpenFile := true;
end;

```

```

procedure CloseFile;
begin
close( outfile );
end;

```

```

function CollectData : boolean;
const
    min_channel = 0;
    max_channel = 3;
    gain = 1;
var
    i, error : integer;
    x : array[min_channel .. max_channel] of WORD;
begin
for i := min_channel to max_channel do
begin
error := Adc_Value( i, gain, x[i] );
if error < > 0 then
writeln( 'Error ', error, ' on channel ', i );
end;
for i := min_channel to max_channel do
begin
write( outfile, x[i]:6 );
end;
writeln( outfile );
(*      CollectData := error = 0; *)
collectdata := true;
end;

```

```

var c: char;
rate : real;
ms : integer;

```

```

BEGIN
clrscr;
writeln ('DATA LOGGING OF SHELL BUCKLING PERFORMANCE WITH
DATA TRANSLATION');

```

```

writeln ('DT2818 SIMULTANEOUS SAMPLING BOARD. ');
writeln;
write('Sampling rate '); readln( rate );
ms := round( 1000.0/rate );
writeln('Sampling every ', ms, ' ms ');
writeln('Enter S to collect single data');
writeln('Enter C to collect continue data');
writeln('Enter Q to quit');
if ConverterSetup then
begin
if OpenFile then
begin
repeat
c := ReadKey;
c := upcase( c );
if c = 'c' then
begin
writeln('Continue data collection');
repeat
if not CollectData then
begin
writeln('Error collecting data');
end;
delay( ms );
until KeyPressed;
end;
else if c = 's' then
begin
writeln('Single data collection');
if not CollectData then
begin
writeln('Error collecting data');
end;
end;
until c = 'Q';
CloseFile;
end;
end;
end.

```

APPENDIX E

CALIBRATION PLOTS

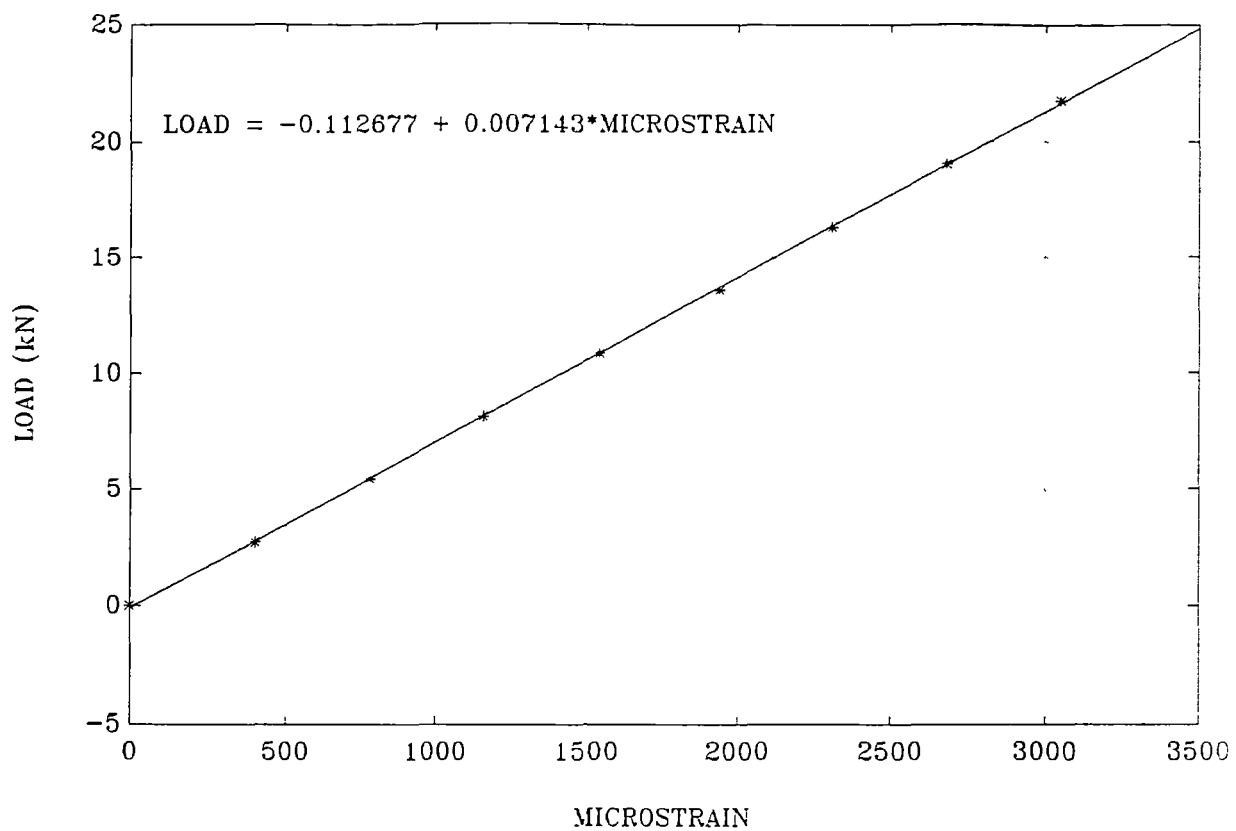


FIGURE E1
CALIBRATION PLOT OF 20kN LOAD CELL

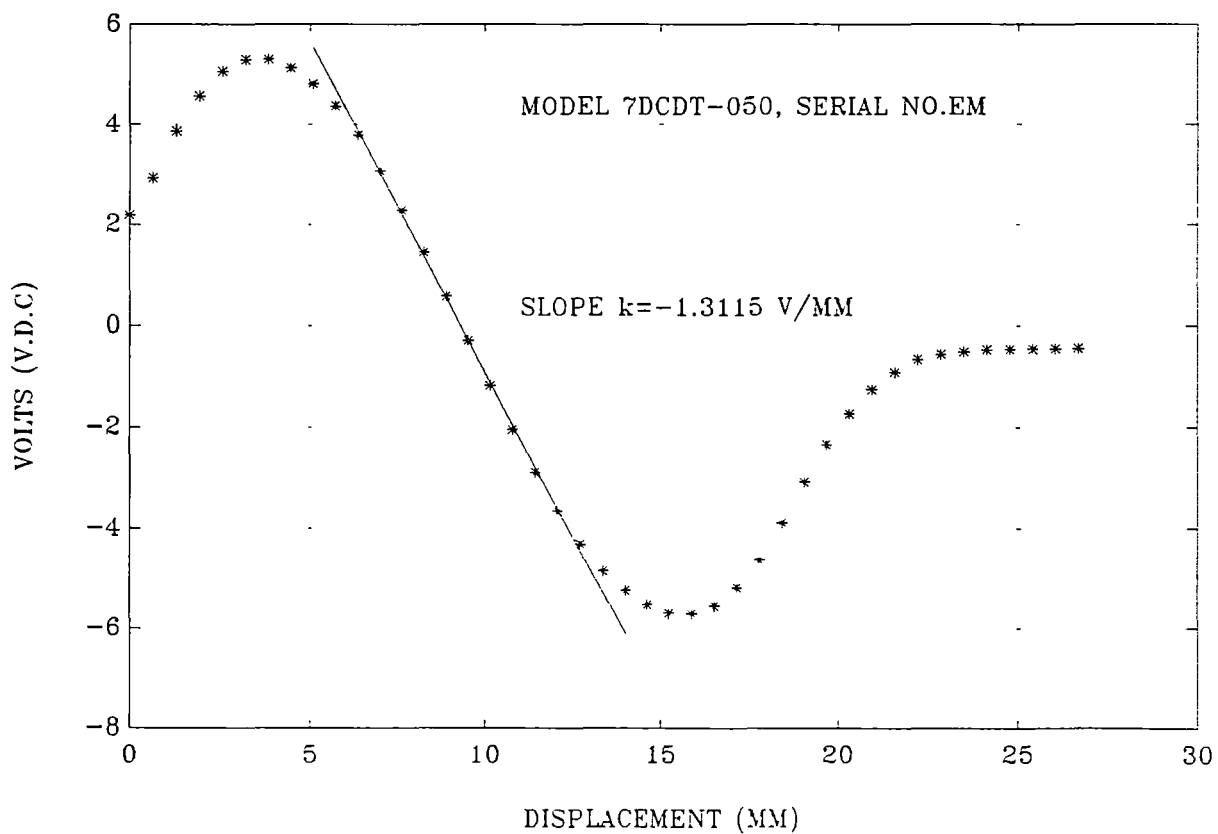


FIGURE E2
CALIBRATION PLOT OF DISPLACEMENT TRANSDUCER

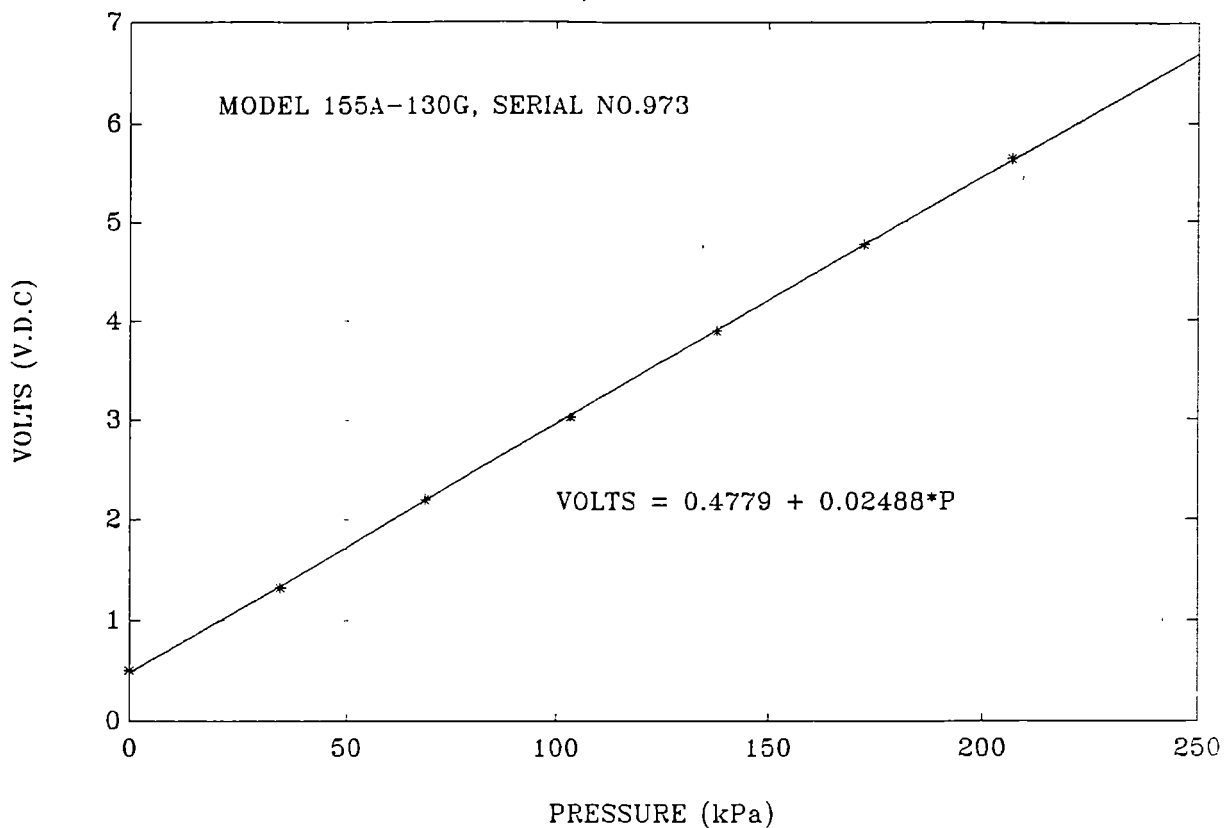


FIGURE E3
CALIBRATION PLOT OF LOW PRESSURE TRANSDUCER

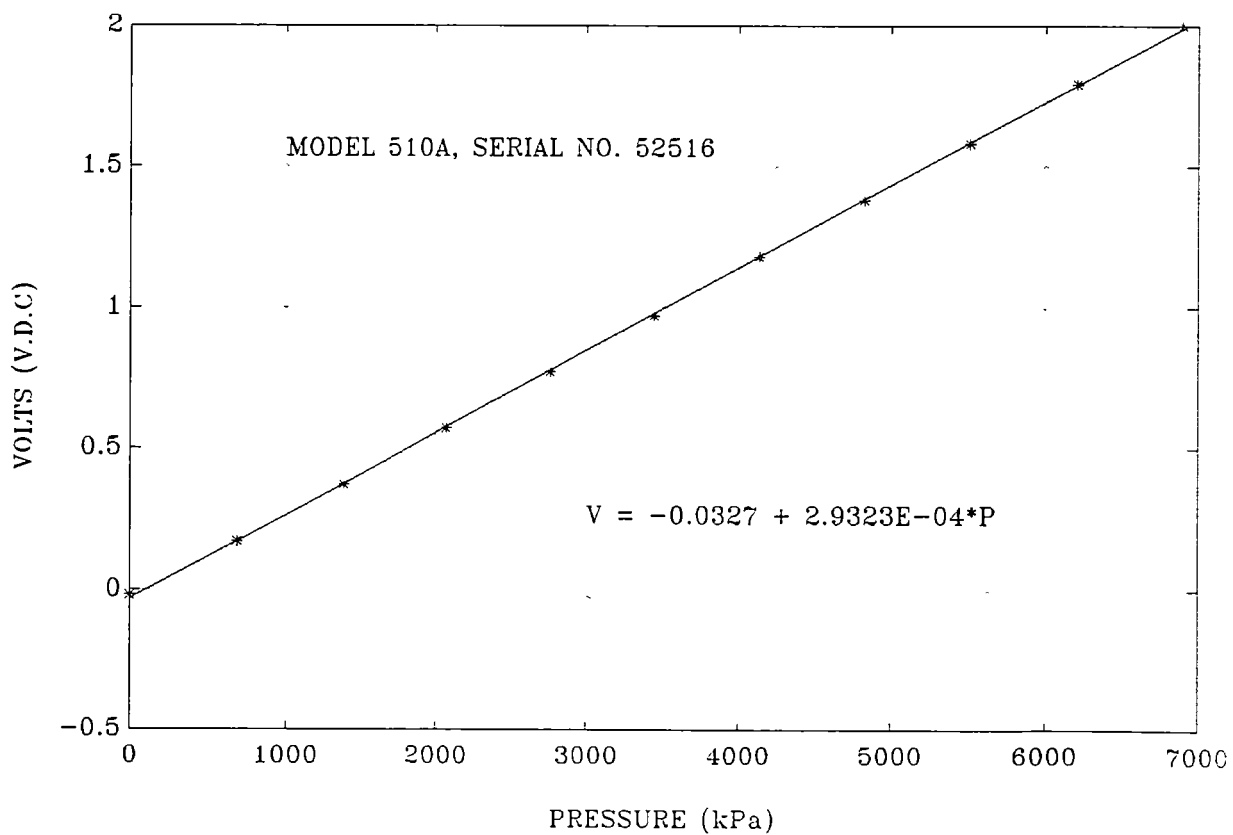


FIGURE E4
CALIBRATION PLOT OF HIGH PRESSURE TRANSDUCER

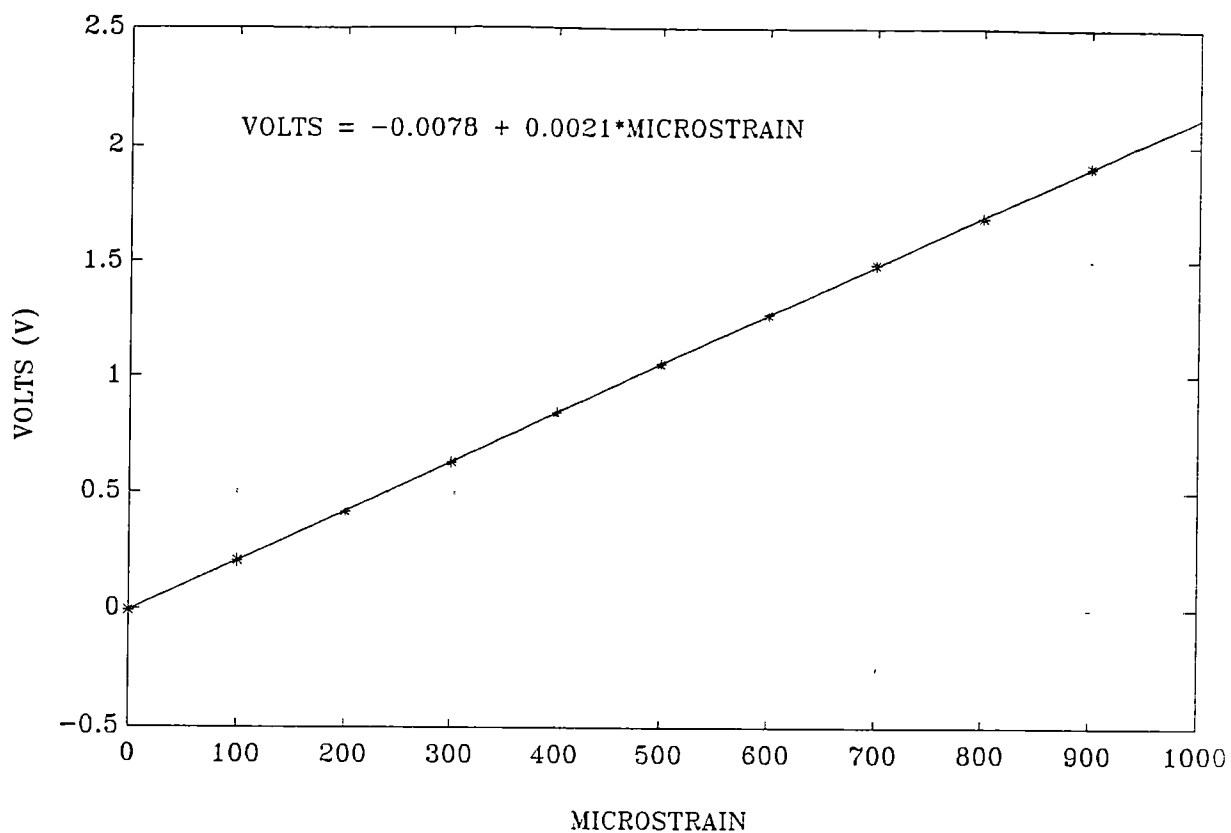


FIGURE E5
CALIBRATION PLOT OF STRAIN INDICATOR

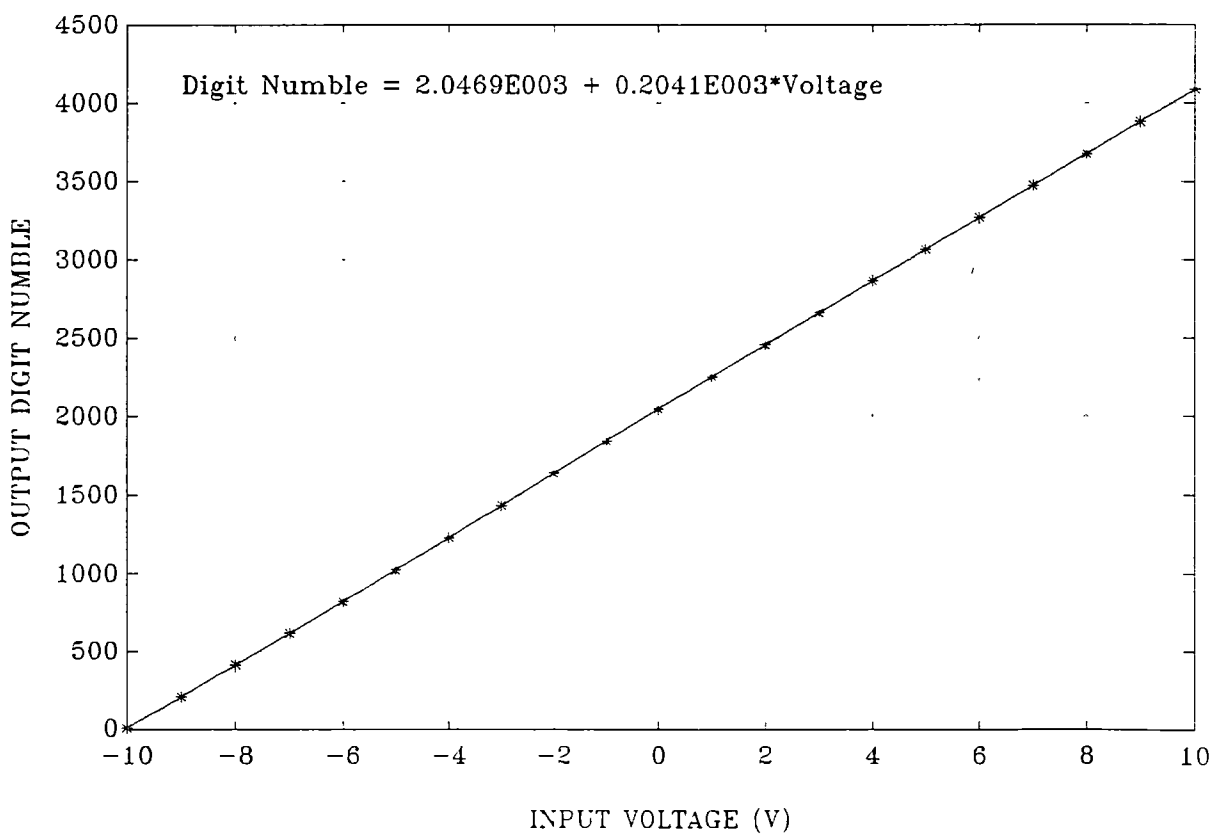


FIGURE E6
CALIBRATION PLOT OF DT2818 DATA LOGGING BOARD

CALIBRATION OF DATA LOGGING BOARD DT2818

VOLTS	CHAN. 0	CHAN. 1	CHAN. 2	CHAN. 3
-10	6	6	7	6
-9	210	210	211	210
-8	414	414	415	415
-7	619	619	620	619
-6	823	823	824	823
-5	1026	1025	1027	1026
-4	1230	1230	1230	1230
-3	1434	1434	1435	1434
-2	1639	1638	1638	1638
-1	1841	1842	1842	1842
0	2047	2046	2048	2047
0	2047	2047	2048	2047
1	2251	2252	2252	2252
2	2456	2456	2456	2456
3	2660	2660	2660	2659
4	2864	2863	2864	2864
5	3068	3067	3068	3068
6	3271	3271	3271	3270
7	3476	3476	3476	3476
8	3678	3678	3679	3678
9	3883	3882	3883	3882
10	4088	4087	4087	4086

APPENDIX F

PROCEDURE LISTING
USED
IN PC-MATLAB

APPENDIX F

PROCEDURE LISTING USED IN PC-MATLAB

```
idata=[
    2142 2043 2045 2155
    2143 2043 2044 2154
    2149 2044 2044 2154
    2153 2046 2044 2155
    2156 2046 2045 2155
    2157 2047 2043 2156
    2159 2048 2044 2154
    .....];
[n,m] = size(idata);
cellpressure = (idata(n,3)-idata(1,3))/204.1/2.021818e-03
externalpressure = (idata(n,4)-idata(1,4))/204.1/0.171571
n1 = idata(:,1);
n2 = idata(:,2);
disp = (n1-n1(1))/204.1 /1.3115*1.0e-03;           [Axial displacement]
newton = (((n2-n2(1))/204.1+0.0078)/0.0021)*7.143;   [Axial load]
num0 = 65;
num1 = 142;
dis = disp(num0:num1);
new = newton(num0:num1);
for j= 1:2
    A1(:,j)=dis.^(2-j);
end;
c = A1\new;
c1 = c(1,1);
c2 = c(2,1);
slope = c1;
pi=3.14159;
R=76.6e-03;
t=1.25e-03;
```

[Data collected from data logging board]

[Finding slope in load-deflection curve]

```

r=0.35e-03;
L=200.00e-03;
A = 2*pi*R*t-360*pi*r*r;
E = c1*L/A [Calculating Young's
modulus of the shell]
x = (3e-4:0.1e-4:19e-4)';
y = polyval(c,x);
n0 = num1;
disp1 = (newton(n0:n) - c2)/c1;
ddisp = disp(n0:n) - disp1; [Calculating change of displacement]
dnewton = ddisp./newton(n0:n); [Calculating change of displacement
/axial load]
for j = 1:2
    B1(:,j) = ddisp.^(2-j);
end;
e = B1\dnewton;
axialload = 1/e(1,1);
u = (-1e-5:0.1e-5:2e-5)';
v = polyval(e,u);
plot(disp,newton,'+ ',x,y,'-',dis,new,'o');
grid;
title('ESTIMATION OF BUCKLING LOAD - SHELL010000');
xlabel('AXIAL DISPLACEMENT (M)');
ylabel(' AXIAL LOAD (N)');

```